SANDY SOIL STABILIZATION BY MICROBIAL INDUCED CALCITE PRECIPITATION (MICP) USING BIO-STIMULATION METHOD

A DISSERTATION SUBMITTED TO THE GRADUATE DIVISION OF THE UNIVERSITY OF HAWAIʻI AT MĀNOA IN PARTIAL FULLFILMENT OF THE REQUIREMENTS FOR THE DEGREE OF

DOCTOR OF PHILOSOPHY

IN

CIVIL ENGINEERING

MAY 2022

By

Yijie Wang

Dissertation Committee:

Ningjun Jiang
Philip Ooi
Tao Yan
Zhenhua Huang
A. Ricardo Archilla

Keywords: microbially induced calcite precipitation (MICP), bio-stimulation, calcareous sand, biochemical response, shearing behaviors, compressibility, erosion

ACKNOWLEDGEMENT

I would like to express my appreciation to the following people and institutions that have supported me throughout my Ph.D.

I would like to extend my deepest gratitude to my supervisor, Dr. Ningjun Jiang, the completion of my dissertation would not be possible without his guidance, patience and support. I also wish to thank the committee members: Dr. Philip Ooi, Dr. Tao Yan, Dr. Zhenhua Huang and Dr. A. Ricardo Archilla for their insightful suggestions in my research.

I gratefully acknowledge the assistance of my lab mates Xiaole Han, Dr. Ogul Doygun for helping with the experimental device set-up, data analysis and paper review. Thanks should also go to our technician Jonathan Imai, for the maintenance on the experimental apparatus.

Lastly, I am also greatful to the encouragement and strong support from my families, especially my wife Yao Huang, who always inspires me.

ABSTRACT

Calcareous sands are often considered as very unstable and evolving materials with large particles allowing an abundance of air space. Their physical properties are usually defined as weak or no structure, free draining with high permeability, poor water retention, and high sensitivity to compaction. In tropic areas, the physical properties of sandy soils are more complicated. A more frequent cycling of wetting and drying can affect the physical properties significantly. These adverse engineering properties make it difficult to manage in the construction field.

Chemical stabilization has been applied in the field for years. Frequently used stabilizers include Portland cement, lime and industrial waste lime, asphalt, and others. However, the major problem of these tradition materials is highly dependent on mass industrial production which requires substantial energy. Some potential environmental issues can be induced due to the high alkaline level of many of these chemical stabilizers. Considering the abovementioned limitations of those traditional additives, alternative technique is required to make the sandy soil stabilization more economic and environmental-friendly.

Microbiologically Induced Calcite Precipitation (MICP) as a new interdisciplinary method combines the microbiological, geochemical, and geotechnical research to fulfill the increasing demands for the sandy soil improvement. The stabilization process can be achieved by inducing calcite precipitation within the sand matrix via microbial ureolysis procedure by ureolytic bacteria. The produced calcite precipitation preferentially accumulates at particle-particle contacts, which can provide extra connection and gain more strength. Because of the widely distribution of ureolytic microbes in the natural soil, the in-situ bio-stimulation of indigenous ureolytic bacteria becomes feasible.

The study in this thesis firstly investigated the effect of enrichment media on the stimulation of native ureolytic bacteria in calcareous sand under solution condition. A series of batch tests were conducted, and the generic and three different selective enrichment media were compared from the biochemical aspects. The results show that the selective enrichment media rich in urea could successfully stimulate and enrich the native ureolytic bacteria by monitoring the ureolytic activity, pH, and electric conductivity. The

nutrients with higher nitrogen sources show better efficiency in improving ureolytic activity.

Secondly, the biochemical and direct shear behaviors of bio-cemented sand treated by bio-stimulated MICP were investigated under sand column condition. It was found that during the enrichment phase, the indigenous ureolytic bacteria can be enriched significantly within 48 hours, though the ureolysis rate was varying with the initial urea concentration. The microbial community changed significantly after enrichment stage. The ureolytic species could be found in the sand. Furthermore, the cementation content increased with the flushing number of cementation solution. The shear strength of bio-cemented sand could be significantly enhanced after MICP treatment. The cohesion and peak friction angle increased with elevated cementation level while declined with the increasing normal stress.

Then, the compressive characteristics of bio-cemented sand was studied under one-dimensional compression tests. It was found that the compressibility of bio-cemented reduced with the increasing cementation content. The samples prepared under higher initial relative density showed less compression. Based on microscopic observations, a conceptual framework based on the interparticle contact modes and their corresponding damage modes during the compression tests was proposed.

After that, to find out a way to preserve the enriched urease within soils as much as possible, and further increase the bio-cementation content, the biochar-amendment was incorporated into MICP. The shear behavior of biochar-amended bio-cemented calcareous sand treated via bio-stimulation was investigated through a series of direct shear test. The results showed that the addition of biochar powders could effectively increase the cementation content as the extra nucleation sites for native ureolytic bacteria. However, too much biochar within bio-cementation may become weak points and thus diminish the contribution of interparticle bonding to the shear strength.

Finally, a preliminary exploration of bio-stimulated MICP in rainfall-induced erosion prevention was conducted by a series of laboratory model tests. The artificial sandy slope was made and subjected to the rainfall. Meanwhile, the photography-based SfM (Structure from Motion) as the new technique was firstly applied to evaluate the slope deformation

under rainfall-induced erosion. The results showed that bio-stimulated MICP could significantly reduce the erosion on a sandy slope, especially in case treated by YE-based enrichment medium with 170 initial urea concentration. It is a good trial to explore a feasible monitoring way for the future full-scale application in field.

TABLE OF CONTENTS

LIST OF TABLES

LIST OF FIGURES

NOMENCLATURE

Roman Symbols

a_v	coefficient of compressibility
a_p	the potential of agglomeration for a given size fraction
a_{po}	pre-compression potential for agglomeration
a_{pf}	post-compression potential for agglomeration
A_t	total agglomeration
A_p	agglomeration potential
A_r	relative agglomeration
B_t	total breakage
B_p	breakage potential
B_r	relative breakage
C_c	coefficient of curvature
CC	cementation content
C_u	coefficient of uniformity
C_r	recompression index
c	cohesion
D	the opening size of sieve
D_r	relative density
e_0	initial void ratio

e_m	modified void ratio
G_s	specific gravity
G_{sg}	specific gravity of sand grains
G_{Ca}	specific gravity of $CaCO_3$
h	horizontal displacement under direct shear
m_{at}	dry mass of sand after MICP treatment
m_{bt}	dry mass of sand before MICP treatment
m_{sg}	mass of sand grains
m_{Ca}	mass of $CaCO_3$
m_B	dry mass of biochar
p'	effective verticle stress
V_t	total volume of sample
v	vertical displacement under direct shear

Greek Symbols

η_p	peak stress ratio
ϕ	friction angle
ψ	dilation angle
ψ_m	maximum dilation angle
ρ_w	mass density of water

Other Symbols

CO_3^{2-}	carbonate ion
Ca^{2+}	calcium ion
$CaCl_2$	calcium chloride
$CaCO_3$	calcium carbonate
$Ca(CH_3COO)_2$	calcium acetate
$C_2H_3O_2^-$	acetate ion
CO_2	carbon dioxide
Fe^{2+}	ferrous ion
$Fe(OH)_3$	ferric hydroxide
H^+	hydrogen ion
H_2O	water
HCO_3^-	bicarbonate ion
HS^-	hydrosulfide ion
Mg^{2+}	magnesian ion
$(NH_2)_2CO$	urea
NH_4^+	ammonium ion
NO_3^-	nitrate ion
N_2	nitrogen gas
OH^-	hydroxyl ion
SO_4^{2-}	sulfate ion

Abbreviations

CEC	cation exchange capability
DNA	deoxyribonucleic acid
EC	electric conductivity
EDS	energy-dispersive X-ray spectroscopy
FTIR	fourier-transform infrared spectroscopy
MICP	microbially induced calcite precipitation
MIP	mercury intrusion porosimetry
OD_{600}	the optical density at 600 nm
OD_{425}	the optical density at 425 nm
OD_{422}	the optical density at 422 nm
PSDs	particle size distribution curves
PV	pore volume
PVC	polyvinyl chloride
SEM	scanning electron microscope
SfM	structure from motion
TGA	thermogravimetric analysis
UA	ureolytic activity
UCS	unconfined compression strength
XRD	X-Ray Diffraction

CHAPTER 1. Literature Review on Bio-mediated Soil Improvement: Processes, Materials, Characterization and Applications

1.1 Introduction

For a long time, geotechnical engineering practice has viewed soil as an inert material for construction, comprising only three phases – mineral solids, pore water and trapped air. The understanding of the fundamentals of soil behavior is primarily based on these three inorganic phases. However, one fact that has been ignored for a long time by geotechnical engineers is that microorganisms including bacteria, archaea and eukaryotes are ubiquitous in soil (Jiang et al., 2020; Mitchell and Santamarina, 2005). The importance of microbes in soil has been well recognized by agricultural, ecological and environmental scientists, and numerous studies have been conducted to reveal the interactions between microbial activities and crop production, ecological conservation, and environmental remediation (DeJong et al., 2015). Microbes have the capacity and capability to alter biogeochemical processes in the local soil environment and the cumulative changes could consequently modify the physical (e.g., density and porosity), mechanical (e.g., strength and compressibility), conductive (e.g., hydraulic and thermal conductivity), and chemical (e.g. buffering and ion exchange capacity) properties of the bulk soil matrix (Ivanov and Chu, 2008; DeJong et al., 2010).

While various natural microbial processes can change soil properties, an engineered process is required for soil treatment. The microbially induced carbonate precipitation (MICP) process has been the primary focus of research in bio-mediated geotechnics to date (Dejong et al., 2013; Zhu and Dittrich, 2016), though other microbial processes can also be used to change soil engineering properties, such as denitrification and other processes involving the use of iron-reducing, nitrifying and oligotrophic bacteria as discussed by Chu et al., (2009). MICP research in geotechnical engineering has experienced rapid developments in the past decade. There have been several published comprehensive review articles on MICP research in the past five years (Jiang et al., 2020; Osinubi et al., 2020; Shashank et al., 2016; Tang et al., 2020; Terzis and Laloui, 2019; Umar et al., 2016; Yu et al., 2020; He et al., 2019; Zhu and Dittrich, 2016; Chu et al., 2015). These reviews have focused on various aspects of MICP, ranging from fundamental processes, influencing factors, raw materials, and multi-scale/multi-disciplinary applications in various fields. In this review paper, the state of the art of MICP and more broadly bio-mediated geotechnics are reviewed based primarily on publications from the past five years. In particular, the following aspects are reviewed to add to the recently published review papers in this field. The current research frontlines, their challenges and future directions are also discussed, as follows:

(1) A comparison between bio-stimulation and bio-augmentation in MICP application.
(2) Some innovative raw materials and additives for MICP.
(3) Emerging tools and testing methodologies for characterizing MICP at multi-scale.
(4) Applications in emerging and/or unconventional geotechnical fields.

1.2 MICP Processes

MICP can be achieved through different pathways, both autotrophic and heterotrophic, such as urea hydrolysis, sulfate reduction, and denitrification. This section will provide a critical review on both popular (i.e., urea hydrolysis) and alternative MICP processes.

1.2.1 Ureolysis: bio-augmentation vs. bio-stimulation

Since MICP was firstly introduced into geotechnical engineering, most studies have focused on ureolysis (Eq. (1-1)) because of its simplicity and high efficiency. Ureolytic bacteria can hydrolyze urea into carbon dioxide (CO_2) and ammonia (NH_3) due to the presence of microbially produced urease, where the hydrolysis rate can be 10^{14} times higher than the natural degradation reaction without urease (Estiu and Merz 2004). The production of hydroxide ions (OH^-) due to the dissolution of ammonia in the water increases the local pH value. Meanwhile, the alkaline solution environment can increase the solubility of aqueous CO_3^{2-}. The bacterial cell walls are usually negatively charged and hence attract calcium ions in the solution, and thus can be used as a suitable nuclear site for crystallization. While most researchers inject known ureolytic bacteria cultivated in the laboratory to complete bio-cementation (i.e. bio-augmentation), enriching indigenous ureolytic bacteria to achieve MICP (i.e. bio-stimulation) is an alternative approach that can potentially reduce complexity, costs, and environmental risks. The comparative study between the bio-augmented and bio-stimulated MICP for soil stabilization (as illustrated in **Fig. 1-1**) has become one of the frontlines of MICP research.

$$(NH_2)_2CO_{(aq)} + H_2O \rightarrow 2NH_{4\,(aq)}^{+} + CO_{3\ (aq)}^{2-} \tag{1-1}$$

Bio-augmentation is an approach where the exogenous bacteria cultured in the laboratory are added into the soil (Mujah et al., 2019; Xiao et al., 2019a; Jain and Arnepalli, 2019). In contrast, the bio-stimulation approach modifies the local environment by injecting nutrient media to enrich indigenous ureolytic bacteria capable of continuously producing a large quantity of urease to generate bio-cementation. There are two ways to achieve bio-stimulation: ex-situ and in-situ. Ex-situ bio-stimulation needs to isolate indigenous bacteria from soil and then performs isolation and purification to obtain pure, enriched ureolytic bacterial strains. The bacteria are finally reinjected into the soil to trigger MICP. In-situ bio-stimulation, instead, can avoid the above-mentioned complicated and lengthy laboratory processes, and simply involves directly injecting selective enrichment media into the soil to stimulate the growth of native ureolytic bacteria and thus generate bio-cementation.

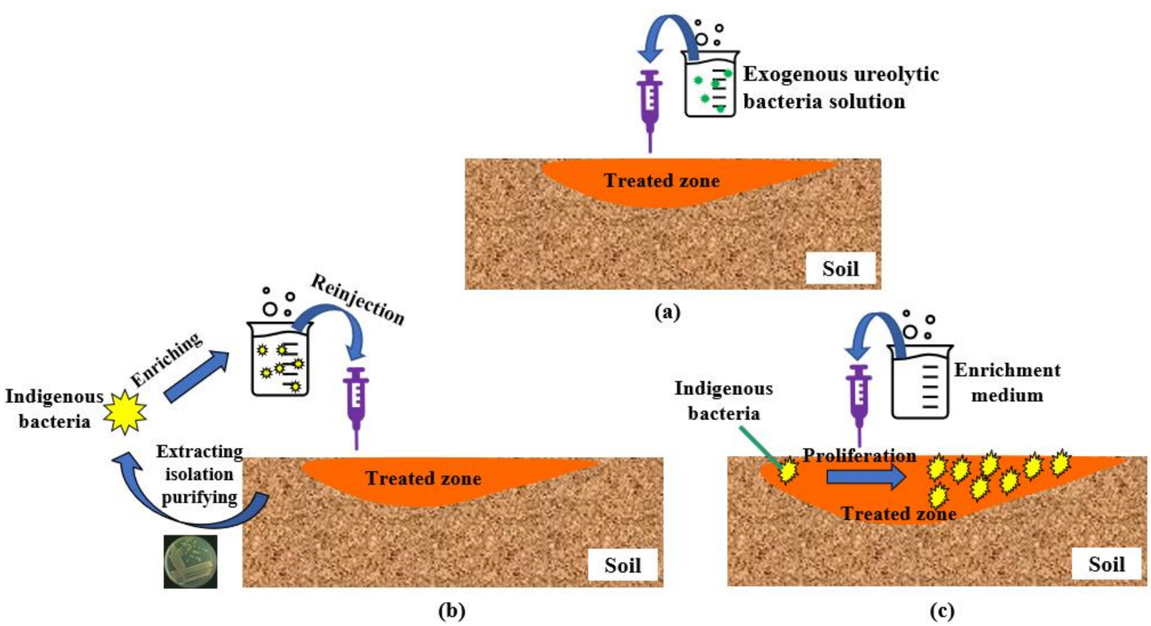

Fig. 1-1 Three pathways of MICP: (a) bio-augmentation; (b) ex-situ bio-stimulation; (c) in-situ bio-stimulation.

Both bio-augmentation and bio-stimulation (include both in-situ and ex-situ ones) have advantages and drawbacks. A comparison among the three approaches from various aspects is summarized in **Table 1-1** (Kadhim and Zheng, 2016; Hamed Khodadadi et al., 2017; Gomez et al., 2017; Terzis and Laloui et al., 2019; Choi et al., 2020; Jiang, 2020). Generally, while bio-augmentation can yield a higher reaction rate and initial ureolytic activity, the competition with other indigenous bacteria may affect the ultimate MICP efficiency (Graddy et al., 2018; Jiang, 2020). Consequently, it is required to repeatedly inject bacteria suspensions to maintain a sufficient amount and activity of urease enzyme within the soil matrix. Though bio-stimulation requires more treatment time than bio-augmentation to achieve comparable ureolytic activity or urea hydrolysis rate, it can significantly reduce costs associated with cultivating bacteria. The successful achievement of bio-stimulation is dependent on whether the ureolytic bacterial species are pre-existing in the environment or not. While bio-augmentation and bio-stimulation are equally effective with respect to improving soil engineering properties (Gomez et al., 2017; Graddy et al., 2018), it does not mean that bio-stimulation can totally replace bio-augmentation. In specific applications, such as cracks and fracture repair or sealing in porous materials (e.g. concrete) under a harsh environment that cannot support sufficient indigenous bacteria, bio-augmentation is still a preferred approach (Ghosh et al., 2005; Phillips et al., 2016; Jadhav et al., 2018; Alazhari et al., 2018; Xu and Wang, 2018; Marin et al., 2020). In addition, the bio-stimulation might not be suitable for a sterile area, such as desert and cold region. The advantages of bio-stimulation over bioaugmentation should not be overestimated.

In recent years, the diversification of urease positive bacterial species upon completion of MICP treatment, either through bio-augmentation or bio-stimulation, has gained more attention. Graddy et al. (2018) compared the diversity of *Sporosarcina*-like bacterial strains during bio-augmentation and bio-stimulation treatment in meter-scale tank experiments (shown in **Fig. 1-2**). They found that a variety of urease positive species was recovered at the end of the investigation in both cases, which was attributed to the numerous ecological niches created by the non-uniform cementation solution injections. Through either bio-augmentation or bio-stimulation, the ureolytic MICP process has been demonstrated to be an effective technique for soil improvement. There have been many studies to investigate the feasibility of the ureolysis process for MICP from the perspective of microbiological behaviors, mechanical properties, and microstructural characteristics (Graddy et al., 2018; Mujah et al., 2019; O'Donnell and Kavazanjian, 2015). However, there are still some challenges and research gaps that deserve further investigation. Below are a few examples:

(1) Ammonium removal during ureolytic MICP.

(2) Regulatory mechanisms of crystal morphology.

(3) Adaptability to complex environments.

(4) Bio-augmentation *v.s.* bio-stimulation in field application.

(5) Protocols for up-scaling field applications in diverse or varying climatic conditions.

Table 1-1 Comparison of bio-augmentation, ex-situ bio-stimulation and in-situ bio-stimulation.

Aspects	Bioaugmentation	Ex-situ biostimulation	In-situ biostimulation
Ureolytic activity	High	High	Low
Urease loss	High	High	High
Reaction rate	High	High	Low
Environmental risks	High	Medium	Low
Estimated Cost	High	Medium	Low
Required labor works	Medium	High	Low
Technical maturity	High	High	Low
Application scope	High	Low	Low

1.2.2 Denitrification

The denitrification process (Eq. (1-2)) involves multiple reactions by denitrifying bacteria. Several enzymes catalyze the reduction of nitrate (NO_3^-) to nitrogen gas (N_2). Using acetate (i.e., $C_2H_3O_2^-$) as the electron donor and nitrate as the electron acceptor, carbonate ions (CO_3^{2-}) can be generated. When free calcium ions (Ca^{2+}) are available, precipitation can be induced spontaneously (Pham et al., 2016; O'Donnell et al., 2019).

$$2.6H^+_{(aq)}+1.6NO^-_{3(aq)}+CH_3COOH^-_{(aq)}\rightarrow0.8N_{2(aq)}+2CO_{2(aq)}+2.8H_2O \quad (1\text{-}2)$$

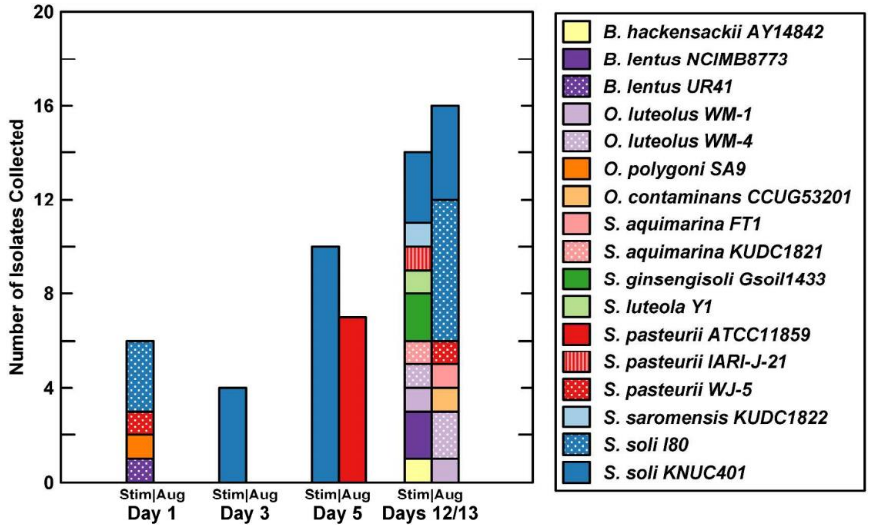

Fig. 1-2 Strain assignments and abundances of isolates collected in experimental tanks treated by bio-augmentation and bio-stimulation (Graddy et al., 2018).

In recent years, although the denitrification-induced bio-cementation process is relatively slow to form a comparable amount of bio-cementation compared with ureolysis (O'Donnell, 2016), denitrification has its own advantages. Usually, denitrifying bacteria occur in wet and anaerobic soil conditions, which has the potential to improve submerged granular soils in deeper locations by forming bio-cementation via denitrification process (Kavazanjian et al., 2015; Pham et al., 2016). Although the peak shear strength of lightly biocemented sand could not be greatly improved, its stiffness and dilatancy, especially under low strain, could still be enhanced significantly (Pham et al., 2016). The other major advantage of the denitrification process for bio-cementation is that there is no ammonia production. On the other hand, the N_2 generated in this process can desaturate sand to increase liquefaction resistance. The partially saturated conditions due to the presence of N_2 gas bubbles can dampen pore pressure buildup and thus increase the undrained shear strength (He et al., 2013; O'Donnell et al., 2017; Hall et al., 2018). However, the potential negative effects of the generated gas bubbles on soil stabilization and the flow rate of various injected solutions should be considered carefully.

To develop denitrification-induced bio-cementation as a feasible and implementable soil improvement technique, further studies are needed on the following aspects:

(1) Increasing bio-cementation amounts and reaction rates.

(2) Developing appropriate substrate recipes to prevent the generation of toxic intermediate nitrogen compounds (i.e., NO_2^-).

(3) Expanding applications under aerobic condition (i.e., surface soil).

(4) Investigating the effects of regionally variable factors such as temperature, physical and chemical properties of local soils on the ultimate success of denitrification.

(5) Enhancing the durability of bio-cementation by denitrification.

1.2.3 Sulfate reduction

Sulfate reduction induced bio-cementation under anoxic conditions is another alternative MICP approach. Sulfate-reducing bacteria have played an important role throughout earth's 4.6 billion years history. They are predominantly anaerobic heterotrophs without oxygen involved in their metabolic activity (Baumgartner et al., 2006). Sulfate-reducing bacteria are able to reduce sulfates to sulfides while oxidizing organic carbon (Eq. 1-3):

$$SO_{4\,(aq)}^{2-}+2[CH_2O]_{(aq)}+OH^-_{(aq)}\rightarrow HS^-_{(aq)}+2HCO^-_{3\,(aq)}+H_2O \qquad (1\text{-}3)$$

When sufficient calcium is present in the solution, the increased alkalinity will move the equilibrium towards calcium carbonate precipitation. However, some obvious disadvantages including the generation of toxic and combustible hydrogen sulphode (H_2S) gas may threaten the environment and human health (Gu et al., 2018). Therefore, challenges such as the treatment of toxic byproducts should be resolved prior to its application in soil improvement. While sulfate-reducing bacteria are not preferred for soil improvement, they can bind with heavy metals, making sulfate reduction a promising method for the immobilization of heavy metal contaminants (Hwang and Jho, 2018; Le Pape et al., 2017).

1.2.4 Iron reduction

Iron reduction (Eq. (1-4)), which induces ankerite and other mixed mineral precipitation, has also been investigated by some researchers as a potential bio-cementation process (Weaver et al., 2011). The redox reactions involved have been shown to be dominant in the anaerobic subsurface environment (Lovely, 1991). While iron-based precipitation is much cheaper, it is less effective, for example, in reducing the permeability of the soil, than calcium-based precipitation (i.e., by urea hydrolysis process) (Ivanov et al., 2010). Zeng and Tice, (2014) found that the mineral composition was unstable, was easily affected by the concentration of other ions (e.g., Mg^{2+} and Ca^{2+}), and that cementation commonly occurred as the co-precipitation of calcite, siderite, and dolomite. The studies related to iron reduction are somewhat limited currently, suggesting that iron reduction may not be a viable solution to induce bio-cementation for soil improvement.

$$4Fe(OH)_3+[CH_2O]_{(aq)}+7H^+_{(aq)}\rightarrow 4Fe^{2+}_{(aq)}+HCO^-_{3(aq)}+10H_2O \tag{1-4}$$

1.3 Materials for MICP

Materials involved in the MICP process include bacteria strains, nutrients, cementation solutions, auxiliary additives, and soils. In this section, the recent developments in the research into materials involved in MICP, in particular, the ureolysis process are reviewed and discussed.

1.3.1 Bacterial Strains

The efficiency of bio-cementation is highly associated with the performance of either the injected exogenous or the enriched native ureolytic bacteria. A widely-accepted assumption of the $CaCO_3$ precipitation process during MICP is that bacterial cells can serve as the nucleation sites for $CaCO_3$ due to the negative charge on the cell walls (EI

Mountassir et al., 2014). Different bacteria have their own preferred environments, and even a slight variation of external conditions may affect their growth. Generally, ureolytic bacteria used for MICP should (1) have a reliable and constantly high enzymatic activity and (2) be harmless to humans and pose a low risk to the local ecosystem.

For the ureolysis process, various ureolytic bacterial strains isolated from the soil environment have been identified and found to be effective for MICP. These include, but are not limited to, *Bacillus* strains, *Sporosarcina* strains, *Shewanella* strains, *Pararhodobacter* strains, and *Lysinibacillus* strains. Some most representative species include *Sporosarcina pasteurii* (Gomez et al., 2015; Kannan et al., 2020), *Bacillus sphaericus* (Saffari et al., 2017; Mujah et al., 2016), *Pararhodobacter sp.* (Amarakoon and Kawasaki, 2017), and *Bacillus megaterium* (Jiang et al., 2016). The bacterial strains could affect MICP efficiency in terms of (1) ureolysis rate (i.e., urease activity); and (2) nucleation and crystallization, which will be reviewed in the next two paragraphs.

On the one hand, different bacterial strains may display very different ureolysis rate. To assess the ureolysis capability of a specific bacterial strain, urease activity is usually used as the key indicator. The urease activity values that wereattained by various bacteria in previous studies are summarized in **Table 1-2**. It should be noted that many factors may affect urease activity, including bacterial type, biomass density, and culturing medium conditions (e.g., concentration of substrate (urea) and byproduct (NH_4^+), pH, and oxygen availability) (Martin et al., 2012; Bachmeier et al., 2002). From **Table 1-2**, it is clear that the microorganism type can make a significant difference to urease activity. Specifically, *Sporosarcina pasteurii* in most previous studies show a higher urease activity than other types of ureolytic bacteria, and higher biomass density results in higher urease activity.

On the other hand, bacterial cells can promote nucleation and crystallization by creating supersaturated alkaline environments and secreting extracellular polymeric materials (i.e. exopolysaccarides (EPS) and capsular polysaccharides (CPS) (Sundaram and Thakur 2018; Ercole et al., 2012). The extracellular polymeric materials produced by microorganisms might be tightly bound to the cell, loosely adherent to cells, or existing in the form of free dissolved matter (Ercole et al., 2012), which can trap calcium ions at a given pH, control crystallization, influence the polymorphic development of $CaCO_3$ crystals (Dupraz et al., 2009; Bains et al., 2015; Yin et al., 2020). For example, in recent years, Szcześ et al. (2016)

investigated *Rhodococcus opacus* cultures and found that the crystal size and polymorph could be controlled by EPS. EPS could stabilize vaterite and this effect is stronger at basic pH. Azulay et al. (2018) indicated that the EPS generated by *Bacillus subtilis* strain affected the crystal's nucleation, and the proteins (TasA and TapA) induced the aggregation of crystallites.

Table 1-2 Urease activity of representative ureolytic bacteria.

Bacteria	Urease activity	Bacterial concentration	Reference
Sporosarcina pasteurii	1.8 mM urea/min	0.8-1.2 (OD_{600})	Xiao et al. (2019b)
Sporosarcina pasteurii	1.4-2.0 mM urea/min	10^7 cells/mL	Xiao et al. (2019a)
Sporosarcina pasteurii	4-5 mM urea/min	N/A	Hoang et al. (2019)
Sporosarcina pasteurii	2.08 mM urea/min/OD_{600}	0.22 (OD_{600})	Jiang et al. (2017)
Lysinibacillus sphaericus	0.4 μM urea/72h	250 mL sporulating bacterial spore solution	Kang et al. (2015)
Bacillus sphaericus	10 μM urea/min	2-2.5 (OD_{600})	Mujah et al. (2016)
Bacillus sp.	20 ± 1 μM urea/min	4.2 ± 0.2 (OD_{600})	Cheng et al. (2019)
Bacillus sp.	15 μM urea/min	3-3.15 (OD_{600})	Hao et al. (2018)

Most of the currently identified ureolytic bacteria are aerobes, and hence are used for MICP under oxic conditions. The aerobic ureolytic bacteria target the surface soil where the oxygen is sufficient for the continuous expression of enzymatic activity. For instance, although the most widely used *Sporosarcina pasteurii* is a facultative anaerobe, it is unable to synthesize urease anaerobically. However, some ureolytic bacterial strains are reportedly able to survive and induce ureolysis under anoxic conditions. There is a controversy regarding the efficiency of ureolysis process that can be achieved in the absence of oxygen. For instance, one the one hand, Jiang et al. (2016) and Martin et al. (2012) observed considerable ureolytic activity of *B. megaterium* (ATCC 14581) and *Sporosarcina pasteurii* under anoxic conditions, which was attributed to the aerobic preculture, and the urease already present in the cells. On the other hand, Mortensen et al. (2011) observed extensive ureolytic activity of *Sporosarcina pasteurii* under anoxic conditions, suggesting that the anoxic environment did not inhibit urease activity. Mitchell et al. (2019) investigated the kinetics of ureolysis and $CaCO_3$ precipitation of *Sporosarcina pasteurii* in the absence of oxygen. The results indicated that *Sporosarcina pasteurii* was capable of ureolysis in anaerobic environments, however, sustained growth over time in the absence of oxygen was not possible. Also, oxygen-free environments did not substantially affect the initial rate of ureolysis or $CaCO_3$ precipitation. The microorganisms used for other MICP processes including denitrification, sulfate reduction and iron reduction, are ubiquitous in the anoxic subsurface environment. Thus, bio-stimulation of indigenous bacteria is preferred in these circumstances.

Finally, there are still research gaps in terms of the role of ureolytic bacterial strains during the MICP process. For example, it was observed that the number of injected bacteria was diminishing with time and the diversity of bacteria was reduced at the end of bio-augmented MICP treatment (Graddy et al., 2018). In addition, the function of EPS to facilitate bio-cementation is still unclear for most ureolytic strains. Therefore, further research is needed on the following aspects:

(1) Maintaining the dominance of injected ureolytic bacteria during bio-augmented MICP.

(2) Understanding the microbiological and biochemical interactions between the exogenous and native bacterial species during the MICP process.

(3) Illustrating the function of EPS to facilitate bio-cementation during the MICP process.

1.3.2 Bacterial culture and enrichment media

Nutrients as the energy sources are crucial to the MICP process, in which bacteria utilize nutrients to sustain their metabolic and enzymatic activity. For the bio-augmentation approach, bacteria are cultivated using specific culture media in the laboratory to the desired concentration (i.e., bacterial culture medium). **Table 1-3** shows some representative culture media for ureolytic bacteria that are found to be able to induce high urease activity with the presence of enzyme-substrate (i.e., urea or ammonium) (Jiang and Soga, 2017; Zamani et al., 2018; Liu et al., 2020a), suggesting that urea is not necessarily the only substrate that can induce high urease activity, ammonium-rich media also have a comparable capability to produce similar urease activity.

For bio-stimulation, the enrichment media play a similar role to the culture media for bio-augmentation, which enriches the indigenous ureolytic bacteria and sustains the enzymatic activity (Wang et al., 2020a). Unlike bio-augmentation, the indigenous bacteria cannot reach the desired ureolytic rate immediately after injection. The primary principle for developing an effective enrichment medium is (1) to maximize the urease activity, and (2) to minimize the enrichment time. Various carbon © sources including molasses, glucose, and sodium acetate have been used to stimulate native heterotrophic ureolytic bacteria (Amini Kiasari et al., 2018), and urea is commonly added as the nitrogen source (Nassar et al., 2018). However, recent studies have shown that using carbohydrates as the only main C source could not induce sufficient urase activity. For instance, Amini Kiasari et al. (2019) investigated the effects of various C and nitrate sources, including yeast extract, sugarcane molasses, sodium acetate, and glucose, on enriching the indigenous ureolytic bacteria for MICP. The results showed that the protein-based media such as yeast extract could yield a higher microbial urease activity, which was consistent with the findings of Cheng and Cord-Ruwisch (2013). Yeast extract is a complex nutrient that can provide vitamins, minerals, nucleic acid, amino acids, as well as growth factors that can increase the growth rate of microorganisms (Gat et al., 2016).

Table 1-3 Representative media for the culture of *Sporosarcina pasteurii*.

Media	Batch condition	pH	Main ingredients
NH_4^+-YE medium	Aerobic	9	20 g/L Yeast extract, 10 g/L $(NH_4)_2SO_4$
Urea-YE medium	Aerobic	7.5	20 g/L Yeast extract, 170 mM urea
NH_4^+-YE medium	Aerobic	N/A	20 g/L Yeast extract, 10 g/L$(NH_4)_2SO_4$, 0.5 M urea

While appropriately designed sterilized culture or enrichment media have been adopted to grow ureolytic bacteria, non-sterilized conditions have also been found to be feasible. Yang et al. (2020b) enriched urease-producing bacteria from activated sludge under non-sterilized conditions for MICP. Although the urease activity of the non-sterile enriched culture started to decrease after 3 days from the initial value of 15 U/ml to 7 U/ml at 10 days, it was still adequate for MICP for bio-cementation. The non-sterile enrichment method can reduce the total energy consumption and production cost by 30% (Yang et al., 2020b). A similar non-sterile method was also performed by Cheng and Cord-Ruwisch (2013). Sharaky et al. (2018) compared the bio-cementation content precipitated in sand achieved by using sterilized and non-sterilized media. It was observed that the amount of precipitation of $CaCO_3$ treated by the non-sterilized media method was equal to that of the sterilized media method.

Finally, for future large-scale field applications, the effectiveness of the culture and enrichment and the cost and environmental risks should be considered carefully. Some alternative inexpensive industrial substrates such as corn steep liquor, vegemite, torula, lactose mother liquor, and food-grade yeast extract that can produce a considerable urease activity have been reported to replace the expensive laboratory-grade yeast extract (Achal et al., 2009; Chaparro-Acuña et al., 2018; Joshi et al., 2018; Omoregie et al., 2019; Babakhani et al., 2020). Moreover, some industrial wastes can also be used as the nutrients such as chicken manure effluent (Yoosathaporn et al., 2016). In these studies, the urease activity induced by the traditional lab-grade nutrients did not show a significant superiority over the industrial substrates. For instance, urease activity in "NB (nutrient broth)-urea medium" and "YE (yeast extract)-urea medium" was only 0.17- and 0.04-fold higher than those in LML (lactose mother liquor)-urea medium (Achal et al., 2009).

The current research gap relating to the bacterial culture and enrichment media lies in reducing the dosage, cost, and environmental risk as much as possible to achieve the requirements for MICP.

1.3.3 Cementation solution

For the bio-augmented ureolytic MICP process, most researchers commonly adopt a two-stage treatment strategy, in which cementation solution is injected following the cultivated bacteria suspension. Urea-calcium composite chemicals are usually adopted as the main ingredients of cementation solutions, sometimes with trace nutrients. For the urea source, researchers have not only used the traditional pure chemical, but have tried natural resources such as pig and human urine (Chen et al., 2019; Lambert and Randall, 2019). For the calcium (Ca) source, common chemicals such as calcium chloride ($CaCl_2$), calcium acetate ($Ca(CH_3COO)_2$), and calcium nitrate ($Ca(NO_3)_2$) have been used. These Ca sources are chemically stable and relatively inexpensive for large-scale applications. Among them, $CaCl_2$ is the most common. However, it is worth noting that, to obtain sufficient cementation content, the amount of $CaCl_2$ required is commonly excessive and may be harmful to the environment. Also, to further minimize the environmental risk, alternative Ca sources are being developed. Choi et al., (2016) compared $CaCl_2$ and Ca from eggshells dissolved by culinary vinegar. The results showed that the Ca produced from eggshells was as good as using $CaCl_2$. Moreover, Liu et al. (2018) utilized the soluble Ca dissolved from calcareous sand by acetic acid to improve the strength and permeability of MICP-treated calcareous sand. Choi et al. (2017) and Casas et al. (2019) released and reused Ca from quarry limestone and Ca-rich silicate quarry, respectively, to apply to MICP.

Previous studies have suggested that the cementation solution plays a role in forming variable morphologies and sizes of $CaCO_3$crystals. It has been reported that the type of cementation solution (i.e. Ca^{2+} source) and the time interval between cementation solution injections could largely affect the mineralogy and morphology of $CaCO_3$. The crystal types of $CaCO_3$ through MICP process usually include calcite, vaterite and aragonite, among which the calcite is the most common and stable. Zhang et al. (2014) found that the samples treated with $CaCl_2$ and $Ca(NO_3)_2$ were more likely to form calcite, whereas the samples treated with $Ca(CH_3COO)_2$ were composed of 88% aragonite and 12% calcite. Burdalski and Gomez (2020) investigated the effect of different Ca^{2+} concentrations of cementation solution on the morphology of $CaCO_3$. When the concentration was 500 mM, the sample showed a dominant calcite phase (96%) with negligible amounts (around 2%) of vaterite and aragonite. If the concentration increased to 1250 mM, calcite was still the dominant phase (75%), and the quantities of vaterite significantly increased to 23%. Wang et al. (2019b) conducted a microchip experiment and found that the size of $CaCO_3$ crystals was highly dependent on the time interval between cementation solution injections. The average size of $CaCO_3$ crystals was considerably larger when the injection interval was 23-25 hours than 3-5 hours.

In short, cementation solution is critical to achieving satisfactory MICP treatment. However, the potential secondary pollution from injecting large amounts of solution into soil remains unexplored. In addition, further reducing the cost by selecting alternative Ca and urea sources is also necessary. Future work is needed to further reduce the cost and environmental risks associated with the cementation solution.

1.3.4 Auxiliary additives

In order to improve bacterial growth, urease activity and bio-cementation content, researchers have developed several auxiliary additives to supplement the culture/enrichment media and cementation solution, or to add directly into the soil matrix.

For the auxiliary additives added into the culture/enrichment media, apart from the common necessary elements (C, N, P, H, O), nickel dichloride ($NiCl_2$) has been used by many researchers, usually in very small amounts (Gat et al., 2016; Amini Kiasari et al., 2018, 2019; Fang et al., 2020; Xu et al., 2020). MICP is highly associated with the metabolic and enzymatic activity of the specific ureolytic bacteria. As a key part of the urease enzyme structure, the nickel ion has been shown to be an essential trace element for maintaining sufficiently high ureolytic activity of urease-producing bacteria (Svane et al. 2020). In addition, Shashank et al. (2018) investigated the effect of buffer solution added with the bacterial suspension on regulating the ureolysis procedure. Adding a buffer solution was found to prevent the instantaneous increase of pH which might lead to a rapid clogging near the injection port during the MICP process.

For the auxiliary additives in the cementation solution, Xu et al. (2020) proposed magnesium ions to modify carbonate crystal polymorphs. The results showed that the incorporation of 0.01-0.5 M magnesium ions with the cementation solution composed of $Ca(CH_3COO)_2$ and urea could promote the formation of acicular aragonite and inhibit the growth of rhombohedral calcite, which resulted in a 40%-200% increase in the unconfined compression strength. Nawarathna et al. (2018) used various concentrations of poly-Lys ranging from 0 to 50 mM as the additive to the cementation solution ($CaCl_2$+urea). The findings indicated that the addition of poly-Lys created stronger cemented sand specimens than those obtained by the conventional method without poly-Lys. Wang et al. (2018a) modified the cementation solution by adding polyvinyl alcohol (PVA) to successfully improve the erodibility of the treated sand.

For the auxiliary additives directly added into the soil matrix, randomly distributed fibers have been used to increase the ductility of sandy soil and to prevent the loss of post-peak strength. Different types of fibers including natural plant bassed and synthetic polymers have been used (Li et al., 2016; Choi et al., 2016; Zhao et al., 2020; Imran et al., 2020). The optimum fiber content was usually between 0.2%-0.3% by weight (Qiu et al., 2019; Li et al., 2016; Fang et al., 2020). Li et al. (2016) used homopolymer polypropylene multifilament fibers as the additive in sand and found the unconfined compression strength gradually increased when the fiber content was between 0.2% and 0.3%, which is the optimum fiber content. Fang et al. (2020) added modified-polyester fibers to improve the engineering properties of MICP-treated calcareous sand. The results showed that the permeability reduced by 2-3 orders of magnitude and UCS increased from 2.78 MPa to 21.65 MPa. Besides randomly distributed fibers, researchers have also added clay particles as an auxiliary additive. Won et al. (2020) added kaolinite into sand as the extra nucleation sites for the calcite precipitation. The results indicated that the kaolinite particles could function as nucleation sites and facilitate the heterogeneous nucleation of calcite. Ma et al. (2020) introduced bentonite into coarse sand, and found that the unconfined compressive strength (UCS) was substantially improved with an optimal bentonite concentration of 20g/L. Higher bentonite concentrations (40 g/L and 80 g/L in this study) might have a negative effect on UCS.

1.3.5 Soil

MICP has been widely investigated for its applicability in different types of soils. **Table 1-4** shows a few examples reported in the past five years. Typically, the size of bacteria for MICP is between 0.5 and 3 μm, making it suitable for a broad range of soil types.

For granular soils, MICP has already been intensively studied to modify the physical (density, gradation, porosity, saturation), mechanical properties (strength, stiffness, shear behavior, compressibility) and hydraulic properties through bio-cementation. The relatively larger pore space in coarse-grained soils allows microbes to move freely within the soil matrix. Thus, it is much easier to conduct MICP treatment in granular soils. It is also necessary to consider the effect of relative density, one of the most important parameters for coarse-grained soils, on strength improvement. The biggest difference between bio-cemented and chemically cemented soil was that soil structure remains intact by using MICP, thus the initial packing of soil governs the formation of cementation within the soil matrix (Terzis and Laloui, 2019). Rowshanbakht et al. (2016) found that increasing the initial relative density resulted in the reduction in cementation content, which wasdue to the decreasing pore volumes for the nucleation sites of calciteand the decreasing amounts of microbes and nutrients that could be absorbed.

In recent years, more and more studies have focused on MICP applications in soils that were traditionally regarded as unsuitable for MICP treatment (i.e. clay soil and loess). For clay soils, percolation may be difficult due to their low permeability and surface charge on the particles. Thus, premixing the bacterial solution with clay soil is one of the primary sample preparation methods (Kannan et al., 2020). Cardoso et al. (2018) suggested that MICP application in clay soils is much more challenging than in sand due to the complex chemical interactions between clay minerals and the injected solutions. For example, Sharma and Ramkrishnan (2016) conducted bio-augmented MICP in clay. A noticeable improvement (1.5–2.9 times higher than the untreated samples) in the unconfined compressive strength was observed. Saffari et al. (2017) found that MICP-treatment could increase the cohesion, friction angle and shear strength in low plasticity clay. For collapsed loess, Atashgahi et al. (2020) reported that MICP could reduce the collapse potential between 24 and 54.8% by enhancing particle-particle contacts between the soil particles. Sun et al. (2020) suggested that the collapsibility of loess soils was significantly decreased at an optimum cementation solution concentration of 0.75-1 M.

Soil is a rather complex mixture consisting of organic matter, minerals, gases, liquids, and organisms (i.e., solid, air, liquid, and organisms). The effects of soil environment on bacterial growth and precipitation formation remain unclear. In future research, it is important to assess whether environmental conditions including pH, oxygen availability, temperature, and humidity within the soil matrix can support the activity of injected microbes before application. Moreover, the sustainability and durability of induced precipitation in various soil environments after MICP treatment also needs to be examined.

1.4 Characterization of MICP processes

As a multidisciplinary research field in the intersection of geotechnics, microbiology, biochemistry, environmental engineering, and material science, the MICP process needs to be characterized using observational and experimental tools from multi-disciplines and at multi-scales (**Fig. 1-3**). This section will review the characterization techniques for the MICP process at nano, micro, meso, element, pilot, and field scales.

Table 1-4 MICP in different types of soils in laboratory studies.

Soil type	Problems	Improvement mechanism	References
Sandy soil	Very loose; low strength and stiffness	Strengthen particle bonds via bio-cementation	Whitaker et al. (2018); Cui et al. (2017)
Sandy soil	Low cohesion; low wind or water erosion resistance	Stabilize the surface layer of soil via bio-cementation	Maleki et al. (2016); Shanahan and Montoya (2016); Wang et al. (2018b); Fattahi et al. (2020)
Mixed soil (gravel-sand/sand-clay)	Internal erosion as the core Materials in embankment dams and levees	Mitigate internal erosion and improve hydraulic condition via bio-cementation and bio-clogging	Jiang and Soga (2017, 2019); Jiang et al. (2017)
Liquefiable sand	Loose; saturated; insufficient cyclic shear strength	Reduce the degree of saturation via generating biogas (denitrification); Solidify and densify soil via calcite precipitation (ureolysis)	Hall et al. (2018)
Clayed soil	Formation of desiccation cracks lead to an increase in hydraulic conductivity	Remediate the desiccation cracks via bio-cementation	Liu et al. (2020b)
Marine clay	Low bearing capacity; high natural water content (close to the liquid limit); be susceptible to large consolidation settlements	Reduce liquid limit and increase strength via bio-cementation; increase strength via bioencapsulation	Kannan et al. (2020); Li et al. (2016); Ivanov et al. (2015); Li et al. (2016)
Loess soil	Potential collapsibility; insignificant adhesion; very unstable	Improve the strength and hydraulic features via bio-cementation and bio-clogging	Atashgahi et al. (2020)
Heavy metal contaminated soil	High environmental and ecological risks	Coprecipitate and then remove the heavy metals with calcite	Cheng and Shahin 2017; Zhu et al. 2016 ; Zhao et al. 2017; Jalilvand et al. 2020

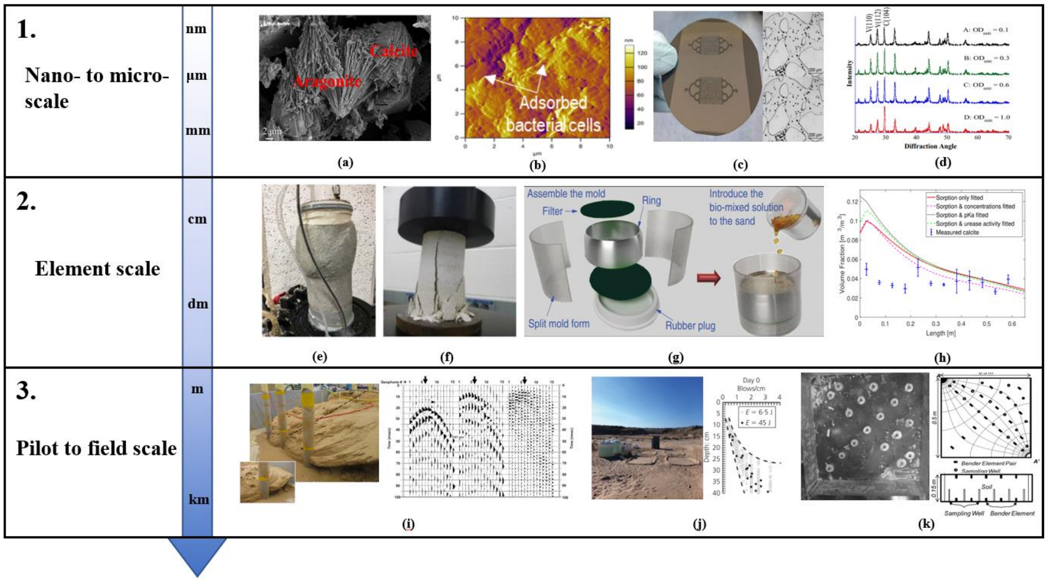

Fig. 1-3 The characterization of MICP at multi-scales: (a) SEM images of precipitation (Xu et al., 2020); (b) AFM peak-force error images of substrates with bacteria cell adhesion (Shashank et al., 2020); (c) the particle-scale behavior of calcite precipitation from a microfluidic chip (Wang et al., 2019a); (d) the XRD patterns of $CaCO_3$ crystals (Wen et al., 2019); (e) shear response of biocemented sand by undrained triaxial test (Nafisi et al., 2019); (f) the unconfined compress (UCS) test (Fang et al., 2020); (g) one-dimensional compression test (Xiao et al., 2020); (h) predicted volume fractions of final calcite by numerical modelling (Hommel et al., 2020); (i) seismic shear-wave data of 100 m^3 large-scale biogrouting test (van Paassen et al., 2010); (j) dynamic cone penetration (DCP) data of field-scale test measuring 2.4 m×4.9 m on loose sand (Gomez et al., 2015); (k) Five-Spot treatment model (Dejong et al., 2014).

1.4.1 Nano-scale

Nano-scale material characterization techniques are used to show the interactions between bacteria and substrate (soil particles) during the MICP process, which can illustrate fundamental mechanisms between microorganisms and their nucleation surface. Atomic force microscopy (AFM) developed in 1986 is an ideal tool which can be applied to acquire the surface topography and texture information with demonstrated resolution on the nanometer scale. Shashank et al. (2020) used AFM to investigate the capability of the biosorption of bacteria on the surface of soil particles. They found that the extent of bacterial adhesion on soils depends on the available hydrophobic binding sites, and bacteria could be entrapped in the pores of formed crystals based on the surface texture parameters during the MICP treatment.

1.4.2 Micro- and meso-scale

The characteristics of calcite crystals and their interactions with soil particles can affect the mechanical properties of bio-cemented soil. Various characterization micro-scale techniques including, but not limited to, scanning electron microscope (SEM) with energy-dispersive X-ray spectroscopy (EDS), X-ray diffraction (XRD), Fourier-transform infrared spectroscopy (FTIR), thermogravimetric analysis (TGA), X-ray CT, and mercury intrusion porosimetry test (MIP), and meso-scale techniques such as microfluidic chip, have been used to provide insight into the evaluation of the crystal shape, size, content, distribution pattern, structure, contact and surface fractures of bio-cemented soils.

The size of the precipitated crystals can be detected clearly using SEM images. For instance, Cheng et al. (2017) observed that different size and distribution patterns were observed by comparing SEM images at different concentrations of cementation solution. Crystals were more likely to be distributed randomly all over the sand grains for the treatment with the low concentration of cementation solution (0.25 M), while the crystals were inclined to accumulate in local areas in the high cementation solution ($\geq$ 0.5M). Choi et al. (2020) and Fang et al. (2020) suggested that bonding at the particle-particle contacts as a bridge and coating on the particle surface are the two primary functions of precipitated crystals within bio-cemented soil. It is found that coating and bridging as the actual distribution pattern usually coexist after MICP treatment under unsaturated conditions (as shown in **Fig. 1-4**).

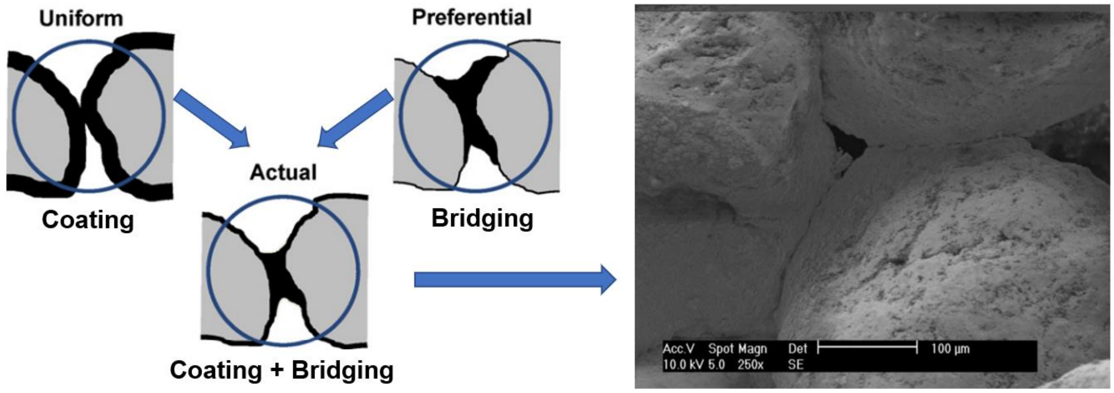

(a) (b)

Fig. 1-4 The precipitated crystals distribution pattern within pore space of soil matrix (modified after Dejong et al., 2010 and Cheng et al., 2013).

The variation in porosity of MICP treated soils can be determined by conducting MIP test and X-ray CT scanning. Amarakoon and Kawasaki (2017) found that the porosity of treated sand samples decreased with depth by analyzing the X-CT images at the top, middle and bottom parts. Gao et al. (2019) conducted MIP test to identify the changes in the pore size distribution of bio-cemented quartz sand. The results also showed that the porosity of the treated sample was significantly reduced from 0.428 to 0.28–0.33 in the surface layer by forming a hard crust and 0.37–0.39 below the crust.

By using EDS, XRD, and FTIR, the crystal morphology can be determined. The rhombohedral, hexahedral, orthorhombic, acicular, spherical, and ellipsoidal crystals commonly appear in the form of calcite, aragonite and vaterite under different environmental conditions (temperature, cementation solution, pH, etc.). For instance, by analyzing the data from XRD and EDS, Xu et al. (2020) found that cementation solution types had an effect on the crystal morphology. The main crystal form was aragonite when $Ca(CH_3COO)_2$ was used as the Ca source. After adding 0.5 M magnesium ions to the cementation solution, a small amount of calcite converts into low-magnesium calcite, however, the growth of aragonite is not inhibited. Wen et al. (2020) conducted XRD tests and found that the concentration of bacteria or urease did not have an apparent effect on the morphology of $CaCO_3$ crystals. Moreover, results from FTIR suggested that vaterite was the major form of $CaCO_3$ crystals within 72 h with calcite increasing over time during the MICP process.

At the meso-scale, Wang et al. (2017; 2019a; 2019b) developed a microfluidic chip, a 2-D representation of porous media, to observe the MICP process and the behavior of bacteria and growth of precipitated crystals under saturated condition (as shown in Fig. 3(c)). It contains an inlet, upstream flow distribution channels, a porous medium, downstream flow distribution channels, and an outlet (Wang et al., 2019a). A computer-controlled microscope is used for image collection. The observations showed that bacteria were distributed evenly after the bacterial suspension injection and $CaCO_3$crystallized at narrow pore throats or open-pore bodies. The precipitated $CaCO_3$ crystal transformed from irregularly shaped amorphous $CaCO_3$ precipitates to spherical vaterite and then to rhombohedral calcite (Wang et al., 2019b). Marzin et al. (2020) also used a microfluidic cell to investigate the influence of the injection time and the ionic strength on the adhesion rate of *Sporosarcina pasteurii* bacteria on sandstone grains and crystals formation during MICP. The results indicated a rise of adhesion rate from 0.005 per minute to 0.03 per minute with an increase of NaCl concentration in solution from 3 g/L to 20 g/L.

1.4.3 Element-scale

A series of element-scale characterization techniques have been applied in the laboratory to assess the improvement of engineering properties including, but not limited to, permeability, unconfined compressive strength, shear behavior, particle breakage and compressibility behavior, cementation content, thermal conductivity, and durability.

The formed bio-cementation, which serves as a clogging material between particle contacts, can reduce the size of pore throats and resist water permeation. In the laboratory, both constant head and falling head tests can be applied to a variety of bio-cemented soils. Bio-grouting using bio-slurry containing preformed urease active calcium carbonate crystals is an emerging technique for soil improvement by reducing the coefficient of permeability. Various types of soils have been studied, which widens the practical applications in terms of the bio-grouting technique in different soil conditions. For example, Peng et al. (2020) reported that the coefficient of permeability of MICP-treated fractured rock was reduced to 3-5×10^{-5} m/s by four orders of magnitude using bio-grouting method. Lian et al. (2019) conducted bio-grouting on hydraulic fill fine sands for reclamation. The permeability coefficient was reduced by approximately three orders of magnitude using the constant head approach. Wu and Chu (2020) used bio-grouting to treat granite aggregates and found a reduction of permeability in both saturated and unsaturated cases. A larger reduction was observed in the unsaturated condition. Pan et al. (2020) successfully applied bio-grouting on sands with grain sizes ranging from 0.30 to 2.36 mm to significantly reduce the coefficient of permeability. Compared with the conventional chemically treated soil, the reduction in permeability via the MICP process is much less. The minor reduction in permeability can, on the one hand, create a good drainage passage which ensures the unhindered penetration of bacterial solution (Chu et al., 2014), and on the other hand, can avoid the development of excess pore water pressure during loading (Mujah et al., 2017).

The unconfined compression test is another popular characterization method at element-scale, which could assess the strength of bio-cemented soils (Rowshanbakht et al., 2016; Terzis et al., 2018; Amini Kiasari et al., 2019; Hoang et al., 2019). Existing studies have primarily focused on the effect of cementation level on unconfined compression strength (UCS), and an empirical correlation between UCS and cementation content was proposed. Specifically, the UCS was found to be positively correlated with the cementation content. The UCS values could fluctuate between 50-100 kPa and 10 MPa with the cementation content varying substantially from less than 2% to 25-30% (Amarakoon and Kawasaki, 2017). Usually, the UCS values were reported when the $CaCO_3$content is over 3%, at which the bio-cemented samples could maintain their integrity and stand alone. However, Terzis and Laloui, (2019) pointed out that the lower cementation content (<2%) could still offer the desired improvement if considering the role of confinement. Choi et al. (2020) gave an empirical correlation between UCS and cementation content (CC, in percentage) based on the compiled data as follows, where α_{UCS}, β_{UCS} are two empirical fitting parameters.

$$UCS\ [\text{kPa}] = \alpha_{UCS} \cdot CC^{\beta_{UCS}},\ \text{when } CC < 30\% \tag{1-5}$$

Researchers have conducted various types of tests to evaluate the shear strength of bio-cemented soils, among which the triaxial compression test and direct shear test are the most common methods. More attention has been placed on the stress-strain relationship and stress-dilatancy behavior of bio-cemented samples. The evolution of cohesion, effective friction angle and failure envelope with the variation of cementation level was the major concerns. Generally, the results suggested that the shear strength performance improves significantly compared with uncemented soils. For instance, Cui et al. (2017) conducted triaxial undrained tests on sand. It was found that the effective cohesion and effective friction angle increased with cementation level with a linear and exponential relationship respectively. The increase in effective cohesion with cementation level has also been observed in other studies (Li, 2014; Wu et al., 2021). However, Wu et al. (2021) found that the effective friction angle did not change when the cementation content exceeded 5%. The major effect of cementation is to increase the cohesion. Thus, the effect of cementation on the friction angle of bio-cemented soils should not be overestimated. Amini Kiasari et al. (2018) performed direct shear tests on bio-cemented sand treated using the bio-stimulation approach. The results showed an increase of 190% in cohesion and 16.79% in the friction angle compared with the uncemented sand. The bonding effect enhancing the interparticle contacts is commonly considered as the main governing role for bio-cemented soils. The cementations deposited on the surface of particles were regarded as ineffective and made little contribution to the enhanced peak shear strength of bio-cemented soils (Dejong et al., 2010; Cui et al., 2017). However, interestingly, O'Donnell and Kavazanjian (2015) reported a significant improvement in stiffness and dilatancy on bio-treated Ottawa 20-30 sand with very little cementation under isotropically undrained triaxial compression (CIUC) tests. They hypothesized that such improvement was possibly from particle roughening due to the coating effect of $CaCO_3$on the particle surface. Current investigations also show variations of shear parameters at critical or residual state. For instance, in triaxial tests, Feng and Montoya (2016) indicated that the residual cohesion is assumed to be zero. The residual friction angle decreased with the increase of confining pressure but was larger at all levels of confinement in heavily and moderately-cemented sand. In contrast, the residual friction angle of lightly-cemented sand is close to that of untreated soil.

Regarding the compression and particle breakage behaviors, while many researchers have investigated them for uncemented soils, very limited studies have been conducted to explore those of bio-cemented sand treated using MICP. The particle breakage and compressibility behavior of MICP-treated sands have been investigated mostly by oedometric compression tests. The extent of particle breakage is usually quantified by the difference in particle size distribution (PSDs) before and after loading. Generally, MICP treatment can effectively reduce the magnitude of grain crushing and compressibility. For example, Lin et al. (2016) conducted confined compression tests and found the MICP-treated specimens were less compressible than untreated specimens. The compressibility decreased with the increase of $CaCO_3$ content. For a given vertical effective stress or input work, specimens with a larger bio-cementation content exhibited smaller particle breakage and vertical strain. The formed bio-cementation serves to restrain particle breakage and compressibility mainly via three mechanisms: (1) increase the effective diameter of soil particles; (2) dissipate energy during loading; and (3) remain in the void and reduce the magnitude of particle contact forces through a cushioning effect (Xiao et al., 2020a, 2020b).

Cementation content is another essential parameter that is characterized at the element-scale, which has a strong correlation with the engineering performance of bio-cemented soils. In previous studies, cementation content measurement was measured mainly using the destructive method. Dissolving samples in hydrochloric acid (HCl) is a conventional destructive method, in which HCl is added to dissolve the formed cementation and then the weight difference of samples or the pressure difference due to the generation of CO_2 is calculated before and after washing by acid (Feng and Montoya, 2015; Xu et al., 2020). Although acid washing is rather convenient, the accuracy of this method is not inferior to any other methods as compared by Choi et al. (2017) due to the non-uniformity of treatment. In recent years, new non-destructive methods have been applied to characterize bio-cementation content. For instance, the bender element test has been conducted to obtain bio-cementation by correlating it with measured shear wave velocity (Nafisi et al., 2018, 2020).

The thermal conductivity of MICP-treated soil has also been studied in recent years. The effect of bio-cementation within the soil matrix is an influential factor on the thermal conductivity. Venuleo et al. (2016) compared the thermal conductivity between MICP-treated and untreated soils. The results showed that the thermal conductivity of MICP treated soils was increased by 250%. The formation of $CaCO_3$ acting as “thermal bridges” among sand grains, offering more highly effective heat transfer path by increasing the surface contact area. Wang et al. (2020b) found that the thermal conductivity was linearly correlated with dry density, treatment cycles, and $CaCO_3$ content in bio-cemented sands. Martinez et al. (2019) investigated the relationship between the degree of saturation and soil thermal conductivity for a poorly graded quartz sand, and results indicated that thermal conductivity increased with the degree of saturation especially at low saturation levels. In the future, the performance of MICP in practical applications related to thermal conductivity properties such as energy piles, ground source heat pumps, etc. could be assessed.

The efficacy of the engineering performance of MICP is another concern. There are many environmental conditions that could reduce durability, such as wet-dry cycles, freeze-thaw cycles, acid rain infiltration, etc. Element-scale experiments have been conducted to characterize the durability of MICP treated soils. For instance, Liu et al. (2019) conducted a series of unconfined compression tests to investigate the durability of bio-cemented sandy soils under various artificial environmental conditions. The results showed that nearly 80% UCS reduction after one wet-dry cycle, 58% UCS reduction after 15 freeze-thaw cycles, and 83% UCS reduction after 15 days immersed in acid rain solution with a pH of 3.5. Gowthaman et al. (2020) investigated the influence of freeze-thaw cycles on slope soil treated by MICP. The results indicated that the erosion induced by freeze-thaw cycles was dependent on the cementation content. Liu et al. (2019) found that fiber-reinforced samples could reduce the strength reduction after wet-dry and freeze-thaw cycles, though their resistance to acid rain attack remained weak.

1.4.4 Pilot- and field-scale

Several pilot and field trials have been conducted in recent years to treat sandy soils using MICP, in which different characterization tools were adopted. Normally, pilot-scale tests are carried out to validate the MICP concept, which are smaller in dimensions and cheaper than the field-scale ones. In addition, although the experimental conditions at pilot-scale are easier to control, the representation of experimental results is not as relevant as those from field-scale tests. Gomez et al. (2015) conducted a pilot-scale test on loose sand deposits measuring 2.4 m by 4.9 m to improve the surficial erosion resistance. Dynamic cone penetrometer (DCP) measurement was applied to the three biotreated test plots to evaluate variations in the penetration resistance. The results showed the improvement could reach to around 28 cm depth. San Pablo et al. (2020) developed 3.7 m long horizontal columns to investigate the spatial uniformity of bio-cementation and the removal of posttreatment ammonium by-product. The results indicated that using bio-stimulated approaches with a low ureolytic rate could reach a farther treatment distance. Do et al. (2020) developed a double wall pile delivery system in a soil box (measuring 0.91 m × 0.91 m × 0.91 m) to improve the submerged sand adjacent to a pile foundation system using MICP treatment. This system involved the cementation of the general area adjacent to the pile in an ellipsoidal shape with few plugging issues.

For the field-scale tests, Dejong et al. (2014) adopted a scaled repeated five-spot treatment model to monitor the efficiency of MICP during treatment. Bender elements were installed to capture the spatial and temporal changes in mechanical properties using shear wave velocity, which is a good proxy for the distribution of calcite precipitation. Phillips et al. (2018) applied MICP in enhancing wellbore cement integrity with a diameter of 24.4 cm (9.625 inches). The treated region was identified using an ultrasonic imaging tool (USIT), providing a continuous image of the quality of the cement bond at the cement-casing interface. Meng et al. (2020) used the MICP technique to control the wind erosion of surface desert soil (with a depth of ~10 cm). Surface penetration tests (penetration depth ~2 cm) by a digital micro-penetrometer were conducted to evaluate soil bearing capacity. Saneiyan et al. (2019) adopted induced polarization (IP), a geophysical method in mineral exploration, to monitor the status of soil strengthening via MICP in the field spatially and temporally. Terzis et al. (2020) applied field-scale bio-grouting to mitigate landslide risk through MICP within the targeted slip zone hit by extreme rainfall in Switzerland. The data collected by drone surveillance indicated a slower movement within the MICP-treated zone after treatment compared with other zones without MICP treatment.

Although some pilot- and field-scale experiments have been conducted, more attention has been placed on the short-term treatment efficiency. There are rather limited large-scale research studies focusing on the long-term durable behaviors. Further work is needed to conduct long-term verification of MICP treatment in the field.

1.4.5 Numerical modelling

Numerical modeling is a useful tool to virtually assess the performance of MICP where the complex coupled bio-geochemical processes are involved. Numerical prediction can be conducted from different aspects, namely biology, chemistry, hydraulics and mechanics as illustrated in **Fig. 1-5**. MICP is the collective result of water flow, solute transport, chemical reactions, and microorganism mobilization, immobilization, growth, decay, and dynamic metabolic potential (Nassar et al., 2018). Recently, much of the numerical modeling of MICP has focused on small-scale experiments in porous media (mostly sand) whereas large-scale modeling is rather limited.

On the biochemical aspect, the developed models normally consider both solid and aqueous phases and take various coupling mechanisms into account including the flow of the aqueous phase, and the transport of the chemical and bacterial components (i.e. advection, diffusion, dispersion, sorption, bacterial decay) in these two phases (Matsubara et al., 2019; Wang and Nackenhorst, 2020). Researchers may have different assumptions for the phase adsorption of diverse species and chemical components, which could either simplify or complicate models. For instance, Wang and Nackenhorst (2020) assumed that both the urea and ammonium were in the liquid phase, while Fauriel and Laloui (2012) divided them into two parts: solute ammonium/urea in the liquid phase and absorbed ammonium/urea in the solid phase. Furthermore, based on the different assumptions of distribution of various aqueous chemicals and reactants, two types of models have been applied in previous studies: macroscopic continuum and pore-scale models (Wang and Nackenhorst, 2020). Macroscopic continuum models are based on homogenization techniques and have been shown to have advantages in large-scale MICP applications (Fauriel and Laloui, 2012; Hommel et al., 2015; Cunningham et al., 2018). The aqueous biochemical components are assumed to be mixed completely, and the impacts of the local incomplete mixing of reactants at the pore throat are not covered. Pore-scale models focus more on the local heterogeneity, thus the variations in porosity and permeability could be considered (Wang and Nackenhorst, 2020; Qin et al., 2016).

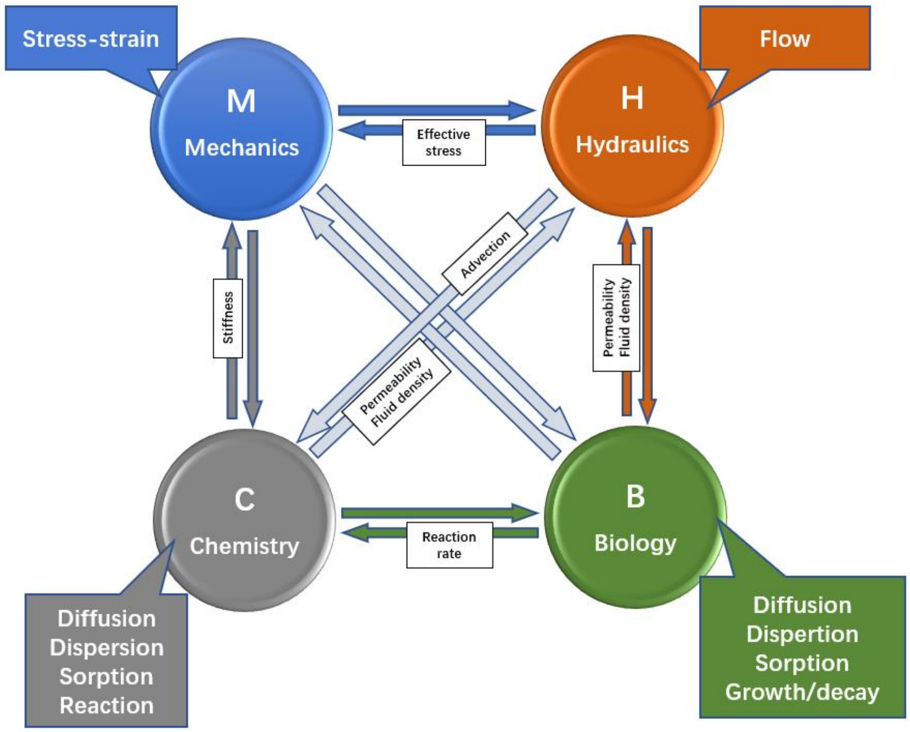

Fig. 1-5 The bio-chemo-hydro-mechanical (BCHM) mechanisms and their couplings (modified after Fauriel and Laloui, 2012).

Various methods have been established on the mechanical aspect to predict the element-scale or pilot-scale properties such as the distribution of calcite precipitation, permeability, and porosity in the solid phase. Zamani and Montoya (2016) conducted simulations in a *Seep/W* program based on the finite-element method to detect the effect of cementation level change on permeability. Feng et al. (2017) conducted three-dimensional DEM simulations using PFC^{3D}. The stiffnesses, shear behaviors, bond breakage, and average void ratio were analyzed. Yang et al. (2017) developed a five-parameter DEM model to simulate the behavior of MICP-treated sands. The peak and residual friction angles predicted by the simulations were very comparable to the experimental results. So far, large-scale numerical modeling is still limited.

In general, numerical modeling is a complex system. Future work is still needed to obtain: (1) a better understating of interactions among coupled bio-chemo-hydro-mechanical processes especially during the bio-stimulation treatment method; (2) the unified rational assumptions regardless of MICP treatment procedures; (3) the more accurate inputs of various modeling parameters for numerical prediction.

In summary, the development of reliable and convenient characterization techniques at various scales is critical for the understanding and implementing of the MICP process. The nano-, micro-, and meso-scale assays help to understand the fundamental mechanisms of MICP. Element-scale tests can provide available methodologies for the mechanical behaviors in the laboratory. In order to apply MICP at a large scale, pilot- and field-scale characterizations are indispensable. Moreover, reliable numerical models are beneficial for understanding fundamental mechanisms and the prediction of engineering behavior of bio-cemented soils. Currently, most characterization techniques at nano-, micro-, element-scales are carried out in the laboratory. However, with further scaling up, there are more challenges during different stages including test setup and preparation, fluid injection, bio-grouting monitoring, and efficiency assessment.

1.5 Promising Applications of MICP

Since the MICP process was firstly explored for its applications in geotechnical engineering, researchers keep exploring new fields that can utilize MICP. While substantial effort is still put into applications in geotechnical engineering such as ground improvement and liquefaction control (Wang et al., 2017), there are an increasing number of studies now focusing on other fields, particularly material modification, disaster alleviation, environmental protection, and energy production/storage (as presented in **Fig. 1-6**). In this section, recent developments in MICP applications in both geotechnical engineering and other fields are reviewed. The existing studies are crucial to provide some insights on this promising technique and potentially help broaden the horizon of MICP applications.

1.5.1 Emerging applications in geotechnical engineering

In recent years, the application of MICP in geotechnical engineering has expanded out of traditional areas such as soil improvement. One such promising application is bio-grouting for soil or rock joints. Studies on the use of bio-grouting for soil and rock joints have been carried out by Chu, (2012). The results have shown that bio-grouting effectively reduces the seepage in soil and rock joints and increases the shear strength of sand (Wu et al., 2019; Wu and Chu, 2020; Pan et al., 2020). However, bio-grouting using the conventional MICP method does have one disadvantage. When the method is used for coarse sand or rock joints with relatively big openings, the number of treatments required to generate sufficient $CaCO_3$to occupy the pores in order to reduce the permeability is excessive. An innovative way to overcome this problem was the use of bio-grouting containing bio-slurry (Cheng et al., 2019). By adjusting the solid content in the bio-slurry, this so-called unified bio-grouting method (Pan et al., 2020) can be used for fine to coarse sand or rock joints of different sizes of the opening.

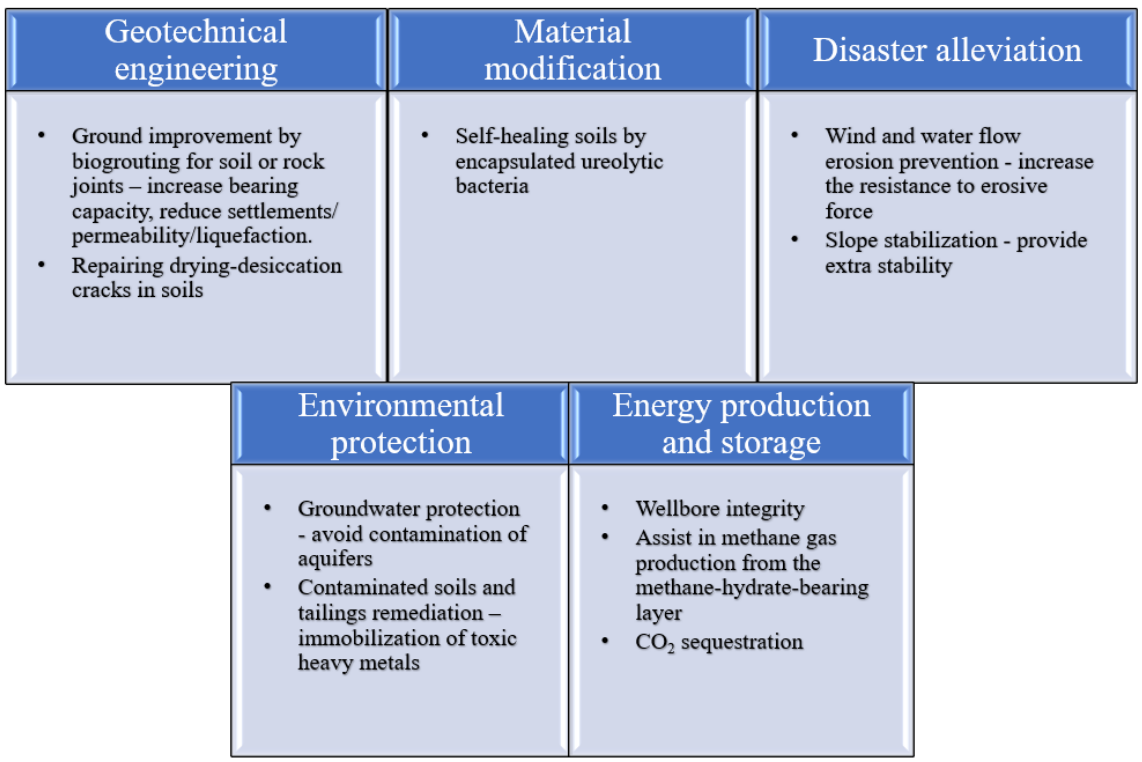

Fig. 1-6 The potential applications of MICP in various fields.

Another promising application is repairing drying-induced cracks in the soil. Drying-induced desiccation cracking of soils is a common natural phenomenon, considerably degrading soil mechanical and hydraulic properties. In recent years, Liu et al. (2020b) applied MICP to remediate desiccation cracking in clayey soils. They found that soils treated with MICP present the highest resistance to cracking (**Fig. 1-7**). Geometrical parameters featuring the crack pattern such as surface crack ratio, average crack width, total crack length, crack width distribution range and the most probable value of crack width decrease significantly with the increasing MICP treatment cycles. Guo et al. (2018) conducted MICP treatment to repair desiccation cracks that occurred in bentonite. It was found that the MICP-treated samples had a larger polygons and smoother surface than the untreated ones after they were totally dried. Liu et al. (2020c) investigated the crack repair in tabia (a traditional artificial Chinese soil which mainly consists of clay, sand and lime) by MICP. The results indicated that the peak recovery rate of flexural and shear strength reached up to 79.92% and 88.54% when the crack with was 5 mm. Wider cracks could lead to a decrease in repair efficiency.

1.5.2 Material modification

While soils, especially coarse-grained ones, are the primary targets of MICP treatment, more and more efforts are being put on the application of MICP on a variety of other materials. The concept of self-healing of materials using MICP has become popular recently. Harbottle et al. (2014) demonstrated the potential of self-healing of sand by MICP to respond to damage by vane shearing the specimens. The results showed a substantial strength increase of 300% to 400% after the initial healing stage. Botusharova et al. (2020) used a spore-forming strain (*Sporosarcina ureae*) for the self-healing procedures in sand. A conceptual process of utilizing sporulated bacteria in porous media was proposed (shown in **Fig. 1-8**). Self-healing via the ureolysis-based MICP process has also been applied in concrete (Jongvivatsakul et al., 2019; Xu et al., 2018; Alazhari et al., 2018; Zhang et al., 2019), which can help reduce the high maintenance costs of concrete in a relatively eco-friendly way. Although most ureolytic bacteria are alkali-tolerant species, which can, to a certain extent, maintain the enzymatic activity in a harsh environment in concrete (pH up to 12-13), encapsulation technique is necessary to further increase the survival of bacteria. Nevertheless, Lee et al. (2018) pointed out that ensuring the survival of bacteria is still the biggest challenge of self-healing concrete. Furthermore, the released byproduct ammonia along with ureolysis process is highly undesirable for the people who live in the buildings with such self-healing concrete.

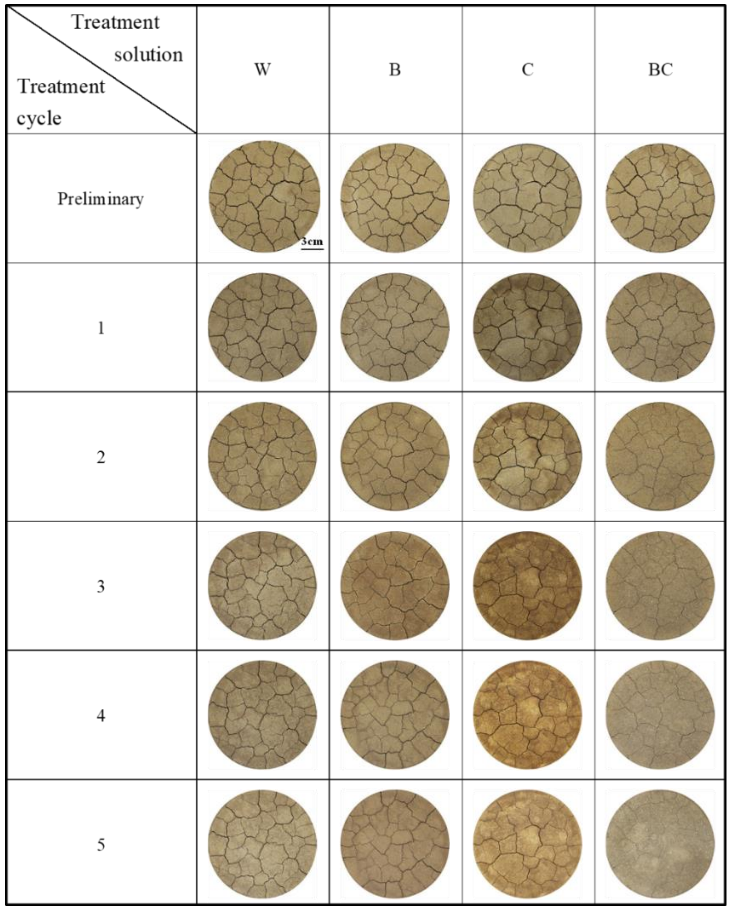

Fig. 1-7 The spatiotemporal evolutions of soil crack patterns after different treatment cycles. W - treated with deionized water; B - treated with bacteria solution; C - treated with cementation solution; BC - treated with both bacteria and cementation solutions (Liu et al., 2020b).

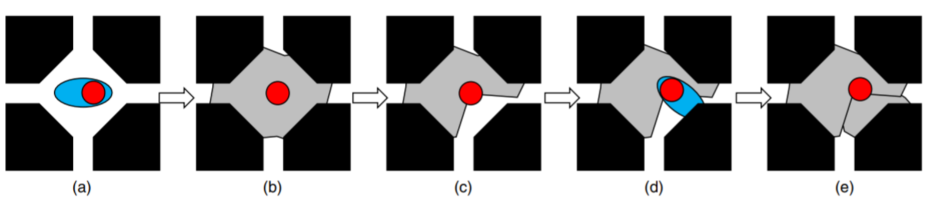

Fig. 1-8 Concept of bacterial self-healing in porous media (Botusharova et al., 2020): (a) sporulating bacteria capable of biomineralization present in the pore space; (b) bacteria produce mineral products, entombing themselves with spores surviving; (c) deterioration of the mineral exposes spores; (d) germination of new cells form spores; and (e) further mineral formation caused by new cells, entombing themselves in the process once more.

1.5.3 Disaster mitigation

MICP techniques have also been applied to mitigate the impacts of natural disasters such as coastal erosion, wind erosion in desert areas, landslides etc. (Chu 2013; Chu et al. 2015). Coastal erosion is mostly caused by storm wave attacks and long-term sea-level rise, which lead to the loss of beach sand dunes and the erosion process related to coastal sediments. The traditional hard structures are expensive and not eco-friendly. MICP-based foreshore sandy slope stabilization is a type of soft structural protection method which has gained increasing interest. Both bio-augmentation and bio-stimulation have been investigated in the laboratory for sandy slope stabilization (Salifu et al., 2016; Liu et al., 2020a; Imran et al., 2019; Gowthaman et al., 2019; Shahin et al., 2020; Kou et al., 2020). However, considering that human activities are sometimes intensive in the beach zones, the issues such as byproduct treatment and durability should be addressed carefully before application in beaches. Alternatively, the creation of artificial beachrocks using natural materials (eg, microbes, sand, shell, pieces of calcareous, and seaweed, etc.) within a short time by MICP method was a milder approach (Imran et al., 2019; Daryono et al., 2020).

Wind erosion is a common problem occurring in arid regions. Fattahi et al. (2020) developed an element-scale cube sand box with a dimension of 10×10×10 cm. A uniform crust was formed and able to provide considerable protection for aeolian sand against erosion by airflow at different velocities. Meng et al. (2021) performed a field-scale test to investigate the efficiency of reducing wind erosion via MICP. Under the optimal condition, the thickness of the soil crust reached up to 12.5 mm and the bearing capacity exceeded 300 kPa. So far, the high cost is the major challenge for the use of MICP in desert areas mainly due to logistics and harsh environments (Meng et al. 2021).

MICP also shows potential for slope stabilization. In order to prevent landslides, it is important to immobilize the ureolytic bacteria within the target surface zones. However, Gowthaman et al. (2019) suggested that well-immobilized bacteria could only exist within the surface zone based on their experimental observations. Factors such as the particle size distribution may limit the treatment in deeper locations. Therefore, it is recommended that the MICP technique is used to enhance the surface cover condition or prevent the instability of surface slopes based on the current knowledge and implementation method.

1.5.4 Environmental protection

Heavy metal contamination in soil and groundwater has been a threat to the ecosystem and human health due to (1) the long-term accumulation in many phases (i.e. air, solid, fluid), and (2) pollution from industrial activities (Jiang et al., 2019; Xia et al., 2019). In recent years, with the development and increasing knowledge of MICP techniques, ureolysis-based MICP has been proven to be an effective approach to stabilize soils contaminated with heavy metals.

Various heavy metals including lead (Pb), cadmium (Cd), zinc (Zn), copper (Cu), mercury (Hg), cobalt (Co), strontium (Sr), barium (Ba), iron (Fe) and nickel (Ni) have been investigated for immobilization efficiency by either bio-stimulated or bio-augmented MICP processes. For example, Kang et al. (2016) found that treatment by four isolated bacterial co-mixtures was more effective in removing mixtures of Pb, Cd, and Cu in soil. Chen et al. (2019) observed that various bio-stimulated ureolytic bacteria could facilitate Cu immobilization by accelerating MICP process. It was proved that the immobilized Cu was mainly in the form of Cu carbonates. Jiang et al. (2019) applied bio-augmented MICP to immobilize Pb in aqueous conditions. The results showed that *S. pasteurii* exhibited compatible resistance to Pb toxicity. The immobilization of Pb might follow a specific sequence, and a hypothesized multi-layer precipitation structure was proposed. In order to investigate the mechanism of ureolytic bacteria in immobilizing heavy metals, Kang and So (2016) isolated six ureolytic bacteria from an abandoned mine. The maximum tolerance concentrations of isolated strains were tested for various heavy metals (Co, Cu, Fe, Cd, Ba, Pb, Sr, and Zn). It was found that the heavy metal resistance of these isolates was closely associated with their resistance to antibiotics. Zhao et al. (2017) utilized *Bacillus sp* isolated from a mine soil to immobilize Cd. Both the efficiency of biosorption and MICP were analyzed. The results indicated that MICP had a greater potential to remove Cd than biosorption process under different factors (initial pH, Cd concentration, contact time). Based on existing studies, the main mechanism of the immobilization process via MICP lies in the co-precipitation of heavy metals in $CaCO_3$ or entering the interstice or defect of the crystal. The heavy metal ions are adsorbed to the bacterial cell wall as a result of Its negative charge, thus resulting in the formation of crystals on the surface of the bacterial cell. Meanwhile, adsorption and redox reactions usually accompany co-precipitation.

It is worth mentioning that co-contaminants often complicate bacterial reactions. While many bacteria possess the potential for biotreatment of various contaminants in laboratory conditions, their survival and enzymatic activity under a real natural environment are vital for field implementation (Rahman et al., 2020). Thus, further research on the impacts of various inhibiting and promoting physio-chemical factors on the capacity and capability of MICP for heavy metal immobilization is needed. Moreover, though the strong absorption of heavy metals on the surface and inside the lattice of calcite occurs, they may possibly suffer under unexpected adverse environmental conditions such as the sudden variation of temperature, pH or microbial population. Thus, the durability of the formed co-precipitation needs to be further studied.

1.5.5 Energy production and storage

Recently, the MICP technique has been developed to assist energy resources production procedures. During the production and extraction of some energy resources such as petroleum and methane hydrate, the disturbance and strength loss of ambient soils or facilities such as wellbores may significantly affect the efficiency of energy production. MICP, as an environmental-friendly approach, can be applied to stabilize the weak soil in these areas. For instance, Phillips et al. (2018) applied MICP in enhancing wellbore cement integrity in the field. The reduced injectivity, reduced pressure fall-off and increased solids showed a successful sealing effect of MICP. Hata et al. (2020) evaluated the feasibility of MICP for ground improvement in the deep ocean using native bacteria. The urease-producing bacteria (i.e. *Sporosarcina newyorkensis*) were isolated from the depressurized core sample in the methane-hydrate-bearing zone. It was found that deep-ocean microbes can still survive in the methane hydrate stable area. The bonding and clogging effects of induced bio-cementation had the potential in preventing sand and water production. In addition, Okyay and Rodrigues (2015), and Okyay et al. (2016) investigated the potential of MICP in CO_2 sequestration to reduce atmospheric CO_2 levels. The results confirm that CO_2 can be removed from the atmosphere through two possible mechanisms: (a) sequestration by MICP biotically and (2) sequestration by increasing the environment pH (i.e. CO_2 solubility) abiotically.

Reference

Achal, V., Mukherjee, A., Basu, P. C., and Reddy, M. S. (2009). Lactose mother liquor as an alternative nutrient source for microbial concrete production by Sporosarcina pasteurii. Journal of Industrial Microbiology and Biotechnology, **36**(3), 433-438.

Al-Thawadi, S. 2008. High strength in-situ biocementation of soil by calcite precipitating locally isolated ureolytic bacteria. Doctoral dissertation, Murdoch University.

Al-Thawadi, S., Cord-Ruwisch, R. and Bououdina, M. 2012. Consolidation of sand particles by nanoparticles of calcite after concentrating ureolytic bacteria in situ. International Journal of Green Nanotechnology, **4**(1), 28-36.

Alazhari, M., Sharma, T., Heath, A., Cooper, R. and Paine, K. 2018. Application of expanded perlite encapsulated bacteria and growth media for self-healing concrete. Construction and Building Materials, **160**, 610-619.

Al Qabany, A., Mortensen, B., Martinez, B., Soga, K. and DeJong, J. 2011. Microbial carbonate precipitation: correlation of S-wave velocity with calcite precipitation. In: Proceedings of Geo-Frontiers: Advances in Geotechnical Engineering, pp. 3993-4001.

Al Qabany, A., Soga, K. and Santamarina, C. 2012. Factors affecting efficiency of microbially induced calcite precipitation. Journal of Geotechnical and Geoenvironmental Engineering, **138**(8), 992-1001.

Al Qabany and Soga, K. 2014. Effect of chemical treatment used in MICP on engineering properties of cemented soils. In: Proceedings of Bio-and Chemo-Mechanical Processes in Geotechnical Engineering: Géotechnique Symposium in Print, ICE Publishing, pp. 107-115.

Amarakoon, GGNN and Kawasaki, S. 2017. Factors Affecting Sand Solidification Using MICP with Pararhodobacter sp. Materials Transactions, M-M2017849.

Amini Kiasari, M., Pakbaz, M. S. and Ghezelbash, G. R. 2019. Comparison of Effects of Different Nutrients on Stimulating Indigenous Soil Bacteria for Biocementation. Journal of Materials in Civil Engineering, **31**(6), 04019067.

Amini Kiasari, M., Pakbaz, M. S. and Ghezelbash, G. R. 2018. Increasing of soil urease activity by stimulation of indigenous bacteria and investigation of their role on shear strength. Geomicrobiology Journal, **35**(10), 821-828.

Arjoon, A., Olaniran, A. O. and Pillay, B. 2013. Enhanced 1, 2-dichloroethane degradation in heavy metal co-contaminated wastewater undergoing biostimulation and bioaugmentation. Chemosphere, **93**(9), 1826-1834.

Atashgahi, S., Tabarsa, A., Shahryari, A. and Hosseini, S. S. 2020. Effect of carbonate precipitating bacteria on strength and hydraulic characteristics of loess soil. Bulletin of Engineering Geology and the Environment.

Azulay, D. N., Abbasi, R., Ben Simhon Ktorza, I., Remennik, S., Reddy M, A., and Chai, L. 2018. Biopolymers from a bacterial extracellular matrix affect the morphology and structure of calcium carbonate crystals. Crystal Growth and Design, **18**(9), 5582-5591.

Babakhani, S., Fahmi, A., Katebi, H., Ouria, A., Majnouni ‐ Toutakhane, A., Ganbarov, K. and Kafil, H. S. 2020. Non ‐ sterile corn steep liquor a novel, cost effective and powerful culture media for Sporosarcina pasteurii cultivation for sand improvement. Journal of Applied Microbiology.

Bains, A., Dhami, N. K., Mukherjee, A., and Reddy, M. S. 2015. Influence of exopolymeric materials on bacterially induced mineralization of carbonates. Applied Biochemistry and Biotechnology, **175**(7), 3531-3541.

Baumgartner, L. K., Reid, R. P., Dupraz, C., Decho, A. W., Buckley, D. H., Spear, J. R., Przekop, K. M. and Visscher, P. T. 2006. Sulfate reducing bacteria in microbial mats: changing paradigms, new discoveries. Sedimentary Geology, **185**(3-4), 131-145.

Bhattacharya, S. 2015. Numerical investigation of Biogrout: a new soil improvement method based on MICP (Doctoral dissertation).

Botusharova, S., Gardner, D., and Harbottle, M. 2020. Augmenting Microbially Induced Carbonate Precipitation of Soil with the Capability to Self-Heal. Journal of Geotechnical and Geoenvironmental Engineering, **146**(4), 04020010.

Burbank, M. B., Weaver, T. J., Green, T. L., Williams, B. C. and Crawford, R. L. 2011. Precipitation of calcite by indigenous microorganisms to strengthen liquefiable soils. Geomicrobiology Journal, **28**(4), 301-312.

Burbank, M. B., Weaver, T. J., Williams, B. C. and Crawford, R. L. 2012. Urease activity of ureolytic bacteria isolated from six soils in which calcite was precipitated by indigenous bacteria. Geomicrobiology Journal, **29**(4), 389-395.

Bang, S., Min, S. H. and Bang, S. S. 2011. Application of microbiologically induced soil stabilization technique for dust suppression. International Journal of Geo-Engineering, **3**(2), 27–37.

Bachmeier, K. L., Williams, A. E., Warmington, J. R. and Bang, S. S. 2002. Urease activity in microbiologically-induced calcite precipitation. Journal of biotechnology, **93**(2), 171-181.

Cardoso, R., Pires, I., Duarte, S. O. and Monteiro, G. A. 2018. Effects of clay's chemical interactions on biocementation. Applied Clay Science, **156**, 96-103.

Casas, C. C., Schaschke, C. J., Akunna, J. C. and Jorat, M. E. 2019. Dissolution experiments on dolerite quarry fines at low liquid-to-solid ratio: a source of calcium for MICP. Environmental Geotechnics, 1-9.

Chaparro-Acuña, S. P., Becerra-Jiménez, M. L., Martínez-Zambrano, J. J. and Rojas-Sarmiento, H. A. 2018. Soil bacteria that precipitate calcium carbonate: mechanism and applications of the process. Acta Agronómica, **67**(2), 277-288.

Chen, H. J., Huang, Y. H., Chen, C. C., Maity, J. P. and Chen, C. Y. 2019. Microbial induced calcium carbonate precipitation (MICP) using pig urine as an alternative to industrial urea. Waste and Biomass Valorization, **10**(10), 2887-2895.

Chen, X. and Achal, V. 2019. Biostimulation of carbonate precipitation process in soil for copper immobilization. Journal of Hazardous Materials, **368**, 705-713.

Cheng, L. and Cord-Ruwisch, R. 2012. In situ soil cementation with ureolytic bacteria by surface percolation. Ecological Engineering, **42**, 64-72.

Cheng, L. and Cord-Ruwisch, R. 2013. Selective enrichment and production of highly urease active bacteria by non-sterile (open) chemostat culture. Journal of Industrial Microbiology and Biotechnology, **40**(10), 1095-1104.

Cheng, L., Cord-Ruwisch, R. and Shahin, M. A. 2013. Cementation of sand soil by microbially induced calcite precipitation at various degrees of saturation. Canadian Geotechnical Journal, **50**(1), 81-90.

Cheng, L., Shahin, M. A., Cord-Ruwisch, R., Addis, M., Hartanto, T., and Elms, C. 2014. Soil stabilisation by microbial-induced calcite precipitation (micp): investigation into some physical and environmental aspects. In: 7th International Congress on

Environmental Geotechnics: iceg2014, Engineers Australia, pp. 1105.

Cheng, L. and Shahin, M. A. 2017. Stabilisation of oil-contaminated soils using microbially induced calcite crystals by bacterial flocs. Géotechnique Letters, **7**(2), 146-151.

Cheng, L., Shahin, M. A. and Cord-Ruwisch, R. 2017. Surface percolation for soil improvement by biocementation utilizing in situ enriched indigenous aerobic and anaerobic ureolytic soil microorganisms. Geomicrobiology Journal, **34**(6), 546-556.

Cheng, L., Shahin, M. A. and Mujah, D. 2017. Influence of key environmental conditions on microbially induced cementation for soil stabilization. Journal of Geotechnical and Geoenvironmental Engineering, **143**(1), 04016083.

Cheng, L., Shahin, M. A. and Chu, J. 2019. Soil bio-cementation using a new one-phase low-pH injection method. Acta Geotechnica, **14**(3), 615-626.

Cheng, L., Shahin, M. A. and Mujah, D. 2017. Influence of key environmental conditions on microbially induced cementation for soil stabilization. Journal of Geotechnical and Geoenvironmental Engineering, **143**(1), 04016083.

Chu, J., Ivanov, V., Lee, M. F., Oh, X. M. and He, J. 2009. Soil and waste treatment using biocement. In: Proceedings of International Symposium on Ground Improvement Technologies and Case Histories (ISGI09), Singapore, 165-170.

Chu, J. 2012. General report on biogrout and other grouting methods. In: Proceedings of ISSMGE - TC 211 International Symposium on Ground Improvement, Brussels, **1**, 177-187.

Chu, J., Stabnikov, V. and Ivanov, V. 2012. Microbially Induced Calcium Carbonate Precipitation on Surface or in the Bulk of Soil. Geomicrobiology Journal, **29**(6), 544–549.

Chu, J. 2013. Innovation in disaster mitigation technologies. Chapter 23 in Geotechnical Predictions and Practice in Dealing with Geohazards, Springer, 375-384.

Chu, J., Ivanov, V., Naeimi, M., Stabnikov, V. and Liu, H. L. 2014. Optimization of calcium-based bioclogging and biocementation of sand. Acta Geotechnica, **9**(2), 277-285.

Chu, J., Ivanov, V., He, J., Naeimi, M. and Wu, S. F. 2015. Use of biogeotechnologies for soil improvement, Chapter 27 in Ground Improvement Case Histories: Chemical, Electrokinetic, Thermal, and Bioengineering Methods, Butterworth-Heinemann, 571-590.

Choi, S. G., Wang, K. and Chu, J. 2016. Properties of biocemented, fiber reinforced sand. Construction and Building Materials, **120**, 623-629.

Choi, S. G., Chang, I., Lee, M., Lee, J. H., Han, J. T. and Kwon, T. H. 2020. Review on geotechnical engineering properties of sands treated by microbially induced calcium carbonate precipitation (MICP) and biopolymers. Construction and Building Materials, **246**, 118415.

Choi, S. G., Wu, S. and Chu, J. 2016. Biocementation for sand using an eggshell as calcium source. Journal of Geotechnical and Geoenvironmental Engineering, **142**(10), 06016010.

Choi, S. G., Park, S. S., Wu, S. F. and Chu, J. 2017. Methods for calcium carbonate content measurement of biocemented soils. Journal of Materials in Civil Engineering, **29**(11), 06017015.

Choi, S. G., Chu, J., Brown, R. C., Wang, K. and Wen, Z. 2017. Sustainable biocement production via microbially induced calcium carbonate precipitation: use of limestone and acetic acid derived from pyrolysis of lignocellulosic biomass. ACS Sustainable Chemistry and Engineering, **5**(6), 5183-5190.

Coleman, M. L. 1993. Microbial processes: controls on the shape and composition of carbonate concretions. Marine geology, **113**(1-2), 127-140.

Corpe, W. A. 1970. Attachment of marine bacteria to solid surfaces. Academic Press, New York.

Cui, M. J., Zheng, J. J., Zhang, R. J., Lai, H. J. and Zhang, J. 2017. Influence of cementation level on the strength behaviour of bio-cemented sand. Acta Geotechnica, **12**(5), 971-986.

Cunningham, A.B., Class, H., Ebigbo, A., Gerlach, R., Phillips, A.J. and Hommel, J. 2018. Field-scale modeling of microbially induced calcite precipitation. Computational Geosciences, **23**(2), 399-414.

Dadda, A., Geindreau, C., Emeriault, F., Du Roscoat, S. R., Filet, A. E. and Garandet, A. 2019. Characterization of contact properties in biocemented sand using 3D X-ray micro-tomography. Acta Geotechnica, **14**(3), 597-613.

Daryono, L. R., Nakashima, K., Kawasaki, S., Suzuki, K., Suyanto, I. and Rahmadi, A. 2020. Investigation of Natural Beachrock and Physical–Mechanical Comparison with Artificial Beachrock Induced by MICP as a Protective Measure against Beach Erosion at Yogyakarta, Indonesia. Geosciences, **10**(4), 143.

DeJong, J. T., Fritzges, M. B. and Nüsslein, K. 2006. Microbially induced cementation to control sand response to undrained shear. Journal of Geotechnical and Geoenvironmental Engineering, **132**(11), 1381-1392.

DeJong, J. T., Mortensen, B. M., Martinez, B. C. and Nelson, D. C. 2010. Bio-mediated soil improvement. Ecological Engineering, **36**(2), 197–210.

Dejong, J. T., Soga, K., Kavazanjian, E., Burns, S., Van Paassen, L. A., Al Qabany, A., Aydilek, A., Bang, S. S., Burbank, M., Caslake, L. F., Chen, C. Y., Cheng, X., Chu, J., Ciurli, S., Esnault-Filet, A., Fauriel, S., Hamdan, N., Hata, T., Inagaki, Y., Jefferis, S., Kuo, M., Laloui, L., Larrahondo, J., Manning, D. A. C., Martinez, B., Montoya, B. M., Nelson, D. C., Palomino, A., Renforth, P., Santamarina, J. C., Seagren, E. A., Tanyu, B., Tsesarsky, M. and Weaver, T. 2013. Biogeochemical processes and geotechnical applications: Progress, opportunities and challenges. Geotechnique, **63**(4), 287–301.

DeJong, J. T., Martinez, B. C., Ginn, T. R., Hunt, C., Major, D. and Tanyu, B. 2014. Development of a scaled repeated five-spot treatment model for examining microbial induced calcite precipitation feasibility in field applications. Geotechnical Testing Journal, **37**(3), 424-435.

DeJong, J., Tibbett, M. andFourie, A. 2015. Geotechnical systems that evolve with ecological processes. Environmental Earth Sciences, **73**(3), 1067–1082.

De Muynck, W., Cox, K., De Belie, N. and Verstraete, W. 2008. Bacterial carbonate precipitation as an alternative surface treatment for concrete. Construction and Building Materials, **22**(5), 875-885.

Duteil, T., Bourillot, R., Grégoire, B., Virolle, M., Brigaud, B., Nouet, J., Braissant, O., Portier, E., Féniès, H., Patrier, P. and Gontier, E., 2020. Experimental formation of clay-coated sand grains using diatom biofilm exopolymers. Geology, **48**(10), 1012-1017.

Ehrlich, H. L., Newman, D. K. and Kappler, A. 2015. Ehrlich's geomicrobiology. CRC press.

Estiu, G. and Merz, K. M. 2004. The hydrolysis of urea and the proficiency of urease. Journal of the American Chemical Society, **126**(22), 6932-6944.

Fang, X., Yang, Y., Chen, Z., Liu, H., Xiao, Y. and Shen, C. 2020. Influence of Fiber Content and Length on Engineering Properties of MICP-Treated Calcareous Sand. Geomicrobiology Journal, 1-13.

Fattahi, S. M., Soroush, A., and Huang, N. 2020. Biocementation Control of Sand against Wind Erosion. Journal of Geotechnical and Geoenvironmental Engineering, **146**(6), 04020045.

Fauriel, S., and Laloui, L. 2012. A bio-chemo-hydro-mechanical model for microbially induced calcite precipitation in soils. Computers and Geotechnics, **46**, 104-120.

Feng, K., Montoya, B. M., and Evans, T. M. 2014. Numerical Investigation of Microbial-Induced Cemented Sand Mechanical Behavior. In: Geo-Congress 2014: Geo-characterization and Modeling for Sustainability. pp. 1644-1653.

Fujita, Y., Ferris, F. G., Lawson, R. D., Colwell, F. S., and Smith, R. W. 2000. Subscribed content calcium carbonate precipitation by ureolytic subsurface bacteria. Geomicrobiology Journal, **17**(4), 305-318.

Fujita, Y., Taylor, J. L., Gresham, T. L., Delwiche, M. E., Colwell, F. S., McLing, T. L., Petzke, L. M. and Smith, R. W. 2008. Stimulation of microbial urea hydrolysis in groundwater to enhance calcite precipitation. Environmental Science and Technology, **42**(8), 3025-3032.

Fujita, Y., Taylor, J. L., Wendt, L. M., Reed, D. W. and Smith, R. W. 2010. Evaluating the potential of native ureolytic microbes to remediate a 90Sr contaminated environment. Environmental Science and Technology, **44**(19), 7652-7658.

Fredrickson, J. K. and Fletcher, M. 2001. Subsurface microbiology and biogeochemistry. Wiley-Liss.

Gai, X. and Sánchez, M. 2019. An elastoplastic mechanical constitutive model for microbially mediated cemented soils. Acta Geotechnica, **14**(3), 709-726.

Gao, Y., Tang, X., Chu, J. and He, J. 2019. Microbially induced calcite precipitation for seepage control in sandy soil. Geomicrobiology Journal, **36**(4), 366-375.

Gat, D., Tsesarsky, M. and Shamir, D. 2011. Ureolytic $CaCO_3$ precipitation in the presence of non-ureolytic competing bacteria. In: Proceedings of Geo-Frontiers 2011: Advances in Geotechnical Engi- neering, ASCE Geotechnical Special Publication 211, Dallas, TX, 3966–3974.

Gat, D., Ronen, Z. and Tsesarsky, M. 2016. Soil bacteria population dynamics following stimulation for ureolytic microbial-induced $CaCO_3$ precipitation. Environmental Science and Technology, **50**(2), 616-624.

Ghosh, P., Mandal, S., Chattopadhyay, B. D. and Pal, S. 2005. Use of microorganism to improve the strength of cement mortar. Cement and Concrete Research, **35**(10), 1980-1983.

Gomez, M. G., Anderson, C. M., Graddy, C. M., DeJong, J. T., Nelson, D. C. and Ginn, T. R. 2017. Large-scale comparison of bioaugmentation and biostimulation approaches for biocementation of sands. Journal of Geotechnical and Geoenvironmental Engineering, **143**(5), 04016124.

Gomez, M. G., Martinez, B. C., DeJong, J. T., Hunt, C. E., deVlaming, L. A., Major, D. W. and Dworatzek, S. M. 2015. Field-scale bio-cementation tests to improve sands. In: Proceedings of the Institution of Civil Engineers-Ground Improvement, **168**(3), 206-216.

Gowthaman, S., Iki, T., Nakashima, K., Ebina, K. and Kawasaki, S. 2019. Feasibility study for slope soil stabilization by microbial induced carbonate precipitation (MICP) using indigenous bacteria isolated from cold subarctic region. SN Applied Sciences, **1**(11), 1480.

Gowthaman, S., Nakashima, K., and Kawasaki, S. (2020). Freeze-thaw durability and shear responses of cemented slope soil treated by microbial induced carbonate precipitation. Soils and Foundations, **60**(4), 840-855.

Graddy, C. M., Gomez, M. G., Kline, L. M., Morrill, S. R., DeJong, J. T. and Nelson, D. C. 2018. Diversity of Sporosarcina-like bacterial strains obtained from meter-scale augmented and stimulated biocementation experiments. Environmental Science and Technology, **52**(7), 3997-4005.

Gu, T., Jia, R., Unsal, T. and Xu, D. 2019. Toward a better understanding of microbiologically influenced corrosion caused by sulfate reducing bacteria. Journal of Materials Science and Technology, **35**(4), 631-636.

Hamed Khodadadi, T., Kavazanjian, E., van Paassen, L. and DeJong, J. 2017. Bio-grout materials: A review. In: Grouting 2017. pp. 1-12.

Hall, C. A., Hernandez, G., Darby, K. M., van Paassen, L., Jr, E. K., DeJong, J. and Wilson, D. 2018. Centrifuge model testing of liquefaction mitigation via denitrification-induced desaturation. In: Geotechnical Earthquake Engineering and Soil Dynamics V: Liquefaction Triggering, Consequences, and Mitigation. American Society of Civil Engineers. Reston, VA. pp. 117-126.

Harbottle, M. J., Lam, M. T., Botusharova, S., and Gardner, D. R. 2014. Self-healing soil: Biomimetic engineering of geotechnical structures to respond to damage.

Harkes, M. P., Van Paassen, L. A., Booster, J. L., Whiffin, V. S. and van Loosdrecht, M. C. 2010. Fixation and distribution of bacterial activity in sand to induce carbonate precipitation for ground reinforcement. Ecological Engineering, **36**(2), 112-117.

Hata, T., Saracho, A. C., Haigh, S. K., Yoneda, J. and Yamamoto, K. 2020. Microbial-induced carbonate precipitation applicability with the methane hydrate-bearing layer microbe. Journal of Natural Gas Science and Engineering, **81**, 103490.

Hataf, N. and Baharifard, A. 2020. Reducing Soil Permeability Using Microbial Induced Carbonate Precipitation (MICP) Method: A Case Study of Shiraz Landfill Soil. Geomicrobiology Journal, **37**(2), 147-158.

Heineck, K. S., Coop, M. R. and Consoli, N. C. 2005. Effect of microreinforcement of soils from very small to large shear strains. Journal of Geotechnical and Geoenvironmental Engineering, **131**(8), 1024-1033.

Hausinger, R. P. 1987. Nickel utilization by microorganisms. Microbiological reviews, **51**(1), 22.

He, J., Chu, J. and Ivanov, V. 2013. Mitigation of liquefaction of saturated sand using biogas. Géotechnique, **63**(4), 267–275.

He, J., Chu, J., Gao, Y. and Liu, H. 2019. Research advances and challenges in biogeotechnologies, Geotechnical Research, **6**(2), 144-155.

Hoang, T., Alleman, J., Cetin, B., Ikuma, K. and Choi, S. G. 2019. Sand and silty-sand soil stabilization using bacterial enzyme–induced calcite precipitation (BEICP). Canadian Geotechnical Journal, **56**(6), 808-822.

Hommel, J., Akyel, A., Frieling, Z., Phillips, A. J., Gerlach, R., Cunningham, A. B. and

Class, H. 2020. A numerical model for enzymatically induced calcium carbonate precipitation. Applied Sciences, **10**(13), 4538.

Hommel, J., Lauchnor, E., Phillips, A., Gerlach, R., Cunningham, A.B. and Helmig, R. 2015. A revised model for microbially induced calcite precipitation: improvements and new insights based on recent experiments. Water Resources Research, **51**(5), 3695–3715.

Hwang, S. K. and Jho, E. H. 2018. Heavy metal and sulfate removal from sulfate-rich synthetic mine drainages using sulfate reducing bacteria. Science of the Total Environment, **635**, 1308-1316.

Imran, M. A., Gowthaman, S., Nakashima, K. and Kawasaki, S. 2020. The Influence of the Addition of Plant-Based Natural Fibers (Jute) on Biocemented Sand Using MICP Method. Materials, **13**(18), 4198.

Imran, M. A., Kimura, S., Nakashima, K., Evelpidou, N. and Kawasaki, S. 2019. Feasibility Study of Native Ureolytic Bacteria for Biocementation Towards Coastal Erosion Protection by MICP Method. Applied Sciences, **9**(20), 4462.

Ivanov, V. and Chu, J. 2008. Applications of microorganisms to geotechnical engineering for bioclogging and biocementation of soil in situ. Reviews in Environmental Science and Biotechnology, **7**(2), 139-153.

Ivanov, V., Chu, J. and Stabnikov, V. 2014. Iron- and calcium-based biogrouts for porous soils, In: Proceedings of the Institution of Civil Engineers-Construction Materials. **167**(1), 36-41

Ivanov, V., Chu, J., Stabnikov, V. and Li, B. 2015. Strengthening of soft marine clay using bioencapsulation. Marine Georesources and Geotechnology, **33**(4), 320-324.

Jadhav, U. U., Lahoti, M., Chen, Z., Qiu, J., Cao, B. and Yang, E. H. 2018. Viability of bacterial spores and crack healing in bacteria-containing geopolymer. Construction and Building Materials, **169**, 716-723.

Jain, S. and Arnepalli, D. N. 2019. Biochemically induced carbonate precipitation in aerobic and anaerobic environments by Sporosarcina pasteurii. Geomicrobiology Journal, **36**(5), 443-451.

Jalilvand, N., Akhgar, A., Alikhani, H. A., Rahmani, H. A. and Rejali, F. 2020. Removal of heavy metals Zinc, Lead, and Cadmium by biomineralization of urease-producing bacteria isolated from Iranian Mine Calcareous soils. Journal of Soil Science and Plant Nutrition, **20**(1), 206-219.

Jiang, N. J., Soga, K. and Kuo, M. 2017. Microbially induced carbonate precipitation for seepage-induced internal erosion control in sand–clay mixtures. Journal of Geotechnical and Geoenvironmental Engineering, **143**(3), 04016100.

Jiang, N. J. and Soga, K. 2019. Erosional behavior of gravel-sand mixtures stabilized by microbially induced calcite precipitation (MICP). Soils and Foundations, **59**(3), 699-709.

Jiang, N. J., Yoshioka, H., Yamamoto, K. and Soga, K. 2016. Ureolytic activities of a urease-producing bacterium and purified urease enzyme in the anoxic condition: Implication for subseafloor sand production control by microbially induced carbonate precipitation (MICP). Ecological Engineering, **90**, 96-104.

Jiang, N. J. and Soga, K. 2017. The applicability of microbially induced calcite precipitation (MICP) for internal erosion control in gravel–sand mixtures. Géotechnique, **67**(1), 42-55.

Jiang, N. J., Liu, R., Du, Y. J. and Bi, Y. Z. 2019. Microbial induced carbonate precipitation for immobilizing Pb contaminants: Toxic effects on bacterial activity and immobilization efficiency. Science of the Total Environment, **672**, 722-731.

Jiang, N. J. 2020. Discussion of "About calcium carbonate precipitation on sand biocementation" by Rafaela Cardoso, Rita Pedreira, Sofia OD Duarte, and Gabriel A. Monteiro. Engineering Geology, 105726.

Jiang, N. J., Tang, C. S., Hata, T., Courcelles, B., Dawoud, O. and Singh, D. N. 2020. Bio-mediated soil improvement: The way forward. Soil Use and Management, **36**(2), 185–188.

Jeong, J. H., Jo, Y. S., Park, C. S., Kang, C. H. and So, J. S. 2017. Biocementation of concrete pavements using microbially induced calcite precipitation. Journal of Microbiology and Biotechnology, **27**(7), 1331-1335.

Jongvivatsakul, P., Janprasit, K., Nuaklong, P., Pungrasmi, W. and Likitlersuang, S. 2019. Investigation of the crack healing performance in mortar using microbially induced calcium carbonate precipitation (MICP) method. Construction and Building Materials, **212**, 737-744.

Kadhim, F. J. and Zheng, J. J. 2016. Review of the Factors That Influence on the Microbial Induced Calcite Precipitation. Civil and Environmental Research, **8**, 69-76.

Kang, C. H., Kwon, Y. J. and So, J. S. 2016. Bioremediation of heavy metals by using bacterial mixtures. Ecological Engineering, **89**, 64-69.

Kannan, K., Bindu, J. and Vinod, P. 2020. Engineering behaviour of MICP treated marine clays. Marine Georesources and Geotechnology, 1-9.

Karatas, I. 2008. Microbiological improvement of the physical properties of soils. Doctoral dissertation, Arizona State University.

Kang, C. H., Kwon, Y. J. and So, J. S. 2016. Soil bioconsolidation through microbially induced calcite precipitation by Lysinibacillus sphaericus WJ-8. Geomicrobiology Journal, **33**(6), 473-478.

Kang, C. H., and So, J. S. 2016. Heavy metal and antibiotic resistance of ureolytic bacteria and their immobilization of heavy metals. Ecological Engineering, **97**, 304-312.

Kou, H. L., Wu, C. Z., Ni, P. P. and Jang, B. A. 2020. Assessment of erosion resistance of biocemented sandy slope subjected to wave actions. Applied Ocean Research, **105**, 102401.

Laloui, L. and Di Donna, A. 2013. Energy geostructures. ISTE and John Wiley and Sons.

Lambert, S. E. and Randall, D. G. 2019. Manufacturing bio-bricks using microbial induced calcium carbonate precipitation and human urine. Water Research, **160**, 158-166.

Lee, M., Gomez, M. G., San Pablo, A. C., Kolbus, C. M., Graddy, C. M., DeJong, J. T. and Nelson, D. C. 2019. investigating Ammonium By-product Removal for Ureolytic Bio-cementation Using Meter-scale experiments. Scientific Reports, **9**(1), 1-15.

Lee, L. M., Ng, W. S., Tan, C. K. and Hii, S. L. 2012. Bio-mediated soil improvement under various concentrations of cementation reagent. In: Proceedings of Applied Mechanics and Materials, **204**, 326-329.

Le Pape, P., Battaglia-Brunet, F., Parmentier, M., Joulian, C., Gassaud, C., Fernandez-Rojo, Guigner, J.M., Ikogou, M., Stetten, L., Olivi, L. and Casiot, C. 2017. Complete removal of arsenic and zinc from a heavily contaminated acid mine drainage via an indigenous SRB consortium. Journal of Hazardous Materials, **321**, 764-772.

Li, B., Chu, J. and Whittle, A. 2016. Biotreatment of fine-grained soil through bioencapsulation method, In: Proceedings of GeoChicago 2016. 14-17.

Li, J., Chen, X., Liu, W. and Tao, Y. 2020. Biostimulation of a marine anammox bacteria-dominated bioprocess by Co (II) to treat nitrogen-rich, saline wastewater. Science of The Total Environment, 141489.

Li, M., Li, L., Ogbonnaya, U., Wen, K., Tian, A. and Amini, F. 2016. Influence of fiber addition on mechanical properties of MICP-treated sand. Journal of Materials in Civil Engineering, **28**(4), 04015166.

Li, M., Wen, K., Li, Y. and Zhu, L. 2018. Impact of oxygen availability on microbially induced calcite precipitation (MICP) treatment. Geomicrobiology Journal, **35**(1), 15-22.

Lian, B., Hu, Q., Chen, J., Ji, J. and Teng, H. H. 2006. Carbonate biomineralization induced by soil bacterium Bacillus megaterium. Geochimica et Cosmochimica Acta, **70**(22), 5522-5535.

Lian, J., Xu, H., He, X., Yan, Y., Fu, D., Yan, S., and Qi, H. 2019. Biogrouting of hydraulic fill fine sands for reclamation projects. Marine Georesources and Geotechnology, **37**(2), 212-222.

Lin, H., Suleiman, M. T., Brown, D. G., and Kavazanjian Jr, E. 2016. Mechanical behavior of sands treated by microbially induced carbonate precipitation. Journal of Geotechnical and Geoenvironmental Engineering, **142**(2), 04015066.

Liu, K. W., Jiang, N. J., Qin, J. D., Wang, Y. J., Tang, C. S. and Han, X. L. 2020. An experimental study of mitigating coastal sand dune erosion by microbial-and enzymatic-induced carbonate precipitation. Acta Geotechnica, 1-14.

Liu, L., Liu, H., Xiao, Y., Chu, J., Xiao, P. and Wang, Y. 2018. Biocementation of calcareous sand using soluble calcium derived from calcareous sand. Bulletin of Engineering Geology and the Environment, **77**(4), 1781-1791.

Liu, S., Wen, K., Armwood, C., Bu, C., Li, C., Amini, F., and Li, L. 2019. Enhancement of MICP-Treated Sandy Soils against Environmental Deterioration. Journal of Materials in Civil Engineering, **31**(12), 04019294.

Liu, B., Zhu, C., Tang, C. S., Xie, Y. H., Yin, L. Y., Cheng, Q. and Shi, B. 2020. Bio-remediation of desiccation cracking in clayey soils through microbially induced calcite precipitation (MICP). Engineering Geology, **264**, 105389.

Lloyd, A. B. and Sheaffe, M. J. 1973. Urease activity in soils. Plant and Soil, **39**(1), 71-80.

Lomboy, G., Sundararajan, S., Wang, K. and Subramaniam, S. 2011. A test method for determining adhesion forces and Hamaker constants of cementitious materials using atomic force microscopy. Cement and Concrete Research, **41**(11), 1157-1166.

Lovley, D. R. 1991. Dissimilatory Fe (III) and Mn (IV) reduction. Microbiology and Molecular Biology Reviews, **55(**2), 259-287.

Madigan, M. T. and Martinko, J. 2005. Brock Biology of Microorganisms (11th Edn.). Upper Saddle River, NJ: Prentice Hall.

Marín, S., Cabestrero, O., Demergasso, C., Olivares, S., Zetola, V. and Vera, M. 2020. An indigenous bacterium with enhanced performance of microbially-induced Ca-carbonate biomineralization under extreme alkaline conditions for concrete and soil-improvement industries. Acta Biomaterialia.

Martin, D., Dodds, K., Ngwenya, B. T., Butler, I. B. and Elphick, S. C. 2012. Inhibition of Sporosarcina pasteurii under anoxic conditions: implications for subsurface carbonate precipitation and remediation via ureolysis. Environmental Science and Technology, **46**(15), 8351-8355.

Martin, D., Dodds, K., Butler, I. B. and Ngwenya, B. T. 2013. Carbonate precipitation under pressure for bioengineering in the anaerobic subsurface via denitrification. Environmental Science and Technology, **47**(15), 8692-8699.

Matsubara, H. and Yamada, T. 2020. Mathematical modelling and simulation of microbial carbonate precipitation: the urea hydrolysis reaction. Acta Geotechnica, **15**(1), 29-38.

Maleki, M., Ebrahimi, S., Asadzadeh, F. and Tabrizi, M. E. 2016. Performance of microbial-induced carbonate precipitation on wind erosion control of sandy soil. International Journal of Environmental Science and Technology, **13**(3), 937-944.

Meng, H., Gao, Y., He, J., Qi, Y. and Hang, L. 2021. Microbially induced carbonate precipitation for wind erosion control of desert soil: Field-scale tests. Geoderma, **383**, 114723.

Mitchell, A. C. Espinosa-Ortiz, E. J. Parks, S. L. Phillips, A. J. Cunningham, A. B. and Gerlach, R. 2019. Kinetics of calcite precipitation by ureolytic bacteria under aerobic and anaerobic conditions. Biogeosciences, **16**(10), 2147-2161.

Mitchell, J. K. and Santamarina, J. C. 2005. Biological Considerations in Geotechnical Engineering. Journal of Geotechnical and Geoenvironmental Engineering, **131**(10), 1222–1233.

Mortensen, B. M. Haber, M. J. DeJong, J. T. Caslake, L. F. and Nelson, D. C. 2011. Effects of environmental factors on microbial induced calcium carbonate precipitation. Journal of Applied Microbiology, **111**(2), 338-349.

Mujah, D., Shahin, M. and Cheng, L. 2016. Performance of biocemented sand under various environmental conditions. In: Proceedings of XVIII Brazilian Conference on Soil Mechanics and Geotechnical Engineering The Sustainable Future of Brazil goes through our Minas COBRAMSEG. pp. 19-22.

Mujah, D., Shahin, M. A. and Cheng, L. 2017. State-of-the-art review of biocementation by microbially induced calcite precipitation (MICP) for soil stabilization. Geomicrobiology Journal, **34**(6), 524-537.

Mujah, D., Cheng, L., and Shahin, M. A. 2019. Microstructural and geomechanical study on biocemented sand for optimization of MICP process. Journal of Materials in Civil Engineering, **31**(4), 04019025.

Nafisi, A. and Montoya, B. M. 2018. A new framework for identifying cementation level of MICP-treated sands. In: Proceedings of IFCEE 2018. pp. 37-47.

Nafisi, A., Montoya, B. M., and Evans, T. M. 2020. Shear strength envelopes of biocemented sands with varying particle size and cementation level. Journal of Geotechnical and Geoenvironmental Engineering, **146**(3), 04020002.

Nassar, M. K., Gurung, D., Bastani, M., Ginn, T. R., Shafei, B., Gomez, M. G., Graddy, C. M., Nelson, D. C. and DeJong, J. T. 2018. Large - scale experiments in microbially induced calcite precipitation (MICP): Reactive transport model development and prediction. Water Resources Research, **54**(1), 480-500.

Nemati, M., Greene, E. A. and Voordouw, G. 2005. Permeability profile modification using bacterially formed calcium carbonate: comparison with enzymic option. Process Biochemistry, **40**(2), 925-933.

O'Donnell, S. T., Hall, C. A., Kavazanjian Jr, E. and Rittmann, B. E. 2019. Biogeochemical Model for Soil Improvement by Denitrification. Journal of Geotechnical and Geoenvironmental Engineering, **145**(11), 04019091.

O'Donnell, S. T., Kavazanjian, E. and Rittmann, B. E. 2017. MIDP: Liquefaction mitigation via microbial denitrification as a two-stage process. II: MICP. Journal of

Geotechnical and Geoenvironmental Engineering, **143**(12), 1–12.

O'Donnell, S. T. and Kavazanjian Jr, E. 2015. Stiffness and dilatancy improvements in uncemented sands treated through MICP. Journal of Geotechnical and Geoenvironmental Engineering, **141**(11), 02815004.

Okyay, T. O. and Rodrigues, D. F. 2015. Biotic and abiotic effects on CO_2 sequestration during microbially-induced calcium carbonate precipitation. FEMS Microbiology Ecology, **91**(3), fiv017.

Okyay, T. O., Nguyen, H. N., Castro, S. L. and Rodrigues, D. F. 2016. CO_2 sequestration by ureolytic microbial consortia through microbially-induced calcite precipitation. Science of the Total Environment, **572**, 671-680.

Omoregie, A. I., Ngu, L. H., Ong, D. E. L., and Nissom, P. M. (2019). Low-cost cultivation of Sporosarcina pasteurii strain in food-grade yeast extract medium for microbially induced carbonate precipitation (MICP) application. Biocatalysis and Agricultural Biotechnology, 17, 247-255.

Osinubi, K. J., Eberemu, A. O., Ijimdiya, T. S., Yakubu, S. E., Gadzama, E. W., Sani, J. E. and Yohanna, P. (2020). Review of the use of microorganisms in geotechnical engineering applications. SN Applied Sciences, **2**(2).

Paerl, H. W. 1997. Coastal eutrophication and harmful algal blooms: Importance of atmospheric deposition and groundwater as "new" nitrogen and other nutrient sources. Limnology and oceanography, **42**, 1154-1165.

Pan, X. H., Chu, J., Cheng, L. and Yang, Y. 2020. A new biogrouting method for fine to coarse sand, Acta Geotechnica, **15**(1), 1-16.

Park, S. S. 2011. Unconfined compressive strength and ductility of fiber-reinforced cemented sand. Construction and Building Materials, **25**(2), 1134-1138.

Peng, S., Di, H., Fan, L., Fan, W. and Qin, L. 2020. Factors Affecting Permeability Reduction of MICP for Fractured Rock. Frontiers in Earth Science, **8**, 217.

Perfumo A., Banat I. M., Marchant R. and Vezzulli L. 2007. Thermally enhanced approaches for bioremediation of hydrocarbon-contaminated soils. Chemosphere, **66**(1), 179-184.

Pham, V. P., Nakano, A., Van Der Star, W. R., Heimovaara, T. J. and Van Paassen, L. A. 2016. Applying MICP by denitrification in soils: a process analysis. Environmental

Geotechnics, **5**(2), 79-93.

Pham, V. P., van Paassen, L. A., van der Star, W. R. and Heimovaara, T. J. 2018. Evaluating strategies to improve process efficiency of denitrification-based MICP. Journal of Geotechnical and Geoenvironmental Engineering, **144**(8), 04018049.

Phillips, A. J., Cunningham, A. B., Gerlach, R., Hiebert, R., Hwang, C., Lomans, B. P., Westrich, J., Mantilla, C., Kirksey, J., Esposito, R. and Spangler, L. 2016. Fracture sealing with microbially-induced calcium carbonate precipitation: A field study. Environmental Science and Technology, **50**(7), 4111-4117.

Qin, C.Z., Hassanizadeh, S.M. and Ebigbo, A. 2016. Pore-scale network modeling of microbially induced calcium carbonate precipitation: insight into scale dependence of biogeochemical reaction rates. Water Resources Research. **52**(11), 8794–8810.

Rahman, Z. 2020. An overview on heavy metal resistant microorganisms for simultaneous treatment of multiple chemical pollutants at co-contaminated sites, and their multipurpose application. Journal of Hazardous Materials, 122682.

Roden, E. E., Leonardo, M. R. and Ferris, F. G. 2002. Immobilization of strontium during iron biomineralization coupled to dissimilatory hydrous ferric oxide reduction. Geochimica et Cosmochimica Acta, **66**(16), 2823-2839.

Rowshanbakht, K., Khamehchiyan, M., Sajedi, R. H. and Nikudel, M. R. 2016. Effect of injected bacterial suspension volume and relative density on carbonate precipitation resulting from microbial treatment. Ecological Engineering, **89**, 49–55.

Saffari, R., Habibagahi, G., Nikooee, E. and Niazi, A. 2017. Biological stabilization of a swelling fine-grained soil: The role of microstructural changes in the shear behavior. Iranian Journal of Science and Technology , **41**(4), 405-414.

Salifu, E., MacLachlan, E., Iyer, K. R., Knapp, C. W. and Tarantino, A. 2016. Application of microbially induced calcite precipitation in erosion mitigation and stabilisation of sandy soil foreshore slopes: A preliminary investigation. Engineering Geology, **201**, 96-105.

San Pablo, A. C., Lee, M., Graddy, C. M., Kolbus, C. M., Khan, M., Zamani, A., Martin, N., Acuff, C., DeJong, J.T., Gomez, M.G. and Nelson, D. C. 2020. Meter-scale biocementation experiments to advance process control and reduce impacts: examining spatial control, ammonium by-product removal, and chemical reductions.

Journal of Geotechnical and Geoenvironmental Engineering, **146**(11), 04020125.

Shahin, M. A., Jamieson, K. and Cheng, L. 2020. Microbial-induced carbonate precipitation for coastal erosion mitigation of sandy slopes. Géotechnique Letters, **10**(2), 211-215.

Shanahan, C. and Montoya, B. M. 2016. Erosion reduction of coastal sands using microbial induced calcite precipitation. In: Proceedings of Geo-Chicago 2016. pp. 42-51.

Sharaky, A. M., Mohamed, N. S., Elmashad, M. E., and Shredah, N. M. 2018. Application of microbial biocementation to improve the physico-mechanical properties of sandy soil. Construction and Building Materials, **190**, 861-869.

Shashank, B. S., Minto, J. M., Singh, D. N., El Mountassir, G. and Knapp, C. W. 2018. Guidance for investigating calcite precipitation by urea hydrolysis for geomaterials. Journal of Testing and Evaluation, **46**(4), 1527-1538.

Shashank, B. S., Sharma, S., Sowmya, S., Latha, R. A., Meenu, P. S. and Singh, D. N. 2016. State-of-the-art on geotechnical engineering perspective on bio-mediated processes. Environmental Earth Sciences, **75**(3), 1–16.

Shashank B., Kuntikana G., Jiang N. J., Singh D. N. 2020. Investigations on biosorption and biogenic calcite precipitation in sands. Soil Use and Management.

Shen, Y. and Buick, R. 2004. The antiquity of microbial sulfate reduction. Earth-Science Reviews, **64**(3-4), 243-272.

Stocks-Fischer, S., Galinat, J. K. and Bang, S. S. 1999. Microbiological precipitation of $CaCO_3$. Soil Biology and Biochemistry, **31**(11), 1563-1571.

Svane, S., Sigurdarson, J. J., Finkenwirth, F., Eitinger, T. and Karring, H. 2020. Inhibition of urease activity by different compounds provides insight into the modulation and association of bacterial nickel import and ureolysis. Scientific Reports, **10**(1), 1-14.

Tang, C. S., Yin, L. yang, Jiang, N. jun, Zhu, C., Zeng, H., Li, H. and Shi, B. 2020. Factors affecting the performance of microbial-induced carbonate precipitation (MICP) treated soil: a review. Environmental Earth Sciences, **79**(5).

Terzis, D. and Laloui, L. 2018. 3-D micro-architecture and mechanical response of soil cemented via microbial-induced calcite precipitation. Scientific Reports, **8**(1), 1-11.

Terzis, D. and Laloui, L. 2019. A decade of progress and turning points in the understanding of bio-improved soils: A review. Geomechanics for Energy and the

Environment, **19**, 100116.

Terzis, D., Laloui, L., Dornberger, S., and Harran, R. 2020. A Full-Scale Application of Slope Stabilization via Calcite Bio-Mineralization Followed by Long-Term GIS Surveillance. In: Geo-Congress 2020: Biogeotechnics. Reston, VA: ASCE. pp. 65-73.

Tsukamoto, M. and Oda, K. 2013. Influence of relative density on microbial carbonate precipitation and mechanical properties of sand. In: Proceedings of the 18th International Conference on Soil Mechanics and Geotechnical Engineering, Paris. pp. 2613-2616.

Umar, M., Kassim, K. A. and Ping Chiet, K. T. 2016. Biological process of soil improvement in civil engineering: A review. Journal of Rock Mechanics and Geotechnical Engineering, **8**(5), 767–774.

Van Der Star, W. R., Taher, E., Harkes, M. P., Blauw, M., Van Loosdrecht, M. C. and van Paassen, L. 2010. Use of waste streams and microbes for in situ transformation of sand into sandstone. In: Proceedings of International Symposium on Ground Improvement Technologies and Case Histories, ISGI'09. pp. 177-182.

Van Paassen, L. A., Daza, C. M., Staal, M., Sorokin, D. Y., van der Zon, W. and van Loosdrecht, M. C. 2010. Potential soil reinforcement by biological denitrification. Ecological Engineering, **36**(2), 168-175.

Van Paassen, L. A., Ghose, R., van der Linden, T. J. M., van der Star, W. R. L. and van Loosdrecht, M. C. M. 2010. Quantifying Biomediated Ground Improvement by Ureolysis: Large-Scale Biogrout Experiment. Journal of Geotechnical and Geoenvironmental Engineering, **136**(12), 1721 – 1728.

Venuleo, S., Laloui, L., Terzis, D., Hueckel, T. and Hassan, M. 2016. Microbially induced calcite precipitation effect on soil thermal conductivity. Géotechnique Letters, **6**(1), 39-44.

Vilain, S., Luo, Y., Hildreth, M. B. and Brözel, V. S. 2006. Analysis of the life cycle of the soil saprophyte Bacillus cereus in liquid soil extract and in soil. Applied and Environmental Microbiology, **72**(7), 4970-4977.

Wang, H. S., Tang, C. S., Gu, K., Shi, B. and Inyang, H. I. 2020. Mechanical behavior of fiber-reinforced, chemically stabilized dredged sludge. Bulletin of Engineering Geology and the Environment, **79**(2), 629-643.

Wang, Y., Soga, K. and Jiang, N. J. 2017. Microbial induced carbonate precipitation (MICP): the case for microscale perspective. In: Proceedings of the 19th international conference on soil mechanics and geotechnical engineering: unearth the future, connect beyond. pp. 1099-1102.

Wang, Y., Soga, K., Dejong, J. T. and Kabla, A. J. (2019a). A microfluidic chip and its use in characterising the particle-scale behaviour of microbial-induced calcium carbonate precipitation (MICP). Géotechnique, **69**(12), 1086-1094.

Wang, Y., Soga, K., DeJong, J. T. and Kabla, A. J. (2019b). Microscale visualization of microbial-induced calcium carbonate precipitation processes. Journal of Geotechnical and Geoenvironmental Engineering, **145**(9), 04019045.

Wang, Y. J., Han, X. L., Jiang, N. J., Wang, J. and Feng, J. 2020a. The effect of enrichment media on the stimulation of native ureolytic bacteria in calcareous sand. International Journal of Environmental Science and Technology, **17**(3), 1795-1808.

Wang, Z., Zhang, N., Cai, G., Jin, Y., Ding, N. and Shen, D. 2017. Review of ground improvement using microbial induced carbonate precipitation (MICP). Marine Georesources and Geotechnology, **35**(8), 1135-1146.

Wang, Z., Zhang, N., Ding, J., Lu, C. and Jin, Y. 2018. Experimental study on wind erosion resistance and strength of sands treated with microbial-induced calcium carbonate precipitation. Advances in Materials Science and Engineering.

Wang, Z., Zhang, N., Ding, J., Li, Q. and Xu, J. 2020b. Thermal conductivity of sands treated with microbially induced calcite precipitation (MICP) and model prediction. International Journal of Heat and Mass Transfer, **147**, 118899.

Wang, X. and Nackenhorst, U. 2020. A coupled bio-chemo-hydraulic model to predict porosity and permeability reduction during microbially induced calcite precipitation. Advances in Water Resources, 103563.

Warthmann, R., Van Lith, Y., Vasconcelos, C., McKenzie, J. A. and Karpoff, A. M. 2000. Bacterially induced dolomite precipitation in anoxic culture experiments. Geology, **28**(12), 1091-1094.

Weaver, T. J., Burbank, M., Lewis, A., Lewis, R., Crawford, R. and Williams, B. 2011. Bio-induced calcite, iron, and manganese precipitation for geotechnical engineering applications. In: Proceedings of Geo-Frontiers 2011: Advances in Geotechnical

Engineering. pp. 3975-3983.

Weil, M. H., DeJong, J. T., Martinez, B. C. and Mortensen, B. M. 2012. Seismic and resistivity measurements for real-time monitoring of microbially induced calcite precipitation in sand. Geotechnical Testing Journal, **35**(2), 330-341.

Wen, K., Li, Y., Amini, F. and Li, L. 2020. Impact of bacteria and urease concentration on precipitation kinetics and crystal morphology of calcium carbonate. Acta Geotechnica, **15**(1), 17-27.

Whitaker, J. M., Vanapalli, S. and Fortin, D. 2018. Improving the strength of sandy soils via ureolytic $CaCO_3$ solidification by Sporosarcina ureae. Biogeosciences, **15**(14), 4367-4380.

Whiffin, V. S., Van Paassen, L. A. and Harkes, M. P. 2007. Microbial carbonate precipitation as a soil improvement technique. Geomicrobiology Journal, **24**(5), 417-423.

Whiffin, V. S. 2004. Microbial $CaCO_3$ precipitation for the production of biocement. Doctoral dissertation, Murdoch University.

Wu, C., and Chu, J. (2020). Biogrouting method for stronger bond strength for aggregates. Journal of Geotechnical and Geoenvironmental Engineering, **146**(11), 06020021.

Wu, S., Li, B., and Chu, J. (2021). Stress-Dilatancy Behavior of MICP-Treated Sand. International Journal of Geomechanics, **21**(3), 04020264.

Wu, C, Chu, J., Wu, S. F. and Guo, W. 2019. Quantifying the permeability reduction of biogrouted rock fracture, Rock Mechanics and Rock Engineering, **52**, 947-954.

Xia, W. Y., Du, Y. J., Li, F. S., Li, C. P., Yan, X. L., Arulrajah, A., Wang, F. and Song, D. J. 2019. In-situ solidification/stabilization of heavy metals contaminated site soil using a dry jet mixing method and new hydroxyapatite based binder. Journal of Hazardous Materials, **369**, 353-361.

Xiao, P., Liu, H., Stuedlein, A. W., Evans, T. M. and Xiao, Y. 2019a. Effect of relative density and biocementation on cyclic response of calcareous sand. Canadian Geotechnical Journal, **56**(12), 1849-1862.

Xiao, Y., He, X., Evans, T. M., Stuedlein, A. W. and Liu, H. 2019b. Unconfined compressive and splitting tensile strength of basalt fiber–reinforced biocemented sand. Journal of Geotechnical and Geoenvironmental Engineering, **145**(9), 04019048.

Xiao, Y., Chen, H., Stuedlein, A. W., Evans, T. M., Chu, J., Cheng, L., Jiang, N. J., Lin, H., Liu, H. and Aboel-Naga, H. M. 2020a. Restraint of particle breakage by biotreatment method. Journal of Geotechnical and Geoenvironmental Engineering, **146**(11), 04020123.

Xiao, Y., Zhao, C., Sun, Y., Wang, S., Wu, H., Chen, H. and Liu, H. 2020b. Compression behavior of MICP-treated sand with various gradations. Acta Geotechnica, 1-10.

Xu, J. and Wang, X. 2018. Self-healing of concrete cracks by use of bacteria-containing low alkali cementitious material. Construction and Building Materials, **167**, 1-14.

Xu, X., Guo, H., Cheng, X. and Li, M. 2020. The promotion of magnesium ions on aragonite precipitation in MICP process. Construction and Building Materials, **263**, 120057.

Yang, D., Xu, G. and Duan, Y. 2020a. Effect of Particle Size on Mechanical Property of Bio-Treated Sand Foundation. Applied Sciences, **10**(22), 8294.

Yang, P., O'Donnell, S., Hamdan, N., Kavazanjian, E. and Neithalath, N. 2017. 3D DEM simulations of drained triaxial compression of sand strengthened using microbially induced carbonate precipitation. International Journal of Geomechanics, **17**(6), 04016143.

Yang, Y, Chu, J., Cao, B., Liu., H. and Cheng, L. 2020b. Biocementation of Soil Using Non-Sterile Enriched Urease-Producing Bacteria from Activated Sludge, Journal of Cleaner Production.

Yoosathaporn, S., Tiangburanatham, P., Bovonsombut, S., Chaipanich, A., and Pathom-Aree, W. (2016). A cost effective cultivation medium for biocalcification of Bacillus pasteurii KCTC 3558 and its effect on cement cubes properties. Microbiological Research, **186**, 132-138.

Yu, F. 2017. Particle breakage and the drained shear behavior of sands. International Journal of Geomechanics, **17**(8), 04017041.

Yu, T., Souli, H., Péchaud, Y. and Fleureau, J. M. 2020. Optimizing protocols for microbial induced calcite precipitation (MICP) for soil improvement–a review. European Journal of Environmental and Civil Engineering, 1–16.

Yu, H., Liang, H., Qu, F., He, J., Xu, G., Hu, H. and Li, G. 2016. Biofouling control by biostimulation of quorum - quenching bacteria in a membrane bioreactor for wastewater treatment. Biotechnology and Bioengineering, **113**(12), 2624-2632.

Zamani, A. and Montoya, B. M. 2016. Permeability reduction due to microbial induced calcite precipitation in sand. In: Proceedings of Geo-Chicago 2016. pp. 94-103.

Zamani, A. and Montoya, B. M. 2018. Undrained Monotonic Shear Response of MICP-Treated Silty Sands. Journal of Geotechnical and Geoenvironmental Engineering, **144**(6), 04018029.

Zeng, Z. and Tice, M. M. 2014. Promotion and nucleation of carbonate precipitation during microbial iron reduction. Geobiology, **12**(4), 362-371.

Zhang, Y., Guo, H. X. and Cheng, X. H. 2014. Influences of calcium sources on microbially induced carbonate precipitation in porous media. Materials Research Innovations, **18**(Sup2), S2-79.

Zhang, J., Zhao, C., Zhou, A., Yang, C., Zhao, L. and Li, Z. 2019. Aragonite formation induced by open cultures of microbial consortia to heal cracks in concrete: Insights into healing mechanisms and crystal polymorphs. Construction and Building Materials, **224**, 815-822.

Zhao, Y., Yao, J., Yuan, Z., Wang, T., Zhang, Y. and Wang, F. 2017. Bioremediation of Cd by strain GZ-22 isolated from mine soil based on biosorption and microbially induced carbonate precipitation. Environmental Science and Pollution Research, **24**(1), 372-380.

Zhao, Q., Li, L., Li, C., Li, M., Amini, F. and Zhang, H. 2014. Factors affecting improvement of engineering properties of MICP-treated soil catalyzed by bacteria and urease. Journal of Materials in Civil Engineering, **26**(12), 04014094.

Zhao, Y., Fan, C., Ge, F., Cheng, X. and Liu, P. 2020. Enhancing Strength of MICP-Treated Sand with Scrap of Activated Carbon-Fiber Felt. Journal of Materials in Civil Engineering, **32**(4), 04020061.

Zhu, Q., Jiang, L., Chen, Y., Xu, J. and Mo, L. 2012. Effect of chloride salt type on chloride binding behavior of concrete. Construction and Building Materials, **37**, 512-517.

Zhu, T. and Dittrich, M. 2016. Carbonate precipitation through microbial activities in natural environment, and their potential in biotechnology: A review. Frontiers in Bioengineering and Biotechnology, **4**, 4.

Zhu, X., Li, W., Zhan, L., Huang, M., Zhang, Q. and Achal, V. 2016. The large-scale process of microbial carbonate precipitation for nickel remediation from an industrial soil. Environmental Pollution, **219**, 149-155.

CHAPTER 2. The Effect of Enrichment Media on the Stimulation of Native Ureolytic Bacteria in Calcareous Sand under Solution Condition

2.1 Introduction

Microbial induced carbonate precipitation (MICP) is a naturally occurring bio-mineralization process, which can be artificially accelerated for engineering applications. MICP involves several microbiological processes: synthesis of urease enzyme via ureolytic bacteria such as *Sporosarcina pasteurii* (Jiang et al., 2014; Jiang and Soga, 2016; Bhaduri et al., 2017), *Bacillus sphaericus* (Cheng et al., 2014) and *Bacillus megaterium* (Lian et al., 2006; Jiang et al., 2016); catalysis of urea and the formation of alkaline environment and carbonate; and formation of calcite precipitation on the surface of bacterial cells when calcium source is available. The ureolytic bacteria is essential to the production of microbial urease. Most of them can use urea as nitrogen source by actively transporting or passively diffusing urea into the cell cytoplasm.

Generated calcite precipitation has cementation property and can be used in various engineering applications including concrete micro-crack repair (Van Tittelboom et al. 2010), wind erosion control in desert area (Maleki et al., 2016), stabilization/solidification for soil remediation (Achal et al., 2011; Kang et al., 2014); and slope stability improvement of mine tailings (Zamani et al., 2018). In particular, MICP works efficiently to enhance the strength and erosion resistance of granular soils (Dejong et al., 2006; Mortensen et al., 2011; Jiang et al., 2014; Jiang et al., 2016). Therefore, it is likely to be able to mitigate coastal erosion along beaches, which consist primarily of loose sand.

Bio-augmentation is one approach to implement MICP in the field, in which bacterial solution is injected into soil with nutrient and cementation media (Gomez et al., 2016). While it has been demonstrated to be effective in many laboratory studies, its compatibility with complex environment in the field is questionable. In addition, the cost of cultivating and transporting ureolytic bacterial strains and possible negative impacts on local ecosystem also make it difficult to be implemented in the field.

Bio-stimulation is an alternative approach, in which native ureolytic bacteria are enriched. The existence of native ureolytic bacteria is the most important prerequisite of MICP application in the field. In representative natural soil environment, the amount of native prokaryotic species in 1cm^3 soil is around 10^{10}-10^{11} and the number of native bacteria varies from a few to thousands (Horner-Devine et al., 2004). Bio-stimulation has been used for bioremediation in environmental engineering for many years (Nakajima et al., 2008; Al-Mailem et al., 2017; Álvarez et al., 2017; Roy et al., 2018). It is found that enriched native bacteria generally have better adaptability to the local environment and can reduce contaminant concentration to acceptable levels. However, the reports on the applications of bio-stimulation based MICP approach in geotechnical and coastal engineering are rather limited (Gomez et al., 2017). Typically, soil is highly heterogeneous in its physical and chemical properties and microbial population. Previous studies on the isolation, enrichment and utilization of native microbes for MICP applications showed that ureolytic bacteria exist in various carriers, namely, sludge, liquefiable soils, sand and tropical peats (Kang et al., 2016; Dhami et al., 2017; Phang et al., 2018). However, the processes of microbial extracting, enriching, purification, and re-injection are complicated and thus it is preferred to directly enrich ureolytic microbes in the field. A majority of ureolytic bacteria can be enriched effectively using media containing urea and/or ammonium (Kang et al., 2016; Phang et al., 2018). Meanwhile, the population of most other aerobic microbes is suppressed at high ammonium and urea concentration. To improve the effectiveness of enriching native ureolytic bacteria in soil, it is necessary to seek appropriate enrichment media. The concentration and composition of the enrichment medium are the most important factors that determine the enrichment efficiency.

The primary objective of this chapter is to investigate the effectiveness of three enrichment media for the stimulation of native ureolytic bacteria in calcareous beach sand. The novelties of the present work are (1) soil type: the Hawaiian calcareous sands which are composed primarily of calcium carbonate are used, instead of the silica sand in the previous work. (2) the feasibility of bio-stimulation of this research can be also provide implications to other tropic regions with similar weather condition as Hawaiian areas. (3) media type: three complex carbon enrichment nutrients with different concentrations of nitrogen source are compared. Furthermore, the effects of initial urea concentration on the enrichment efficiency are specifically examined through a batch-type experiment. The bio-precipitation process is not in the schedule of the present work. This research was carried out in University of Hawaii at Manoa from September to November of 2018.

2.2 Materials and Methods

2.2.1 Soil and enrichment media

For the present work, beach sand was collected from 5 cm depth of the supratidal zones of the Waikiki Beach on the Oahu Island, Hawaii. The grain size distribution of the sand samples is shown in **Fig. 2-1**. Three enrichment media (i.e., yeast extract (YE), malt extract (ME) and nutrient broth (NB)) were used to enrich native ureolytic bacteria. YE, ME and NB are all complex and the most common nutrients for the enrichment of microorganisms. However, the total nitrogen contents are different among them. YE is made of innoxious *Saccharomycetes* by removing their cell walls, extracting the cell contents, drying and concentrating. Therefore, it is abundant in proteins, amino acids, vitamins and enzymes. YE is widely used as a non-selective bacteria culture medium, which serves as both carbon and nitrogen sources. ME is the extract from malt, germinated cereal grains. The produced enzymes during the malting process are able to transform the grain starch into different sugars. Different from YE, ME contains little nitrogen (about 0.5% in total), however is abundant in carbohydrates (George et al., 2008). NB is one of the most nourishing media for bacteria culturing. It is a mixture of peptone and beef extract. The peptone can provide amino acids and long-chained fatty acids, which can be digested into organic nitrogen. The beef extract supplies the bacteria with additional vitamins, carbohydrates, salts and organic nitrogen compounds. The total nitrogen content is comparable to YE or even higher than YE. In the present work, YE, ME and NB media contained 20 g/L yeast extract, malt extract and nutrient broth in distilled water, respectively, which could supply excessive nutrients. The three enriching media were deemed to be generic media, as they contained a variety of proteins, amino acids, vitamins, carbohydrates, and minerals, which supported the growth of most fastidious bacteria (Atlas, 2005). In the present work, the three media were also amended with urea (50, 100 and 170 mM), making them selective enrichment media only favorable for ureolytic bacterial growth (designated as YEU, MEU and NBU). All raw chemical materials were sterilized prior to the enrichment experiments.

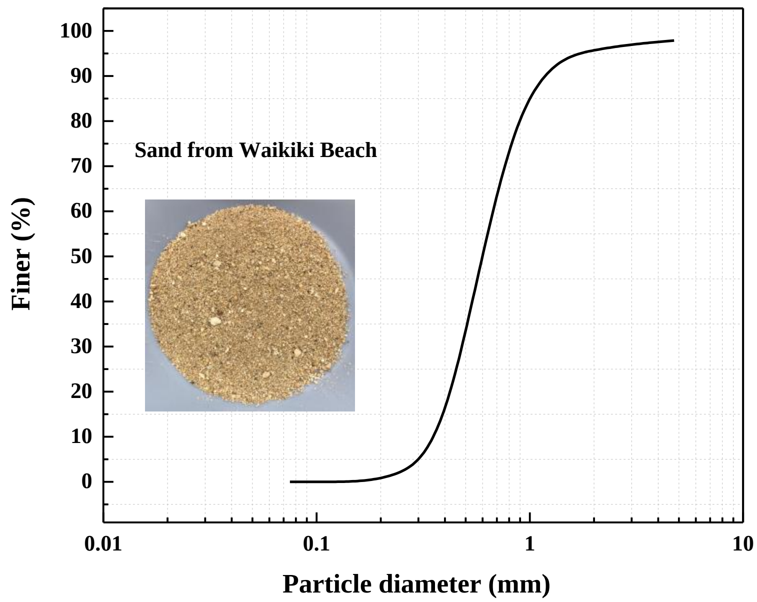

Fig. 2-1 Grain size distribution curve of the Waikiki Beach sand.

2.2.2 Batch-type enrichment test

The scheme of the experimental procedures is illustrated in **Fig. 2-2**. The enrichment test was conducted by shaking-incubating beach sand/enrichment media mixtures in sterilized conical-bottom polyethylene centrifuge tubes (50 mL). A small hole was drilled on the top of the flat-top cap of the centrifuge tubes to allow air circulation. However, as the entire centrifuge tube was almost filled up, the solution tended to be oxic at the top, but anoxic at the bottom during bacterial growth (Somerville and Proctor, 2013). Within each tube, 1.0 g fresh sand sample was mixed with 50 mL enrichment media. Triplicate samples were prepared to ensure the results reliable. The centrifuge tubes were then put into the shaking incubator and the experiment was conducted at 200 rpm (0.425 g-force) at 30 °C for 72 h. The ureolytic activity, electric conductivity (EC), pH, and viable cell number were measured and/or calculated in the course of the test at 6, 12, 24, 48, and 72 h, respectively.

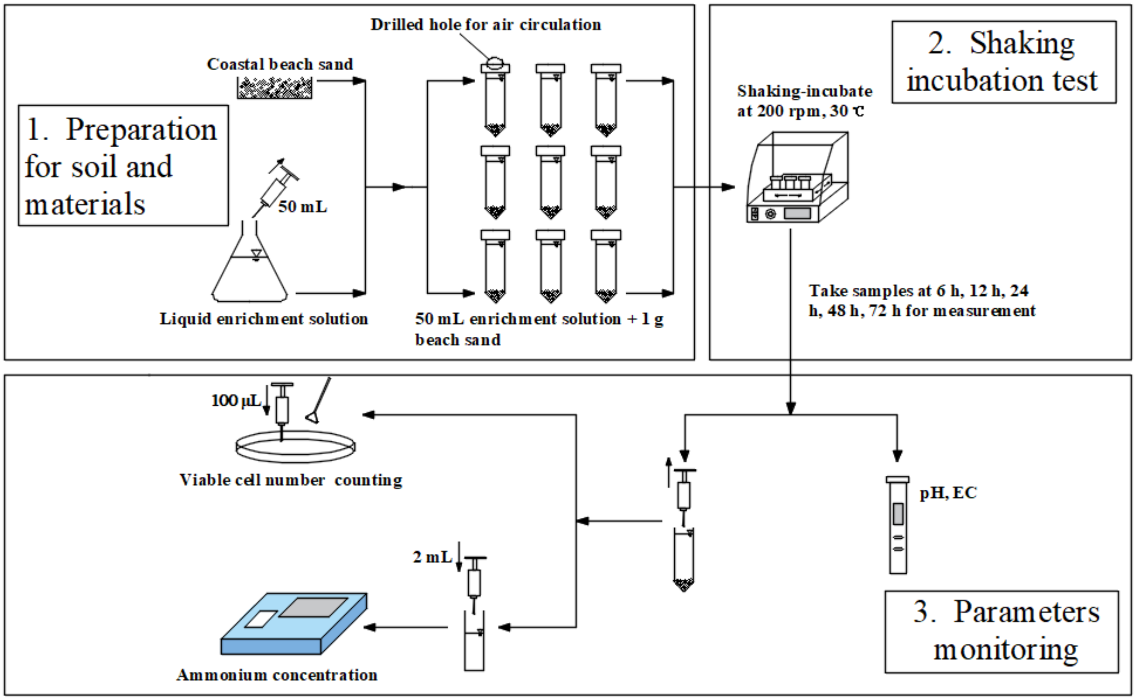

Fig. 2-2 Schematic of experimental procedures.

2.2.3 Chemical and microbial measurements

All chemical and microbial measurements in the present work were based on the solution sampled from the sand/enrichment media mixtures at prescribed time. Before sampling, the solution had been shaken to ensure uniformity. The pH was measured using a disinfected pH meter with a precision of 0.01 and the EC value was determined using a disinfected conductivity meter with a precision of 1 μS. Viable cell number was determined using the plate counting method. 100 μL sampled solution was spread evenly onto the surface of a solid agar medium (20 g/L yeast extract, 15 g/L agar) on a petri dish, which was then incubated overnight at 37 °C for counting. As mentioned earlier in the text, yeast extract was a basic bacteriological medium component and was used as a non-selective medium. Therefore, the counting results could reflect the overall bacterial population in the enrichment solutions. To get valid viable cell number between 30 and 300 on a plate, series dilution was conducted. The ureolytic activity (expressed in mM completely hydrolyzed urea per min) reflects the rate of urea hydrolysis by urease enzyme in the solution, which can be calculated using Eq. (2-1) (Whiffin, 2004). It was determined based on the EC (in mS/cm) increase between 1st and 9th min after mixing 1mL sampled solution with 9 mL of 1.5 M urea solution. In Eq. (2-1), the coefficient value of 10 reflects the dilution during the measurement, and the coefficient value of 11 reflects the relationship between EC change and hydrolyzed urea concentration (Van Paassen, 2009).

$$\textit{Ureolytic Activity} = \frac{(EC_{9\mathrm{min}} - EC_{1\mathrm{min}})}{8} \times 10 \times 11 \ (\mathrm{mM\ urea/min}) \qquad (2\text{-}1)$$

2.3 Results

In the present work, the effects of enrichment medium type and initial urea concentration on the bio-stimulation efficiency were interpreted based on the results of ureolytic activity, change rate of EC, pH value, and viable cell number.

2.3.1 Ureolytic activity

Ureolytic activity is the most straightforward variable showing the enrichment efficiency of native ureolytic bacteria. **Fig. 2-3** shows the variations of ureolytic activity with time. In all generic media (i.e., YE-0, ME-0 and NB-0), the increase in ureolytic activity with time was rather limited (< 0.2 mM urea/min). This indicates that most indigenous bacteria in sampled sand were not able to produce urease enzyme constitutively and bacteria capable of producing urease enzyme inducibly (hereafter defined as ureolytic bacteria) could not be effectively enriched in a medium without urea. In selective media with low urea concentration (50 mM), ureolytic activity in the NBU medium showed a slight increase. However, in the YEU and MEU media, ureolytic activity barely increased. In selective media with urea at 100 and 170 mM, noticeable increase in ureolytic activity was observed after enrichment. However, the ureolytic activity at 100 and 170 mM urea did not show remarkable difference. This is attributed to the nature of enzyme, in which the activity increases with substrate concentration (urea in the present work) until a threshold is reached. After that, further increase in substrate concentration cannot elevate enzyme activity anymore (Copeland, 2000).

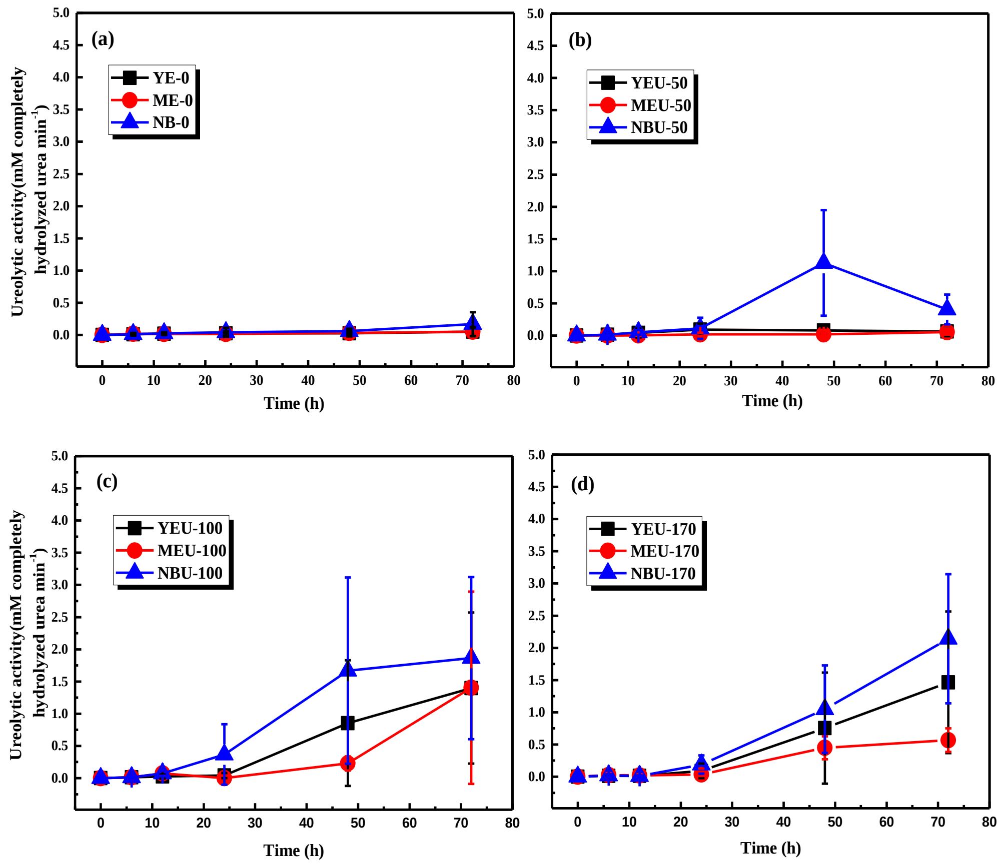

Fig. 2-3 Variations of ureolytic activity with time ((a). without urea (b). 50mM urea (c). 100mM urea (d). 170mM urea).

When comparing the effect of the three enriching media, the NBU medium induced the highest ureolytic activity at all urea concentrations. For the other two media, their stimulated ureolytic activity was negligible at 50 mM urea. At higher urea concentrations, YEU was slightly better than MEU to stimulate ureolytic bacteria. The differences among the three media are primarily due to their different compositions. NB, a mixture of peptone and beef extract, is one of the most nourishing media for bacteria culturing. It is not surprising that the ureolytic activity is the highest in the NB cases. On the other hand, ME contains little nitrogen (about 0.5% in total), however is abundant in carbohydrates. Thus, it is expected that its ability to stimulate ureolytic activity is weaker.

2.3.2 Electrical conductivity (EC) change rate

According to Noble (1999), Krishnamurti and Kate (1951), and Allison et al. (1938), subtle changes in ionic composition of a culture medium can affect EC. The metabolism of bacteria cells leads to the decomposition of stable large organic molecules like proteins into small molecules and electrolytic ions, which increases EC accordingly. In this sense, EC change rate can be used to represent bacterial activity. Actually, EC was already used by other researchers to characterize bacterial activity in a bio-stimulation practice (Graddy et al., 2018).

In this experiment, the bacterial activity (i.e., EC change rate) has two predominant sources: (1) ureolytic activity from bacteria which are able to produce enzyme inducibly (i.e., ureolytic bacteria) and (2) non-ureolytic metabolic activity of all bacteria. At different stages, either one may prevail. **Fig. 2-4** shows the evolutions of the EC change rate (i.e., bacterial activity) with time. In generic media, only limited EC change rate (< 0.2 mS/cm/h) could be detected in all the three media. As no urea was amended and very low level of ureolytic activity was detected in the case of generic media, the EC change rate (i.e., bacterial activity) here was supposed to be prevailed by the non-ureolytic metabolic activity of bacteria. Because YE and NB contained both carbon and nitrate sources, whereas ME only had carbon (George et al., 2008), the metabolic activity of bacteria in YE and NB was more intensive than in ME.

In the selective media amended with urea, elevated EC change rate was detected for all three media. In 50 mM urea, the EC change rate in the case of NBU was the highest especially after 12-24 h, peaking at ~ 0.4 mS/cm/h and stabilizing after 24-48 h. YEU yielded the second highest EC change rate peaking at ~ 0.2 mS/cm/h, although it was equalized by MEU between 48 and 72 h. In 100 mM urea, the evolution of EC change rate changed dramatically. For NBU and MEU, EC change rate soared to 0.9~1.0 mS/cm/h between 24 and 48 h before dropping to almost zero between 48 and 72 h. YEU also showed the bell-shaped trend, but with peak at ~0.4 mS/cm/h. Finally, in 170 mM urea, bell-shaped curves were also observed. YEU (~0.8 mS/cm/h) and NBU (~0.5 mS/cm/h) peaked between 12 and 24 h while MEU (~0.5 mS/cm/h) between 24 and 48 h.

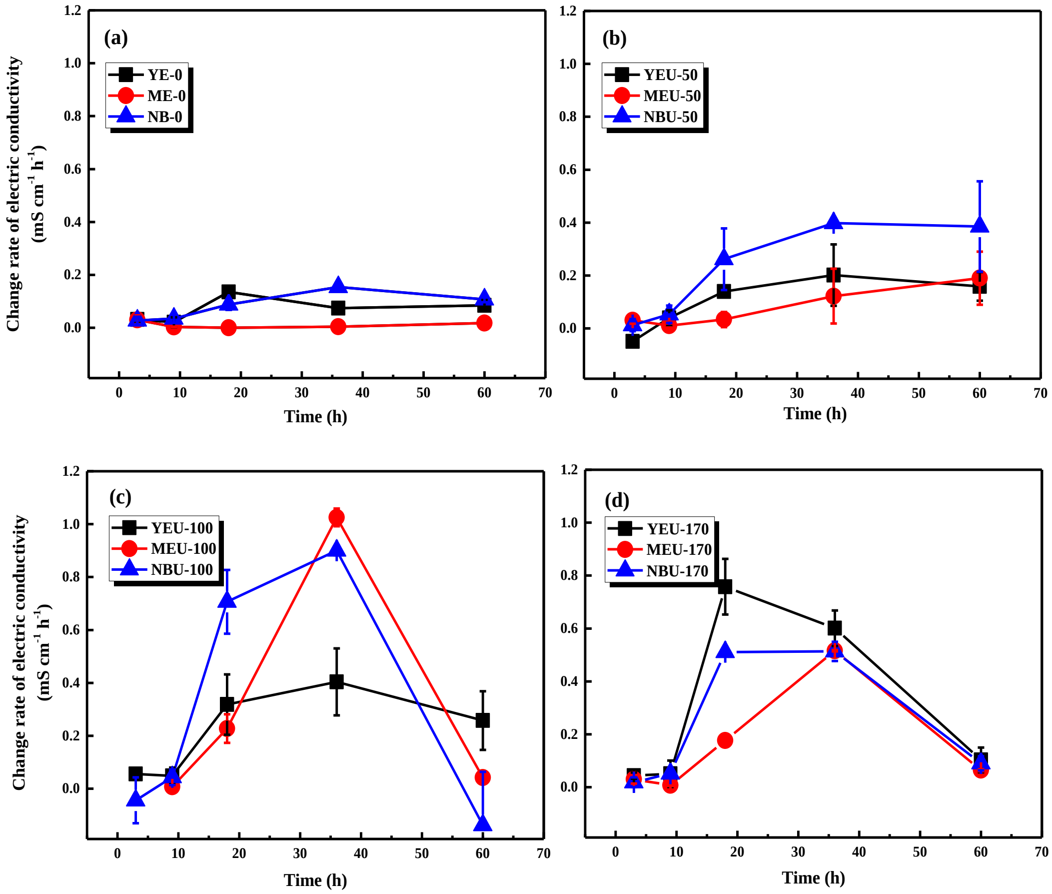

Fig. 2-4 Evolutions of EC change rate (bacterial activity) with time ((a). without urea (b). 50mM urea (c). 100mM urea (d). 170mM urea).

The observed bacterial activity evolution via EC change rate fundamentally was determined by the viability and adaptability of native soil bacteria under elevated urea environment. Firstly, many natural ureolytic bacteria can express urease inducibly and thus are enzymatically ready for ureolysis when urea is present (Kaltwasser et al., 1972; Morsdorf and Kaltwasser, 1989). Therefore, when a urea-rich environment is present, ureolytic bacteria will rapidly utilize urea as both carbon and nitrate sources for growth and metabolism (Bibi et al., 2018). The ureolytic activity of urease enzyme increases with urea concentration until a threshold urea concentration is reached (Copeland, 2000). Secondly, when bacteria encounter unsuitable environments, they are forced to constantly expend energy on coping with the adverse environments, leaving limited energy for growth and other maintenance functions (Graddy et al., 2018). Usually, special gene-induced-stress proteins will be synthesized in response to the adverse environment stresses (Hecker and Völker, 2001). This process will lead to the increased level of decomposition of nutrients necessary for the synthesis of gene-induced-stress proteins. In the present work, the presence of NH_4^+-NH_3 (generated through ureolysis by ureolytic bacteria) in solution is an adverse environment for most native soil bacteria, which are usually neutrophilic (Booth, 1985; Müller et al., 2006) and not capable of producing urease enzyme. Therefore, their non-ureolytic metabolic activity increases substantially for a certain period to cope with this adverse environment.

In the present work, in general, EC change rate at 50 mM urea was smaller than that at 100 and 170 mM urea. This is likely attributed to elevated ureolytic activity at higher urea concentration (See **Fig. 2-3)**. At 100 and 170 mM urea, the EC change rate dropped to a low level between 48 and 72 h. This is likely due to the depletion of urea in the enrichment solution and the cease of ureolysis by ureolytic bacteria. Then, at 100 and 170 mM urea, a burst of EC change rate was observed between 24 and 48 h and between 12 and 48 h in the case of 100 mM and 170 mM urea, respectively (See **Fig. 2-4 © and (d)**). This appears to be attributed to the exposure of native soil bacteria to elevated NH_4^+-NH_3 concentration from urea hydrolysis, which forces them to expend energy by decomposing more nutrients to cope with. It is also noted that the peak EC change rate at 100 mM urea was higher than at 170 mM urea. It is likely that 170 mM urea is too high for native soil bacteria incapable of producing urease so that they cannot survive for a long time. Thus, the viability of native soil bacteria at 170 mM declines more quickly and decomposes fewer nutrients against the adverse urea-rich condition.

2.3.3 pH value

The pH of the enrichment solution during the test is controlled by several factors. On one hand, the hydrolysis of urea by ureolytic bacteria alkalinizes the solution. On the other hand, aerobic bacterial respiration and anaerobic bacterial fermentation result in the acidification of solution (Cheng et al., 2018).

Fig. 2-5 shows the changes in pH value during the enrichment process. In the generic media, pH value dropped between 12 and 48 h before recovering later. The pH drop at early stage was likely due to the aerobic respiration of bacteria at the top part of the solution

(Mookerjee et al., 2015) and the anaerobic fermentation of bacteria at the bottom part of the solution (Cheng et al., 2018). The pH recovery at later stage was likely attributed to the accumulation of NH_4^+-NH_3 in the solution, which came from the decomposition of nitrate source in the enrichment solution. However, with limited experimental program conducted in the present work, this hypothesis cannot be fully verified.

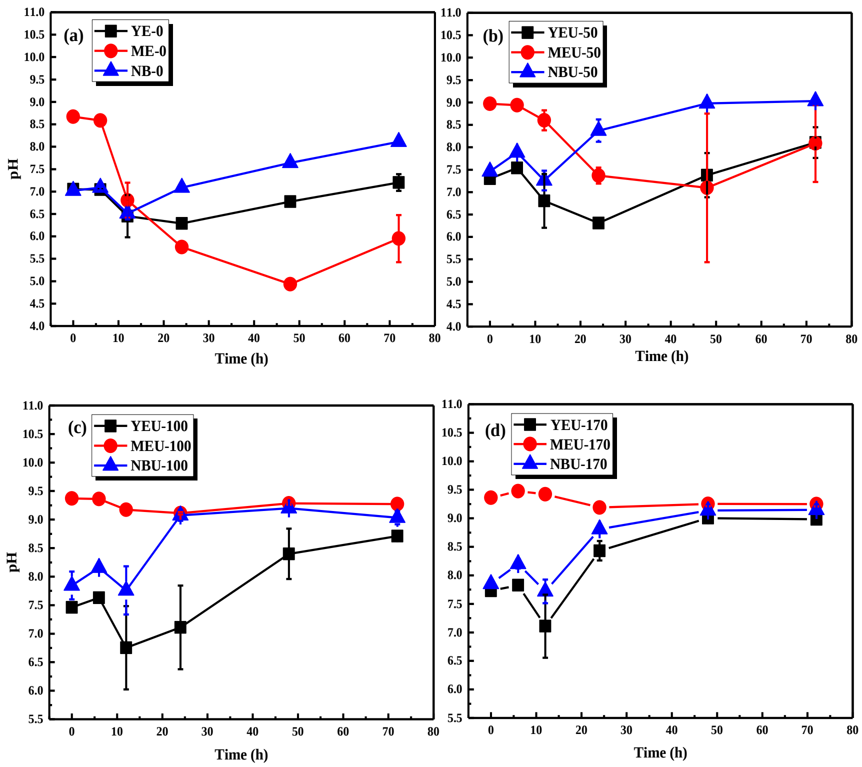

Fig. 2-5 Variations of pH with time ((a). without urea (b). 50mM urea (c). 100mM urea (d). 170mM urea).

Compared with the generic media, although the pH-time relationship of selective media still showed a concave shape, a faster pH recovery could be observed with elevated urea concentration. More specifically, pH of YEU started to rebound at 48 h, with pH raised to 7.4, 8.3, and 8.7 at 50, 100 and 170 mM urea, respectively. For MEU, the rebound started at 72h and the addition of 50, 100 and 170 mM urea were able to recover pH to 8.0, 9.2, and 9.3, respectively. For NBU, the pH value rebounded at 24 h and recovered to 8.4, 9.1, and 9.0 with the amendment of 50, 100 and 170 mM urea, respectively.

With the increase in urea concentration, ureolytic activity becomes more intense, leading to faster urea hydrolysis and NH_4^+-NH_3 production. Theoretically, with the accumulation of NH_4^+/NH_3, the system pH is elevated and finally stabilized at 9.3 (pK_a for the NH_4^+/NH_3 equilibrium) (Graddy et al., 2018). It is apparent that the higher the amended urea concentration, the faster the system approaches to the equilibrium pH value.

2.3.4 Viable cell number

Viable cell number is a more suitable parameter over optical density at 600 nm (OD_{600}) as OD_{600} is uncertain when the environment has different species with diverse size and mass. In addition, OD_{600} readings are affected by environmental factors, such as the pigments, the sample preparations and the presence of colloid particles in solution (Sutton 2006). Therefore, only viable cell number, expressed in colony-forming unit (CFU), was reported to give the growth trend of enriched native bacteria. The change of viable cell number with time is shown in **Fig. 2-6**. Regardless of medium type and urea concentration, viable cell number increased exponentially within initial 24 h from 10^4 CFU/mL to 10^6~10^9 CFU/mL, indicating that the stimulated bacteria were in the exponential growth phase. After 24 h, in the generic media (YE-0, ME-0 and NB-0) and selective media with 50 mM urea (YEU-50, MEU-50 and NBU-50), the viable cell number ceased to increase and maintained stable, indicating that the bacteria were in the stationary phase (Kolter et al. 1993). However, in the selective media with higher urea concentration (i.e., 100 and 170 mM), the overall viable cell number started to decline, indicating that large amounts of bacteria, mostly not capable of producing urease, started to die. Furthermore, the effect of enrichment medium type on viable cell number was not obvious in the first 24 h. After 24 h, the viable cell number in the YEU and NBU media were more than that in the MEU medium.

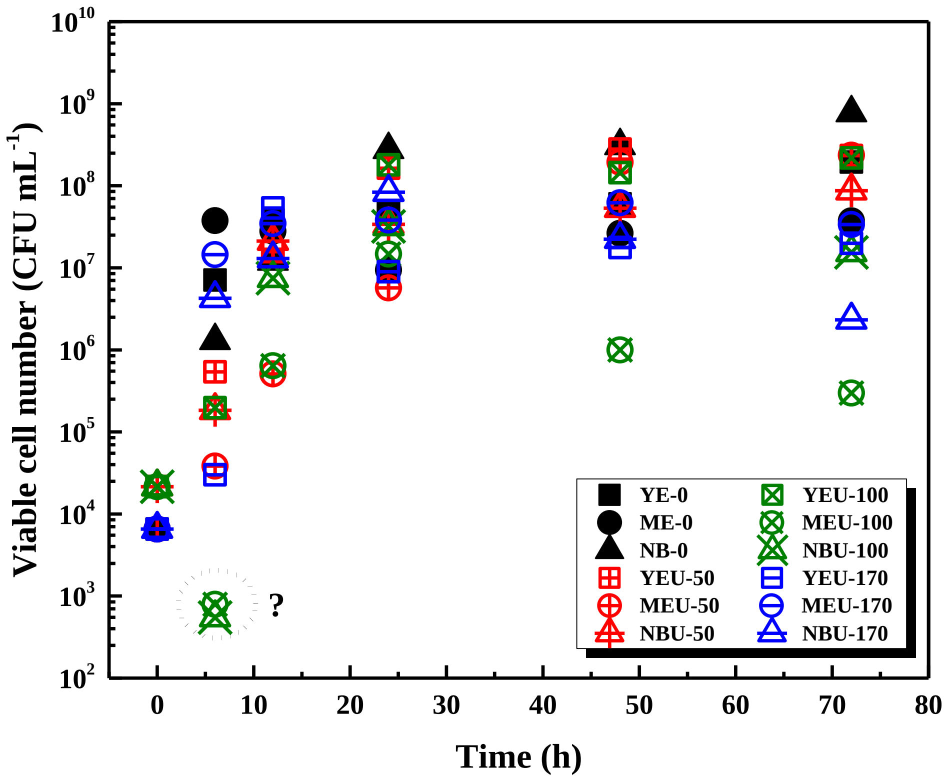

Fig. 2-6 Variations of viable cell number with time.

2.4 Discussion

2.4.1 Relationship between pH and ureolytic activity

Fig. 2-7 shows how ureolytic activity changed with pH. It is obvious that the most significant ureolytic activity occurred at pH range between 8.4 and 9.2 in the present work. For the YEU media, ureolytic activity started to rise up at pH 8.1 and peaked at pH 8.4. As there was no more alkaline condition for the YEU media, it is not possible to confirm the ureolytic activity at pH>8.5. For the MEU media, ureolytic activity was only very significant around pH 9.2 while any slightly acidic or alkaline conditions severely diminished ureolytic activity. For the NBU media, the ureolytic activity started to increase at pH 8.7 and peaked at pH 9.1. Similarly, it is not clear how ureolytic activity behaves at pH>9.1 due to limited alkalinity of the NBU media.

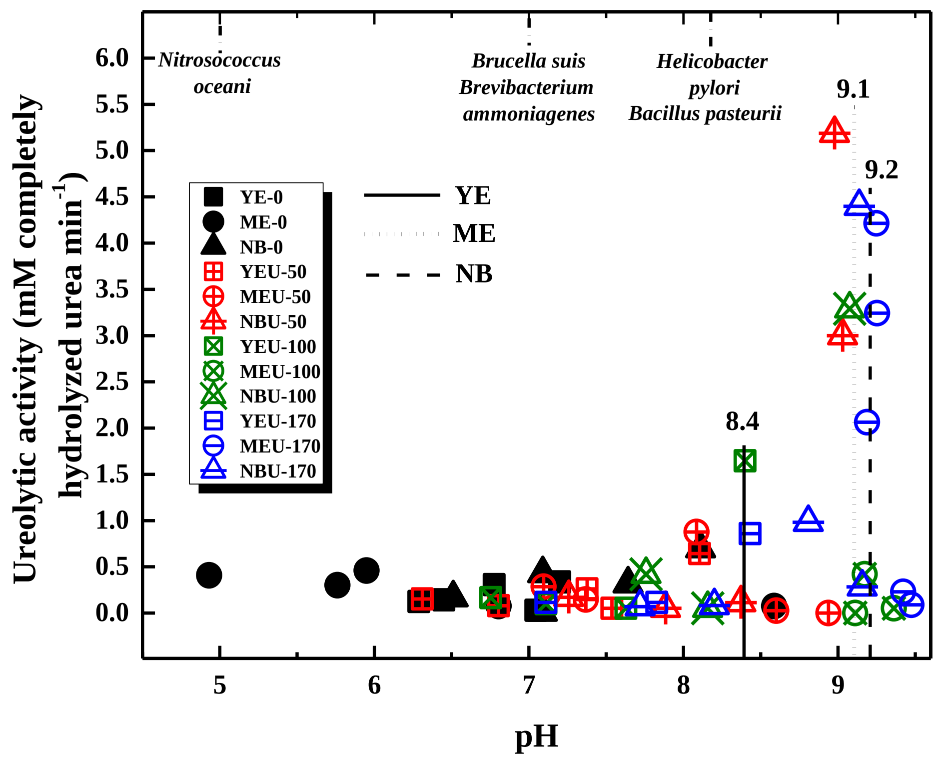

Fig. 2-7 Relationship between ureolytic activity and pH value.

Fundamentally, the effect of pH on ureolytic activity is related to the pH-dependent behavior of both urease enzyme and bacterial cell. Firstly, for urease enzyme, the change in pH not only impacts the stability of enzyme but also alters the reactivity of functional groups composing active sites of the enzyme. For a certain enzyme, there exists an optimal pH range, within which the enzyme displays an optimal catalytic activity. Regarding pure microbial urease enzyme, many researchers have reported its optimal pH range to be between 5.0 and 8.2 (Watson 1965; Contreras-Rodriguez et al. 2008; Evans et al. 1991). It should be noted that the optimal pH reported in the present work does not exactly match those reported previously. This is because that, the optimal enzymatic pH for a certain enzyme is not constant, but rather depends on the enzyme purity, substrate type and properties, and the presence of buffer agents and/or inhibitors. As the testing condition and solution composition may not be the same between our study and those reported previously, the optimal enzymatic pH may also differ.

Secondly, the viability and metabolism of bacteria highly depend on pH of surrounding environment. Most soil bacteria are neutrophilic and maintain their cytoplasmic pH between 7.5 and 8.0 (Booth 1985). However, for many bacteria capable of producing urease constitutively or inducibly, they are usually alkali-tolerant, which can tolerate an internal pH greater than 9. Their optimal growth pH value is normally around 9.25~9.5 (Wiley and Stokes 1962; Hoddinott et al. 1978; Jahns 1996). Under this condition, the activity of other neutrophilic soil bacteria is severely inhibited, thus leaving nutrients to ureolytic bacteria and enhancing their urease production rate. In the present work, the optimal pH was much closer to the optimum pH for ureolytic bacteria growth (9.25~9.5) rather than the optimal pH value for the expression of pure microbial urease enzyme ($\leqslant$ 8.2). It can be assumed the competitive relation between non-ureolytic and ureolytic bacteria could delay the expression of microbial urease.

2.4.2 The dominance of ureolytic activity over other bacterial metabolic activities

Earlier, EC change rate could be taken as an indicator of bacterial metabolic activity. Thus, the EC value of the enrichment solution can be viewed as cumulative bacterial activity during the enrichment process, which includes both ureolytic activity of ureolytic bacteria and non-ureolytic metabolism of all bacteria. **Fig. 2-8** shows how ureolytic activity changes with increase in EC value (EC_{now}-$EC_{baseline}$). The $EC_{baseline}$ refers to the initial EC of sand-medium solution. It is apparent that during the initial increase in EC up to 10 mS/cm, there was not noticeable increase in ureolytic activity. This indicates that the early stage of enrichment process is dominated by non-ureolytic metabolism rather than ureolytic activity. Fundamentally, as the ureolytic bacteria population at the early stage is still small, not sufficiently high NH_4^+-NH_3 concentration has been generated to inhibit the growth of most soil bacteria that are neutrophilic and not capable of producing urease enzyme. Therefore, from the viable cell number results, we did not see much difference in overall bacterial population within initial 24 h. In another set of experiments, 100 mM NH_4Cl was premixed with the enrichment solution in the case of YEU-170 to inhibit soil bacteria that are neutrophilic and not capable of producing urease enzyme. The 100 mM NH_4Cl is high enough to enhance the ureolysis process (Gomez et al. 2017), which can effectively inhibit the non-ureolytic bacteria. The change in viable cell number, as shown in **Fig. 2-9,** has clearly showed that ureolytic bacterial population was only around 10~10^2 per milliliter initially and 10^3~10^4 per milliliter after 12 h of enrichment, only a very small fraction of overall bacterial population.

Then, with further increase in EC (i.e., cumulative bacterial activity), ureolytic bacterial also increases and displays a linear relationship with EC increase. This appears to demonstrate that at later stage of enrichment, ureolytic activity becomes dominant of overall bacterial activity. This is fundamentally due to the dominance of ureolytic bacteria and the decline in non-ureolytic bacterial population under NH_4^+-NH_3-rich condition at this stage, which can be confirmed by the viable cell number results in **Fig. 2-6** and **Fig. 2-9**.

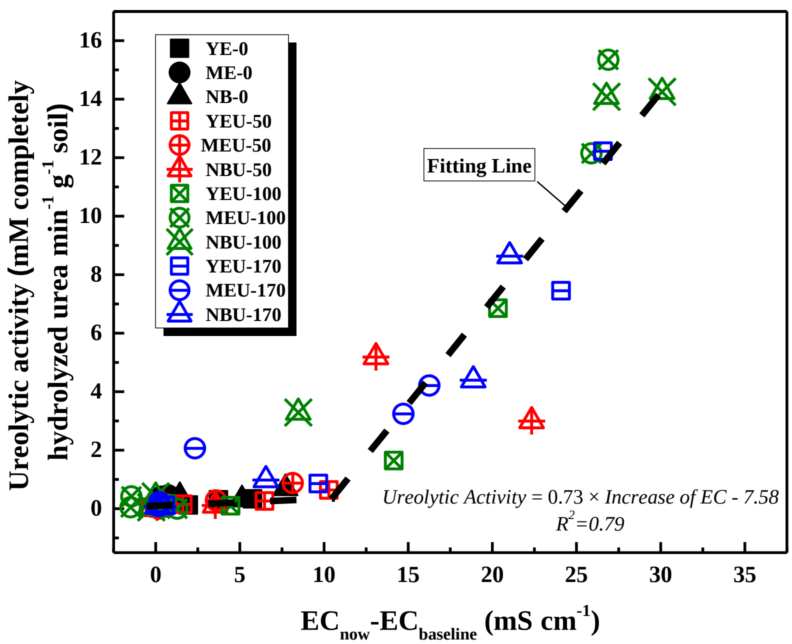

Fig. 2-8 Relationship between ureolytic activity and increase of electric conductivity (EC_{now}-$EC_{baseline}$).

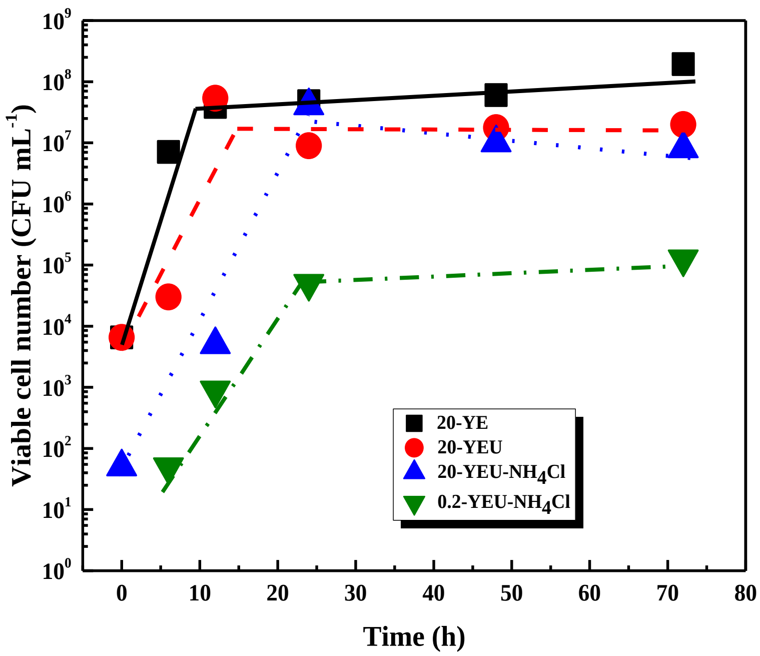

Fig. 2-9 Variations of viable cell number under initially ammonium-rich and reduced nutrient conditions (■: 20 g/L YE only; ●: 20 g/L YE with 170 mM urea; ▲: 20 g/L YE with 170 mM urea and 100 mM NH_4Cl; ▼: 0.2 g/L YE with 170 mM urea and 100 mM NH_4Cl).

2.4.3 Effect of viable cell number on ureolytic activity

Fig. 2-10 shows the relationship between viable cell number and ureolytic activity in the three different enrichment media. Under no urea or low urea concentration (≤50 mM) conditions, ureolytic activity is rather low regardless of the viable cell number, indicating that the bacterial population is not dominated by ureolytic bacteria at low urea concentration. Then, at higher urea concentration (100 and 170 mM), ureolytic activity becomes significant when a certain level of viable cell number is reached (ranging from 10^8 ~10^9 per milliliter depending on the specific enrichment media), indicating that ureolytic bacteria start to prevail overall bacterial population. After the threshold is reached, ureolytic activity increases significantly, which is accompanied by the gradual decline in overall bacterial population, mostly likely due to a decline in non-ureolytic bacterial population under elevated NH_4^+-NH_3 condition.

In previous studies, bacterial cell concentration has been found to be linearly correlated to the ureolytic activity/rate when exotic ureolytic bacteria species are used for hydrolysis (e.g., *S. pasteurii*) (Okwadha and Li 2010; Tobler et al. 2011; Lauchnor et al. 2015). In the present work, due to the presence of native soil bacteria incapable of producing urease enzyme, a linear relationship was not observed. In a similar aqueous bio-stimulation test reported by Gomez et al. (Gomez et al. 2017), ureolysis rate was also found to be negligible when aqueous total cell density was below 10^7 cells/mL. Beyond that, ureolysis rate increased dramatically with cell concentration changed little. Their threshold value 10^7 cells/mL is slightly smaller than that in our study (4×10^7~ 4×10^8 cells/mL based on 2×10^9 ~ 2×10^{10} per gram soil), possibly due to the inhibition on non-ureolytic bacteria when NH_4Cl was added into the enrichment solution.

2.4.4 The rationale to select effective medium type and urea concentration

From the analysis of the relationship between pH, electric conductivity, viable cell number and ureolytic activity, it can be found that the selection of effective medium type and urea concentration depends on whether a particular enrichment medium can:

(1) achieve the optimal pH range.
(2) establish the dominance of ureolytic activity over other metabolic activities; and
(3) stimulate sufficient native soil bacteria (thus enough ureolytic bacteria).

Based on the above discussions, two essential considerations on the selection of the enrichment media can be made:

(1) Nitrogen-rich complex enrichment media such as YE and NB are more suitable for the enrichment, especially the NBU medium.
(2) 170 mM and 100 mM urea concentration have comparable efficiency. Economically, 100 mM urea concentration is better to apply within 72 h enrichment.

From the microbiological aspect, these two measures can induce higher rate of ureolysis and higher bacterial growth rate. They will facilitate the pH reaching the optimal value of ureolytic activity, help establish the dominance of ureolytic process, and ensure enough amounts of ureolytic bacteria. Nevertheless, some other measures from engineering aspect such as the injection method, the enriching depth and the enriching duration might be also considerable.

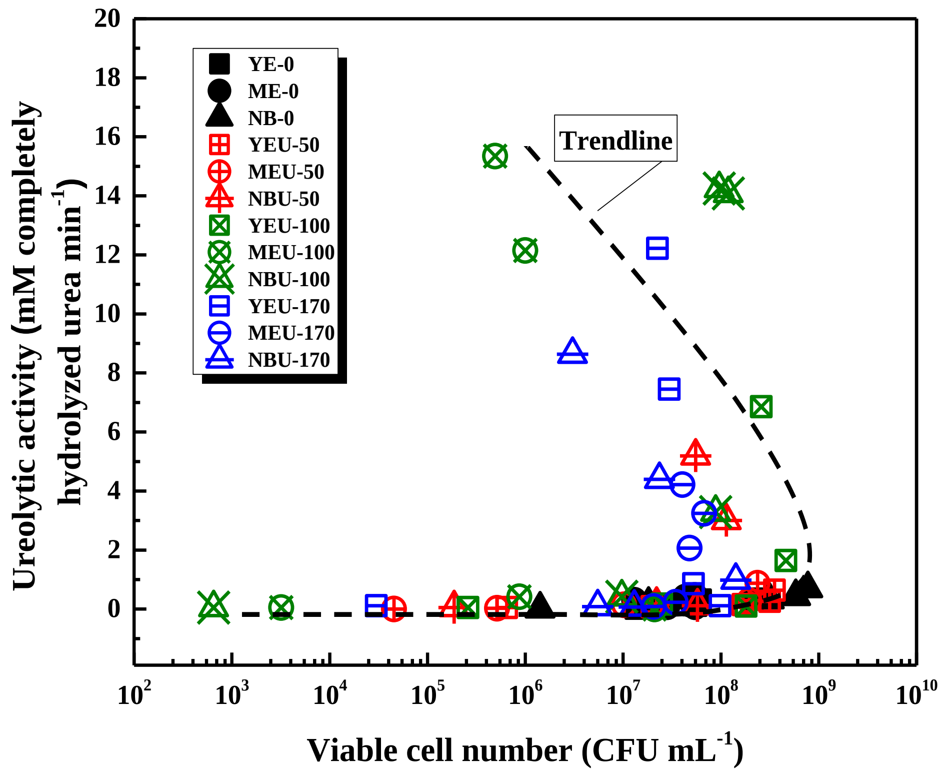

Fig. 2-10 Relationship between ureolytic activity and viable cell number.

2.4.5 The bio-stimulation in calcareous sand

According to the previous research (Harkes et al., 2010; Burbank et al., 2011; Chu et al., 2012; Cheng et al., 2013; Gat et al., 2016; Gomez et al., 2017), the bio-stimulation has already been successfully applied to the silica and other types of sand except for the calcareous sand. Calcareous sands are abundant in the coastal areas. For the further potential MICP application in the coastal areas, it is significant to ensure the successful bio-stimulation on the calcareous sand for the first step. In this section, the comparisons of the bio-stimulation results between the calcareous sand in the present work and other sands from the previous research are made.

In the solution optimization study by Gomez et al. (2017) for the native ureolytic microorganisms in quarried sands, a similar aqueous viable cell number versus elapsed time (**Fig. 2-6**) was observed. The total cell densities are both ranged from 10^7 to 10^8 approximately with a fast growing at early stage and a low growing rate at late stage of growing period. Moreover, the trends of ureolytic activity (i.e., ureolysis rate) versus viable cell number (**Fig. 2-10**) were similar for both studies, though the thresholds numbers were slightly different. In addition, the majority of urea hydrolysis process occurred within a narrow range of pH values between 9.2 and 9.4, which is consistent with the values around 9.1 and 9.2 (**Fig. 2-7**) in the present work for the higher urea concentration cases. Furthermore, a similar pH evolution trend was observed in the research conducted by Gat et al. (2016) on the stimulation in silica sand. By comparison, the results of the present work indicate that bio-stimulation can be also applied to the calcareous sand. The difference of sand properties may not have essential influence on the bio-stimulation process.

2.4.6 Effect of reduced nutrients and ammonium amendment on enrichment efficiency

As an effort to further improve the effectiveness of an ureolytic enrichment medium, two additional experiments were performed. In the first additional experiment, 100 mM NH_4Cl was added to the enrichment medium. In the second, 0.2 g/L instead of 20 g/L enrichment medium was used, which could avoid providing excess organic matters and inducing anaerobic fermentation during enriching. These two cases were first applied to the case of YEU-170.

In **Fig. 2-9**, the viable cell number and ureolytic activity were compared under two conditions: (1) initially ammonium-rich: 20 g/L YE with 170 mM urea and 100 mM NH_4Cl (20-YEU- NH_4Cl) and (2) initially reduced nutrients: 0.2 g/L YE with 170 mM urea and 100 mM NH_4Cl (0.2-YEU-NH_4Cl). It is apparent that the initially ammonium-rich condition inhibited the growth of most native soil bacteria that are neutrophilic and not capable of producing urease enzyme. Under ammonium-rich condition, enzymes inside neutrophilic bacteria can be inactivated and their vitality is lost soon (i.e., ammonium intoxication) (Sprott and Patel, 1986). That is why the total bacterial population, most of which was ureolytic bacteria, was only $10\sim10^2$ and $10^3\sim10^4$ at 0 h and 12 h, respectively. However, with elapsed time, the ureolytic bacterial population was able to reach the same order as in the case of "20-YEU", though still lower than that in the case of generic medium

(20-YE). This is because sufficient carbon and nutrient source from YE (20 g/L) and urea (170 mM) enabled the continuous growth of ureolytic bacteria. Moreover, as ureolytic bacteria were more prevailing in the case of "20-YEU-NH_4Cl" than in the case of "20-YEU", the measured ureolytic activity was also slightly higher. The above results suggest that the amendment of ammonium in the enrichment solution, though initially delays the bacteria growth, can finally lead to elevated ureolytic activity due to the elimination of non-ureolytic bacteria at the very start stage of enrichment.

On the other hand, when the nutrient level was reduced to 0.2 g/L, the bacteria growth was severely inhibited and it is likely that all nutrient sources were consumed after 24 h, resulting in the inability of bacteria for further reproduction. That is why the maximum viable cell number was below 10^5/mL in the reduced nutrient case. However, the optimal concentration of nutrient of enrichment medium still needs further research. Moreover, although the reduced nutrient condition triggered moderate ureolytic activity at 24 h, the further increase in ureolytic activity was not possible due to the depletion of YE. The above results suggest that reduced nutrients in the enrichment medium can slow the bacterial reproduction, and further limit the population of ureolytic bacteria, resulting in relatively low ureolytic activity.

2.5 Conclusions

In the present work, the effects of the enrichment medium type and initial urea concentration on the enrichment of native ureolytic bacteria in calcareous beach sand were investigated. The following conclusions are drawn from this study:

(1) The increase in ureolytic activity with time was limited in the generic media, whereas a noticeable increase could be observed in most selective media. In general, YE and NB with higher nitrogen sources have better efficiency than ME. Two different bacterial activities dominate at different stages of bio-stimulation. At the early stage when the cumulative EC value is less than 10 mS cm^{-1}, non-ureolytic bacterial metabolism is dominant. The ureolytic activity due to ureolysis process becomes dominant making the cumulative EC surpass the 10 mS cm^{-1} threshold at the later stage.

(2) Higher initial urea concentration (100 and 170 mM) inhibits the bacterial reproduction at the later stage in the selective media. In generic media and the selective media with 50 mM urea, viable cell number maintained stable until the end of the test.

(3) Reduced nutrients slow down the bacterial reproduction, and further limit the population of ureolytic bacteria, resulting in relatively low ureolytic activity. The amendment of ammonium to the enrichment media, though initially delays the bacteria growth, can finally elevates ureolytic activity due to the elimination of non-ureolytic bacteria at the very start stage of enrichment.

Further work of this research includes: (1) enriching native ureolytic bacteria in beach sands with different origins and geographical locations; (2) enriching native ureolytic bacteria in a large-scale test in real coastal environment (sand column and field); and (3) developing the protocol of MICP implementation via enriched native ureolytic bacteria.

References

Atlas RM (2005) Handbook of media for environmental microbiology, CRC Press.

Allison JB, Anderson JA, Cole WH (1938) The Method of electrical conductivity in studies on bacterial metabolism. J Bacteriol 36(6):571-586.

Al-Mailem DM, Al-Deieg M, Eliyas M, Radwan SS (2017) Biostimulation of indigenous microorganisms for bioremediation of oily hypersaline microcosms from the arabian gulf kuwaiti coasts. J Environ Manage 193:576-583. https://doi:10.1016/j.jenvman.2017.02.054.

Achal V, Pan X, Zhang D (2011) Remediation of copper-contaminated soil by kocuria flava CR1, based on microbially induced calcite precipitation. Ecol Eng 37(10):1601-1605. https://doi:10.1016/j.ecoleng.2011.06.008

Álvarez LM, Ruberto LAM, Balbo AL, Mac Cormack WP (2017) Bioremediation of hydrocarbon-contaminated soils in cold regions: development of a pre-optimized biostimulation biopile-scale field assay in antarctica. Sci Total Environ 590:194-203. https:// doi:10.1016/j.scitotenv.2017.02.204

Booth IR (1985) Regulation of cytoplasmic pH in bacteria. Microbiol. Rev. 49(4):359-378.

Bhaduri S, Ghosh T, Montemagno C, Kumar A (2017) *Sporosarcina Pasteurii* can form nanoscale crystals on cell surface. BioRxiv 184184. https://doi.org/10.1101/184184

Bibi S, Oualha M, Ashfaq MY, Suleiman MT, Zouari N (2018) Isolation, differentiation and biodiversity of ureolytic bacteria of qatari soil and their potential in microbially induced calcite precipitation (MICP) for soil stabilization. RSC Adv 8(11):5854-5863. https:// doi:10.1039/c7ra12758h

Burbank MB, Weaver TJ, Green TL, Williams BC, Crawford RL (2011) Precipitation of calcite by indigenous microorganisms to strengthen liquefiable soils. Geomicrobiol J 28(4):301-312. https:// doi:10.1080/01490451.2010.499929

Contreras-Rodriguez A, Quiroz-Limon J, Martins AM, Peralta H, Avila-Calderon E, Sriranganathan N, Boyle SM, Lopez-Merino A (2008) Enzymatic, immunological and phylogenetic characterization of brucella suis urease. BMC Microbiol 8(1):121. https:// doi:10.1186/1471-2180-8-121

Copeland RA (2000) Enzymes, a practical introduction to structure, mechanism, and data analysis, 2nd Ed., Wiley-VCH, New York.

Cheng L, Cord-Ruwisch R, Shahin MA (2013) Cementation of sand soil by microbially induced calcite precipitation at various degrees of saturation. Can Geotech J 50(1):81-90. https:// doi:10.1139/cgj-2012-0023

Cheng L, Shahin MA, Cord-Ruwisch R, Addis M, Hartanto T, Elms C (2014) Soil stabilisation by microbial-induced calcite precipitation (MICP): Investigation into some physical and environmental aspects. In Proceedings of 7th International Congress on Environmental Geotechnics: iceg2014, pp. 1105.

Cheng L, Yang Y, Chu J (2018) In-situ microbially induced Ca_2^+-alginate polymeric sealant for seepage control in porous materials. Microb Biotechnol 12(2):324-333. https:// doi:10.1111/1751-7915.13315

Chu J, Stabnikov V, Ivanov V (2012) Microbially induced calcium carbonate precipitation on surface or in the bulk of soil. Geomicrobiol J 29(6):544-549. https:// doi:10.1080/01490451.2011.592929

Dejong JT, Fritzges MB, NÜSslein K (2006) Microbially induced cementation to control sand response to undrained shear. J Geotech Geoenviron. Eng. 132(11):1381-1392. https:// doi:10.1061/(asce)1090-0241(2006)132:11(1381)

Dhami NK, Quirin MEC, Mukherjee A (2017) Carbonate biomineralization and heavy metal remediation by calcifying fungi isolated from karstic caves. Ecol Eng 103:106-117. https:// doi:10.1016/j.ecoleng.2017.03.007

Evans Jr DJ, Evans DG, Kirkpatrick SS, Graham DY (1991) Characterization of the helicobacter pylori urease and purification of its subunits. Microbiol Pathogenesis 10(1):15-26. https:// doi:10.1016/0882-4010(91)90062-f

Gat D, Ronen Z, Tsesarsky M (2016) Soil bacteria population dynamics following stimulation for ureolytic microbial-induced $CaCO_3$ precipitation. Environ Sci Technol 50(2):616-624. https:// doi:10.1021/acs.est.5b04033

Gomez MG, Anderson CM, Graddy CM, DeJong JT, Nelson DC, Ginn TR (2016) Large-scale comparison of bioaugmentation and biostimulation approaches for biocementation of sands. J Geotech Geoenviron Eng 143(5):04016124. https:// doi:10.1061/(asce)gt.1943-5606.0001640

Gomez MG, Graddy CM, DeJong JT, Nelson DC, Tsesarsky M (2017) Stimulation of native microorganisms for biocementation in samples recovered from field-scale treatment depths. J Geotech Geoenviron Eng 144(1):04017098. https:// doi:10.1061/(asce)gt.1943-5606.0001804

Graddy CMR, Gomez MG, Kline LM, Morrill SR, DeJong JT, Nelson DC (2018) Diversity of sporosarcina-like bacterial strains obtained from meter-scale augmented and stimulated biocementation experiments. Environ Sci Technol 52(7):3997-4005. https:// doi:10.1021/acs.est.7b04271

George EF, Hall MA, De Klerk GJ (2008) The components of plant tissue culture media ii: organic additions, osmotic and pH effects, and support systems, In: plant propagation by tissue culture, Dordrecht, pp. 115-173. https:// doi:10.1007/978-1-4020-5005-3_4

Harkes MP, Van Paassen LA, Booster JL, Whiffin VS, van Loosdrecht MC (2010) Fixation and distribution of bacterial activity in sand to induce carbonate precipitation for ground reinforcement. Ecol Eng 36(2):112-117. https:// doi:10.1016/j.ecoleng.2009.01.004

Horner-Devine MC, Carney KM, Bohannan BJ (2004) An ecological perspective on bacterial biodiversity. Proc R Soc Lond B. 271(1535):113-122. https:// doi:10.1098/rspb.2003.2549

Hoddinott MH, Reid GA, Ingledew WJ (1978) The respiratory chain and proton electrochemical gradient in the alkalophile *Bacillus Pasteurii*. Biochem Soc Trans 6: 1295−1298. https:// doi:10.1042/bst0061295

Hecker M, Völker U (2001) General stress response of bacillus subtilis and other bacteria. Microb Physiol 44:35-91. https:// doi:10.1016/s0065-2911(01)44011-2

Jahns T (1996) Ammonium urea-dependent generation of a proton electrochemical potential and synthesis of ATP in *Bacillus pasteurii*. J Bacteriol 178(2):403−409. https:// doi:10.1128/jb.178.2.403-409.1996

Jiang NJ, Soga K (2016) The Applicability of microbially induced calcite precipitation (MICP) for internal erosion control in gravel–sand mixtures. Géotechnique 67:42-55. https:// doi:10.1680/jgeot.15.p.182

Jiang NJ, Soga K, Dawoud O (2014) Experimental study of the mitigation of soil internal erosion by microbially induced calcite precipitation. In Geo-Congress. 1586-1595. https:// doi:10.1061/9780784413272.155

Jiang NJ, Soga K, Kuo M (2016) Microbially induced carbonate precipitation for seepage-induced internal erosion control in sand–clay mixtures. J Geotech Geoenviron Eng 143(3): 04016100. https:// doi:10.1061/(asce)gt.1943-5606.0001559

Kang CH, Han SH, Shin Y, Oh SJ, So JS (2014) Bioremediation of Cd by microbially induced calcite precipitation. Appl Biochem Biotechnol 172(6):2907-2915. https:// doi:10.1007/s12010-013-0626-z

Krishnamurti K, Kate SR (1951) Changes in electrical conductivity during bacterial growth. Nature 168(4265):170. https:// doi:10.1038/168170b0

Kaltwasser H, Krämer J, Conger WR (1972) Control of urease formation in certain aerobic bacteria. Archiv FÜR Mikrobiologie 81(2):178-196. https:// doi:10.1007/bf00412327

Kang CH, Shin Y, Anbu P, Nam IH, So JS (2016) Biosequestration of copper by bacteria isolated from an abandoned mine by using microbially induced calcite precipitation. J Gen Appl Microbiol 62(4):206-212. https:// doi:10.2323/jgam.2016.03.001

Kolter R, Siegele DA, Tormo A (1993) The stationary phase of the bacterial life cycle. Annu Rev Microbiol 47(1):855-874. https:// doi:10.1146/annurev.mi.47.100193.00423

Lian B, Hu Q, Chen J, Ji J, Teng HH (2006) Carbonate biomineralization induced by soil bacterium *Bacillus megaterium*. Geochim Cosmochim Acta 70(22):5522-5535. https:// doi:10.1016/j.gca.2006.08.044

Lauchnor EG, Topp DM, Parker AE, Gerlach R (2015) Whole cell kinetics of ureolysis by *Sporosarcina pasteurii*. J Appl Microbiol 118(6):1321-1332. https:// doi:10.1111/jam.12804.

Maleki M, Ebrahimi S, Asadzadeh F, Tabrizi ME (2016) Performance of microbial-induced carbonate precipitation on wind erosion control of sandy soil. Int J Environ Sci Technol 13(3):937-944. https:// doi:10.1007/s13762-015-0921-z.

Mookerjee SA, Goncalves RL, Gerencser AA, Nicholls DG, Brand MD (2015) The contributions of respiration and glycolysis to extracellular acid production. Biochim Biophys Acta 1847(2):171-181. https:// doi:10.1016/j.bbabio.2014.10.005.

Mortensen BM, Haber MJ, DeJong JT, Caslake LF, Nelson DC (2011) Effects of environmental factors on microbial induced calcium carbonate precipitation. J Appl Microbiol 111(2): 338-349. https:// doi:10.1111/j.1365-2672.2011.05065.x.

Morsdorf G, Kaltwasser H (1989) Ammonium assimilation in *Proteus vulgaris*, *Bacillus pasteurii*, and *Sporosarcina urea*. Arch Microbiol 152(2):125-131.

Müller T, Walter B, Wirtz A, Burkovski A (2006) Ammonium toxicity in bacteria. Curr Microbiol 52(5):400-406.

Noble PA (1999) Hypothetical model for monitoring microbial growth by using capacitance measurements-a minireview. J Microbiol Methods 37(1):45–49. https:// doi:10.1016/s0167-7012(99)00041-x.

Nakajima J, Sakka M, Kimura T, Furukawa K, Sakka K (2008) Enrichment of anammox bacteria from marine environment for the construction of a bioremediation reactor. Appl Microbiol Biotechnol 77(5):1159-1166. https:// doi:10.1007/s00253-007-1247-7.

Okwadha GD, Li J (2010) Optimum conditions for microbial carbonate precipitation. Chemosphere 81(9):1143-1148. https:// doi:10.1016/j.chemosphere.2010.09.066.

Phang IRK, San Chan Y, Wong KS, Lau SY (2018) Isolation and characterization of urease-producing bacteria from tropical peat. Biocatal Agric Biotechnol 13:168-175. https:// doi:10.1016/j.bcab.2017.12.006.

Roy A, Dutta A, Pal S, Gupta A, Sarkar J, Chatterjee A, Saha A, Sarkar P, Sar P, Kazy SK (2018) Biostimulation and bioaugmentation of native microbial community accelerated bioremediation of oil refinery sludge. Bioresour Technol 253:22-32. https:// doi:10.1016/j.biortech.2018.01.004.

Sutton S (2006) Measurement of cell concentration in suspension by optical density. Microbiology 585: 3-12.

Sprott GD, Patel GB (1986) Ammonia toxicity in pure cultures of methanogenic bacteria. Syst Appl Microbiol 7(2-3):358-363. https:// doi:10.1016/s0723-2020(86)80034-0.

Somerville GA, Proctor RA (2013) Cultivation conditions and the diffusion of oxygen into culture media: the rationale for the flask-to-medium ratio in microbiology. BMC Microbiol 13(1):9. https:// doi:10.1186/1471-2180-13-9.

Tobler DJ, Cuthbert MO, Greswell RB, Riley MS, Renshaw JC, Handley-Sidhu S, Phoenix VR (2011) Comparison of rates of ureolysis between *Sporosarcina pasteurii* and an indigenous groundwater community under conditions required to precipitate large volumes of calcite. Geochim Cosmochim Acta 75(11):3290-3301. https:// doi:10.1016/j.gca.2011.03.023.

Van Paassen LA (2009) Biogrout, ground improvement by microbial induced carbonate precipitation [dissertation]: Delft University of Technology, Netherlands.

Van Tittelboom K, De Belie N, De Muynck W, Verstraete W (2010) Use of bacteria to repair cracks in concrete. Cem Concr Res 40:57-166. https:// doi:10.1016/j.cemconres.2009.08.025.

Watson SW (1965) Characteristics of a marine nitrifying bacterium, *Nitrosocystis Oceanus Sp. N. 1*. Limnol Oceanogr 10 (suppl):R274-R289.

Whiffin VS (2004) Microbial $CaCO_3$ precipitation for the production of biocement [dissertation]: Murdoch University, Perth, Australia.

Wiley WR, Stokes JL (1962) Requirement of an alkaline pH and ammonia for substrate oxidation by *Bacillus pasteurii*. J Bacteriol 84(4):730−734.

Zamani A, Liu Q, Montoya BM (2018) Effect of microbial induced carbonate precipitation on the stability of mine tailings. In IFCEE2018, pp. 291-300. https:// doi:10.1061/9780784481615.024.

CHAPTER 3. Biochemical Characteristics under Sand Column Condition and Shearing Behaviors of Bio-cemented Calcareous Sand

3.1 Introduction

In the previous chapter, the effect of enrichment media and the biochemical characteristics under solution condition have been investigated. In this chapter, the biochemical properties under sand column situation were studied. Furthermore, we conducted a comprehensive experimental program to systematically investigate the shear behavior of bio-cemented calcareous sand treated by bio-stimulated MICP through direct shear tests.

In terms of the shearing behaviors, DeJong et al. (2010) confirmed that the densification and bonding effect of bio-cementation could improve the shear strength and stiffness of silica sand. Nafisi et al. (2020) indicated the effect of cementation was more pronounced at lower confining stress, and surface roughness due to precipitation was recognized as a significant contributor to the shear strength of MICP-treated samples. Feng and Montoya (2016) reported that the stiffness, peak shear strength, and dilatancy of sand increased with the elevated calcite content at a given effective confining pressure. Liu et al. (2019) found that the peak cohesion intercept increased with increasing cementation solution/sample volume ratio, while the peak friction angles remained constant. Cui et al. (2017) reported a significant improvement of triaxial shear strength of bio-cemented calcareous sand with the increasing cementation level in terms of the strength parameters such as the effective frictional angle and effective cohesion. It is worth noting that most of these studies used the bio-augmented MICP approach, and there are rather limited studies examining the shear behavior of bio-cemented sand treated by the bio-stimulated MICP approach.

3.2 Materials and Methods

3.2.1 Sand

The sand in this study was sampled from the supratidal zone of Waikiki beach, Honolulu, Hawaii, USA. The sand was collected from the surface layer (depth up to 5 cm) where most aerobic microbes could survive. Its grain size distribution curve is shown in **Fig. 3-1**. Prior to the experiment, the sand was passed through No.10 sieve with opening size of 2 mm to remove oversized grains. Small twigs and grass were also picked out from the samples. Other basic physical properties of the calcareous sand are listed in **Table 3-1**.

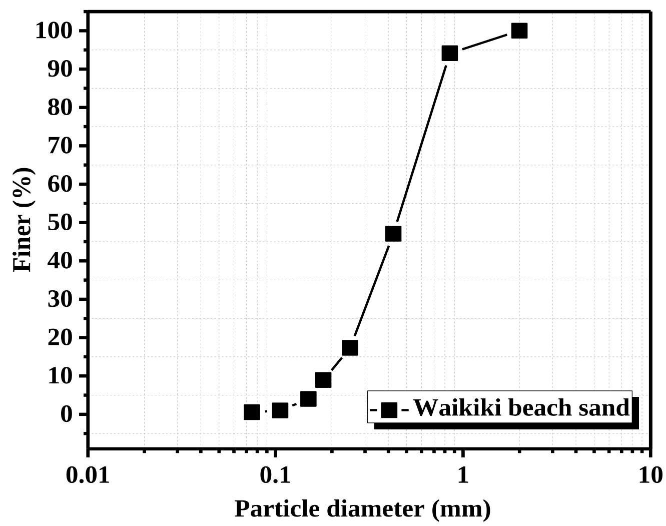

Fig. 3-1 Particle size distribution curve of sampled calcareous sand.

3.2.2 Enrichment Media and Cementation Solution

Two selective enrichment media were developed in this study to stimulate native urease-positive bacteria. The first one contained 20 g/L yeast extract (YE) + urea and the second one contained 20 g/L nutrient broth (NB) + urea. The selection of the nutrient concentration was based on the author's previous study (Wang et al. 2020), in which 20g/L showed the highest ureolytic activity. The Urea concentration in the enrichment media ranged from 0 to 170 mM. The cementation solution consisted of equivalent concentration (i.e., 0.3 or 0.5 M) of urea and $CaCl_2$ with 0.2 g/L YE or NB. The purpose of adding 0.2 g/L YE or NB was to maintain bacteria viability during the cementation stage.

3.2.3 Enrichment Test

The bio-stimulated MICP was achieved through two stages: bacteria enrichment and cementation. An enrichment test was firstly conducted to identify optimized enrichment parameters for the subsequent cementation stage. 300 g Fresh calcareous sand was firstly mixed thoroughly with 35 mL enrichment media under partially saturated condition (approximately 50% saturation and 12% water content). Then the moist sand was tamped into cylindrical PVC columns with height of 10.4 cm and inner diameter of 5.2 cm in three layers to reach the initial relative density (D_r) of 67.2%. Specimens were prepared in duplicate. The sand columns were left at 20°C and 52% relative humidity for up to 72 hours for bacteria enrichment. It should be noted that the sand was only mixed with enrichment solution once during the process of sample preparation, thus no additional enrichment solution was injected. The viable cell number, and urea/ammonium concentration during enrichment were measured at 0, 6, 12, 18, 24, 48 and 72 hours, respectively. Therefore, the total amounts of sand columns that needed to be prepared for enrichment were 14 (7×2). The measuring methods will be interpreted later in another independent section. The results obtained from enrichment tests were used to determine the optimized initial urea concentration and enrichment time for the subsequent bio-cementation process.

Table 3-1 The physical properties of collected sand.

Characteristic	Value
Soil classification (ASTM D2487)	SP
Coefficient of curvature C_c	0.816
Coefficient of uniformity C_u	2.5
Specific gravity, G_s (g/cm^3)	2.7
Maximum void ratio e_{max}	0.888
Minimum void ratio e_{min}	0.271
Carbonate content (%)	⩾99.5
Initial natural moisture content (%)	1-2

3.2.3 Microbial Community Analysis of Bio-stimulated Samples

The microbial community present in the pore fluid before and after the enrichment stage was determined by 16S metagenomic sequencing. The additional three soil samples (i.e., untreated, YE-treated, and NB-treated) were made for the analysis. The DNA was extracted from 1 g moisture soil samples using Omega® Soil DNA Extraction Kit. The total extracted DNA concentrations were 0.43 ng/μL, 10.13 ng/μL, and 5.99 ng/μL for untreated, YE-treated, and NB-treated sample, respectively, measured with Quant-iT

PicoGreen. Triplicate 16S V3-V4 amplicons for high-throughput analysis were generated using the primers (Forward Primer = 5'TCGTCGGCAGCGTCAGATGTGTATAAGAG ACAGCCTACGGGNGGCWGCAG; Reverse Primer = 5'GTCTCGTGGGCTCGGAGA TGTGTATAAGAGACAGGACTACHVGGGTATCTAATCC).

3.2.4 Bio-cemented Samples for Direct Shear Test

Based on the optimized enrichment parameters obtained from the enrichment test in Chapter 2, bio-cemented samples were prepared for the direct shear test. Direct shear samples were prepared using brass rings with height of 2.54 cm and inner diameter of 6.35 cm. The preparation method was the same as the samples used for the above enrichment tests. Specifically, the fresh sand was firstly mixed with 14 mL corresponding enrichment medium. The solid-to-liquid ratio was the same as that in the enrichment test. Then, it was compacted in brass rings to achieve two distinct relative densities (16.2% and 54.6%). The specimens were left for 48 hours to stimulate the growth of native bacteria. After that, cementation solution was flushed from top to bottom of the specimens by surface percolation without applying extra confining pressure once per day for consecutive 5 or 10 days. The volume of flushed cementation solution each cycle was 1.5 PV. The flushing rate was kept around 2 mm/min. The effluent liquid was collected for the immediate measurement of aqueous urea and ammonium concentration. Upon the completion of the bio-cementation treatment, the specimens were carefully extruded from brass rings and oven dried for 24 hours prior to the direct shear test, thus the dry bio-cemented specimens were used for direct shear tests. A total of 80 tests were then performed on the specimens at 50, 100, 200, 400, and 600 kPa normal stresses using the Geocomp® ShearTrac-II-DSS Direct Shear Apparatus. The shear rate was kept constant at 1 mm/min. For comparison, untreated sand samples with the same relative densities were also tested. All cases tested in the study are listed in **Table 3-2**. The designation "*a*M_*b*d_*c*(*d*)" represents the bio-cemented sample treated with *b* days of flush of *a*M cementation solution. *c* is the nutrient type (YE or NB) and *d* is relative density level (low or high).

3.2.5 Biochemical and Microstructural Monitoring

The biochemical measurements included viable cell number, urea and ammonium concentration, and cementation content. Plate counting method was used to obtain the viable cell number, and the concentrations of urea and ammonium were determined spectrophotometrically via measuring the absorbance at 425 and 422 nm wavelength, respectively (Greenburg et al., 1992; Knorst et al., 1997). More details of the measurements could be found in our preliminary study (Wang et al., 2020). The cementation content was determined by measuring the dry weight difference of the intact sand specimens prior to and after the MICP treatment. The specimen after bio-stimulated MICP treatment was flushed by distilled water to wash away residual dissoluble chemicals. Moreover, the microstructural features of bio-cemented sand and the shearing interface were characterized through optical microscopy using a Nikon SMZ1500 stereo microscope.

Table 3-2 The program of bio-cemented sand for direct shear tests.

Specimen	D_r (%)	Enrichment		Bio-cementation			Direct shear
		[Nutrient] (g/L)	[Urea] (mM)	[$CaCl_2$] (M)	[Urea] (M)	Time (days)	Normal stress (kPa)
0.3M_5d_YE(L)	16.2	20	170	0.3	0.3	5	50, 100, 200, 400, 600
0.3M_10d_YE(L)				0.3	0.3	10	
0.5M_5d_YE(L)				0.5	0.5	5	
0.5M_10d_YE(L)				0.5	0.5	10	
0.3M_5d_NB(L)				0.3	0.3	5	
0.3M_10d_NB(L)				0.3	0.3	10	
0.5M_5d_NB(L)				0.5	0.5	5	
0.5M_10d_NB(L)				0.5	0.5	10	
0.3M_5d_YE(H)	54.6	20	170	0.3	0.3	5	
0.3M_10d_YE(H)				0.3	0.3	10	
0.5M_5d_YE(H)				0.5	0.5	5	
0.5M_10d_YE(H)				0.5	0.5	10	
0.3M_5d_NB(H)				0.3	0.3	5	
0.3M_10d_NB(H)				0.3	0.3	10	
0.5M_5d_NB(H)				0.5	0.5	5	
0.5M_10d_NB(H)				0.5	0.5	10	

3.3 Results and Data Interpretation

3.3.1 Ureolytic activity (UA)

Fig. 3-2 showed the change in viable bacterial cell number with time at the bio-stimulation stage. It could be seen that the viable cell number raised from around 10^4 /g soil to 10^7/g soil at the first 18 h, regardless of the initial urea concentration. Starting from 24 h, the cases with higher initial urea concentration saw a drop in viable cell number. For example, in YE-170 mM and NB-170 mM, the viable cell number was only around 10^5 /g sand after 72 h. On the other hand, the cases with lower initial urea concentration had only marginal reduction (100 mM urea case) or even slight increase (50 mM urea case) in viable cell number. Finally, the evolution of viable cell numbers was quite similar among the two enrichment media.

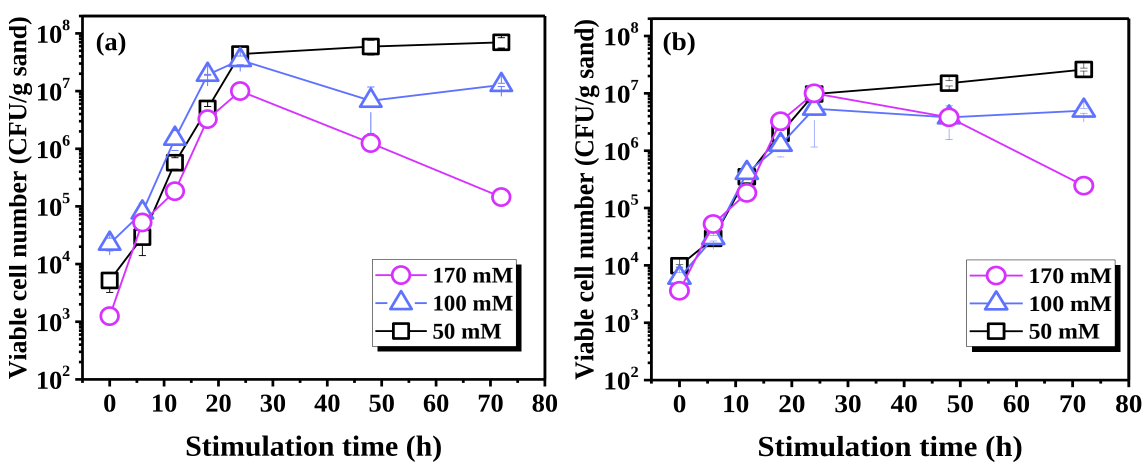

Fig. 3-2 The change in viable cell number with time: (a) yeast extract (YE), (b) nutrient broth (NB).

During the first 18 h, the similar viable cell number pattern among all cases was attributed to the non-selective growth of indigenous bacteria. This was substantiated by urea and ammonium concentration results which showed relatively low ureolytic activity in initial 18 h, meaning that ureolytic bacteria was not dominant during this period. After 24 h of enrichment, the microbial population was dominated by ureolytic bacteria, as evidenced by more significant ureolysis. The production of massive ammonium from ureolysis at this stage suppressed the growth and survival of non-ureolytic bacteria (Wang et al. 2020). In particular, more non-ureolytic bacteria became non-viable at higher urea concentration, leading to the drop in overall viable cell number.

3.3.2 Urea and Ammonium Concentrations at Enrichment Stage

Urea is the key component in the selective enrichment media for indigenous ureolytic bacteria. During bio-stimulation process, urea is hydrolyzed to aid the growth and reproduction of native ureolytic bacteria (Tsesarsky et al., 2016). Therefore, if bio-stimulation is effectively occurring in soil, a reduction in urea and increase in ammonium (product of ureolysis) concentration is expected. The urea hydrolysis or ammonium production rate could be used to evaluate the generated ureolytic activity in soil (Tsesarsky et al., 2016; Gat et al., 2016).

The evolution of urea and ammonium concentration with time in this study was shown in **Fig. 3-3**. In both YE and NB cases, urea concentration dropped gradually with time. At 170 mM urea concentration, the ureolysis rate was relatively slow at the first 18 h. From 24 h onward, urea was hydrolyzed at a much faster rate and was almost depleted at 48 h after the start of bio-stimulation. For lower urea concentration (50 and 100 mM), the urea was hydrolyzed at a slower but steady rate, and was almost fully depleted at 48 h. For ammonium concentration, it remained undetected at the first 12 h in both YE and NB case regardless of initial urea concentration, indicating the ureolysis was not significant during this period. Between 12 h and 48 h, higher urea concentration cases (i.e., 170 mM) showed the fastest ammonium production rate in both YE and NB case. After 24h in the lower urea concentrations cases (i.e., 50mM and 100 mM), ammonium concentration either increased very slowly or started to drop, indicating the completion of urea hydrolysis. It should be noted that the stoichiometric relationship between hydrolyzed urea and produced ammonium concentration did not strictly follow 1:2. This was likely due to the ammonification process, in which large organic molecules were depolymerized into ammonium.

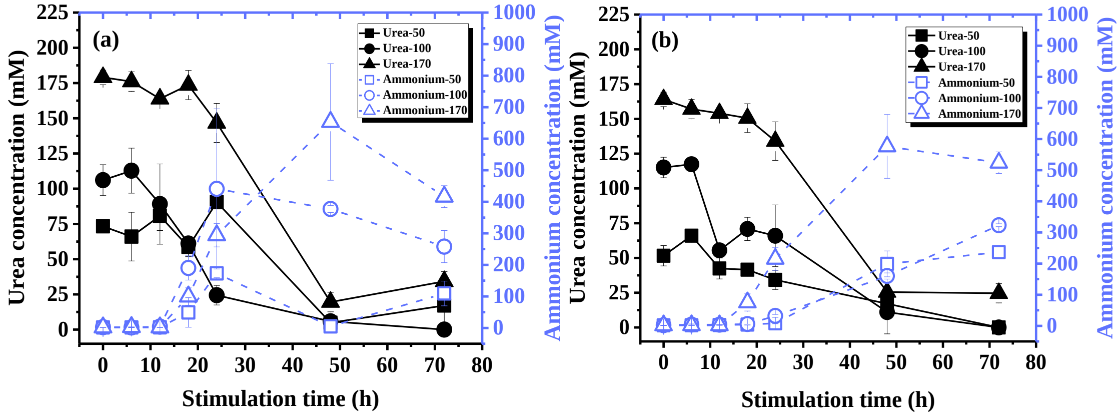

Fig. 3-3 The evolution of urea and ammonium concentration with time: (a) cases amended with yeast extract (YE), (b) cases amended with nutrient broth (NB).

3.3.3 Microbial Community Analysis

The relative abundance of different microbial community presented in **Fig. 3-4** also confirmed such similarity. It was apparent that the microbial community changed significantly due to the enrichment process. In the original soil without treatment, the microbial genera were diverse and 39% were *Actinobacteriota*, while Firmicutes took over after enrichment in both YE- and NB-treated soil. The microbial community exhibited a similar pattern in YE- and NB-treated soil where the abundance of common urease-positive genera such as Sporosarcina and Bacillus increased from less than 0.1% to 19% and 25%, respectively. This was also shown in the study by Graddy et al. (2021). In addition, the existence of genus *lysinibacillus* was found to contribute to MICP process (Kang and Kwon, 2016; Ekprasert et al., 2020).

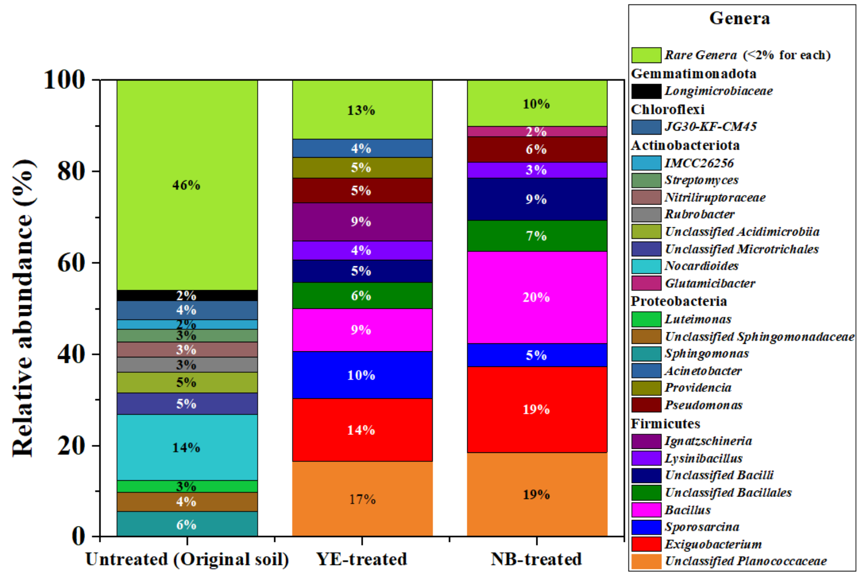

Fig. 3-4 High-throughput 16S community analysis. (Note: Plots are colored according to genus-level classification).

3.3.4 Biochemical Response at Bio-cementation Stage

At the bio-cementation stage, the effluent from the samples during each cycle of cementation solution flushing was subjected to the urea concentration measurement and the results were shown in **Fig. 3-5**. Clearly, the urea concentration decreased substantially after the first two days of cementation solution flush. This indicated that rapid ureolysis occurred due to the presence of high ureolytic activity in sand after the enrichment process. Then, with further cycles of cementation solution flushing, the urea concentration in effluent recovered gradually (probably due to the error caused by large dilution factor) or remain stable, which was a result of the stable or slightly decreasing ureolysis rate. At the end of 10 d of cementation solution flush, the urea concentration in the four cases were 190 mM (0.3M_YE), 425 mM (0.5M_YE), 275 mM (0.3M_NB), and 360 mM (0.5M_NB). The measured urea concentration changed clearly demonstrated the effectiveness of the bio-stimulated bio-cementation approach, as urea was found to be continuously depleted during the bio-cementation process.

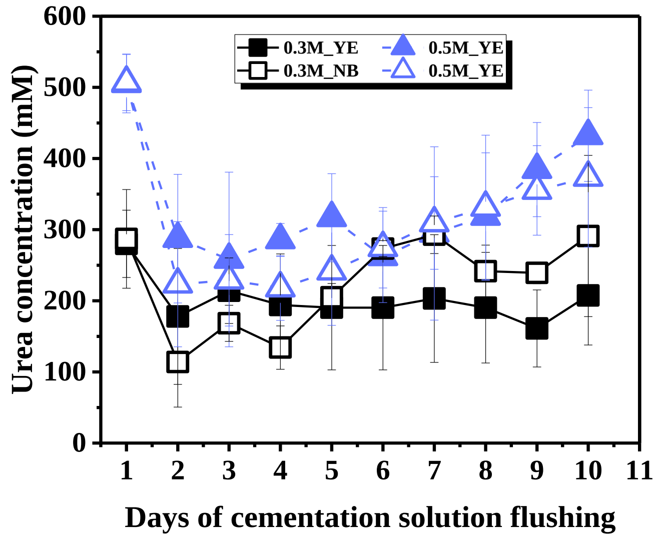

Fig. 3-5 The urea concentration during the bio-cementation stage.

The measured cementation content of samples in all 16 cases was shown in **Table 3-3**, which ranged from 1.40% to 6.79%. It could be seen that, for a specific nutrient medium and initial D_r, cementation content increased with cementation solution concentration as well as days of flushing. Furthermore, increasing initial D_r resulted in the reduction in cementation content in almost all cases, assuming other conditions the same. This phenomenon was also observed by other researchers (Tsukamoto et al., 2013; Rowshanbakht et al., 2016), which was, on one hand, due to the decreasing pore volumes for the nucleation sites of calcite in higher initial D_r, and on the other hand, the decreasing amounts of microbes and nutrients that could be absorbed in the higher initial D_r samples. Finally, while the measured cementation content of NB samples was in general slightly smaller than that of YE ones, it seemed the small difference did not lead to very different shear strength behaviors based on the shear strength results reported in the following section.

3.3.5 Peak Stress Ratio

Stress ratio is the shear stress normalized by the normal stress under the direct shear condition, which is widely used in previous studies to represent sand shear behavior during direct shear tests (Dai et al. 2016; van Paassen et al. 2012). From the direct shear test, the stress ratio - shear strain and vertical displacement - shear strain relationships could be immediately obtained. **Fig. 3-6** showed an example of a representative case (0.5M_5d_NB (H)). An evident peak in stress ratio occurred at various normal stress levels. With the increase of normal stress, the peak tended to diminish gradually. The bio-cemented sand exhibited an evolution from a brittle strain softening behavior towards a gentle strain softening behavior. Also, at lower normal stress, the cementation can significantly enhance the dilative behavior as shown in the vertical displacement response.

Table 3-3 Cementation content of bio-cemented calcareous sand.

Specimen	Cementation content (%)
0.3M_5d_YE (L)	1.86 (±0.54)
0.5M_5d_YE (L)	3.63 (±0.30)
0.3M_10d_YE (L)	4.27 (±0.34)
0.5M_10d_YE (L)	6.33 (±1.13)
0.3M_5d_NB (L)	1.55 (±0.06)
0.5M_5d_NB (L)	2.22 (±0.27)
0.3M_10d_NB (L)	3.80 (±0.24)
0.5M_10d_NB (L)	6.79 (±0.24)
0.3M_5d_YE (H)	1.58 (±0.22)
0.5M_5d_YE (H)	2.88 (±0.41)
0.3M_10d_YE (H)	3.60 (±0.15)
0.5M_10d_YE (H)	6.26 (±0.56)
0.3M_5d_NB (H)	1.40 (±0.20)
0.5M_5d_NB (H)	2.83 (±0.25)
0.3M_10d_NB (H)	2.31 (±0.39)
0.5M_10d_NB (H)	5.87 (±0.40)

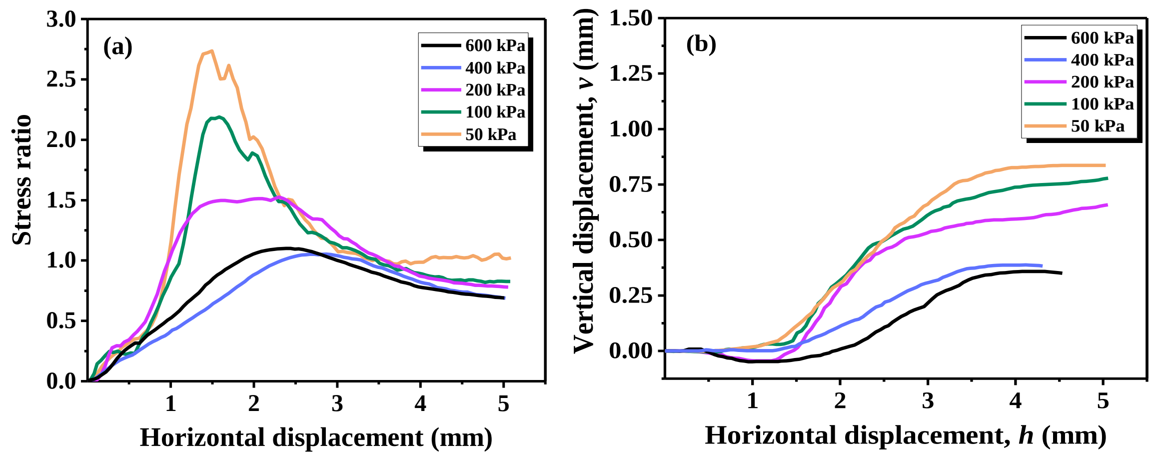

Fig. 3-6 The shear response of representative bio-cemented samples (0.5M_5d_NB(H)) at different cementation level and normal stress.

The results of peak stress ratio (η_p), which indicates the failure of samples, and its relationship with cementation content were exhibited in **Fig. 3-7**. Firstly, it can be clearly seen that η_p increased with cementation content at an identical normal stress, regardless of initial D_r. However, the effect of cementation content on η_p was diminishing with elevated normal stress. For instance, for all samples at 50 kPa normal stress, the η_p increased from 1.37 at 1.86% cementation to 5.84 at 6.33% cementation. However, the η_p at 600 kPa normal stress only increased from 0.72 at 2.22% cementation to 1.52 at 5.87% cementation. Secondly, it was obvious that η_p in general decreased with elevated normal stress at an identical cementation content. In addition, the initial D_r also affected η_p. More specifically, at an identical normal stress, higher initial D_r was corresponding to larger η_p in 32 out of 40 cases. For high initial D_r samples, the η_p was reduced from 2.16~5.54 at 50 kPa to 0.93~1.52 at 600 kPa normal stress. For low initial D_r samples, it was reduced from 1.37~4.26 at 50 kPa to 0.72~0.90 at 600 kPa normal stress. Finally, the effect of nutrient type on η_p seemed to be marginal, though NB outperformed YE in 24 out of 40 cases.

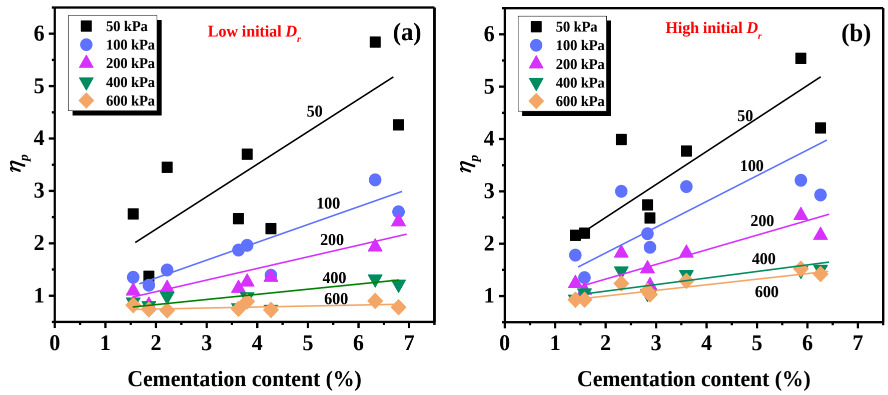

Fig. 3-7 The evolution of η_p as a function of cementation content: (a) low initial D_r; (b) high initial D_r.

To better capture the variation of η_p in various specimens with different cementation contents. **Fig. 3-8** presented the evolution of η_p as a function of normal stress in different specimens. The main observations are quite similar with that shown in **Fig. 3-7**. However, one thing worth mentioning was that at high normal stress, the η_p values of low initial D_r specimens were slightly smaller than that of untreated clean sands. For high initial D_r specimens, however, this did not happen. This observation was probably due to the localized bonding breakage during shearing that changed the interlocking and particle rearrangement behaviors of the shear interface. More detailed explanation will be presented in the "Discussion" section.

Finally, some results performed by other researchers were also presented here for comparison in terms of η_p as an important strength parameter. Van Paassen et al. (2012) found that the maximum η_p of bio-cemented gravel ranged from 2 to 4.5 at the cementation ($CaCO_3$) content between 10 and 65 kg/m^3 under 5 kPa normal stress. According to the research conducted by Amini Kiasari et al. (2019), the maximum of η_p of bio-cemented poorly graded silica sand through bio-stimulation could reach 1.72 at 54 kPa after 21-day treatment. Azadi et al. (2017) reported the η_p of bio-cemented silica sand was approximately 16.2, 9.5, 6.67 and 5.65 at 50, 100, 150 and 200 kPa, respectively.

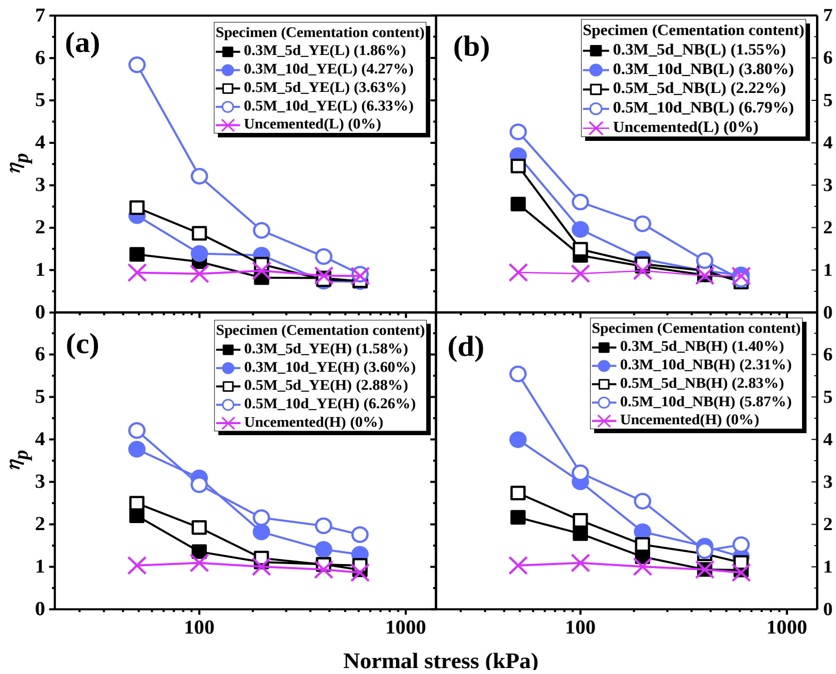

Fig. 3-8 The evolution of η_p as a function of normal stress in semi-log scale.

3.3.6 Failure Envelopes

The linear Mohr-Coulomb (M-C) failure envelope is widely used to predict the state of stresses at failure by strength parameters (c and ϕ). The shear strength of soil includes both “friction” and “cohesion” components. In the system of direct shear, the intercept of this linear failure envelope towards zero normal stress at which the “friction” component equals zero gives a cohesion (c). However, the experimental evidence shows that the failure envelope is curved for some types of soils. It is also found that the linear M-C model could overestimate cohesion at lower stress levels (Lefebvre, 1981; Maksimovic, 1989). These issues can be abated by developing a more accurate model for the estimation of strength parameters. In this study, the M-C linear as well as bilinear failure envelopes were adopted to obtain strength parameters of the bio-cemented sand (Nouri et al., 2006; Consoli et al., 2007; Hajiabdolmajid et al., 2002). In particular, the bilinear failure envelope was composed of two segments of best fitting straight lines. The shear strength parameters were estimated for these two normal stress ranges, with the first one ranging from 50 kPa to 200 kPa, and the second one from 200 kPa to 600 kPa. However, it should be mentioned that

200 kPa was not necessarily the exact turning point of the bilinear failure envelope. The selection of 200 kPa was merely targeted to predict the cohesion in a more accurate way. Therefore, two sets of peak friction angle and cohesion were obtained from the bilinear failure envelope (i.e., ϕ_1, c_1, and ϕ_2, c_2). The shear strength parameters obtained from M-C linear and bilinear failure envelopes for various specimens were listed in **Table 3-4** and **3-5**. It was found that, for 13 out of 16 specimens, the friction angle (ϕ_2) at higher normal stress (i.e., 200-600 kPa) was smaller than that (ϕ_1) at lower normal stress (i.e., 50-200 kPa). In addition, at a given initial D_r and normal stress range, the peak friction angle of specimens with lower cementation content (< 3.8%) did not change significantly (within 6°-7°) as compared with specimens with higher cementation content (>5.87%) which had a notable increase in the peak friction angle of up to 18°. Such obvious increase in peak friction angle with cementation content was also observed by Cui et al. (2017) and Marri et al. (2012) in the cemented sand treated by MICP and ordinary Portland cement. Moreover, for 11 out of 16 specimens, the cohesion (c_2) at lower normal stress (i.e., 50-200 kPa) was smaller than the that (c_1) at lower normal stress (i.e., 200-600 kPa).

To better illustrate the trends of failure envelopes, **Fig. 3-9** and 3-**10** presented the characteristics of linear and bilinear failure envelopes of the specimens with low (1.40%-1.86%) and high (5.87%-6.79%) cementation content, respectively. Meanwhile, the variation of cohesion obtained from bilinear failure envelopes as a function of cementation content was also plotted in **Fig. 3-11** to reveal factors that may affect the cohesion. Also, the linear failure envelopes of uncemented sand without cohesion were also plotted for comparison. At first glance, there was no significant difference between linear and bilinear failure envelopes for the specimens with lower cementation content as the normal stress increased (as shown in **Fig. 3-9)**, suggesting that small amounts of cementation could not substantially influence the failure envelope. However, an evident curved feature was observed for the specimens with higher cementation content as the normal stress increased (as shown in **Fig. 3-10)**. More specifically, the slope of failure envelopes (i.e., peak friction angle) declined with the increase in normal stress (i.e., $\phi_2 < \phi_1$ in **Table 3-5**, **Fig. 3-10**), which indicated that the peak shear strength of biocemented specimens was significantly reduced when specimens are sheared at high normal stress. Such reduction occurred due to the breakage of interparticle bonds by shearing at higher normal stress. In addition, it was obvious that the linear M-C failure envelopes overestimated the cohesion intercept for the specimens with high cementation content in **Fig. 3-10**. For instance, the overestimated value could be up to 110 kPa in 0.5M_10d_NB (L). Thus, the values of cohesion hereafter were all obtained from bilinear failure envelopes. This observation was in an agreement with the previous study by Nafisi et al. (2020). In **Fig. 3-11**, it was found that the cohesion obtained from bilinear failure envelopes in general increased as the cementation content elevated, which was attributed to the formation of more effective interparticle bonds. Also, it seemed that the initial D_r did not show a significant influence on cohesion as the cementation content. More data were required to further investigate the effect of the initial D_r. Finally, it should be noted that the cohesion values obtained in this study were larger than those from other researchers (Cui et al., 2017; Cheng et al., 2013). This was likely attributed to the fact that the specimens in this study were oven-dried prior to direct shear, whereas full saturation before shearing was achieved in prior studies, which might have weakened the bonds.

Table 3-4 The cohesion and friction angle based on the M-C linear failure envelope.

Specimen	Cementation content (%)	Peak friction angle (°)	Cohesion (kPa)
0.3M_5d_YE (L)	1.86	34.1	40.8
0.5M_5d_YE (L)	4.27	28.9	101.9
0.3M_10d_YE (L)	3.63	28.7	111.7
0.5M_10d_YE (L)	6.33	25.9	282.4
0.3M_5d_YE (H)	1.58	40.2	61.4
0.5M_5d_YE (H)	2.88	45.2	135.2
0.3M_10d_YE (H)	3.60	41.2	83.1
0.5M_10d_YE (H)	6.26	57.2	168.1
0.3M_5d_NB (L)	1.55	34.5	80.2
0.5M_5d_NB (L)	2.22	28.7	136.3
0.3M_10d_NB (L)	3.80	28.7	127.1
0.5M_10d_NB (L)	6.79	25.1	242.9

0.3M_5d_NB (H)	1.40	37.7	84.1
0.5M_5d_NB (H)	2.83	44.1	178.4
0.3M_10d_NB (H)	2.31	43.7	108.6
0.5M_10d_NB (H)	5.87	46.8	226.7

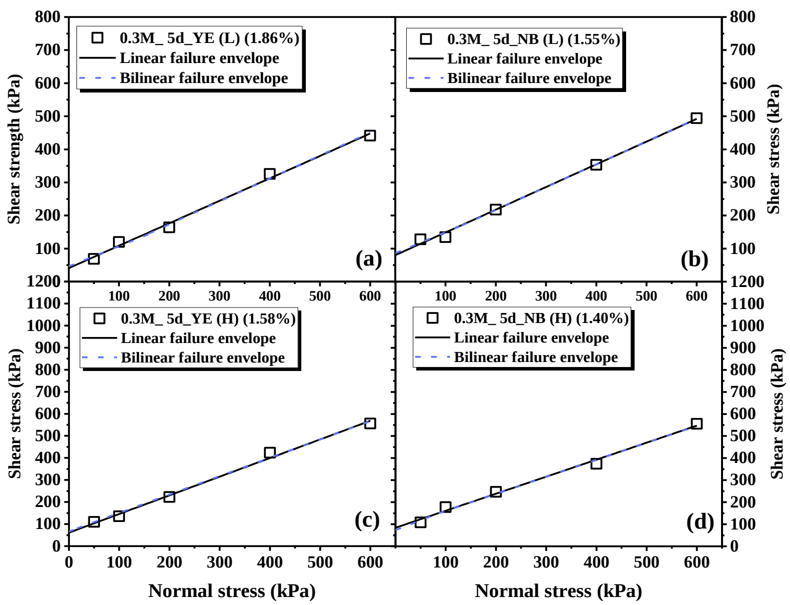

Fig. 3-9 Comparison between linear and bilinear failure envelopes for the specimens with low cementation content (1.40%-1.86%): (a) 0.3M_5d_YE (L); (b). 0.3M_5d_NB (L); (c) 0.3M_5d_YE (H); (d). 0.3M_5d_NB (H).

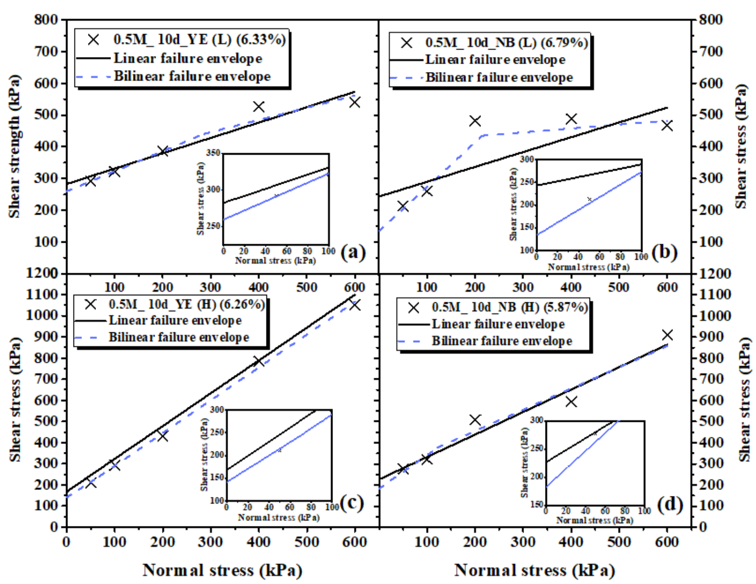

Fig. 3-10 Comparison between linear and bilinear failure envelopes for the specimens with high cementation content (5.87%-6.79%): (a) 0.5M_10d_YE (L); (b). 0.5M_10d_NB (L); (c) 0.5M_10d_YE (H); (d). 0.5M_10d_NB (H).

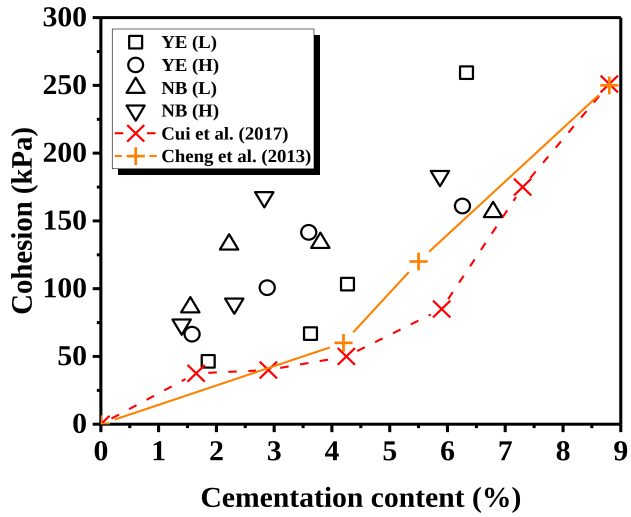

Fig. 3-11 Variation of cohesion of different specimens with cementation content (YE and NB in the legend represent nutrient medium; L and H represent initial D_r).

3.3.6 Peak Dilation Angle

The tangent of dilation angle (ψ) is defined as the ratio between the incremental vertical and horizontal displacements during the direct shear test, which is mathematically represented as:

$$\tan \psi = \delta v / \delta h \quad (3\text{-}1)$$

where δv and δh are the incremental vertical and horizontal displacements, respectively. The peak dilation angle is an indication of the rate of dilation and corresponds to the maximum interlock that can be mobilized during shearing (Dai et al., 2016). It is nominated as ψ_m in this study. The relationship between ψ_m and normal stress was shown in **Fig. 3-12**. For all cases, the peak dilation angle decreased with elevated normal stress, with only a few exceptions such as 0.3M_10d_NB (H) and 0.5M_10d_NB (H) between 50 and 100 kPa. In addition, ψ_m was found to increase with initial D_r at an identical normal stress in 37 out of 40 bio-cemented samples. Meanwhile, it was apparent that more cementation resulted in larger ψ_m at an identical normal stress. It should be noted that the elevated ψ_m

due to cementation was diminishing with the increase in normal stress. For low initial D_r cases at 600 kPa normal stress, the ψ_m of all cemented samples converged to around -2.5°~2.5°, which was lower than that of untreated one (7.8°). However, for high initial D_r cases, the convergent trend of the ψ_m of samples with different cementation levels was less significant. Even at the highest normal stress level, the ψ_m of bio-cemented samples was still higher than that of untreated one. Finally, the nutrient type seemed to have insignificant effect on ψ_m.

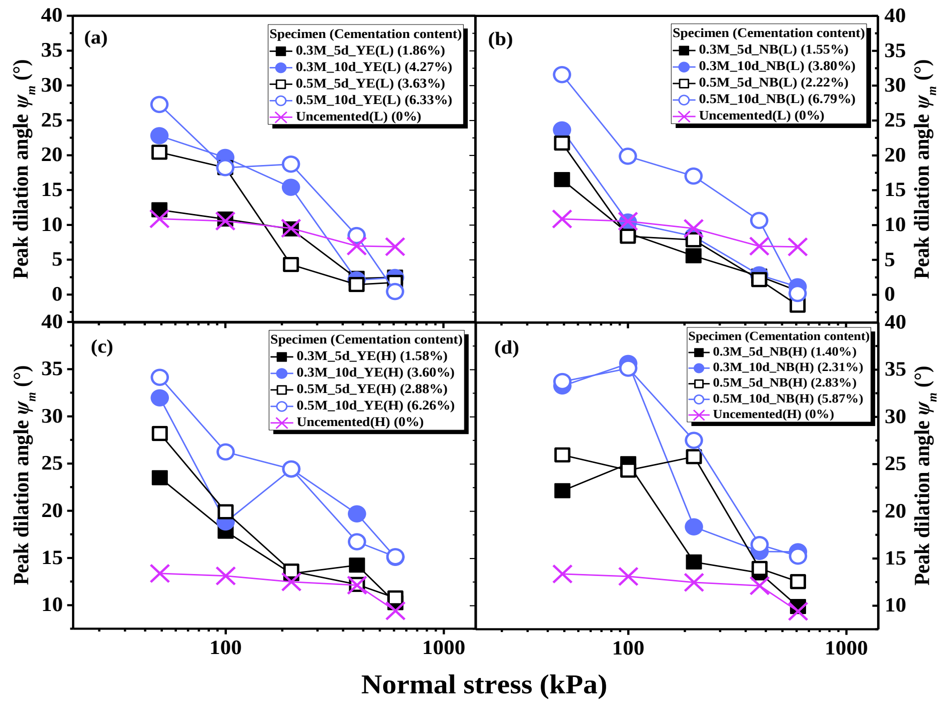

Fig. 3-12 The evolution of peak dilation angle as a function of normal stress in semi-log scale.

In other research regarding the ψ_m of cemented sand, Amini et al. (2014) prepared cemented quartz sand-gravel mixture with Portland cement (up to 2% content) and conducted direct shear tests under different normal stresses and relative densities. Results showed that the magnitude of ψ_m varied between 17° and 40° at 2% cement content with normal stress ranging from 77 to 150 kPa, and relative density from 30% to 90%. This range was similar to that reported in current study.

Table 3-5 The peak friction angle and cohesion based on the bilinear failure envelope.

Specimen	Cementation content (%)	50-200 kPa		200-600 kPa	
		ϕ_1 (°)	c_1 (kPa)	ϕ_2 (°)	c_2 (kPa)
0.3M_5d_YE (L)	1.86	31.4	46.4	30.0	33.1
0.5M_5d_YE (L)	4.27	34	103.4	26.9	119.1
0.3M_10d_YE (L)	3.63	33.0	66.8	29.1	106.6
0.5M_10d_YE (L)	6.33	35.4	259.4	34.1	330.5
0.3M_5d_YE (H)	1.58	32.3	86.3	34.7	78.5
0.5M_5d_YE (H)	2.88	35.0	133.8	31.9	112.8
0.3M_10d_YE (H)	3.60	37.5	132.6	26.7	149.8
0.5M_10d_YE (H)	6.26	54.5	156.5	7.0	408.6
0.3M_5d_NB (L)	1.55	37.5	66.3	39.8	67.4
0.5M_5d_NB (L)	2.22	42.2	141.5	41.7	156.5
0.3M_10d_NB (L)	3.80	36.2	100.7	43.5	47.7
0.5M_10d_NB (L)	6.79	55.5	161.0	53.2	135
0.3M_5d_NB (H)	1.40	41.8	73.5	37.6	84.1
0.5M_5d_NB (H)	2.83	45.9	167.5	43.3	189.4
0.3M_10d_NB (H)	2.31	47.7	88.9	41.6	140.1
0.5M_10d_NB (H)	5.87	57.9	183.1	45.1	255.1

3.3.7 Stress - Dilatancy Relationship

Stress – dilatancy relationship of bio-cemented calcareous sand is manifested in terms of the stress ratio-dilatancy relationship, which demonstrates the shear behavior of granular materials. Dilatancy is defined as the ratio between incremental vertical and horizontal displacements which was also applied by Hossain and Yin (2015) in their direct shear tests. These were different from the stress ratio and dilatancy obtained from triaxial testing results (Wang and Leung, 2008). Therefore, it is not expected to be directly compared between direct shear and triaxial shear testing results.

Taking YE samples as examples, **Fig. 3-13** showed the stress-dilatancy relationship for representative bio-cemented and uncemented samples in this study. For uncemented calcareous sand (**Fig. 3-13(a) and (d)**), the stress-dilatancy relationship was manifested by two approximately straight lines, one representing the pre-peak stage and the other post-peak stage. The normal stress and initial D_r appeared to have little influence on the stress-dilatancy relationship. For cemented calcareous sand samples, while two-segment linear relationship was still apparent for samples at high normal stress (>200 kPa), cemented samples at low normal stress (⩽200 kPa) exhibited a loop-shaped stress-dilatancy relationship (e.g., 0.3M_5d_YE(L), 0.3M_5d_YE(H) and 0.5M_10d_YE(H)), indicating that the development of dilatancy was delayed compared with stress. The area of the closed loop was larger for samples with higher cementation level and at lower normal stress. To further illustrate the asynchronous development of stress ratio and dilatancy rate in bio-cemented calcareous sand samples, the stress-dilatancy relationships at the state of peak stress and maximum dilatancy were plotted in **Fig. 3-14(a)** and **(b)**, respectively. It could be more clearly seen that the disparity between the state of peak stress ratio and maximum dilatancy was the most significant on samples with the cementation content ranging from 5.87% to 6.33% at normal stress between 50 and 200 kPa. Similar results were also reported by Wang and Leung (2008) for Portland cement treated silica sand and by Porcino and Marcianò (2017) for weakly cemented sand under 20 kPa normal stress, both under triaxial condition. This asynchronous stress-dilatancy response indicated that the state-dependent dilatancy of bio-cemented calcareous sand was not only related to stress ratio, but also to cementation level which defined the structure of bio-cemented soil (Wang and Leung, 2008; Leroueil and Vaughan, 1990).

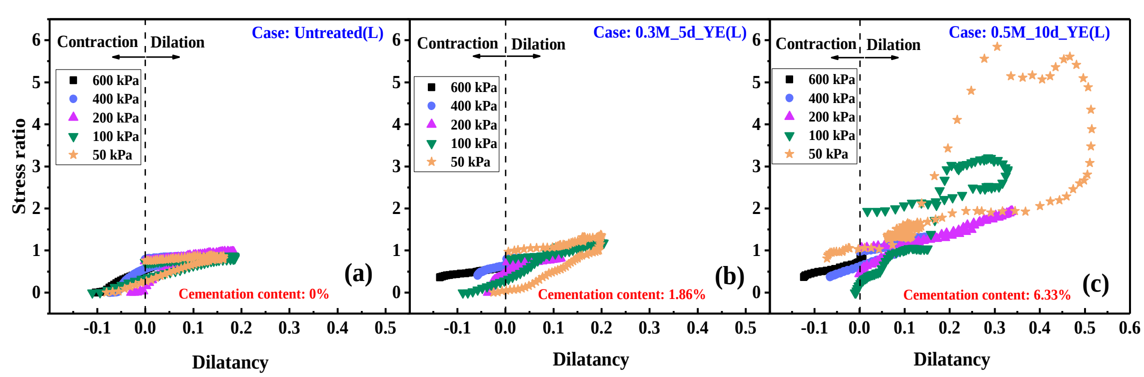

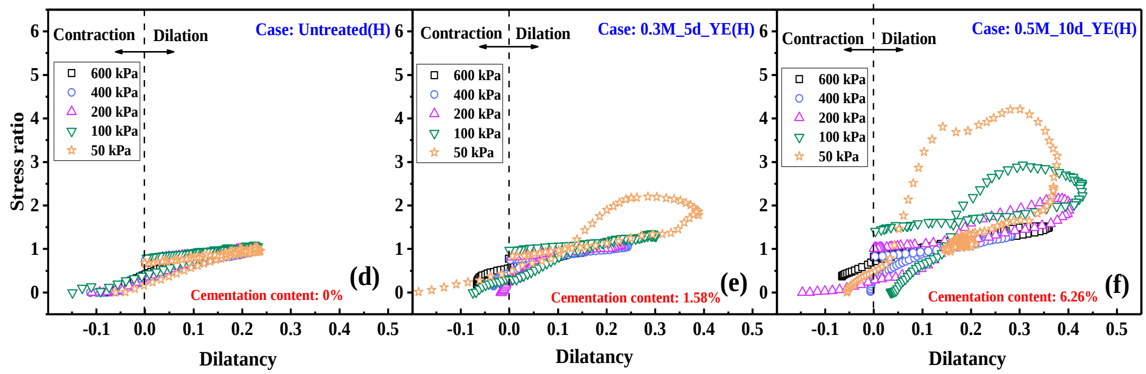

Fig. 3-13 The stress-dilatancy relationship in different cases.

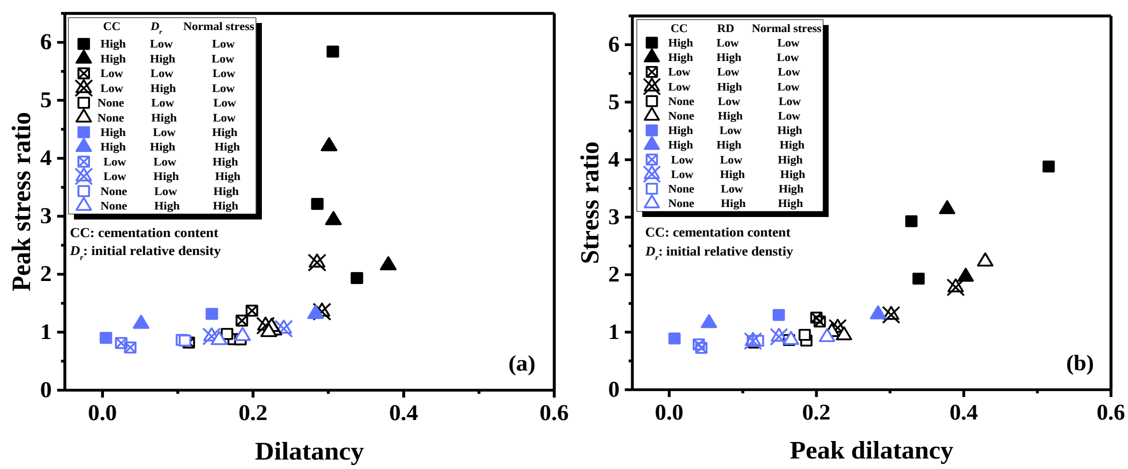

Fig. 3-14 The stress-dilatancy relationship at the state of (a) peak stress ratio; and (b) maximum dilatancy (Note: High CC = 5.87 - 6.79%; Low CC = 1.40 - 1.86%; High initial D_r = 54.6%; Low initial D_r = 16.2%; High normal stress = 400, 600 kPa; Low normal stress = 50, 100, 200 kPa).

3.3.8 Microscopic and Mineralogical Characteristics

Representative microscopic images of bio-cemented calcareous sand were shown in **Fig. 3-15**. **Fig. 3-15(a)** displays the image of untreated sand. Individual sand particles could be clearly observed without bonding between them. **Fig. 3-15(b)** showed the case of 0.3M_5d_YE(L), which had a cementation content of 1.86%. White calcite precipitates could be sparsely spotted between particles. **Fig. 3-15(c)** and **(d)** showed the case of 0.5M_10d_YE(L), which had a cementation content of 6.33%. In this case, substantial white calcite precipitates could be observed between sand particles and bind them together. In addition, many sand particle surfaces were found to be coated by the calcite precipitates.

The microscopic images of shear planes after the direct shear test were shown in **Fig. 3-16**. In the case of untreated sand (**Fig. 3-16(a)**), the sand particles remained intact after shearing at 600 kPa normal stress, indicating that sand particle crushing did not happen at this normal stress level. To verify it, the mechanical sieve analysis was also conducted. The particle size distribution curves (PSDs) of the original uncemented sands before and after shearing under 600 kPa normal stress were presented in **Fig. 3-17**. Clearly, there was hardly any visible difference in PSDs for the sand with 54.6% and 16.2% initial D_r, suggesting that the high normal stress up to 600 kPa did not cause noticeable crushing of calcareous sand particles. For the bio-cemented sample, however, variable shear plane features were observed. For instance, in the case of 0.5M_10d_YE which represented a high cementation level (**Fig. 3-16(b), (c)** and **(d)**), white fines were found to appear on the shear plane upon the completion of the direct shear test. Since the possibility of sand particle crushing has been ruled out, the white fines could only be calcite precipitates. Compared with the sample prior to the direct shear test (**Fig. 3-16(e)**), these fines seemed to be the crushed pieces of calcite precipitates. Furthermore, by comparing in detail among the three shear planes in **Fig. 3-16(b), (c)** and **(d),** it could be seen that the low initial D_r sample at low normal stress (**Fig. 3-16(b)**) had the fewest but coarsest fines of broken bonds. However, loading higher normal stress (**Fig. 3-16(c)**) or increasing initial D_r (**Fig. 3-16(d)**) could both generate more and finer fines of broken bonds.

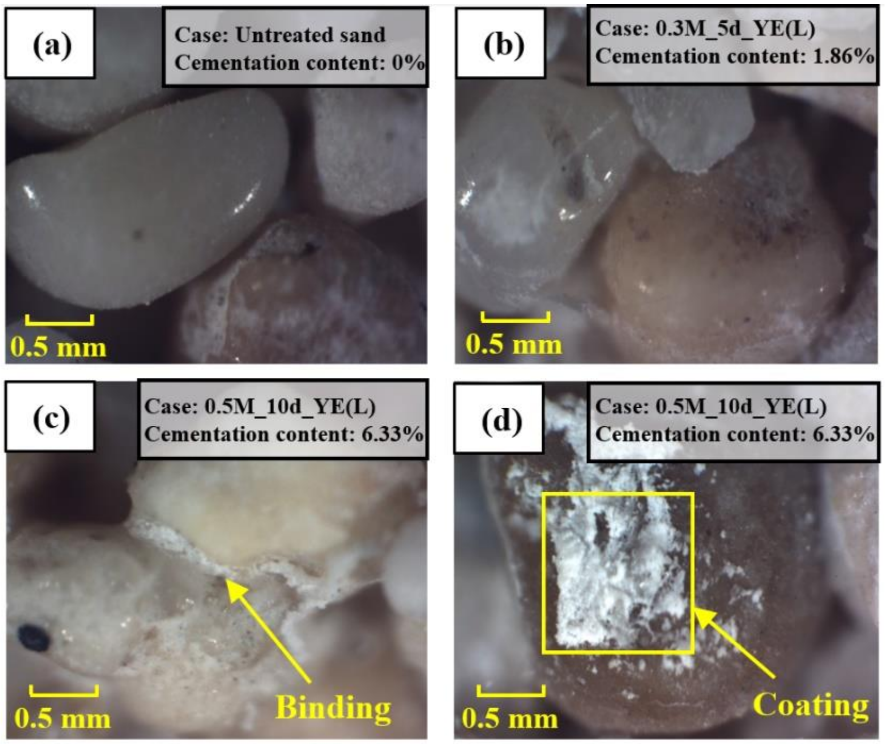

Fig. 3-15 Microscopic images of bio-cementation morphologies.

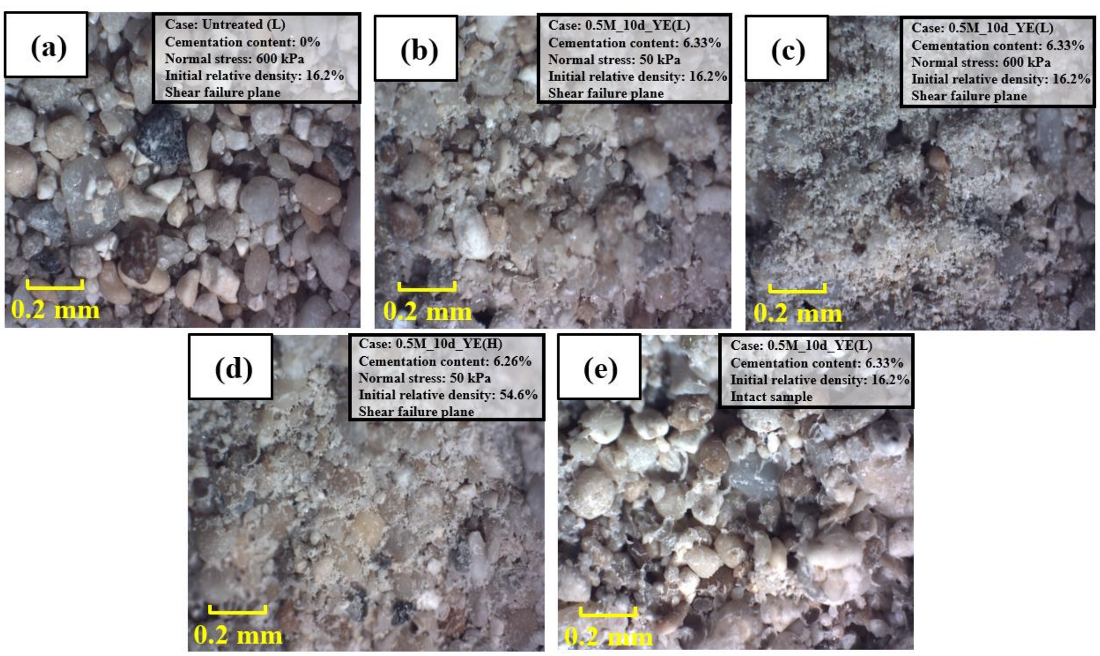

Fig. 3-16 Microscopic images of shear failure plane ((a). un-cemented sample; (b)~(d). sheared cemented samples; (e). intact cemented samples).

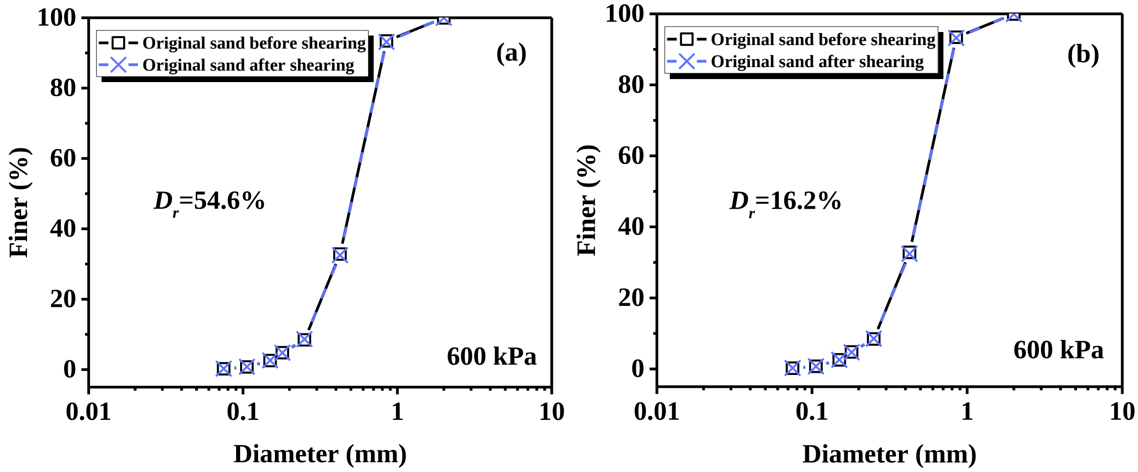

Fig. 3-17 The particle size distribution curves of the original uncemented sands before and after shearing under 600 kPa normal stress: (a) with high initial D_r; (b) with low initial D_r.

3.4 Discussion

In this section, a conceptual framework was proposed to analyze the peak state shear behavior of bio-cemented calcareous sand, as shown in **Fig. 3-18**. The interdependence between external influential factors (cementation level, initial D_r, and normal stress) and strength contributors (interparticle friction, interlocking (dilatancy), particle rearrangement, interparticle bonds, and particle crushing) at the peak state were illustrated in detail. It is worth noting that due to the normal stress applied in this study was limited up to 600 kPa, the proposed framework might not be applicable to explain the higher stress conditions including the sand particle breakage.

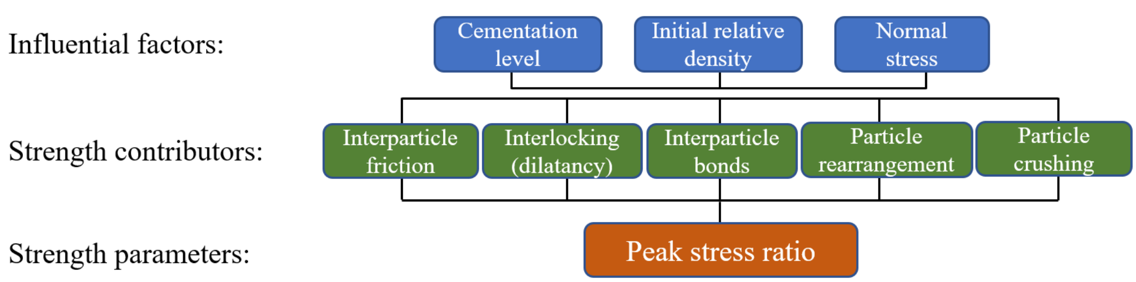

Fig. 3-18 The conceptual framework of shear strength for bio-cemented calcareous sand.

At the peak state, the shear strength of bio-cemented calcareous sand represented by the peak stress ratio is contributed by the interparticle friction, dilation, particle rearrangement, interparticle bonds, and particle crushing. The interparticle fiction angle is roughly constant for a given mineral (calcite in this study), although it was hard to be measured directly in this study (Mitchell and Soga, 2005). In addition, the microstructural observation in **Fig. 3-16(a)** and sieve analysis in **Fig. 3-17** confirmed that particle crushing did not occur in the stress range in this study. Thus, only the other three strength contributors: dilation, particle rearrangement, and interparticle bonds are discussed here.

The effects of cementation level, initial D_r, and normal stress on dilation, particle rearrangement, and interparticle bonds are shown in **Fig. 3-19**. For the effect of cementation level (**Fig. 3-19(a)**), assuming all other factors the same, dilatancy is more significant at higher cementation level. The underlying mechanism is twofold: (1) The size of individual sand particle is enlarged as small individual particles are bonded to form cemented aggregates; (2) The sand particles become more angular and rougher as more produced calcite precipitates coating on particle surfaces (Guo and Su, 2007). All these mechanisms will lead to the enhanced interlocking among sand particles and thus larger dilatancy can be observed at higher cementation level. Microstructural observations shown in **Fig. 3-15(c)** and **(d)** can support these two mechanisms. Furthermore, the contribution of particle rearrangement is diminishing with increasing cementation level due to the constriction of sand particle movement as they are cemented by formed calcite precipitates. Finally, interparticle bonding effect becomes greater as the cementation content increases due to the formation of more effective interparticle cementation. Overall, the superposition of these three mechanisms results in the increased η_p with growing cementation content.

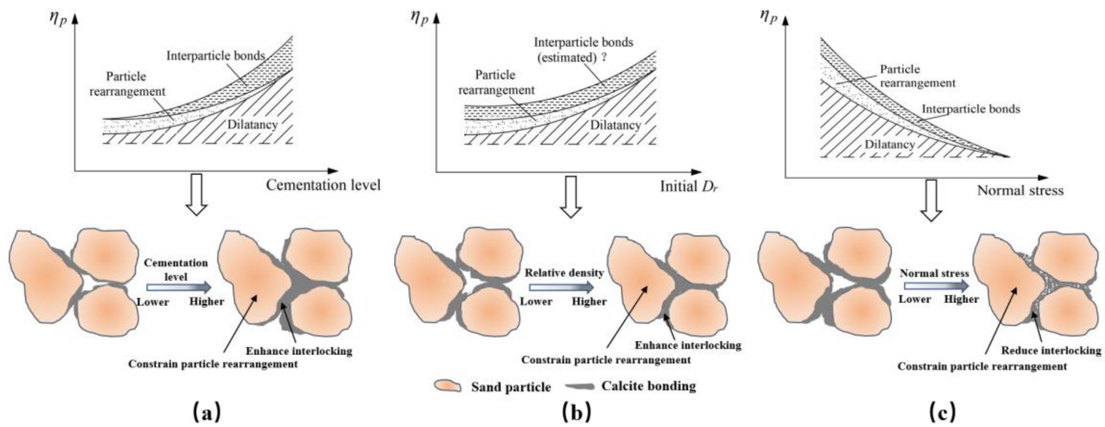

Fig. 3-19 The conceptual illustrations for the peak state: (a) the effect of cementation level; (b) the effect of initial D_r; (c) the effect of normal stress.

With respect to the effect of initial D_r (**Fig. 3-19(b)**), the contribution of dilatancy is more dominant when the bio-cemented sand is initially at dense state. The underlying mechanism is that sand particles have better interlocking effect at dense state as have been widely reported in clean sand (Mitchell and Soga, 2005). On the other hand, the contribution of particle rearrangement is suppressed at high initial D_r, which is similar as clean sand. This is because that dense packing and better interlocking at high initial D_r will further constrain particle movement. Finally, it is assumed that the initial D_r has little effect on the interparticle bonds due to the limited data in current study, and further research is necessary. Overall, η_p increases with the initial D_r considering both dilatancy and particle rearrangement, which is widely recognized for clean sand as well (Holtz et al., 1981).

Regarding the effect of normal stress (**Fig. 3-19(c)**), assuming all other factors the same, dilatancy, particle rearrangement and interparticle bonding effect decrease with the increasing normal stress. More specifically, at lower normal stress, particles can easily roll over one another, which promotes the dilatancy and particle rearrangement, and thus contributes more to η_p. On the contrary, larger normal stress inhibits soil dilation and particle rearrangement resulting a reduce in η_p. These mechanisms are similar to those reported in the case of clean sand. In addition, while sand particle kept intact in this study (**Fig. 3-17**), bonding breakage could occur under a high normal stress level. This may lead to a decrease of interparticle bonds, which makes η_p even become slightly lower than that of clean sand at high normal stress. In the current study, this phenomenon happened when normal stress was higher than 400 kPa (**Fig. 3-8(a) and (b)**). The broken bonding is manifested as fines and likely to reduce interlocking effect of calcareous sand particles. This is different from that reported for silica sand, which shows an increase in particle interlocking (DeJong et al., 2010; Montoya and DeJong, 2015). The difference lies in the fact that calcareous sand particles themselves are much more angular and rougher than silica ones and therefore, additional fines are likely to fill into cavities of uneven surfaces and thus reduce interlocking effect. Finally, at higher normal stress, significantly more bonds breakage is expected to occur and diminishes more dilatancy potential, which can make the ψ_m even smaller than that of clean sand.

It is worth noting that the effect of normal stress, cementation, and initial D_r on η_p are interdependent. For instance, at low normal stress, the effect of cementation on η_p is more pronounced than that of initial D_r (**Fig. 3-8(a) and (c)**). At higher normal stress, however, the initial D_r is more dominant than cementation level. Moreover, while we use "dilatancy" in **Figs. 3-13** and **3-14**, it refers to both dilatancy (positive dilation angle) and contraction (negative dilation angle), as adopted by Wang and Leung (2008). Even though contraction is less likely to happen in calcareous sand due to its much larger particle roughness, contraction instead of dilatancy may still happen on low density, low cementation samples at high normal stress. The case of 0.5M_5d_NB (L) in this study is an example (**Fig. 3-12(b)**).

3.5 Conclusions

In this chapter, the biochemical responses of bio-cemented sand under sand column condition during enrichment and cementation stage were investigated. Also, a series of direct shear tests were conducted on the bio-stimulated calcareous sand at varying cementation levels, initial D_r, and normal stresses. The main conclusions are drawn as follows:

(1) During the enrichment phase, the indigenous ureolytic bacteria can be enriched significantly within 48 hours, though the ureolysis rate was varying with the initial urea concentration. A higher ureolysis rate was maintained in the 170 mM cases until the end of 48 hours, while for 50 mM and 100 mM cases, the ureolysis rate increased slowly or

started to drop after 24 h. In addition, the microbial community changed significantly after enrichment stage. The ureolytic species could be found in the sand.

(2) Peak stress ratio (η_p) increased with increasing cementation content and initial D_r, whereas decreased with increasing normal stress. The η_p of low initial relative density (D_r = 16%) samples could be even smaller than that of untreated clean sand when normal stress was higher than 400 kPa. The effects of cementation content and initial D_r on peak strength parameters diminished with the elevated normal stress.

(3) The linear Mohr-Coulomb failure envelopes overestimated the cohesion. Instead, the bilinear failure envelop could more accurately predict the cohesion of bio-cemented sand, especially for the sands with higher cementation level. It was found that the cohesion and peak friction angle increased with elevated cementation level while declined with the increasing normal stress.

(4) For bio-cemented calcareous sand, the stress ratio and dilatancy exhibited a loop-shaped relationship at low normal stress ($\leqslant$ 200 kPa), and an apparent asynchronism between the state of η_p and maximum dilatancy was observed on samples with higher cementation content ranging from 5.87% to 6.33%.

(5) A conceptual framework to analyze peak state shear behavior of bio-cemented calcareous sand was proposed. The interdependence between external influential factors (cementation level, initial D_r, and normal stress) and strength contributors (interparticle friction, dilatancy, particle rearrangement, interparticle bonding, and particle crushing) at the peak state were illustrated in detail. The validity of this framework was further confirmed through microscopic observations.

References

Amini, Y., Hamidi, A., and Asghari, E., 2014. Shear strength–dilation characteristics of cemented sand–gravel mixtures. International Journal of Geotechnical Engineering 8(4), 406-413.

Allman, M. A., and Poulos, H. G., 1988. Stress-strain behaviour of an artificially cemented calcareous soil. In Proceedings of the International Conference on Calcareous Sediments, Perth, Western Aus-tralia (eds R.J. Jewell and D.C. Andrew), Balkema, Rotterdam, 1:5l-60.

Azadi, M., Ghayoomi, M., Shamskia, N., and Kalantari, H., 2017. Physical and mechanical properties of reconstructed bio-cemented sand. Soils and Foundations 57(5), 698-706.

Cui, M. J., Zheng, J. J., Zhang, R. J., Lai, H. J., and Zhang, J., 2017. Influence of cementation level on the strength behaviour of bio-cemented sand. Acta Geotechnica 12(5), 971-986.

Consoli, N. C., Heineck, K. S., Casagrande, M. D. T., and Coop, M. R., 2007. Shear strength behavior of fiber-reinforced sand considering triaxial tests under distinct stress paths. Journal of Geotechnical and Geoenvironmental Engineering 133(11), 1466-1469.

Cheng, L., Cord-Ruwisch, R., and Shahin, M. A., 2013. Cementation of sand soil by microbially induced calcite precipitation at various degrees of saturation. Canadian Geotechnical Journal 50(1), 81-90.

Dai, B. B., Yang, J., and Zhou, C. Y., 2016. Observed effects of interparticle friction and particle size on shear behavior of granular materials. International Journal of Geomechanics 16(1), 04015011.

DeJong, J. T., Mortensen, B. M., Martinez, B. C., and Nelson, D. C., 2010. Bio-mediated soil improvement. Ecological Engineering 36(2), 197-210.

Ekprasert, J., Fongkaew, I., Chainakun, P., Kamngam, R. and Boonsuan, W., 2020. Investigating mechanical properties and biocement application of $CaCO_3$ precipitated by a newly-isolated *Lysinibacillus sp*. WH using artificial neural networks. Sci. Rep. 10(1), 1-13. https://doi.org/10.1038/s41598-020-73217-7.

Fannin, R. J., Eliadorani, A., and Wilkinson, J. M. T., 2005. Shear strength of cohesionless soils at low stress. Géotechnique. 55(6), 467-478.

Feng, K., and Montoya, B. M., 2016. Influence of confinement and cementation level on the behavior of microbial-induced calcite precipitated sands under monotonic drained loading. Journal of Geotechnical and Geoenvironmental Engineering 142(1), 04015057.

Gat, D., Ronen, Z., and Tsesarsky, M., 2016. Soil bacteria population dynamics following stimulation for ureolytic microbial-induced $CaCO_3$ precipitation. Environmental science and technology 50(2), 616-624.

Ghadakpour, M., Choobbasti, A. J., and Kutanaei, S. S., 2020. Experimental study of impact of cement treatment on the shear behavior of loess and clay. Arabian Journal of Geosciences, 13(4), 1-11.

Guo, P., and Su, X., 2007. Shear strength, interparticle locking, and dilatancy of granular materials. Canadian Geotechnical Journal 44(5), 579-591.

Gomez, M. G., Graddy, C. M., DeJong, J. T., Nelson, D. C., and Tsesarsky, M., 2018. Stimulation of native microorganisms for biocementation in samples recovered from field-scale treatment depths. Journal of Geotechnical and Geoenvironmental Engineering 144(1), 04017098.

Graddy, C. M., Gomez, M. G., DeJong, J. T. and Nelson, D. C. 2021. Native bacterial community convergence in augmented and stimulated ureolytic MICP biocementation. Environ. Sci. Technol. 55(15), 10784-10793. https:// doi.org/10.1021/acs.est.1c01520.

Greenberg, A.E., Clesceri, L.S., and Eaton, A.D., 1992. Standard methods for the examination of water and wastewater. 18th edn. American Public Health Association, Washington.

Hajiabdolmajid, V., Kaiser, P. K., and Martin, C. D., 2002. Modelling brittle failure of rock. International Journal of Rock Mechanics and Mining Sciences 39(6), 731-741.

Holtz, R. D., Kovacs, W. D., and Sheahan, T. C., 1981. An introduction to geotechnical engineering (Vol. 733). Englewood Cliffs, NJ: Prentice-Hall.

Hossain, M. A., and Yin, J. H., 2015. Dilatancy and strength of an unsaturated soil-cement interface in direct shear tests. International journal of Geomechanics 15(5), 04014081.

Hull, T. S., Poulos, H. G., and Alehossein, H., 1988. The static behaviour of various calcareous sediments. In Proceedings of the International Conference on Calcareous Sediments, Perth, Western Aus-tralia (eds R.J. Jewell and D.C. Andrew), Balkema, Rotterdam, 87-96.

Jiang, M. D., Yang, Z. X., Barreto, D., and Xie, Y. H., 2018. The influence of particle-size distribution on critical state behavior of spherical and non-spherical particle assemblies. Granular Matter 20(4), 80.

Jiang, N. J., 2020. Discussion of “About calcium carbonate precipitation on sand biocementation” by Rafaela Cardoso, Rita Pedreira, Sofia OD Duarte, and Gabriel A. Monteiro. Engineering Geology 105726.

Kang, C. H., Kwon, Y. J. and So, J. S., 2016. Soil bioconsolidation through microbially induced calcite precipitation by Lysinibacillus sphaericus WJ-8. Geomicrobiol. J. 33(6), 473-478. https://doi.org/10.1080/01490451.2015.1053581.

Knorst, M. T., Neubert, R., and Wohlrab, W., 1997. Analytical methods for measuring urea in pharmaceutical formulations. Journal of pharmaceutical and biomedical analysis 15(11), 1627-1632.

Lee, K. L., and Seed, H. B., 1967. Drained strength characteristics of sands. Journal of Soil Mechanics and Foundations Div 93(SM6),117–141.

Lefebvre, G., 1981. Fourth canadian geotechnical colloquium: Strength and slope stability in Canadian soft clay deposits. Canadian Geotechnical Journal 18 (3): 420–442.

Leroueil, S., and Vaughan, P. R., 1990. The general and congruent effects of structure in natural soils and weak rocks. Géotechnique, 40(3), 467-488.

Liu, L., Liu, H., Stuedlein, A. W., Evans, T. M., and Xiao, Y., 2019. Strength, stiffness, and microstructure characteristics of biocemented calcareous sand. Canadian Geotechnical Journal 56(10), 1502-1513.

Maksimovic, M., 1989. Nonlinear Failure Envelope for Soils. Journal of Geotechnical Engineering 115(4), 581–586.

Mitchell, J. K., and Soga, K., 2005. Fundamentals of soil behavior (Vol. 3). New York, John Wiley and Sons.

Marri, A., Wanatowski, D., and Yu, H. S., 2012. Drained behaviour of cemented sand in high pressure triaxial compression tests. Geomechanics and Geoengineering, 7(3), 159-174.

Montoya, B. M., and DeJong, J. T., 2015. Stress-strain behavior of sands cemented by microbially induced calcite precipitation. Journal of Geotechnical and Geoenvironmental Engineering 141(6), 04015019.

Nafisi, A., Montoya, B. M., and Evans, T. M., 2020. Shear Strength Envelopes of Biocemented Sands with Varying Particle Size and Cementation Level. Journal of Geotechnical and Geoenvironmental Engineering 146(3), 04020002.

Nouri, A., Vaziri, H., Kuru, E., and Islam, R., 2006. A comparison of two sanding criteria in physical and numerical modeling of sand production. Journal of Petroleum Science and Engineering 50(1), 55–70.

Pakbaz, M. S., Ghezelbash, G. R., and Afzal, A., 2020. Sugarcane Molasses: A Cheap Carbon Source for Calcite Production in Different Class of Soils using Stimulation of Indigenous Urease-producing Bacteria. Geomicrobiology Journal 37(3), 213-229.

Porcino, D. D., and Marcianò, V., 2017. Bonding degradation and stress–dilatancy response of weakly cemented sands. Geomechanics and Geoengineering 12(4), 221-233.

Rowshanbakht, K., Khamehchiyan, M., Sajedi, R. H., and Nikudel, M. R., 2016. Effect of injected bacterial suspension volume and relative density on carbonate precipitation resulting from microbial treatment. Ecological Engineering 89, 49–55.

Tsesarsky, M., Gat, D., and Ronen, Z., 2016. Biological aspects of microbial-induced calcite precipitation. Environmental Geotechnics 5(2), 69-78.

Tsukamoto, M., and Oda, K., 2013. Influence of relative density on microbial carbonate precipitation and mechanical properties of sand. In Proceedings of the 18th International Conference on Soil Mechanics and Geotechnical Engineering. Paris. 2613-2616.

Van Paassen, L. V., Hemert, W. V., Star, W. V. D., Zwieten, G. V., and Baalen, L. V., 2012. Direct shear strength of biologically cemented gravel. In Proceedings of Geo-Congress 2012: State of the Art and Practice in Geotechnical Engineering. 968-977.

Wang, Y. H., and Leung, S. C., 2008. Characterization of cemented sand by experimental and numerical investigations. Journal of Geotechnical and Geoenvironmental Engineering 134(7), 992-1004.

Wang, Y. J., Han, X. L., Jiang, N. J., Wang, J., and Feng, J., 2020. The effect of enrichment media on the stimulation of native ureolytic bacteria in calcareous sand. International Journal of Environmental Science and Technology 17(3), 1795-1808.

Xiao, Y., Long, L., Matthew Evans, T., Zhou, H., Liu, H., and Stuedlein, A. W., 2019. Effect of particle shape on stress-dilatancy responses of medium-dense sands. Journal of Geotechnical and Geoenvironmental Engineering 145(2), 04018105.

CHAPTER 4. Compressive Characteristics of Bio-Cemented Calcareous Sand Treated by Bio-stimulated Microbial Induced Calcite Precipitation

4.1 Introduction

Over the past decade, the compressibility and associated particle breakage behaviors of calcareous sand have been extensively investigated via a variety of testing methods, such as one-dimensional compression test (Altuhafi and Coop, 2011; Xiao et al., 2020), consolidated undrained or drained triaxial test (Dehnavi et al., 2010; Shahnazari and Rezvani, 2013), and impact loading test (Xiao et al., 2018; Lv et al., 2020). It is found that calcareous sand is more compressible and can be crushed more easily than silica one due to its higher internal porosity (Coop et al., 2004; Lv et al., 2019; Xiao et al., 2019, 2020). The factors influencing compressibility and particle breakage behaviors of calcareous sand mainly include soil gradation (Wang et al., 2020c), particle shape (Wei et al., 2020), grain size (Liu et al., 2020), initial density (Shahnazari and Rezvani, 2013; Xiao et al., 2017), external loading (Shahnazari and Rezvani, 2013; Xiao et al., 2020), carbonate content (Bryaant et al., 1974), and fines content (Xiao et al., 2020). Considering that calcareous sand is widely used as foundation or backfill materials in coastal regions, it becomes more and more urgent to implement suitable ground improvement methods to reduce its compressibility.

Since MICP, either via bio-augmentation or bio-stimulation, could cement loose sand particles, it could be used for reducing the compressibility of calcareous sand. Currently, only a few studies have been conducted to examine the compressibility behavior of bio-cemented sand. These studies mostly focus on silica sand treated through bio-augmented MICP. For instance, Xiao et al. (2020a) conducted one-dimension compression tests on bio-augmented MICP-treated silica sand at varying cementation levels. The results indicated that bio-augmented MICP treatment could effectively restrain particle breakage, and thus reduce the compressibility of silica sand. Xiao et al. (2021) investigated the effect of gradation on the compression behaviors of bio-cemented silica sands by bio-augmentation MICP. The results revealed that the compressibility of specimens increased with increasing coefficient of uniformity. Arboleda-Monsalve et al. (2019) studied the compressibility behavior of bio-cemented silica loose sands. They pointed out that the MICP treatment was suitable for vertical effective stress levels below 200 kPa. Lin et al. (2016) conducted confined compression tests on two MICP-treated silica sands. It was found that the compressibility of the treated soil specimens decreased as the $CaCO_3$ content increased. Cardoso et al. (2016) conducted confined compressibility tests on MICP-treated sands, and they found that the compressibility index was very similar between the MICP-treated and untreated sand though the reduction of porosity was obvious. To the authors' knowledge, there have not been any reported studies on the compressibility behaviors of bio-stimulated MICP treated calcareous sand.

The objective of this chapter is to investigate the compressibility behavior of calcareous sand treated via the bio-stimulated MICP approach. A series of one-dimension compression tests were conducted to obtain the compressibility of bio-cemented calcareous sand, which was manifested by the compression curves and particle size distribution curves (PSDs). Then, the relevant parameters including cementation content (*CC*), the coefficient of compressibility (a_v), relative breakage (B_r), and relative agglomeration (A_r) of the bio-cemented sand based on the method proposed by Hardin (1985) were discussed.

4.2 Materials and methods

4.2.1 Calcareous sand

The calcareous sand used in this study was sampled from the shallow surface of Waikiki Beach, Oahu Island, Hawaii, USA. After taken to the laboratory, the sand was firstly sieved through US No.10 sieve (2 mm opening size) to remove oversized grains as well as twigs and grass. The basic physical properties of the post-sieving calcareous sand are listed in **Table 4-1**.

4.2.2 Enrichment and cementation solutions

Two enrichment media were developed in this study to enrich native ureolytic bacteria in the collected calcareous sand. The first one, named YE, contained 20 g/L yeast extract plus urea and the second one, named NB, contained 20 g/L nutrient broth plus urea. Yeast extract and nutrient broth are both organic nutrients containing sufficient proteins and amino acids to facilitate the growth of bacteria. Besides, urea was added as a selective ingredient for the stimulation of ureolytic bacteria and elimination of non-ureolytic ones. The urea concentration used in the enrichment media was 170 mM (~10 g/L). The cementation solution consisted of equal mole concentration (0.3 M or 0.5 M) of urea and $CaCl_2$ plus 0.2 g/L yeast extract or nutrient broth accordingly. The purpose of adding trace amount of yeast extract or nutrient broth was to supply further nutrients to maintain the bacterial viability at the cementation stage.

Table 4-1 The physical and index properties of the collected calcareous sand after sieving.

Physical and Index Properties	Value
Soil classification (ASTM D2487)	SP
Median particle diameter, D_{50} (mm)	0.360
Coefficient of curvature C_c	0.816
Coefficient of uniformity C_u	2.5
Specific gravity, G_s (g/cm^3)	2.73
Maximum void ratio e_{max}	0.888
Minimum void ratio e_{min}	0.271
Carbonate content (%)	⩾99.5
Natural moisture content (%)	1-2
Average circularity	0.839
Average aspect ratio	1.511

4.2.3 Procedures for bio-stimulated MICP treatment

The bio-stimulated MICP treatment consisted of two stages: enrichment and cementation. Specimens were prepared using brass rings with height of 2.54 cm and inner diameter of 6.35 cm. Firstly, fresh calcareous sand was thoroughly mixed with 0.5 pore volume (PV) of either the YE or NB medium. Then, the moist sand was compacted in the brass ring to achieve two initial relative densities (16.2% and 54.6%). The detailed specifications of prepared samples during bio-stimulated MICP treatment were presented in **Table 4-2**. After that, all specimens were left at room temperature and humidity for 48 hours, which were found in previous study to be able to enrich enough native urease-positive bacteria (Wang et al., 2020a). After the completion of the enrichment stage, the cementation solution was flushed through specimens via surface percolation once per day for consecutive 5 or 10 days at relatively small flow rate (2 mL/min) to avoid noticeable disturbance. The flow rate was controlled by a calibrated valve which was connected to the bottom of the solution container. The volume of flushed cementation solution each time was 1.5 PVs of the respective sand specimen. It should be mentioned that during the enrichment and cementation phase, all specimens were treated without any vertical stress. Upon the completion of the cementation stage, the specimens were flushed using 3PVs of deionized water for 5 times to remove residual dissolved salts and then oven-dried at 105 ℃ for 24 hours.

Table 4-2 The specifications of prepared samples during bio-stimulated MICP treatment.

Initial D_r of sample	Mass of collected sand (g)	1 Pore volume (cm^3)
Lower (16.2%)	100	43.1
Higher (54.6%)	120	35.5

4.2.4 One-dimension compression test

The one-dimension compression test was conducted using Geocomp® LoadTrac-II incremental consolidation system. The incremental loading from 12.5 kPa to 6400 kPa and unloading from 6400 kPa to 25 kPa were conducted and the deformation of specimen was recorded continuously for each loading and unloading sequence. Each loading/unloading step lasted for 24h in the current study. All specimens were saturated prior to the compression test. The detailed experimental program of the one-dimensional compression test is shown in **Table 4-3**. The designation "*a_b_c*(*d*)" represents the bio-cemented specimens treated with "*b*" flushes (days) of "*a*" mol/L (M) cementation solution. "*c*" is the nutrient type (YE or NB) and "*d*" is initial D_r level ("L" representing low (16.2%) or "H" representing high (54.6%)).

4.2.5 Cementation content measurement

The cementation content was determined by measuring the increased mass of sand specimens after bio-stimulated MICP treatment and it could be expressed as:

$$\text{Cementation content } (CC) = \frac{m_{at} - m_{bt}}{m_{bt}} \times 100\% \tag{4-1}$$

Where, m_{bt} is the dry mass of sand prior to MICP treatment; m_{at} is the dry mass of sand after MICP treatment.

Table 4-3 Experimental program of the one-dimension compression test.

Specimen nomenclature	*Initial* D_r (%)	Enrichment stage		Cementation stage		
		[Nutrient] (g/L)	[Urea] (mM)	[$CaCl_2$] (M)	[Urea] (M)	Time (days)
0.3_5_YE(L)	16.2	20	170	0.3	0.3	5
0.3_10_YE(L)				0.3	0.3	10
0.5_5_YE(L)				0.5	0.5	5
0.5_10_YE(L)				0.5	0.5	10
0.3_5_NB(L)				0.3	0.3	5
0.3_10_NB(L)				0.3	0.3	10
0.5_5_NB(L)				0.5	0.5	5
0.5_10_NB(L)				0.5	0.5	10
0.3_5_YE(H)	54.6	20	170	0.3	0.3	5
0.3_10_YE(H)				0.3	0.3	10
0.5_5_YE(H)				0.5	0.5	5
0.5_10_YE(H)				0.5	0.5	10
0.3_5_NB(H)				0.3	0.3	5
0.3_10_NB(H)				0.3	0.3	10
0.5_5_NB(H)				0.5	0.5	5
0.5_10_NB(H)				0.5	0.5	10

4.2.6 Sieve analysis

To assess the breakage properties of bio-cemented specimens, the mechanical sieve analysis was conducted based on ASTM D-422 (ASTM, 2007) after the one-dimensional compression test. The opening size (D) designation of sieves used were 0.075 mm, 0.106 mm, 0.15 mm, 0.18 mm, 0.25 mm, 0.425 mm, 0.85 mm, 2 mm and 12.5 mm in this study.

4.2.7 Microstructural observations

To characterize the microstructural features of the bio-cemented calcareous sand, optical microscopy imaging was performed using a Nikon SMZ1500 stereo microscope equipped with lenses providing a magnification in the range between 3.75 and 540.

4.3 Testing results and data interpretation

4.3.1 Cementation content

The cementation content of bio-cemented sand is one of the most important indices which reflects the overall efficiency of MICP treatment. **Fig. 4-1** shows the cementation content of bio-cemented calcareous sand subjected to varying treatment schemes. The measured cementation content for all specimens ranged from 1% to 6.8%. More specifically, for a given enrichment medium and initial D_r, higher concentration of cementation solution (0.5 M) and more treatment flushes (10 times) led to higher cementation content. Additionally, provided other conditions the same, cementation content was found to be slightly higher in low initial D_r specimens in 7 out of 8 cases. The above observation, on the one hand, was due to the less pore volume in the sand specimens with higher initial D_r and on the other hand, due to the decreasing net surface area (Tsukamoto et al., 2013; Rowshanbakht et al., 2016). Finally, it was found that there was no significant difference regarding the effect of enrichment medium type (i.e., YE or NB) on the cementation content, confirming that these two enrichment media were functionally similar. Thus, the results and discussions were mainly based on the cases treated by NB-based enrichment medium.

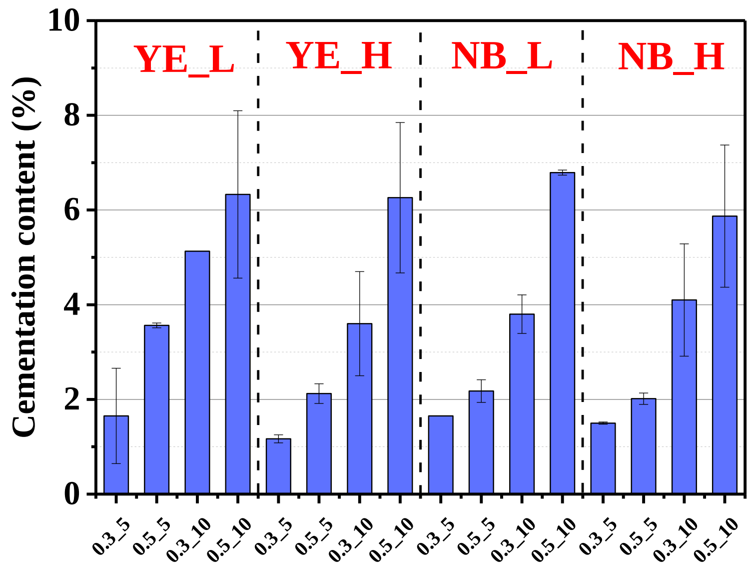

Fig. 4-1 The cementation contents of bio-cemented specimens with varying treatment scheme and initial D_r (notation: YE—yeast extract, NB—nutrient broth, L—low initial D_r, H—high initial D_r, 0.3/0.5—concentration of cementation solution, 5/10—duration of cementation stage).

4.3.2 Compression curves

The representative compression curves (including both e-p and e-log$p$ curves) of the bio-cemented calcareous sand treated by NB-based enrichment medium are shown in **Fig. 4-2**. The rest compression curves are presented in **Fig. 4-3**. The concept of normalized void ratio (e_m/e_0) was adopted here, in which e_m was the modified void ratio at the end of each loading, and e_0 is the initial modified void ratio. Jafari et al. (2020) used similar concept to investigate the isotropic compression behaviors of cemented paste backfill. In the current study, the formed bio-cementation within the voids of sand matrix was incorporated into the calculation of modified void ratio and thus e_m is defined as:

$$e_m = \frac{\rho_w V_t - (m_{sg} / G_{sg} + m_{Ca} / G_{Ca})}{m_{sg} / G_{sg} + m_{Ca} / G_{Ca}} \tag{4-2}$$

where, ρ_w is the mass density of water; V_t is the total volume of sample; m_{sg} and m_{Ca} are the mass of sand grains and $CaCO_3$; G_{sg} and G_{Ca} are the specific gravity of sand grains and $CaCO_3$ (Xiao et al., 2020).

Taking NB-treated bio-cemented sand as an example, firstly, with the increase in the cementation content, a higher value of e_m/e_0 was observed. This phenomenon was also reported previously in terms of other types of cemented soils treated by Portland cement or bio-augmented MICP (Rotta et al. 2003; Silva dos Santos et al. 2010; Xiao et al. 2020a). Then, it can be seen from the e_m/e_0-log$p$ curves (**Fig. 4-2(c), (d)**) that, at lower vertical stress ranging from 12.5 kPa to 400 kPa, all specimens' compression curves were approximately linear and showed smaller reduction in e_m/e_0 compared with the specimens at higher vertical stress, indicating that the bio-cementation provided effective interparticle bonding between sand particles. It was also found that, at low vertical stress range, the compression curve shifted upward with increased cementation content, which was due to the existence of more interparticle bonds. At higher vertical stresses, however, the compression curve began to change from linearity to curvature, indicating that more soil compression occurred at the same vertical stress increment. This was likely due to that the interparticle bonds were significantly broken as vertical stress increased. A distinct transition stress appeared at around 800 (±100) kPa for all specimens in this study. Thereafter, the breakage continued until all interparticle bonds broke. Due to the limit of maximum load, the complete interparticle bonds breakage was not fully achieved in this study.

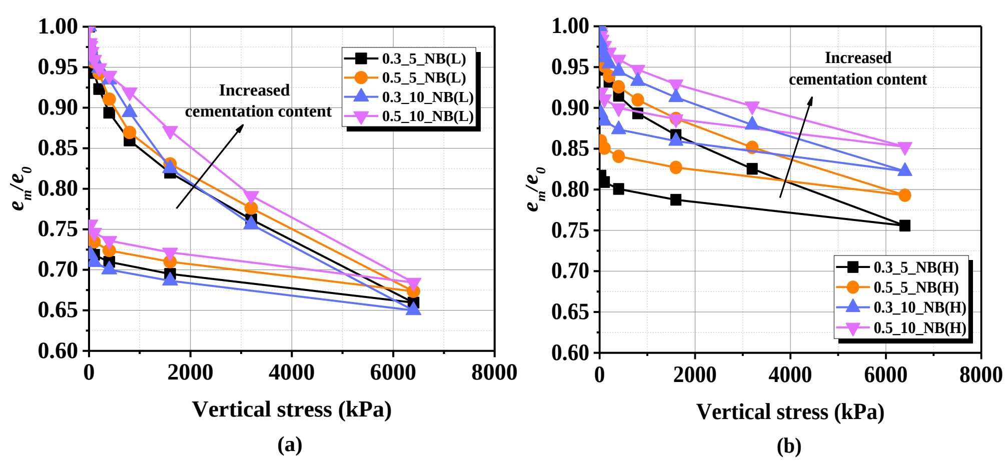

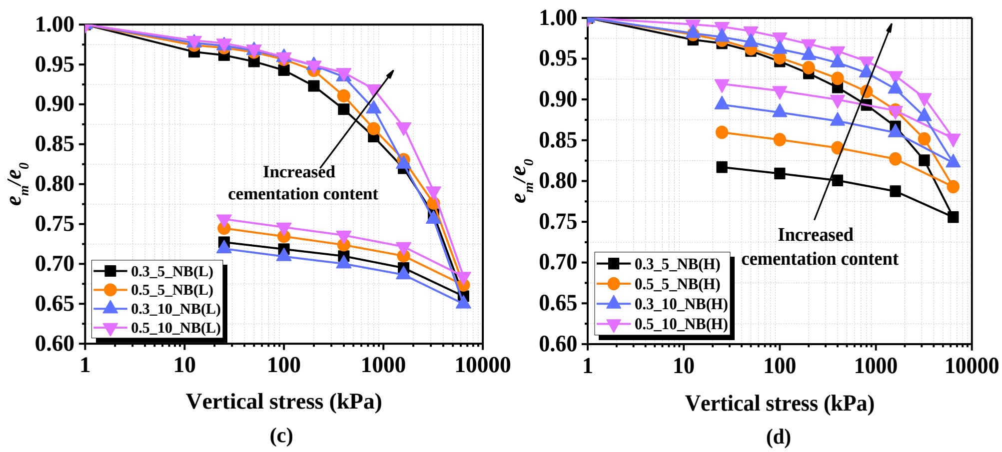

Fig. 4-2 The representative compression curves of the bio-cemented sand treated by NB enrichment medium: (a), (b) in linear scale; (c), (d) in semi-logarithmic scale.

4.3.3 Coefficient of compressibility

The coefficient of compressibility (a_v) was calculated in this study to quantify the compressibility of bio-cemented sand. The a_v is defined as the decrease in modified void ratio (Δe_m) per unit increase in effective vertical stress ($\Delta p'$), which can be derived from the *e* versus *p'* compressibility curves.

Fig. 4-4 depicts the variations of a_v with cementation content at various average vertical stress, which is defined as the average of the initial and final vertical stress for each load increment (Bohnhoff and Shackelford, 2014). In general, the values of a_v decreased with increasing average vertical stress for all specimens, which was consistent with the observations by Yamamuro and Lade (1997) regarding the Nevada sand and Bohnhoff and Shackelford (2014) regarding a backfill soil. Moreover, it is found that a_v decreased gradually with the increase in cementation content for a given initial D_r and enrichment medium, indicating that the more bio-cementation in soil matrix could work effectively as the interparticle bonds. However, it should be noted that such observation was more obvious at low average vertical stresses. More specifically, for the cases of YE_L, YE_H, NB_L, and NB_H, a_v decreased from 7.3×10^{-4} kPa^{-1} to 3.4×10^{-4} kPa^{-1}, from 3.9×10^{-3} kPa^{-1} to 1.6×10^{-4} kPa^{-1}, from 2.4×10^{-3} kPa^{-1} to 1.8×10^{-4} kPa^{-1}, and from 2.8×10^{-3} kPa^{-1} to 1.5×10^{-4} kPa^{-1}, respectively at the average vertical stress of 18.75 kPa, whereas less than 5×10^{-6} kPa^{-1} reduction could be seen at the average vertical stress of 4800 kPa for all specimens.

This indicated that the bio-cementation lost its interparticle bonding function with the increase in vertical stress. Finally, when treated by a given enrichment medium, the a_v values of the specimens with higher initial D_r were approximately 20%-70% smaller than their counterparts with lower initial D_r, especially within average vertical stress range between 18.75 kPa and 4800 kPa for YE-treated specimens, and between 150 kPa and 4800 kPa for NB-treated specimens. This was consistent with the results reported by Yamamuro and Lade (1997).

4.3.4 Recompression index

The recompression index C_r in this study was determined from the graphs representing the variation of modified void ratio e_m as a function of the vertical stress plotted in the semi-logarithmic scale during unloading period, which were not shown in this paper. The last three points were used for the calculation. **Fig. 4-5** shows the effects of cementation content and initial D_r on the variation of C_r for all specimens. It is apparent that higher initial D_r resulted in larger C_r. Additionally, it was evident that the C_r decreased with increasing cementation content, which was consistent with the observation by Lee et al. (2013) on silty residual soil. In their study, the C_r declined linearly with the amount of precipitated calcium carbonate.

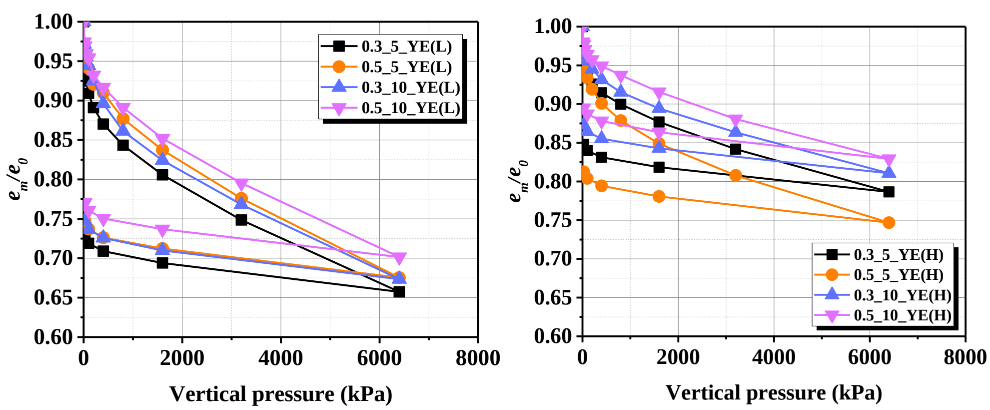

(a) (b)

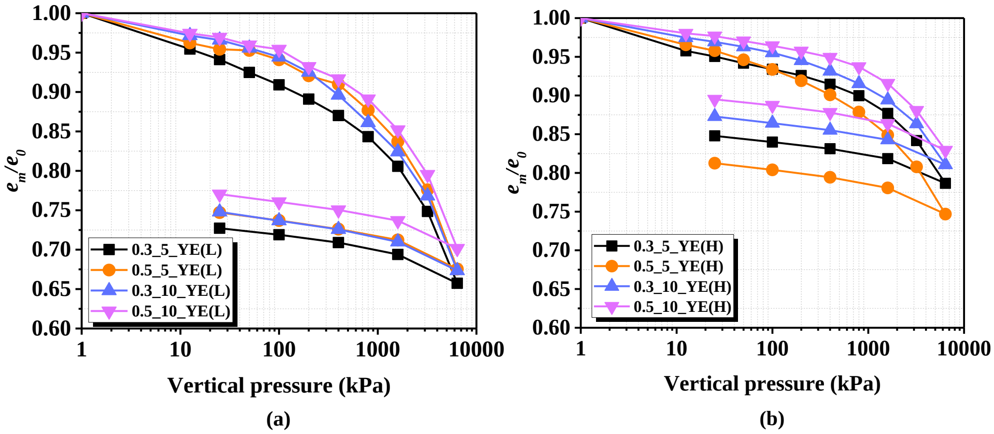

Fig. 4-3 The compression curves of the bio-cemented sand treated by YE enrichment medium: (a), (b) in linear scale; (c), (d) in semi-logarithmic scale.

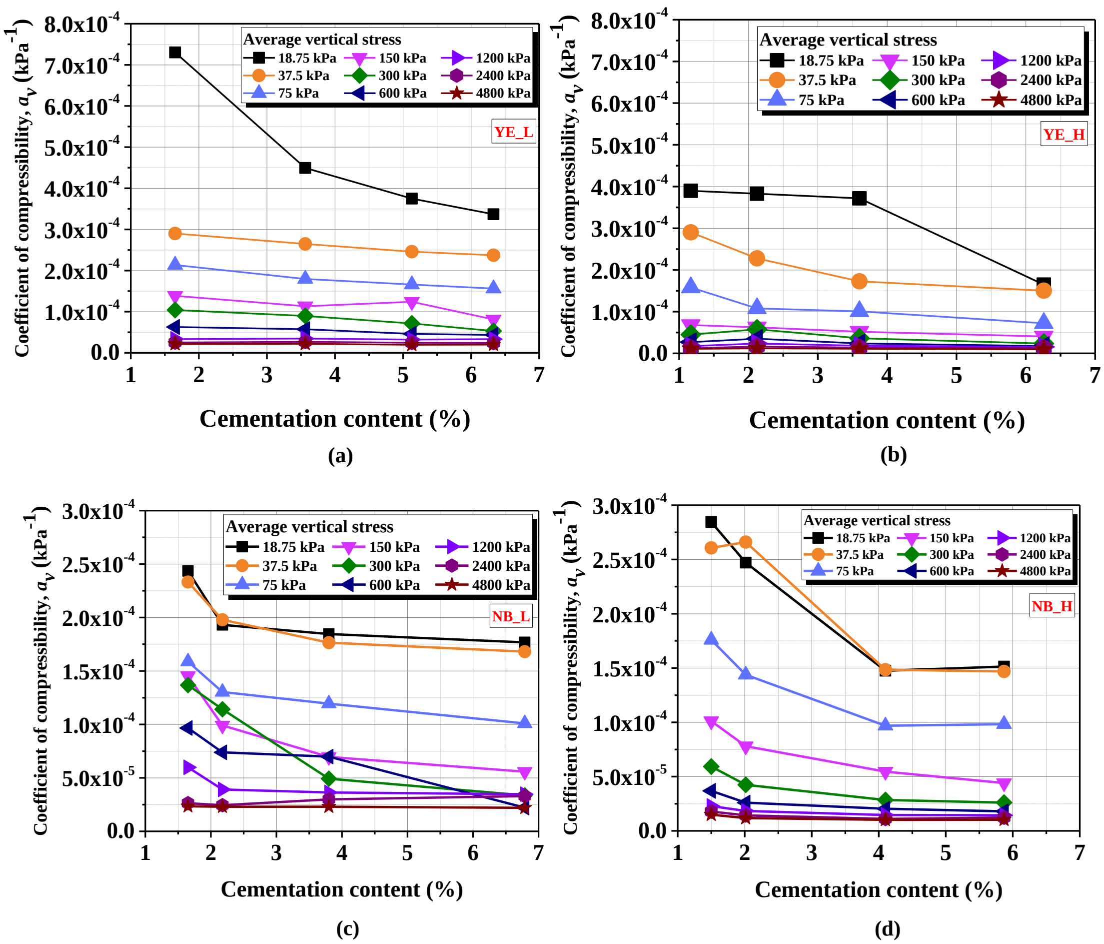

Fig. 4-4 The variations of coefficient of compressibility with cementation content at different average vertical stress: (a) specimens treated by YE with low initial D_r; (b)

specimens treated by YE with high initial D_r; (c) specimens treated by NB with low initial D_r; (d) specimens treated by NB with high initial D_r.

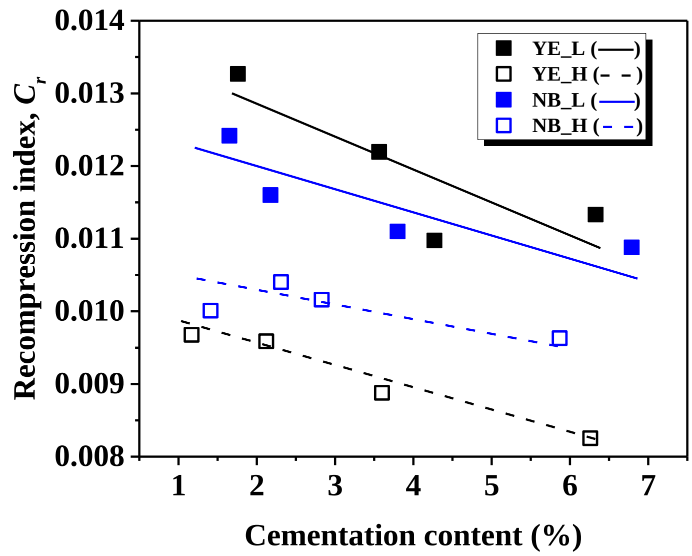

Fig. 4-5 Effects of cementation content and initial D_r on the variation of recompression index.

4.3.5 Interparticle bonding breakage

Fig. 4-6 shows the PSDs of the bio-cemented specimens and the original sand before and after the one-dimensional compression test. Based on the sieve analysis results, a conceptual representation of how PSDs are affected by bio-cementation is depicted in **Fig. 4-7**. It can be seen that the intersection point divides the PSDs of bio-cemented sand into two portions. At the intersection point, the same percent of sands pass through the corresponding particle size for both bio-cemented and clean sand. On the right-side portion (i.e., coarse portion), the downward shift of PSDs means that larger size lumps are generated. On the left-side portion (i.e., fine portion), the upward shift of PSDs indicates the increased percentage of the finer particles. It should be noted that the interference of sand particle breakage could be excluded in terms of the above-mentioned shifts of PSDs, as it could be confirmed that no noticeable sand particle breakage occurred at the level stresses encountered in the current study (**Fig. 4-8**). Thus, the extent of interparticle bonding breakage was quantified using the Relative Breakage (B_r) which was proposed by Hardin (1985) and defined by **Eq (4-3)**:

$$B_r = \frac{B_t}{B_p} = \frac{S_{FOG}}{S_{ABOG}} \tag{4-3}$$

where B_t is the total breakage; B_p is the breakage potential; S_{FOG} and S_{ABOG} are the patterned and pink areas in **Fig. 4-7**.

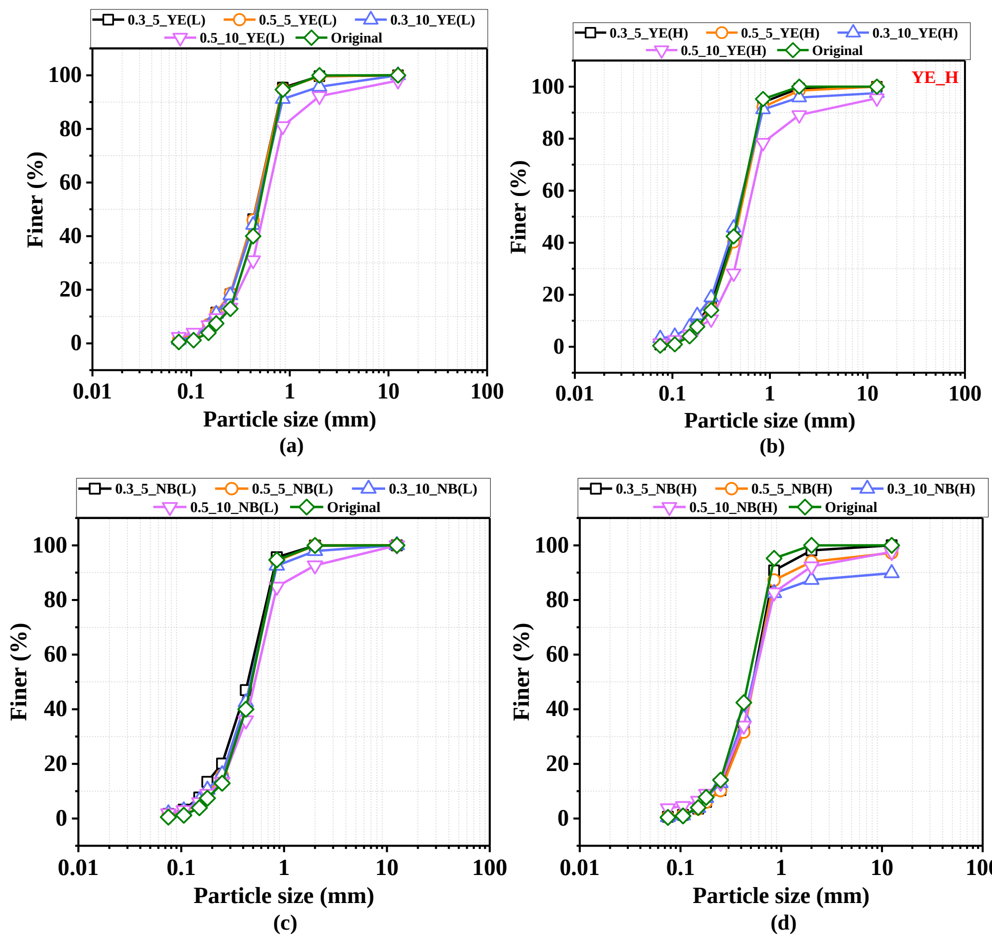

Fig. 4-6 The post-compression PSDs of the original clean sand and the bio-cemented sand: (a), (b) specimens treated by YE with low and high initial D_r; (c), (d) specimens treated by NB with low and high initial D_r.

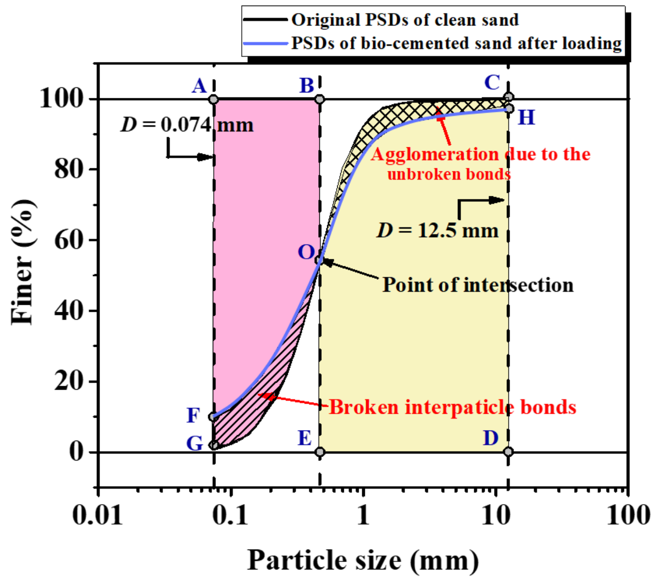

Fig. 4-7 The conceptual PSDs of bio-cemented sand after compression.

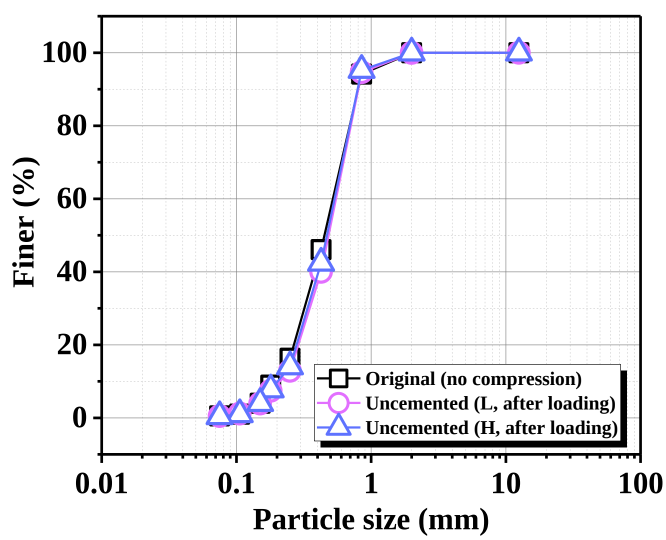

Fig. 4-8 The comparison of pre-compression and post-compression PSDs of untreated calcareous sand.

Meanwhile, the increased coarse portion of bio-cemented sand compared with that of uncemented sand after compression was likely attributed to the agglomeration effect of the remaining unbroken interparticle bonding. Due to the unbroken interparticle bonds, some larger cemented lumps were generated after compression. To quantify how coarse portion of bio-cemented sand PSDs was affected by the cementation content after compression, an analogical concept of Relative Agglomeration (A_r) was proposed in the current study, which is defined as:

$$A_r = \frac{A_t}{A_p} = \frac{S_{OCHO}}{S_{OCDE}} \tag{4-4}$$

where A_t is the total agglomeration; A_p is the potential of agglomeration for the whole sand specimen; S_{OCHO} and S_{OCDE} are the patterned and yellow areas illustrated in **Fig. 4-7**. The total agglomeration (A_t) is defined as:

$$A_t = S_{OCO} = \int_{\mathrm{y}}^{1} (a_{po} - a_{pf}) df \tag{4-5}$$

where, df is a differential of "finer (%)"; a_{po} is the pre-compression potential for agglomeration, a_{pf} is the post-compression potential for agglomeration. The potential of agglomeration (a_p) for a given size fraction (D) is defined as:

$$a_p = \log_{10}\left[\frac{D_c \text{ mm}}{D \text{ in mm}}\right] (\text{for } D \leq 12.5\text{mm}) \tag{4-6}$$

$$a_p = 0 \ (\text{for } D > 12.5\text{mm}) \tag{4-7}$$

where, D_c =12.5 mm is the maximum sieve opening size used in the current study. The potential of agglomeration (A_p) for the whole sand specimen can be expressed as:

$$A_p = S_{OCDE} = \int_{\mathrm{y}}^{1} a_p df \tag{4-8}$$

Where, y is the "finer (%)" of the intercept point between PSDs of original sand and PSDs of bio-cemented specimen.

The calculated B_r and A_r are shown in **Fig. 4-9**. Clearly, they were both significantly influenced by initial D_r and cementation content. On the one hand, at a similar cementation content, the specimens with higher initial D_r had smaller B_r ranging from 0.3% to 3.4%, while larger B_r ranging from 1.7% to 6.25% was observed in the specimens with lower initial D_r. This observation implied that the dense packing reduced the distance between particles, and stronger interparticle bonds could be formed. In addition, it could be found that B_r gradually decreased with the increase of cementation content for a given initial D_r, suggesting that elevated cementation content could also induce more interparticle bonds. On the other hand, in contrast to B_r, the higher initial D_r and more cementation content resulted in a larger A_r. The larger A_r indicated that more interparticle bonds remained effective. These phenomena suggested that the interparticle bonding breakage during compression could be effectively reduced by increasing the initial D_r and the cementation content. It should also be noted that B_r and A_r values in this study did not show significant difference between the specimens treated by YE and NB enrichment media.

4.3.6 Microscopic observations

To further explain the features of the fine and coarse portion in the PSDs of bio-cemented sand, the images of post-compression samples passing through the 0.075mm sieve and retained on the 12.5 mm sieve were shown in **Fig. 4-10** and **Fig. 4-11**, respectively.

Firstly, the fine portion of the post-compression microscopic images of uncemented and bio-cemented sand (taking 0.5_10_YE(L) as an example) are presented in **Fig. 4-10**. In the case of uncemented sand, individual small sand particles could be seen clearly without interparticle bonding. In contrast, in the case of bio-cemented sand (**Fig. 4-10 (b))**, the sand particles were covered by large amounts of white powders, which were presumably regarded as loose fine calcium carbonate crystals from the breakage of interparticle bonding. This observation was in agreement with the PSD results that the percentage of fine portion (D < 0.075 mm) increased in bio-cemented sand after the completion of the one-dimensional compression test.

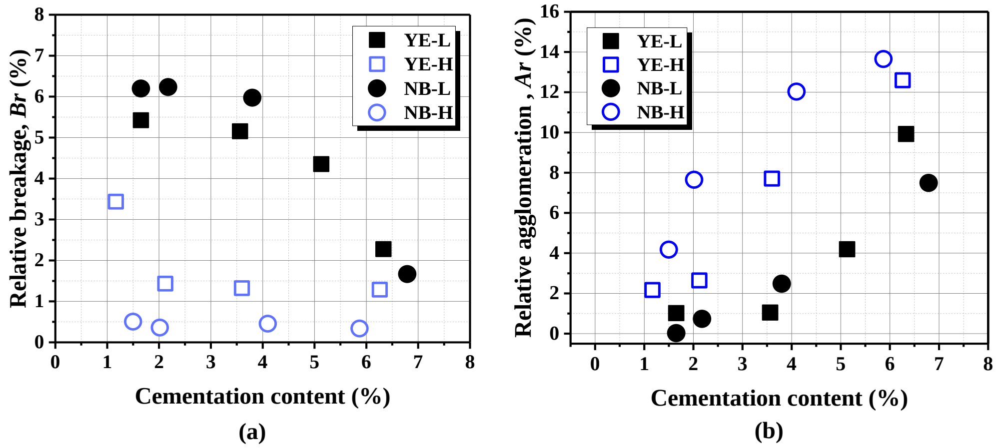

Fig. 4-9 The relationship between cementation content and (a) relative breakage; (b) relative agglomeration.

Secondly, the representative micro-features of the lump with dimensions of 2 cm×2 cm (maximum length ×maximum width) collected from the specimen of 0.5_10_YE(L) are shown in **Fig. 4-11**. The sample shown in **Fig. 4-11 (c)** was the same as that in **Fig. 4-11 (a)**, but carefully washed by deionized water to remove the loose debris around the lump. **Fig. 4-11(b)** and **(d)** are the magnified images (2.7×) of **Fig. 4-11 (a)** and **(c)**, respectively. It could be found from **Fig. 4-11 (a)** and **(b)** that the entire lump was covered by many tiny loose white crystals on the surface of sand particles. These crystals possibly came from the breakage and abrasion of interparticle cementation bonding. Then in **Fig. 4-11 (c)** and **(d),** in which the lump was carefully washed by the deionized water, the cemented sand particle aggregates could be observed. In summary, the microstructural observation results could reveal that most interparticle bonds of bio-cemented sand were broken at the stress level encountered in the current study. However, there were still some unbroken interparticle bonds remaining within the cemented sand aggregates.

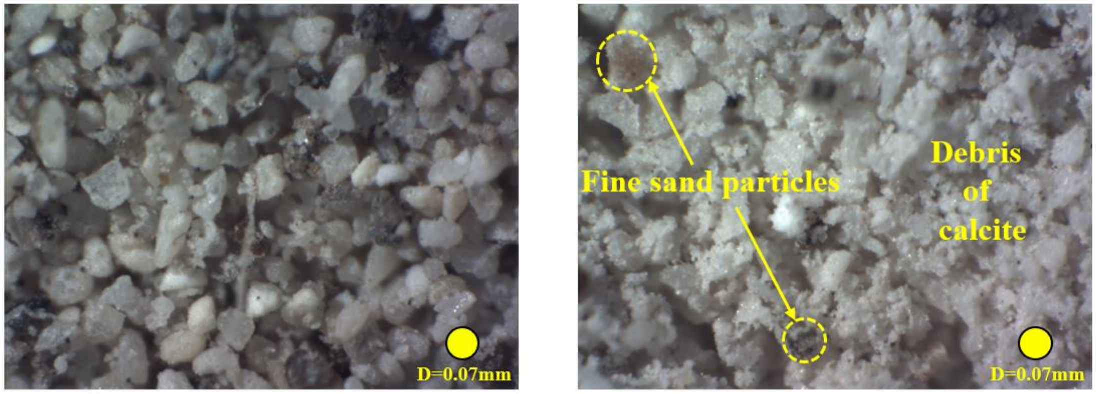

(a) (b)

Fig. 4-10 The post-compression microscopic images of (a) uncemented sand and (b) bio-cemented sand (take 0.5_10_YE(L) as an example).

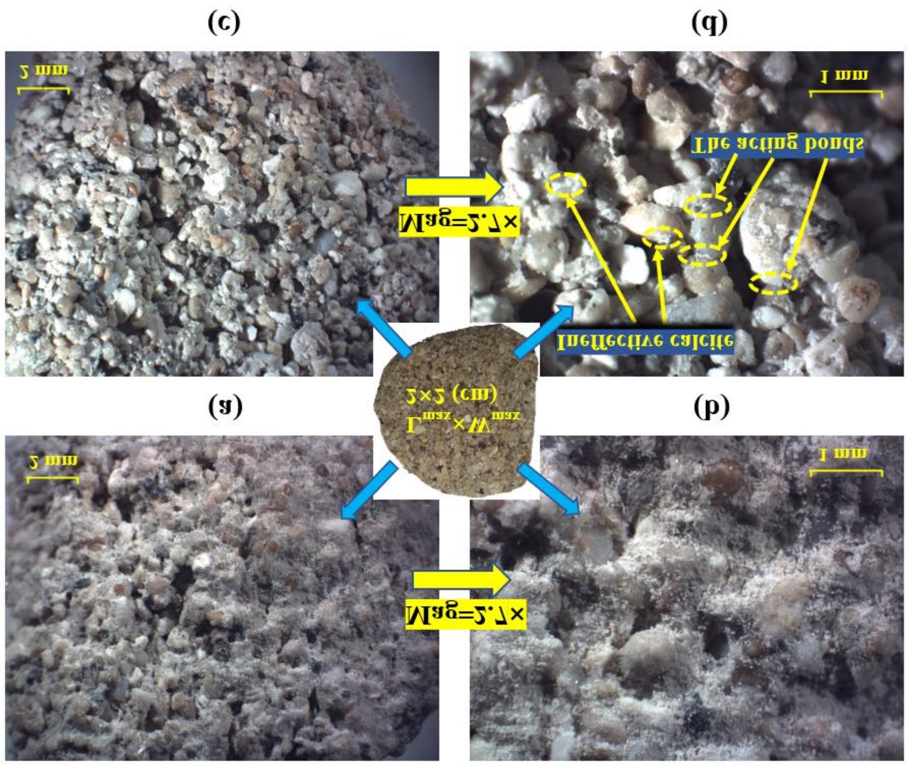

Fig. 4-11 The micro-features of a representative lump collected from the specimen of 0.5_10_YE(L) after compression test: (a) filled with cementation debris; (b) the magnified image of (a); (c) filled without cementation debris; (d) the magnified image of (c).

4.4 Discussion

4.4.1 Conceptual framework for the compressibility behavior of bio-cemented calcareous sand

To facilitate a better understand the compressibility behavior of bio-cemented calcareous sand, a conceptual framework showing the external factors, interparticle contact mode, and damage mode was proposed in the current study as shown in **Fig. 4-12**. This framework was inspired by numerous previous studies on the compressibility of sand with fines. For instance, Yamamuro and Lade (1997) and Yamamuro and Wood (2004) presented a series of possible grain contacts (i.e., large particle-large particle, large particle-small particle-large particle, large particle-small particle-void) when silty sand was deposited among larger sand particles, which could have effect on the compressibility of silty sand. Analogous to the influence of silt grains in their studies, bio-cementation is present among large calcareous sand particles to form different contact modes and can be easily damaged during compression through different modes. Therefore, the evolution of bio-cementation during compression and the interactions between bio-cementation and its neighboring calcareous sand particles are critical to the compressibility behavior of bio-cemented sand.

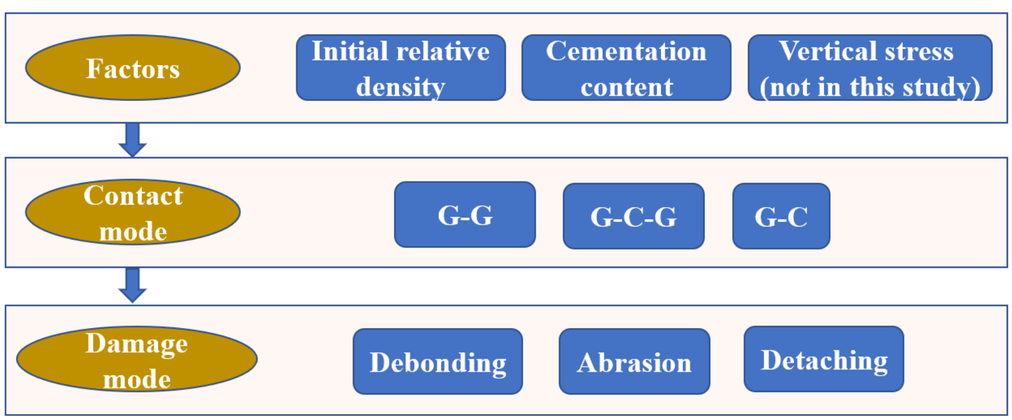

Fig. 4-12 A conceptual framework for understanding compressibility behavior of bio-cemented sand (note: G-grain; C-cementation).

The core of this conceptual framework is the three interparticle contact modes: G-G (grain to grain), G-C-G (grain to cementation to grain), and G-C (grain to cementation), as demonstrated in **Fig. 4-13(a)**. G-G contact is normally considered as a frictional and unstable contact in uncemented sand, and grain rearrangement may occur during compression or shearing. However, in bio-cemented sand, the presence of bio-cementation significantly reduces the G-G contacts (frictional contacts), and consequently the proportions of other contact modes related to bio-cementation (G-C and G-C-G) increase accordingly (Dadda et al., 2019). Since the existence of bio-cementation restricts the movement of sand particles, the unstable G-G contact in bio-cemented sand became less compared with the uncemented sand. Secondly, G-C-G contacts are the unique to bio-cemented sand. Bio-cementation, as a bridge, connects two adjacent sand particles and forms a force chain. The force transfer through G-C-G contacts is largely dependent on the abundance and strength of interparticle bonding, which can be seen as a stable contact. Thirdly, G-C is the weakest contacts in the bio-cemented sand. Large amounts of calcium carbonate deposit on the surface of sand particles, which do not contact with other sand particles. The attached calcium carbonate can be easily detached during the rearrangement of sand particles. Finally, it worth mentioning that these three contact modes co-exist in a typical bio-cemented sand.

Debonding, detachment, and abrasion as shown in **Fig. 4-13(b)** are the three proposed damage modes for bio-cemented calcareous under compression. Debonding refers to the breakage of the interparticle bonds under normal compressive stress; detachment refers to the separation of attached or coated bio-cementation from sand particle surfaces; Abrasion refers to the bio-cementation is ground into several much smaller pieces under tangential shear stress. The three damage modes discussed here derive from either pure compression under normal stress or shearing under tangential stress.

The damage modes associated with the three contact modes (i.e., G-G, G-C-G, and G-C) are different during the compression test. The G-G contact, as a pure frictional contact mode in clean sand, is reduced substantially in the bio-cemented sand. Even if all interparticle bonds of bio-cementation are destroyed during compression, the damage to individual calcareous sand particles is still negligible at the stress levels set in the current study. Consequently, none of the three damage modes are associated with the G-G contact.

However, sliding and particle rearrangement can still occur for the G-G contact, as those in the case of uncemented sand. For the G-C-G contact, firstly debonding evolves with the increasing vertical stress, which is the main contributor for overall volumetric deformation. Then, with debonding and detachment damage progresses, abrasion becomes more and more predominant as particle rearrangement and relocation dominate at this stage. During particle rearrangement and relocation, the interparticle friction forces abrade the bio-cementation progressively and thus lead to further overall volumetric compression. Finally for the G-C contact, the calcium carbonate deposited on the surface can be easily detached from its parent particle because of the particle rearrangement. The increased finer particles observed in **Fig. 4-7** are assumed to be the results of the combining effects of these damage modes. The detached fine calcium carbonate crystal particles simply reside or fill in the voids between larger grains and their primary role is to increase the density of specimen.

With the proposed conceptual framework of contact and damage modes, the macro-scale irreversible volumetric deformation of bio-cemented sand could be associated with these contact and damage modes. In the following paragraphs, the effect of external factors (i.e., initial D_r, cementation content, and vertical stress) on the compressibility behavior of bio-cemented calcareous sand will be interpreted based on the conceptual framework.

Initial D_r: At a given cementation level and vertical stress, the effect of initial D_r on the compressibility of bio-cemented sand is primarily attributed to the following three mechanisms: (1) Similar to the uncemented sand, increasing initial D_r can reduce the compressibility of bio-cemented sand by densification (i.e., sliding, rotation, etc.). (2) By increasing the initial D_r (i.e., reducing the interparticle distance), sand particles can be more readily bridged by bio-cementation. The interparticle bio-cementation is favorable to prevent the occurrence of particle rearrangement due to the bonding effect by forming the effective G-C-G contacts. (3) The amounts of G-G contact can be increased by elevating the initial D_r, which is a stable contact if particle rearrangement can be effectively constrained by G-C-G contacts around the G-G contact points. In this way, more G-G contacts could withstand the applied compressive force, thus reducing the crushing of interparticle cementation. This explains why the PSDs shift upward on the left-side portion (i.e., fine portion) in **Fig. 4-7** and smaller B_r values (**Fig. 4-9(a)**) are obtained in the specimen with higher initial D_r. With the combined role of the three above mentioned mechanisms, the compressibility can be improved significantly in the specimens with higher initial D_r specimens, resulting in a 20%-70% smaller a_v value as observed in **Fig. 4-4**.

Cementation Content: at a given initial D_r and vertical stress, the effect of the cementation content on the compressibility of bio-cemented sand is due to the following two mechanisms: (1) The higher cementation content, the more effective interparticle bonds (i.e., G-C-G contacts) and the stronger interparticle bonding strength can be formed within the soil matrix. Consequently, a decreasing B_r is observed with the increasing cementation content (as shown in **Fig. 4-9(a)**). Also, it should be noted that more interparticle bonds will not be broken with the increasing cementation content when the vertical load reaches up to 6.4MPa in the current study, which explains the increase of A_r with the elevated cementation content (as shown in **Fig. 4-9(b)**). (2) The increasing cementation content can elevate the density of bio-cemented sand by filling pores to form more G-C and G-C-G contacts, and the space available for particle rearrangement is limited, which can make severe abrasion and result in the increase of much smaller fine particles.

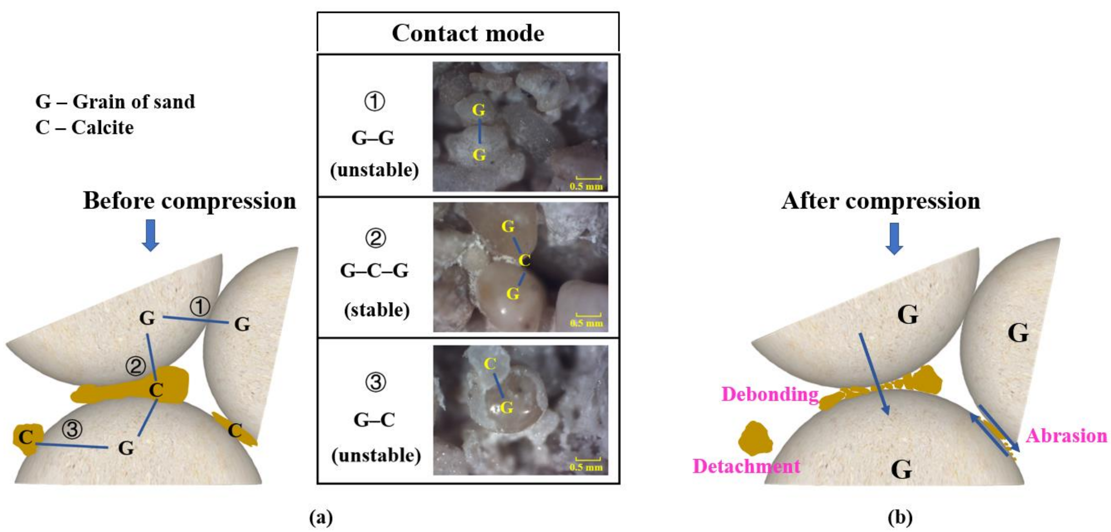

Fig. 4-13 The explanation of conceptual framework: (a) the contact modes before compression; (b) the damage modes after compression.

4.5 Implications for engineering practice

This study investigated the compressibility behavior of bio-cemented calcareous sand treated through bio-stimulated MICP. The results are likely to benefit the design and construction of structures on problematic calcareous sand by providing a technically sound and new soil stabilization method.

Many studies including the current one has clearly shown that bio-cementation can improve the compressibility of granular soils. The observations from the current study provide some implications for the application of bio-stimulated MICP in the field. The bio-cemented sand in the field may not experience an extremely high vertical stress to break all interparticle cementation bonds and even the sand particles. To ensure the bearing capacity of bio-cemented sand, such high stress that may cause the bio-cementation to lose the efficacy in resisting compressibility should be prevented. Therefore, prior to the field implementation of bio-cementation, it is crucial to accurately estimate the potential maximum vertical stresses that the bio-cemented calcareous sand may experience.

4.6 Conclusion

In this study, a series of one-dimension compression tests were conducted to investigate the compressive behaviors of bio-cemented calcareous sand treated using the bio-stimulated MICP approach. The main conclusions are drawn as follows:

(1) The a_v value was found to decrease with the increasing cementation content. Contrarily, the specimens with higher initial D_r had smaller (approximately 20%-70%) a_v values than their counterparts with lower initial D_r. In terms of C_r value, higher initial D_r resulted in a larger C_r, and C_r decreased with the increasing cementation content.

(2) Based on the analysis of PSDs curves after compression, the specimen with higher initial D_r and more CC resulted in a smaller B_r and a larger A_r. More fines were generated in bio-cemented specimens with higher cementation content and lower initial D_r. The increased fines mainly came from the debris of calcium carbonate, which is revealed by microscopic images. Additionally, some larger lumps appeared as the result of residual agglomeration effect of some undamaged cementations.

(3) A conceptual framework based on the interparticle contact modes (i.e., G-G; G-C-G; G-C) and their corresponding damage modes (i.e., detachment; debonding; abrasion)

during the compression tests was proposed. Compared with G-G and G-C modes, the G-C-G was the strongest contact mode for the bio-cemented sand. During compression, debonding and detachment firstly occurred in the G-C-G and G-C contacts mode, respectively. Abrasion damage mode then became predominant as debonding and detachment progressed during particle rearrangement and relocation.

Reference

Altuhafi, F. N. and Coop, M. R., 2011. Changes to particle characteristics associated with the compression of sands. Géotechnique, 61(6), 459-471. https://doi:10.1680/geot.9.p.114.

Arboleda-Monsalve, L. G. Zapata-Medina, D. G. and Galeano-Parra, D. I., 2019. Compressibility of biocemented loose sands under constant rate of strain, loading, and pseudo K0-triaxial conditions. Soils Found. 59(5), 1440-1455. https://doi:10.1016/j.sandf.2019.06.008.

ASTM International. 2017. ASTM D6913/D6913M-17, Standard test method for particle-size distribution (gradation) of soils using sieve analysis.

Bohnhoff, G. L. and Shackelford, C. D., 2014. Consolidation behavior of polymerized bentonite-amended backfills. J. Geotechn. Geoenviron. 140(5), 04013055. https://doi:10.1061/(asce)gt.1943-5606.0001079.

Bryant, W. R. Deflache, A. P. and Trabant, P. K., 1974. Consolidation of marine clays and carbonates. In Deep-sea sediments. Springer, Boston, MA, pp. 209-244.

Cecconi, M. Viggiani, G. and Rampello, S., 1998. An experimental investigation of the mechanical behaviour of a pyroclastic soft rock. The geotechnics of hard soils-soft rocks. Proceedings of the second international symopsium on hard soils-soft rocks, Naples, pp. 473-482.

Coop, M. R. Sorensen, K. K. Bodas Freitas, T. and Georgoutsos, G., 2004. Particle breakage during shearing of a carbonate sand. Géotechnique, 54(3), 157-163. https://doi:10.1680/geot.2004.54.3.157.

Cuccovillo, T. and Coop, M. R., 1999. On the mechanics of structured sands. Géotechnique, 49(6), 741-760.

Dadda, A. Geindreau, C. Emeriault, F. Du Roscoat, S. R. Filet, A. E. and Garandet, A., 2019. Characterization of contact properties in biocemented sand using 3D X-ray micro-tomography. Acta Geotech. 14(3), 597-613. https://doi:10.1007/s11440-018-0744-4.

Dehnavi, Y. Shahnazari, H. Salehzadeh, H. and Rezvani, R., 2010. Compressibility and undrained behavior of Hormuz calcareous sand. Electron. J. Geotech. Eng. 15(1), 1684-1702.

DeJong, J. T. Mortensen, B. M. Martinez, B. C. and Nelson, D. C., 2010. Bio-mediated soil improvement. Ecol. Eng. 36(2), 197-210. https://doi.org/10.1016/j.ecoleng.

Hardin, B. O., 1985. Crushing of soil particles. J. Geotech. Eng. 111(10), 1177-1192.

Jafari, M. Shahsavari, M. and Grabinsky, M., 2020. Experimental Study of the Behavior of Cemented Paste Backfill under High Isotropic Compression. J. Geotechn. Geoenviron. 146(11), 06020019. https://doi:10.1061/(asce)gt.1943-5606.0002383.

Lee, M. L. Ng, W. S. and Tanaka, Y., 2013. Stress-deformation and compressibility responses of bio-mediated residual soils. Ecol. Eng. 60, 142-149. https://doi:10.1016/j.ecoleng.2013.07.034.

Lin, H. Suleiman, M. T. Brown, D. G. and Kavazanjian Jr, E., 2016. Mechanical behavior of sands treated by microbially induced carbonate precipitation. J. Geotech. Geoenviron. 142(2), 04015066. https://doi:10.1061/(asce)gt.1943-5606.0001383.

Liu, H. Zeng, K. and Zou, Y., 2020. Particle breakage of calcareous sand and its correlation with input energy. Int. J. Geomech. 20(2), 04019151. https://doi:10.1061/(asce)gm.1943-5622.0001541.

Lv, Y. Li, X. and Wang, Y., 2020. Particle breakage of calcareous sand at high strain rates. Powder Technol. 366, 776-787. https://doi:10.1016/j.powtec.2020.02.062.

Lv, Y. Liu, J. and Xiong, Z., 2019. One-dimensional dynamic compressive behavior of dry calcareous sand at high strain rates. J. Rock Mech. Geotech. Eng. 11(1), 192-201. https://doi:10.1016/j.jrmge.2018.04.013.

McDowell, G. R., 2002. On the yielding and plastic compression of sand. Soils Found. 42(1), 139-145. https://doi:10.3208/sandf.42.139.

Roscoe, K. H. Schofield, A. and Thurairajah, A., 1963. Yielding of clays in states wetter than critical. Geotechnique, 13(3), 211-240.

Rotta, G. V. Consoli, N. C. Prietto, P. D. M. Coop, M. R. and Graham, J., 2003. Isotropic yielding in an artificially cemented soil cured under stress. Geotechnique, 53(5), 493-501. https://doi:10.1680/geot.2003.53.5.493.

Rowshanbakht, K. Khamehchiyan, M. Sajedi, R. H. and Nikudel, M. R., 2016. Effect of injected bacterial suspension volume and relative density on carbonate precipitation resulting from microbial treatment. Ecol. Eng. 89, 49-55. https://doi:10.1016/j.ecoleng.2016.01.010.

Shahnazari, H. and Rezvani, R., 2013. Effective parameters for the particle breakage of calcareous sands: An experimental study. Eng. Geol. 159, 98-105. https://doi:10.1016/j.enggeo.2013.03.005.

Shipton, B. and Coop, M. R., 2012. On the compression behaviour of reconstituted soils. Soils Found., 52(4), 668-681. https://doi:10.1016/j.sandf.2012.07.008.

Silva dos Santos, A. P. Consoli, N. C. Heineck, K. S. and Coop, M. R., 2010. High-stress isotropic compression tests on fiber-reinforced cemented sand. J. Geotech. Geoenviron. 136(6), 885-890. https://doi:10.1061/ASCEGT.1943-5606.0000300.

Tsukamoto, M. and Oda, K., 2013. Influence of relative density on microbial carbonate precipitation and mechanical properties of sand. In Proceedings of the 18th International Conference on Soil Mechanics and Geotechnical Engineering, Paris, pp. 2613-2616.

Wang, J. Fan, P. Wang, M. Dong, L. Ma, L. and Gao, L., 2020b. Experimental study of one-dimensional compression creep in crushed dry calcareous sand. Can. Geotech. J. 57(12), 1854-1869. https://doi:10.1139/cgj-2019-0406.

Wang, X. Shan, H. Wu, Y. Meng, Q. and Zhu, C., 2020c. Factors affecting particle breakage of calcareous soil retrieved from South China Sea. Geomech. Eng. 22(2), 173-185. https://doi.org/10.12989/gae.2020.22.2.173.

Wang, Y. J. Han, X. L. Jiang, N. J. Wang, J. and Feng, J., 2020a. The effect of enrichment media on the stimulation of native ureolytic bacteria in calcareous sand. Int. J. Environ. Sci. Technol. 17(3), 1795-1808. https://doi:10.1007/s13762-019-02541-x.

Wei, H. Zhao, T. Meng, Q. Wang, X. and Zhang, B., 2020. Quantifying the morphology of calcareous sands by dynamic image analysis. Int. J. Geomech. 20(4), 04020020. https://doi:10.1061/(ASCE)GM.1943-5622.0001640.

Xiao, Y. Chen, H. Stuedlein, A. W. Evans, T. M. Chu, J. Cheng, L. Jiang, N. Lin, H. Liu, H. and Aboel-Naga, H. M., 2020a. Restraint of particle breakage by biotreatment method. J. Geotech. Geoenviron. 146(11), 04020123. https://doi:10.1061/(asce)gt.1943-5606.0002384.

Xiao, Y. Liu, H. Chen, Q. Ma, Q. Xiang, Y. and Zheng, Y., 2017. Particle breakage and deformation of carbonate sands with wide range of densities during compression loading process. Acta Geotech. 12(5), 1177-1184. https://doi:10.1007/s11440-017-0580-y.

Xiao, Y. Yuan, Z. Chu, J. Liu, H. Huang, J. Luo, S. N. Wang, S. and Lin, J., 2019. Particle breakage and energy dissipation of carbonate sands under quasi-static and dynamic compression. Acta Geotech. 14(6), 1741-1755. https://doi:10.1007/s11440-019-00790-1.

Xiao, Y. Yuan, Z. Lv, Y. Wang, L. and Liu, H., 2018. Fractal crushing of carbonate and quartz sands along the specimen height under impact loading. Constr. Build. Mater. 182, 188-199. https://doi:10.1016/j.conbuildmat.2018.06.

Xiao, Y. Yuan, Z. Desai, C. S. Zaman, M. Ma, Q. Chen, Q. and Liu, H., 2020b. Effects of Load Duration and Stress Level on Deformation and Particle Breakage of Carbonate Sands. Int. J. Geomech. 20(7), 06020014. https://doi:10.1061/(asce)gm.1943-5622.0001731.

Xiao, Y. Zhao, C., Sun, Y. Wang, S. Wu, H. Chen, H. and Liu, H., 2021. Compression behavior of MICP-treated sand with various gradations. Acta Geotech. 16(5), 1391-1400. https://doi:10.1007/s11440-020-01116-2.

Yamamuro, J. A. and Lade, P. V., 1997. Static liquefaction of very loose sands. Can. Geotech. J. 34(6), 905-917. https://doi.org/10.1139/t97-057.

Yamamuro, J. A. and Wood, F. M., 2004. Effect of depositional method on the undrained behavior and microstructure of sand with silt. Soil Dyn. Earthq. 24(9-10), 751-760. https://doi:10.1016/j.soildyn.2004.06.004.

CHAPTER 5. The Shearing Behaviors of Biochar-amended Bio-cemented Calcareous Sand Treated by Bio-stimulation

5.1 Introduction

As mentioned in the previous chapters, existing studies have shown a notable potential of MICP in improving the soil's mechanical performances. Obtaining as much urease activity within soils as possible is highly necessary to reduce the cost of in-situ application of MICP (Cheng and Cord-Ruwisch, 2012). It was found that the treatment method has great impact on the preservation of urease activity is soil. For example, the commonly used bacterial fixation and distribution method used by Harkes et al. (2010) can result in about 15% loss and 70% loss for submersed and percolation treatment method (Cheng and Cord-Ruwisch, 2012). The loss of urease activity in soils may restrict the increase of bio-cementation content and soil strength. Therefore, it is necessary for researchers to find a way to preserve the enriched urease within soils as much as possible, to further increase the bio-cementation content.

Biochar is a stable solid residue produced through the pyrolysis of leaves, branches, wood chip or other agricultural wastes under anoxic condition. It is normally rich in carbon and can endure in soil for thousands of years. It is evident that biochar has several positive effects on enhancing soil physical and chemical properties (Verheijen et al. 2010). Firstly, the presence of biochar in soil can increase the overall net surface area of soil particles (Chan et al., 2008), and the porous structure makes biochar effective at retaining both water and water-soluble nutrients (Verheijen et al., 2010; Downie et al., 2012). Secondly, biochar possesses high cation exchange capacity that cations from the aqueous phase can be adsorbed onto the surface by ionic interactions (Downie et al. 2012). Based on these physical and chemical characteristics, efforts have been made to use biochar as an amendment in heavy metals (including Cd, Pb, As and Zn) fixation for contaminated soils (Puga, 2015; Houben et al., 2013; Yu et al., 2017; Tan et al., 2020). Thirdly, biochar could also contribute to the strength improvement and hydration reaction enhancement of cementitious materials (Han et al., 2020; Berti et al., 2021; Gupta et al., 2018; Wang et al., 2020). Fourthly, according to Kolb et al. (2009), biochar can also improve the soil-microbe interactions. That is to say, the micropores within biochar become refugia for microorganisms, which is likely to be one of the mechanisms for the increase of microbial biomass in soil. Based on these superior functions of biochar, it is rational to assume that the bio-stimulated MICP approach, a process that highly relies on the microbial activities in soil, could be enhanced by amending biochar.

In this chapter, the shear behavior of biochar-amended bio-cemented calcareous sand treated via bio-stimulation was investigated through a series of direct shear test. The samples underwent enrichment phase and cementation phase to enrich ureolytic bacteria and form bio-cementation. Upon the completion of bio-stimulated MICP treatment, direct shear test was performed to obtain the shear behaviors and shear parameters including peak stress ratio, friction angle and cohesion. Meanwhile, the specimens were subjected to cementation content measurement and microscopic observations to reveal the fundamentals of the enhancement effect of biochar on bio-cemented calcareous sand.

5.2 Materials and Methods

5.2.1 Calcareous Sand

The calcareous sand used in this study was collected from the Waikiki Beach, Oahu Island, Hawaii, USA. The sand on the beach surface (up to 5 cm depth) was sampled to ensure the presence of sufficient aerobic microbes. The particle size distribution of the sampled calcareous sand is shown in **Fig. 3-1**. After taking to the laboratory, the sand was firstly sieved through US No.10 sieve (2 mm opening size) to remove oversized grains. Small twigs, grass and microplastic particles were also removed from the collected samples. Other basic physical and index properties of the calcareous sand are listed in **Table 3-1**.

5.2.2 Biochar

The biochar used in this study was produced by Pacific Biochar (Santa Rosa, CA) purely from softwood forestry residues, which had a bulk density of 155.8 kg/m^3. The Butane activity was 7%, and the cation exchange capacity was 21.5 meq/100g. The chemical contents in biochar are shown in **Table 5-1**. Before mixed with soil, the air-dried biochar was sieved through US No.325 sieve to remove grains larger than 0.045 mm. This was to achieve a uniform distribution within soil matrix.

Table 5-1 The biochar chemical content in mass.

Ingredient	Content (%)
N	0.7
P_2O_5	0.8
K_2O	3.3
Ca	4.5
Mg	0.5
C	90.2

5.2.3 Enrichment and Cementation Solutions

The enrichment medium containing 20 g/L yeast extract (YE) and 10.21 g/L urea was used in this study, which had been proved to be effective in enriching the indigenous ureolytic bacteria (Wang et al., 2018; 2020b). In it, YE was one of the organic complex nutrients containing sufficient proteins, amino acids and growth factors for bacteria. Urea served as a selective substrate which favored the growth of ureolytic bacteria in soil. The cementation solution consisted of equal mole concentration (0.5 M) of urea and $CaCl_2$ plus 0.2 g/L YE. The additional 0.2 g/L YE was to supply further nutrients to maintain the bacterial viability during the cementation phase.

5.2.4 Procedures for MICP Treatment through Bio-stimulation

Samples were prepared using brass rings with height of 2.54 cm and inner diameter of 6.35 cm. The fresh calcareous sand was firstly mixed uniformly with the air-dried biochar powder, which was followed by the introduction of 0.5 PVs (pore volumes) enrichment medium. Then, the moist sand-biochar mixture was compacted in three layers in a brass ring to achieve two different initial relative densities (D_r = 16.2% and 54.6%) using the moist temping method. After that, all specimens were left for 48 hours for stimulating the growth of indigenous ureolytic bacteria at 20°C. It should be noted that the sand was only mixed with enrichment solution once during the process of sample preparation. Upon the completion of the enrichment phase, the cementation solution was flushed through specimens by surface percolation once per day for consecutive 5 or 10 days to achieve varying cementation content level. The flushing rate was kept at 2 mL/min to avoid too much disturbance on soil structure. The volume of flushed cementation solution each time was 1.5 PVs of the sand specimen. After the completion of the cementation phase, all specimens were flushed with 3PVs deionized water for 5 times to remove residual dissolved salts and then oven-dried (under 105 ℃) for 24 hours. The dried bio-cemented specimens with various biochar contents (i.e., 0%, 0.1%, 0.3% and 0.5%) were exhibited in **Fig. 5-1**.

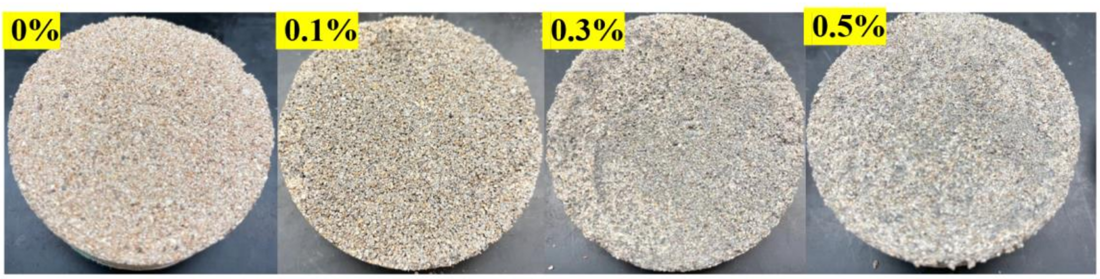

Fig. 5-1 The top views of bio-cemented calcareous sand amended with 0%, 0.1%, 0.3%, and 0.5% biochar content.

5.2.5 Direct Shear Test

The direct shear tests were performed using the Geocomp® Shear Trac-II-DSS system, and at five normal stress levels, i.e., 50, 100, 200, 400, 600 kPa, respectively. The shear rate was kept constant at 1 mm/min. For comparison, the corresponding specimens without biochar and treated under the same situation were also tested. All cases tested in this study are listed in **Table 5-2**.

5.2.6 Determination of Cementation Content

The cementation content (*CC*) was determined by measuring the mass change before and after bio-stimulated MICP treatment. It could be expressed as:

$$\text{Cementation content } (CC) = \frac{m_{at} - m_{bt} - m_B}{m_{bt}} \times 100\% \tag{5-1}$$

Where, m_{bt} is the dry mass of specimen prior to MICP treatment; m_{at} is the dry mass of specimen after MICP treatment; m_B is the dry mass of added biochar.

Table 5-2 Experimental program of the direct shear test.

Specimen (*X_Y_Z*) [a]	Initial relative density (%)	Biochar content [b] (% in *W/W*)	Flushes during cementation phase	Normal stress (kPa)
0%_5_L	16.2	0	5	50, 100, 200, 400, 600
0%_5_H	54.6			
0%_10_L	16.2		10	
0%_10_H	54.6			
0.1%_5_L	16.2	0.1	5	
0.1%_5_H	54.6			
0.1%_10_L	16.2		10	
0.1%_10_H	54.6			
0.3%_5_L	16.2	0.3	5	
0.3%_5_H	54.6			
0.3%_10_L	16.2		10	
0.3%_10_H	54.6			
0.5%_5_L	16.2	0.5	5	
0.5%_5_H	54.6			
0.5%_10_L	16.2		10	
0.5%_10_L	54.6			

[a] The designation "*X_Y_Z*" represents the bio-cemented specimens treated with "*Y*" days of flushing with "*X*" biochar content. The "*Z*" represents the initial relative density level ("L" representing low (16.2%) and "H" representing high (54.6%))
[b] The biochar content equals to the weight ratio of dry biochar to dry sand.

5.2.7 Microstructural Images

The microstructural images of bio-cemented specimens were characterized through optical microscopy using a Nikon SMZ1500 stereo microscope. The zoom ratio of 15 to 1 provided the SMZ1500 with a range of total magnifications from 3.75x up to 540x, depending on the oculars and objectives selected.

5.3 Results

5.3.1 Cementation Content

The *CC* of all specimens were shown in **Fig. 5-2**. Generally, the addition of biochar could yield significant increase in *CC* compared with the specimens without biochar. In addition, the *CC* increased with the elevated amount of biochar for the specimen prepared and treated under the same conditions. More specifically, for the "5_L" specimens (5 – 5-day treatment, L – low initial D_r) containing 0.1%, 0.3%, and 0.5% biochar, the *CC* had 2.5%, 2.6%, and 4% increase compared with those without biochar, respectively. Similarly, 2.1%, 2.4%, and 4.2% increase were observed in the "5_H" specimens (5 – 5-day treatment, H – high initial D_r), 1.6%, 1.65%, and 1.7% increase occurred in the "10_L" specimens (10 – 10-day treatment, L – low initial D_r), and 2.1%, 2.6%, and 2.85% increase were found in the "10_H" specimens (10 – 10-day treatment, H– high initial D_r). It could also be found that *CC* increased with the duration of cementation solution treatment when the initial D_r was the same, which was in an agreement with many other previous studies (Cui et al. 2017; Nafisi et al. 2020; Feng and Montoya 2016). Moreover, it seemed that lower D_r could resulted in a higher *CC* when the other conditions were the same, which was also observed by other researchers (Tsukamoto and Oda 2013; Rowshanbakht et al. 2016). This was likely, on one hand, due to the decreasing pore volumes for the nucleation sites of cementation in higher initial D_r, and on the other hand, the decreasing amounts of microbes and nutrients that could be absorbed in the higher initial D_r samples.

5.3.2 Shear Behavior from the Direct Shear Test

Fig. 5-3 showed the representative stress *v.s.* horizontal displacement curves of the specimens with high initial D_r and high *CC* (i.e., "10_H" case) and the ones with low initial D_r and low *CC* (i.e., "5_L" case) under various normal stresses. For the high initial D_r and high *CC* specimens, it could be observed that the shear stress gradually increased with horizontal displacement and reached the peak shear stress, after which it decreased to a relatively constant value with respect to horizontal displacement. In other words, the specimens showed an evident post-failure strain softening behavior. It could be also seen that as the normal stress increased, the peak shear stress increased accordingly for both "10_H" and "5_L" specimens. This was due to the fact that the elevated normal stress increased the interparticle contact areas and thus increased the frictional resistance, which led to a higher peak shear stress. For the low initial D_r and low *CC* specimens, similar trend and pattern could be observed under low normal stresses of 50, 100, 200 and 400 kPa. However, the shear stress–horizontal displacement curve showed strain hardening at high normal stress of 600 kPa, and the residual or critical shear stress could not be achieved due to the limit of shear displacement that could be reached.

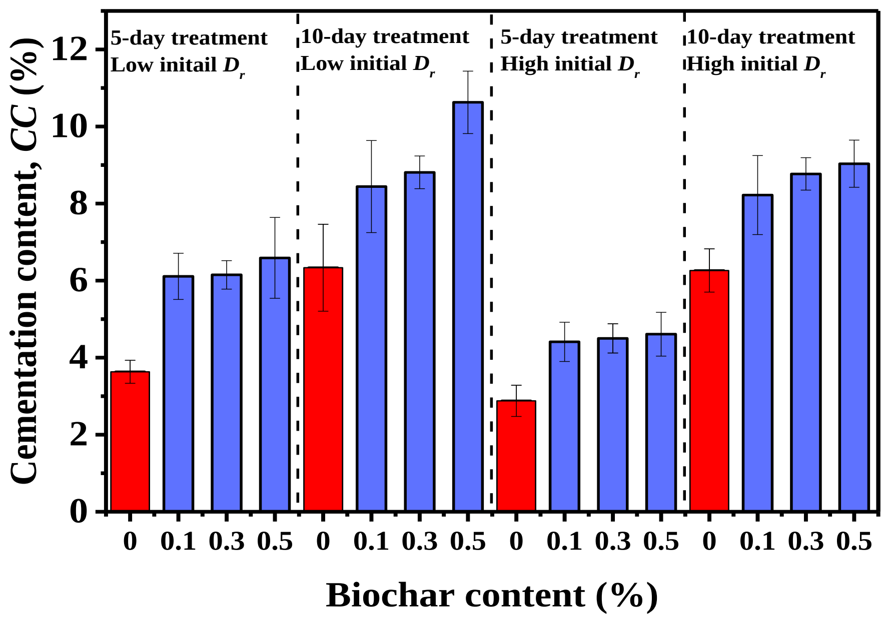

Fig. 5-2 The cementation content of bio-stimulated MICP treated sand for each condition.

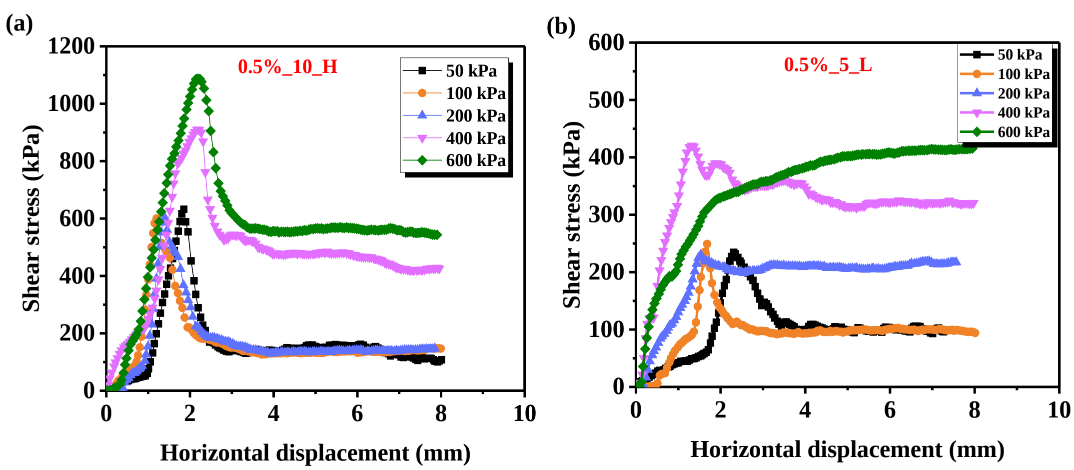

Fig. 5-3 Shear stress *v.s.* horizontal displacement curves for specimen (a) 0.5%_10_H; and (b) 0.5%_5_L.

Fig. 5-4 illustrated the typical shear displacement *v.s.* vertical displacement curves of specimens with high initial D_r and high *CC* (i.e., 10_H case) and the ones with low initial D_r and low *CC* (i.e., 5_L case). For the high initial D_r and high *CC* specimens, it is clear that the development of vertical displacement had two stages. Within a relatively small horizontal displacement (i.e., less than 1 mm), the specimens underwent a very slight vertical contraction stage. This was possibly due to the breakage of some weak interparticle cementation at the beginning, which was also observed by van Paassen et al. (2012) and Pakbaz et al. (2018). At the second stage, as the loading progressed, the specimen exhibited expansion due to dilatancy, and lower normal stress yielded greater expansion. The dilatancy could be attributed to the interlocking effect and particle rearrangement. For the low initial D_r and low *CC* specimens under low normal stresses (i.e., 50, 100, and 200 kPa), a similar evolution trend of vertical deformation including the above mentioned two stages was observed. In contrast to the high initial D_r and high *CC* specimens, however, with the increase of normal stress up to 400 and 600 kPa, the dilative trend was significantly suppressed by higher normal stress. This indicated a decreasing dilatancy, which was associated with the global breakage of interparticle cementation and the restriction of particle rearrangement.

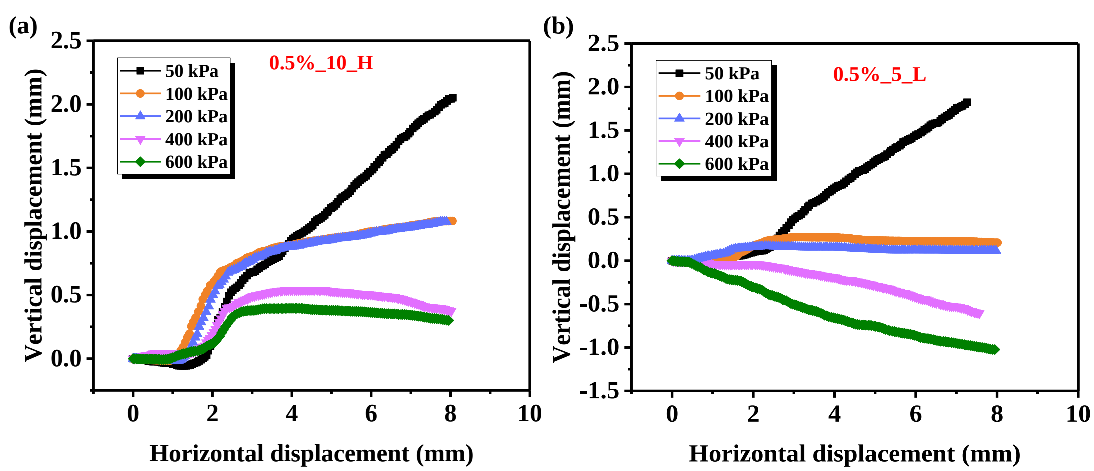

Fig. 5-4 Vertical displacement *v.s.* horizontal displacement curves for specimen (a) 0.5%_10_H; and (b) 0.5_5_L.

5.3.3 Peak Stress Ratio

Stress ratio is the ratio between shear stress and the normal stress under the direct shear condition (Shibuya 1997), indicting the failure of samples. It has been widely used in previous studies to describe sand shear strength obtained from direct shear tests (Van Paassen et al. 2012; Dai et al. 2016; Jewell and Wroth 1987). **Fig. 5-5** exhibited the normalized peak stress ratio (η_p/η_0), which was determined by the ratio between the peak stress of specimens with biochar amendment and that of their counterparts without biochar amendment. The "η_p/η_0>1" indicated an enhancement of shear strength compared with the specimen without biochar amendment, while the "η_p/η_0<1" meant a reduction.

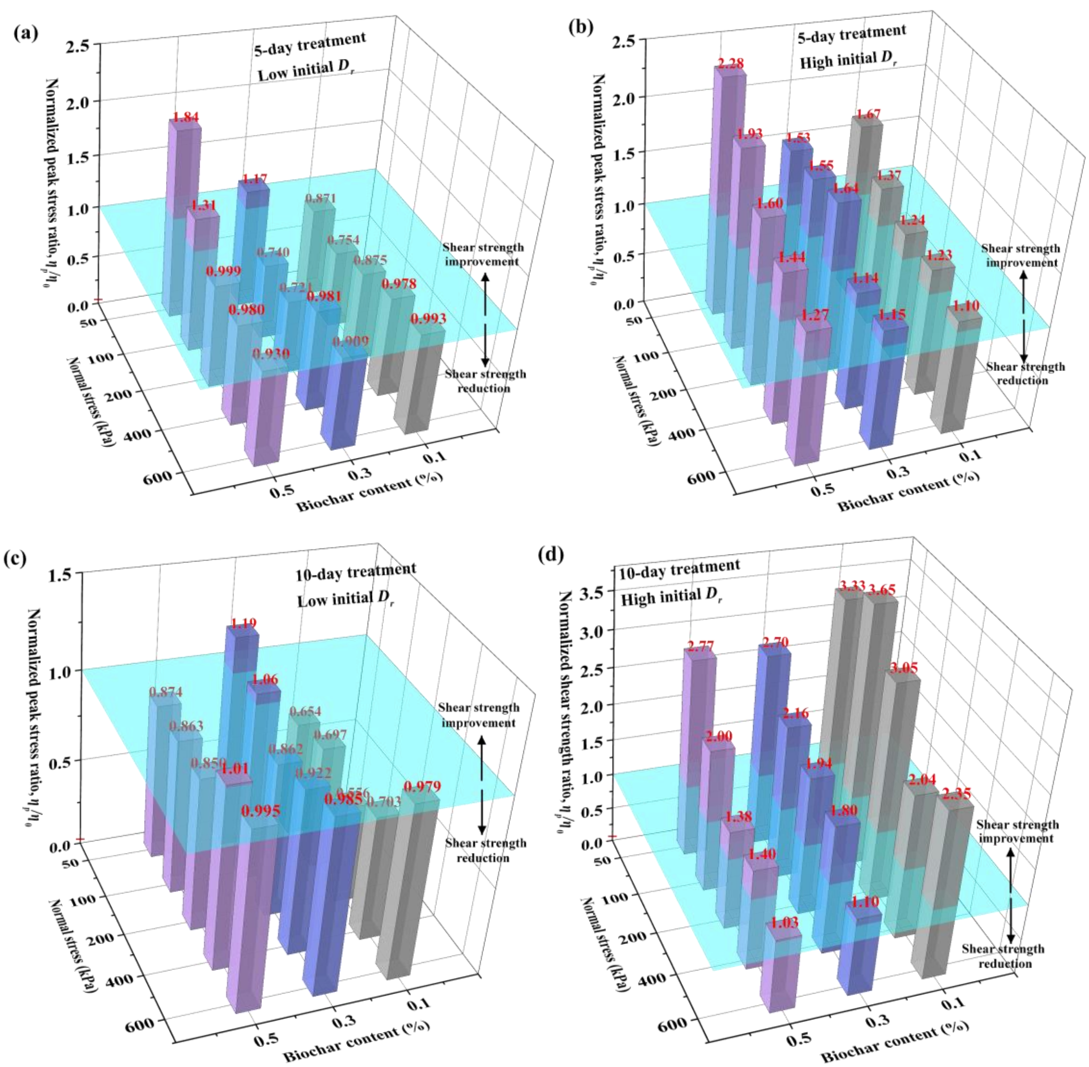

Fig. 5-5 The comparison of normalized peak stress ratio (η_p/η_0) in the specimens with (a) low initial D_r after 5-day cementation; (b) high initial D_r after 5-day cementation; (c) low initial D_r after 10-day cementation; (d) high initial D_r after 5-day cementation.

It could be seen that the specimens prepared under high initial D_r in general showed the greatest η_p/η_0 regardless of the duration of cementation phase (**Fig. 5-5(b)**, **(d)**). In particular for the specimens subjected to 5-day treatment (**Fig. 5-5(b)**), when the biochar content increased from 0.1% to 0.5%, the η_p/η_0 increased from 1.67 to 2.28, 1.37 to 1.93, 1.24 to 1.6, 1.23 to 1.44, and 1.1 to 1.27 under the normal stress of 50 kPa, 100 kPa, 200 kPa, 400 kPa, and 600 kPa, respectively. On the other hand, for the specimens subjected to 10-day treatment (**Fig. 5-5(d)**), with the increase of biochar content from 0.1% to 0.5%, a decreasing trend of η_p/η_0 was observed though the η_p/η_0 values were all larger than 1, indicating that shear strength was still enhanced. Then, for the specimens prepared under low initial D_r, much smaller η_p/η_0 values were observed compared with those in the cases of high initial D_r specimens. More specifically, 24 out of 30 cases of low initial D_r specimens had the η_p/η_0 values smaller than 1.0, indicating a reduction in shear strength. It suggested that low initial D_r had an adverse effect on the shear strength of biochar-amended bio-cemented sand.

5.3.4 Direct Shear Parameters

The typical failure envelopes based on the Mohr–Coulomb failure criterion were shown in **Fig. 5-6**, which shows that shear stress increased approximately linearly with the elevated normal stress. It was generally found that higher shear stress could be reached as the *CC* and initial D_r increased. The direct shear parameters at peak state including cohesion I and friction angle (ϕ) were obtained by performing linear regression and were presented in **Table 5-3**. To further investigate the effect of biochar on the variations of c and ϕ, the evolutions of normalized cohesion (c/c_0) and normalized friction angle (ϕ/ϕ_0) representing the improvement ($\phi/\phi_0 > 1$) or reduction ($\phi/\phi_0 < 1$) of cohesion and friction angle are illustrated in **Fig. 5-7** and **Fig. 5-8**, respectively, where c_0 and ϕ_0 were the cohesion and friction angle of the corresponding bio-cemented specimens without biochar amendment.

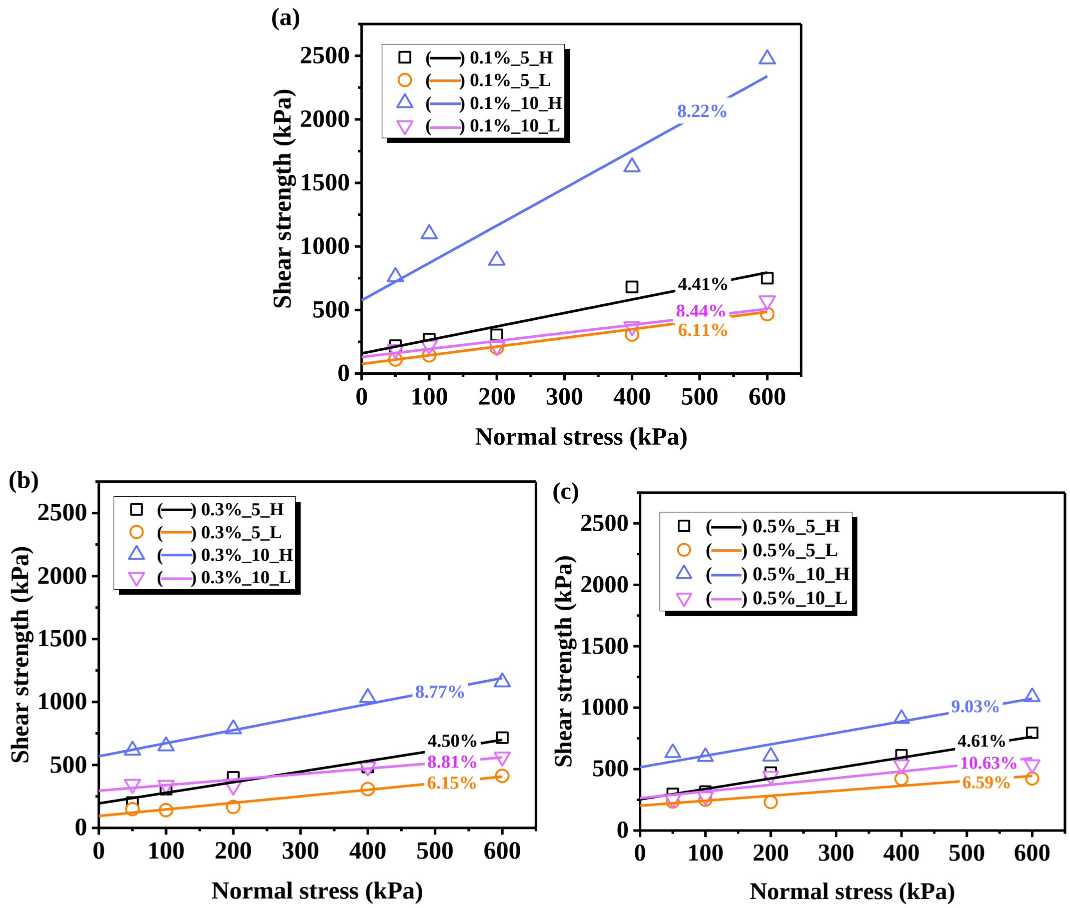

Fig. 5-6 The failure envelopes of biocemented sand amended with (a) 0.1% biochar; (b) 0.3% biochar; (c) 0.5% biochar.

As can be seen from **Fig. 5-7**, the specimens prepared under high initial D_r and subjected to 10-day cementation solution treatment (i.e., 10_H) showed the greatest c/c_0 among all the cases, though with the increase of biochar content from 0.1% to 0.3% and 0.5%, the c/c_0 value decreased slightly from 4.1 to 4.05 and 3.67, respectively. For the specimens prepared under high initial D_r and subjected to 5-day cementation solution treatment (i.e., 5_H), an obvious improvement of cohesion was also observed and with the increase of biochar content from 0.1% to 0.3% and 0.5%, the c/c_0 value increased from 1.78 to 2.20 and 2.86, respectively. On the other hand, for the specimens prepared under low initial D_r and subjected to 10-day cementation solution treatment (i.e., 10_L), the c/c_0 values were merely 0.71, 1.61 and 1.44 in the specimens with 0.1%, 0.3% and 0.5% biochar content, respectively. Meanwhile, the specimens prepared under low initial D_r and subjected to 5-day cementation solution treatment (i.e., 5_L) showed the smallest c/c_0. In this worse case, although the increasing trend of c/c_0 against increasing biochar content could be observed, the cohesion improvement only occurred in the specimen with 0.5% biochar content (c/c_0 =1.76).

Table 5-3 The peak friction angle and cohesion obtained from Mohr-Coulomb failure envelope.

Specimen	Shear strength parameter	
(X_Y_Z)[a]	ϕ_p (°)	c (kPa)
0%_5_L	28.7	114.9
0%_5_H	41.1	88.5
0%_10_L	33.8	183.6
0%_10_H	53.8	140.4
0.1%_5_L	32.2	130.2
0.1%_5_H	46.6	158.3
0.1%_10_L	34.3	75.6
0.1%_10_H	71.2	576.1
0.3%_5_L	27.4	95.1
0.3%_5_H	40.0	194.7
0.3%_10_L	32.7	295.2
0.3%_10_H	46.0	568.8
0.5%_5_L	21.9	202.3
0.5%_5_H	40.3	253.3
0.5%_10_L	28.5	263.6
0.5%_10_H	42.9	515.2

[a] The designation "*X_Y_Z*" represents the bio-cemented specimens treated with "*Y*" days of flushing with "*X*" biochar content. The "*Z*" represents the initial relative density level ("L" representing low (16.2%) and "H" representing high (54.6%))

Fig. 5-8 showed the normalized friction angle (ϕ/ϕ_0) as a function of the biochar content. At first glance, for the specimens under a given initial D_r and duration of cementation solution treatment, it was evident that ϕ/ϕ_0 decreased with the increasing biochar content. More specifically, the friction angle improvement (i.e., ϕ/ϕ_0 >1) was only observed in the specimens with 0.1% biochar content. As the biochar content increased to 0.3% and 0.5%, a slight friction angle reduction was observed, and the ϕ/ϕ_0 values were between 0.75 and 1. Furthermore, the initial D_r and the duration of cementation solution treatment seemed to have an insignificant effect on ϕ/ϕ_0 among the four cases (i.e., 5_L, 5_H, 10_L, and 10_H).

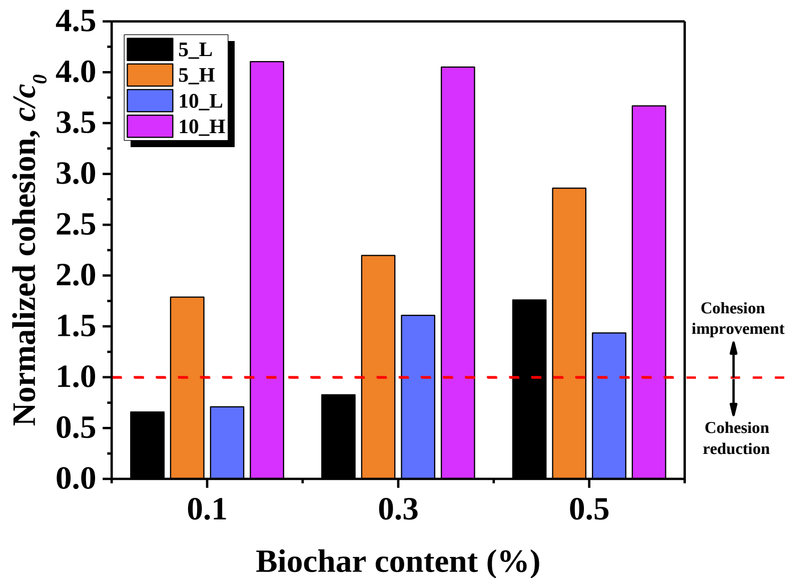

Fig. 5-7 The normalized cohesion against various biochar content (note: "5/10" represent the treatment days; "L/H" represent the level of initial D_r).

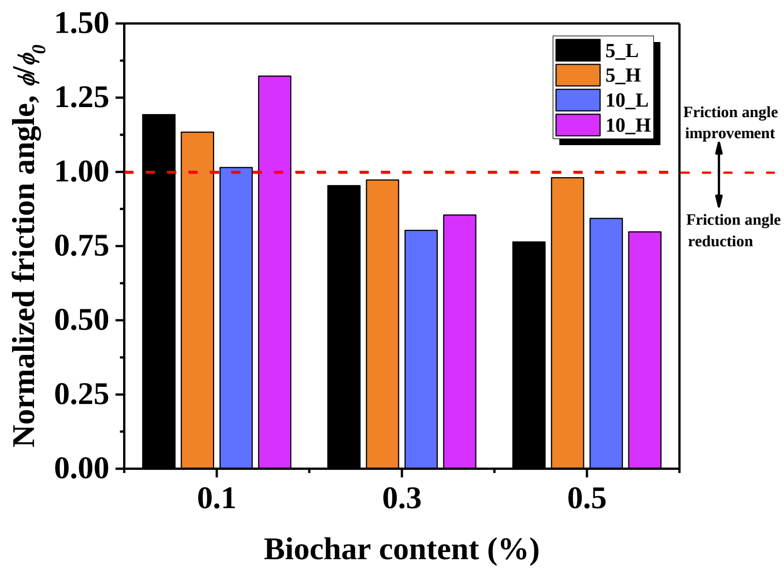

Fig. 5-8 The normalized friction angle against various biochar content.

5.3.5 Microscopic Characteristics

The representative microscopic images of the specimens prepared under high initial D_r were displayed in **Fig. 5-9**. **Fig. 5-9(a)** represented the case of uncemented sand. In this case, only the sand particles could be clearly seen in the image. **Fig. 5-9 (b)** represented the case of bio-cemented specimen without biochar. The obvious white interparticle cementation was observed in this case serving as interparticle bonding that bridged the adjacent sand particles together. **Fig. 5-9(c)** and **(d)** represented the bio-cemented specimens with 0.1% and 0.5% biochar content, respectively. Compared with the bio-cementation in the specimen without biochar, it was found that more bio-cementation could be generated. In addition, the dark color in the specimens with 0.1% and 0.5% biochar was observed, which was due to that the biochar was entombed within the bio-cementation. It was obvious that the 5% biochar content created the most bio-cementation among the three cases with the darkest color indicating more entombed biochar. Additionally, the entombment of biochar was a common phenomenon in the biochar-amended bio-cemented sand, although few independent biochar that was not involved in the process of MICP could still be observed on the surface of sand particles.

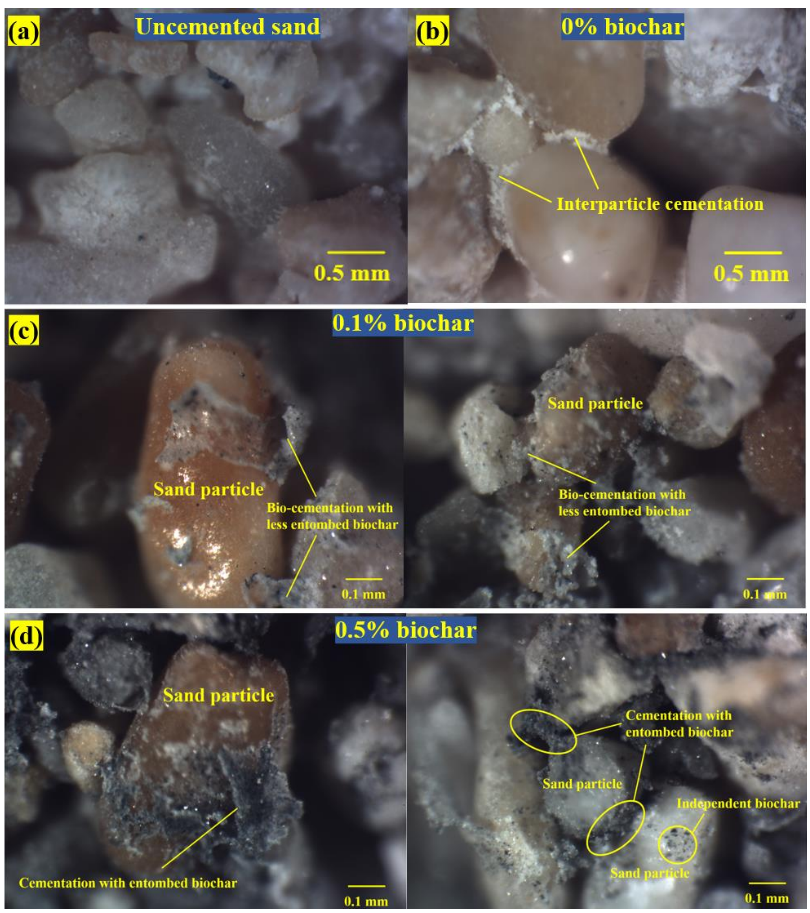

Fig. 5-9 Microscopic images of (a) uncemented sand; (b)bio-cemented sand without biochar; (c)bio-cemented sand with 0.1% biochar content; and (d) bio-cemented sand with 0.5% biochar content.

5.4 Discussion

5.4.1 Effect of Biochar on Bio-Cementation Level

Results from **Fig. 5-2** show that more bio-cementation can be generated in biochar-amended specimens than those without biochar. The underlying mechanisms are presumably to be twofold:

The interaction between biochar and microorganisms: as can be seen from the microscopic images (**Fig. 5-9(c), (d)**), entombment is common in the biochar-amended specimens, indicating that biochar serves as extra nucleation sites for enriched the enriched ureolytic bacteria. The highly porous nature of biochar grains provides a suitable habitat or refuge for the enriched ureolytic microorganisms by protecting them from predation and drying (Kolb et al., 2009; Downie et al., 2012).

Physicochemical properties of biochar: biochar normally has high cation exchange capability (CEC) and possesses negative surface charges, meaning that cations from the aqueous phase can be adsorbed onto the biochar grain surfaces by ionic interactions (Downie et al., 2012). As a result, the adsorbed cations can also participate in attracting anions such as carbonate onto the surface of biochar and thus promote the generation of bio-cementation.

Due to the above two mechanisms, it is reasonable to see that the *CC* increases with the biochar content. Based on the abovementioned two mechanisms, a schematic structure of interparticle bio-cementation is proposed and visualized more clearly in **Fig. 5-10**.

5.4.2 Effect of Biochar on the Shear Strength of Bio-Cemented Calcareous Sand

The shear strength of cemented sands (including bio-cemented ones) is normally contributed by several components including interparticle friction, particle rearrangement, particle crushing, interparticle bonding (i.e., cementation), and dilatancy (i.e., interlocking)

(Mitchell and Soga, 2005). These contributing components are influenced by external factors including cementation level, effective normal stress, particle size/shape, and density (Cui et al., 2017; Nafisi et al., 2018, 2020).

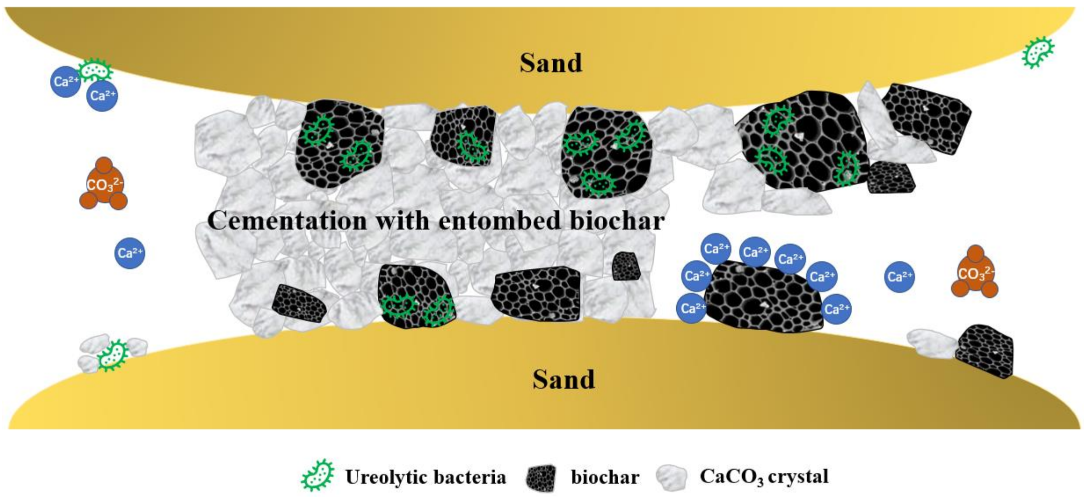

Fig. 5-10 Schematic diagram of biochar-amended biocemented sand.

Based on the experimental results in the current study, the introduction of biochar in the bio-cementation process can affect the shear strength of bio-cemented sands by altering the above-mentioned strength contributing components. Functionally, for one thing, biochar serving as the extra nucleation sites for native ureolytic bacteria can increase *CC* within specimens as shown in **Fig. 5-2**. The increase of *CC* can enhance the interparticle bonding, which improves the shear strength, especially for the specimens prepared under high initial D_r as shown in **Fig. 5-6**. This is mostly attributed to the much closer interparticle distance which makes the formation of interparticle bonds much easier. Secondly, the entombment of biochar within bio-cementation could become weak points, thus diminishing the contribution of interparticle bonding to shear strength. Generally, as the biochar content increases, more biochar will be entombed in the interparticle bio-cementation and impairs the shear strength. The underlying mechanism is illustrated more clearly in **Fig. 5-11**. Specifically, the diminishing effect is the most significant in the case of "10_L" and "10_H". For instance, in the case of "10_L", the η_p and *c* cannot be further improved when the biochar content increases from 0.3% to 0.5%. Also, for the "10_H" case, a continuously decline trend of η_p and c is observed with the increasing biochar content as shown in **Fig. 5-5** and **5-7**. However, it should be mentioned that the diminishing effect is not found in the specimen with 5-day treatment, which can be attributed to the less generated bio-cementation. Thirdly, the un-entombed tiny biochar powders that are distributed randomly on the surface of sand particles (**Fig. 5-9(d)**) may change the interparticle friction properties. Due to the porous properties of calcareous sand, the biochar powders may fill in the voids and reduce the surface roughness. For example, as shown in **Fig. 5-8**, for the specimens with a given initial D_r and duration of cementation solution treatment, a decreasing ϕ/ϕ_0 against increasing biochar content is observed, which indicates that the introduction of biochar may reduce the interparticle friction.

It should be noted that the effect of biochar on the strength contributing component such as particle crushing is not included in the current study due to the lack of sufficient data.

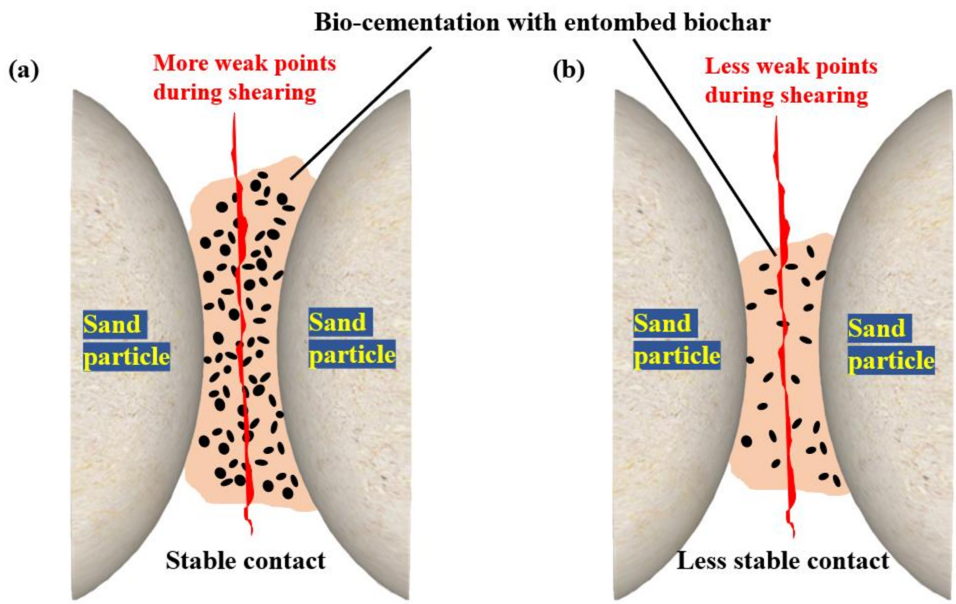

Fig. 5-11 The conceptual illustrations during shearing for specimens with (a) high biochar content; and (b) low biochar content.

5.4.3 Biochar vs. Other Additives

Apart from biochar, other soil amendments have also been considered as additives to enhance the shear strength of bio-cemented sand. These additives include, but not limited to, homopolymer polypropylene multifilament fibers, jute fibers, glass fibers, polyester fibers, wool fibers, PVA fibers, and hemp fibers (Li et al., 2016; Imran et al., 2020; Zhao et al., 2021; Fang et al., 2020; Choi et al., 2016; Yao et al., 2021). These soil amendments could promote bacteria fixation and provide extra nucleation sites for the interparticle biogenetic cementation. The enhancement mechanism of biochar in bio-cemented sand is very similar to these alternative additives in further increasing *CC* and various strength parameters such as peak shear stress, cohesion, and friction angle (Liu et al., 2021; Li et al., 2016). Moreover, the durability of soil amendments is essential for in-situ application regarding the efficacy and low cost. According to the microscopic observation, it is reasonable to believe that biochar powders used in the current study, unlike other organic soil amendments, are not readily worn or damaged under loading due to the entombment effect. During the formation of bio-cementation, the biochar can be protected inside the bio-cementation carefully, and the variation of surrounding environment may have little effect on the stability of biochar. Finally, compared with the industrial synthetic fiber, biochar is a recycled product which is obtained from heated biomass, such as wood, manure or leaves. The resource base for biochar production is diverse which can exist in urban, industrial and rural areas (Lehmann and Joseph, 2015).

5.5 Conclusions

The direct shear tests of biochar-amended bio-cemented calcareous sand treated by bio-stimulation were conducted in this study. The following conclusions are drawn based on the findings from the experiment.

(1) The addition of biochar powders could effectively increase the cementation content of bio-cemented sand treated by bio-stimulation method. Assuming the other conditions were the same, the *CC* increased with the elevated amount of biochar. The addition of biochar yielded a 31%-81% increase in *CC* compared with the specimens without biochar. The specimens with lower initial D_r had slightly higher *CC* than that with higher initial D_r.

(2) The bio-cemented sand with biochar amendment showed a much more significant increase of peak stress ratio ($\eta_p/\eta_0>1$) in the specimens prepared under higher initial D_r than those under lower initial D_r. The primary strength improvement came from the

increase of cohesion, and the significant cohesion improvement (c/c_0>1) was also observed under higher initial D_r situation. The friction angle improvement (i.e., ϕ/ϕ_0 >1) was only observed in the specimens with 0.1% biochar content, indicating that the introduction of biochar may reduce the interparticle friction.

(3) Based on the observation of microscopic images, biochar was able to alter the structure of interparticle cementation to influence the shear strength indirectly. It was found that the entombment of biochar within the cementation was a common phenomenon, making the bio-cementation a dark color. Some independent biochar which was not involved in the process of MICP could be observed on the surface of sand particles.

(4) According to the responses of shear strength parameters, the effects of biochar in the shear strength of bio-cemented sands are three folds. Firstly, biochar used as the extra nucleation sites for native ureolytic bacteria, could increase *CC* within specimens. Secondly, too much biochar within bio-cementation may become weak points and thus diminish the contribution of interparticle bonding to the shear strength. Thirdly, as biochar content increases, more un-entombed tiny biochar powders that are distributed randomly on the surface of sand particles can reduce the interparticle friction.

Reference

Berti, D., Biscontin, G. and Lau, J. 2021. "Effect of Biochar Filler on the Hydration Products and Microstructure in Portland Cement–Stabilized Peat." J. Mater. Civ. Eng., 33(10), 04021263.

Chan, K. Y., Van Zwieten, L., Meszaros, I., Downie, A. and Joseph, S. 2008. "Agronomic values of greenwaste biochar as a soil amendment." Soil Res., 45(8), 629-634.

Cheng, L. and Cord-Ruwisch, R. 2012. "In situ soil cementation with ureolytic bacteria by surface percolation." Ecol. Eng., 42, 64-72.

Choi, S. G., Wang, K. and Chu, J. 2016. "Properties of biocemented, fiber reinforced sand." Constr. Build. Mater., 120, 623-629.

Cui, M. J., Zheng, J. J., Zhang, R. J., Lai, H. J. and Zhang, J. 2017. "Influence of cementation level on the strength behaviour of bio-cemented sand." Acta Geotech., 12(5), 971-986.

Dai, B. B., Yang, J. and Zhou, C. Y. 2016. "Observed effects of interparticle friction and particle size on shear behavior of granular materials." Int. J. Geomech., 16(1), 04015011. https://doi:10.1061/(asce)gm.1943-5622.0000520.

Downie, A., Crosky, A. and Munroe, P. 2012. "Physical properties of biochar." In Biochar for environmental management., 45-64.

Fang, X., Yang, Y., Chen, Z., Liu, H., Xiao, Y. and Shen, C. 2020. "Influence of fiber content and length on engineering properties of MICP-treated coral sand." Geomicrobiol. J., 37(6), 582-594.

Feng, K. and Montoya, B. M. 2016. "Influence of confinement and cementation level on the behavior of microbial-induced calcite precipitated sands under monotonic drained loading." J. Geotech. Geoenviron., 142(1), 04015057.

Gupta, S., Kua, H. W. and Koh, H. J. 2018. "Application of biochar from food and wood waste as green admixture for cement mortar." Sci. Total Environ., 619, 419-435.

Han, X. L., Jiang, N. J. and Wang, Y. J. 2020. "Stabilization of calcareous sand by applying the admixture of alkali-activated slag (AAS) and biochar." In Geo-Congress 2020: Foundations, Soil Improvement, and Erosion, 469-475. Reston, VA: American Society of Civil Engineers.

Houben, D., Evrard, L. and Sonnet, P. 2013. "Beneficial effects of biochar application to contaminated soils on the bioavailability of Cd, Pb and Zn and the biomass production of rapeseed (Brassica napus L.)." Biomass Bioenergy, 57, 196-204.

Imran, M. A., Gowthaman, S., Nakashima, K. and Kawasaki, S. 2020. "The Influence of the Addition of Plant-Based Natural Fibers (Jute) on Biocemented Sand Using MICP Method." Mater., 13(18), 4198.

Jewell, R. A. and Wroth, C. P. 1987. "Direct shear tests on reinforced sand." Geotechnique., 37(1), 53-68.

Jiang, N. J. and Soga, K. 2017. "The applicability of microbially induced calcite precipitation (MICP) for internal erosion control in gravel–sand mixtures." Géotechnique, 67(1), 42-55.

Kolb, S. E., Fermanich, K. J. and Dornbush, M. E. 2009. "Effect of charcoal quantity on microbial biomass and activity in temperate soils." Soil Sci Soc Am J., 73(4), 1173-1181.

Lehmann, J. and Joseph, S. (Eds.). 2015. Biochar for environmental management: science, technology and implementation. Routledge.

Li, M., Li, L., Ogbonnaya, U., Wen, K., Tian, A. and Amini, F. 2016. “Influence of fiber addition on mechanical properties of MICP-treated sand.” J. Mater. Civ. Eng., 28(4), 04015166.

Liu, S., Du, K., Huang, W., Wen, K., Amini, F. and Li, L. 2021. “Improvement of erosion-resistance of bio-bricks through fiber and multiple MICP treatments.” Constr. Build. Mater., 271, 121573.

Mitchell, J. K. and Soga, K. 2005. Fundamentals of soil behavior (Vol. 3). New York: John Wiley and Sons.

Nafisi, A., Khoubani, A., Montoya, B. M. and Evans, M. T. 2018. “The effect of grain size and shape on mechanical behavior of MICP sand I: Experimental study.” In Proceedings of the 11th National Conf. in Earthquake Eng., Research Ins. Los Angeles.

Nafisi, A., Montoya, B. M. and Evans, T. M. 2020. “Shear strength envelopes of biocemented sands with varying particle size and cementation level.” J. Geotech. Eng., 146(3), 04020002.

Pakbaz, M. S., Behzadipour, H. and Ghezelbash, G. R. 2018. “Evaluation of shear strength parameters of sandy soils upon microbial treatment.” Geomicrobiol. J., 35(8), 721-726.

Puga, A. P., Abreu, C., Melo, L. C. A. and Beesley, L. 2015. “Biochar application to a contaminated soil reduces the availability and plant uptake of zinc, lead and cadmium.” J. Environ. Manage., 159, 86-93.

Rowshanbakht, K., Khamehchiyan, M., Sajedi, R. H. and Nikudel, M. R. 2016. “Effect of injected bacterial suspension volume and relative density on carbonate precipitation resulting from microbial treatment.” Ecol. Eng. 89, 49–55. https://doi:10.1016/j.ecoleng.2016.01.010.

Shibuya, S., Mitachi, T. and Tamate, S. 1997. “Interpretation of direct shear box testing of sands as quasi-simple shear.” Geotechnique. 47(4), 769-790. https://doi:10.1680/geot.1997.47.4.769.

Tan, Z., Yuan, S., Hong, M., Zhang, L. and Huang, Q. 2020. “Mechanism of negative surface charge formation on biochar and its effect on the fixation of soil Cd.” J. Hazard. Mater., 384, 121370.

Tsukamoto, M. and Oda, K. 2013. “Influence of relative density on microbial carbonate precipitation and mechanical properties of sand.” In Proceedings of the [1]8th International Conference on Soil Mechanics and Geotechnical Engineering, Paris. 2613-2616.

Van Paassen, L. V., Hemert, W. V., Star, W. V. D., Zwieten, G. V. and Baalen, L. V. 2012. “Direct shear strength of biologically cemented gravel.” In Proceedings of Geo-Congress 2012: State of the Art and Practice in Geotechnical Engineering. 968-977. https://doi:10.1061/9780784412121.100.

Verheijen, F., Jeffery, S., Bastos, A. C., Van der Velde, M. and Diafas, I. 2010. “Biochar application to soils.” A critical scientific review of effects on soil properties, processes, and functions. EUR, 24099, 162.

Wang, L., Chen, L., Tsang, D. C., Guo, B., Yang, J., Shen, Z., Hou, D., Ok, Y.S. and Poon, C.S. and Poon, C. S. 2020. “Biochar as green additives in cement-based composites with carbon dioxide curing.” J. Clean. Prod., 258, 120678.

Wang, Y. J., Han, X. L. and Jiang, N. J. 2018. “Enriching Indigenous Ureolytic Bacteria in Coastal Beach Sand.” In The International Congress on Environmental Geotechnics, 340-347, Springer, Singapore.

Wang, Y., Jiang, N. and Han, X. 2021. “A preliminary study of carbonate sand stabilization by bio-stimulation based MICP method.” Japanese Geotechnical Society Special Publication, 9(6), 282-286.

Yao, D., Wu, J., Wang, G., Wang, P., Zheng, J. J., Yan, J., Xu, L. and Yan, Y. 2021. “Effect of wool fiber addition on the reinforcement of loose sands by microbially induced carbonate precipitation (MICP): mechanical property and underlying mechanism.” Acta Geotech., 16(5), 1401-1416

Yu, Z., Qiu, W., Wang, F., Lei, M., Wang, D. and Song, Z. 2017. “Effects of manganese oxide-modified biochar composites on arsenic speciation and accumulation in an indica rice (Oryza sativa L.) cultivar.” Chemosphere, 168, 341-349.

Zhao, J., Tong, H., Shan, Y., Yuan, J., Peng, Q. and Liang, J. 2021. “Effects of Different Types of Fibers on the Physical and Mechanical Properties of MICP-Treated Calcareous Sand.” Mater., 14(2), 268.

CHAPTER 6. The Explorations of MICP in Rainfall-induced Erosion Prevention

6.1 Introduction

Nowadays, the coastal erosion in tropical regions due to the heavy rainfall and frequent storm attack is becoming more severe. While it is a popular practice to build hard structures such as revetments and seawalls along the shoreline, it has been proven to be expensive and not environmental-friendly. Bio-stimulated MICP in coastal areas to form cementation that can bind loose sand grains is a promising approach to mitigate rainfall-induced erosion. Compared with traditional mechanical coastal hard structures which may damage coastal ecosystem, the bio-stimulation for MICP is a relatively eco-friendly method. Although there has been some existing research in bio-stimulation of ureolytic bacteria, the application in preventing coastal rainfall-induced erosion is still unexplored. In this chapter, a meso-scale laboratory model was made to investigate the deformation on artificial sandy slope treated by bio-stimulated MICP method. Also, it is the first time that the photography-based SfM (Structure from Motion) method is applied to evaluate the rainfall-induced erosion of bio-cemented soils, which is a good trial to explore a feasible monitoring way for the full-scale application in field.

6.2 Materials and methods

6.2.1 Calcareous sand

The calcareous sand used was purchased from the Home Depot, which is a commercial sand manufacturing by the company PRO-PAK®. Its particle size distribution curve was shown in **Fig. 6-1**. The initial water content was 1%-2%. The calcium carbonate content of coral sand was 99.5%.

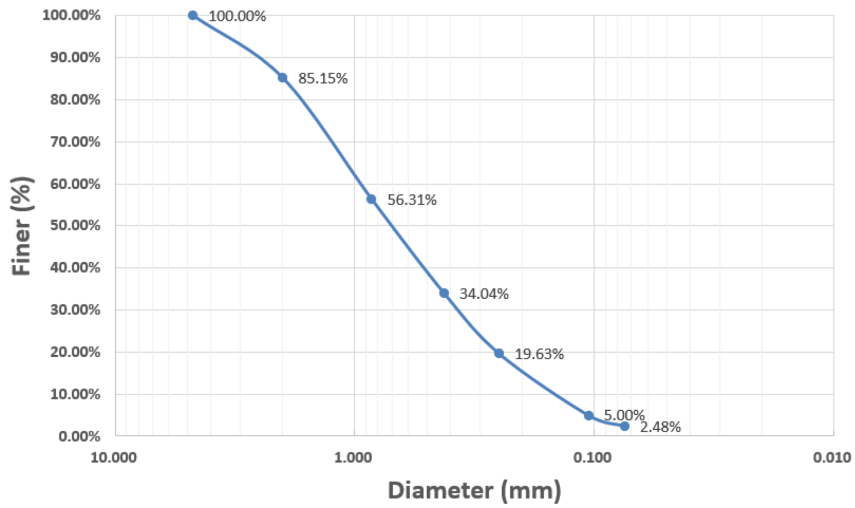

Fig. 6-1 The particle size distribution curve of the commercial Hawaiian coral sand.

6.2.2 Enrichment Media and Cementation Solution

Three nutrient types were used in this study, namely yeast extract (YE), malt extract (ME), and nutrient broth (NB). Generally, YE and NB are protein-based while ME is carbohydrate-based complex medium. These media were prepared by dissolving 20 g yeast extract, malt extract or nutrient broth with 10 g urea in 1 L distilled water, respectively. For cementation solution, the concentration of 500 mM urea and $CaCl_2$ were adopted.

6.2.3 Experimental Setup

To perform the rainfall-induced erosion test, an artificial sandy slope measuring 28.5 cm × 30 cm × 20 cm (L×W×H) with 35° slope angle was prepared in a rectangular box with one side cut off. Firstly, the box was tilted at 35° and fixed firmly. The 12.5 kg sands were then poured into the container by dry pluviation method to reach final relative density of approximately 15%. The surface of slope was flattened after pouring. Then, the box was carefully laid down to complete the preparation of the 35° sandy slope. The schematic diagram of a representative prepared sandy slope is illustrated in **Fig. 6-2**. Upon the completeness of sandy slope preparation, 900 mL enrichment media solution was sprayed onto the slope surface evenly by spraying bottle and the sand slope was left for a 48-hour enrichment stage as did in the sand column cases. After that, 900 mL cementation solution was sprayed and left for 24 hours for bio-cementation to form. The selected volume of 900 mL equaled to the pore volume of the 2-cm-thick sand from the slope surface. Finally, the sandy slope was subjected to the simulated rainfall-induced erosion.

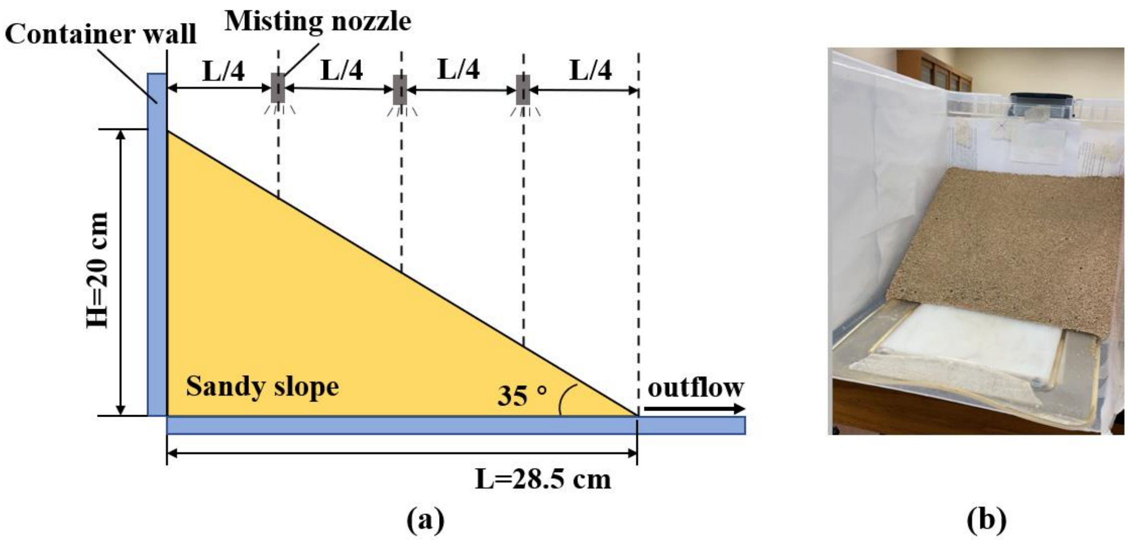

Fig. 6-2 The schematic diagrams of prepared sandy slope: (a) side view; (b) overview of the built sandy slope.

The rainfall was simulated using three misting nozzles with misting range of 50-100 cm placed over the sandy slope. The system was calibrated to produce a continuous rainfall intensity as high as 80 mm/h. The simulated rainfall in total lasted for 1 hours.

To evaluate the erosion-resistance of uncemented and bio-cemented sandy slopes, a photogrammetric approach based on the structure-from-motion (SfM) technique was conducted. Firstly, a series of 2D images from various angles were captured by a high-resolution digital camera (Sony α7II) prior and after the erosion test. The 3D models of sandy slopes were then reconstructed using the software Pix4D, in which the point clouds and digital elevation models (DEMs) were generated. Finally, DEMs were feed into the software CloudCompare v2.12 to obtain the change in elevation of the slopes prior and after rainfall erosion. It worth mentioning that the reconstructed model and DEMs were carefully calibrated using several external check points to make sure the dimensions and positions were correct.

6.3 Results and Discussions

A representative reconstructed 3D model and change of elevation of the slopes prior to and after rainfall erosion are presented in **Fig. 6-3(a)** and **(b)~(e)**, respectively. In **Fig. 6-3(b)-(e)**, the blue color indicated soil erosion (i.e., negative elevation change), and the red color soil accumulation (i.e., positive elevation change). Apparently, for the untreated sandy slope, large areas showed significant erosion. In contrast, the sandy slopes after bio-stimulated MICP treatment generally exhibited much milder erosion.

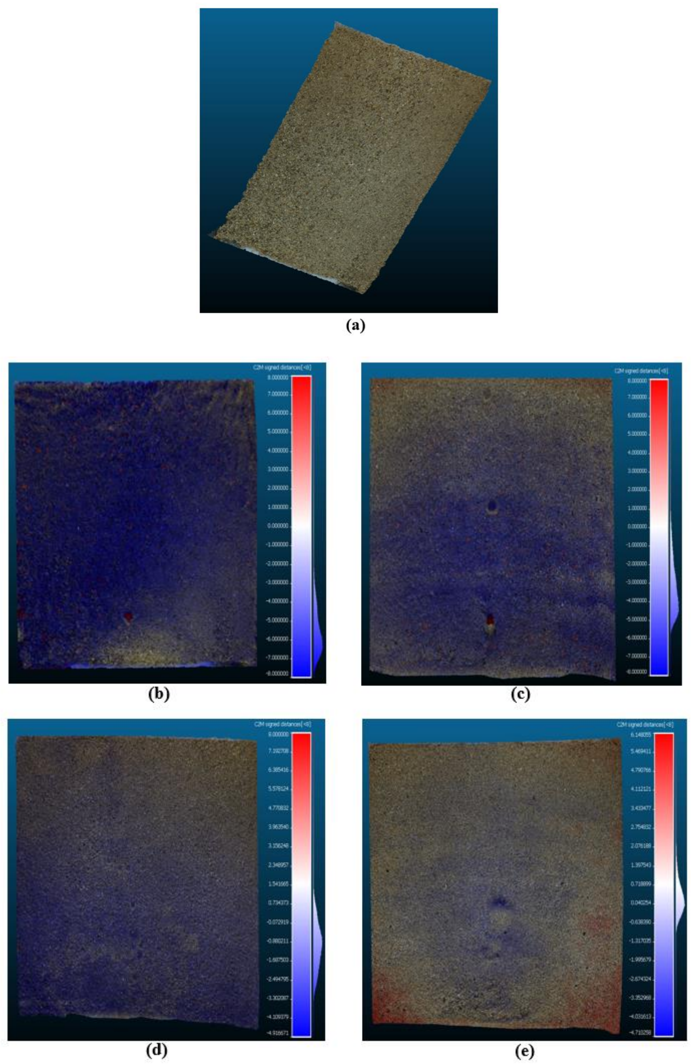

Fig. 6-3 (a) The representative reconstructed 3D slope models after rainfall; and the computed surface elevation change of (b) untreated slope; (c) ME-170 treated slope; (d) NB-170 treated slope; (e) YE-170 treated slope.

To quantify the change in elevation in different cases, a colored histogram of elevation change distribution across the entire slope surface is shown in **Fig. 6-4**. The parameter *R* (count percentage of cloud points), defined as the ratio of cloud point numbers at a given elevation change to the total count of cloud points, was calculated to quantify the elevation change distribution. As shown in **Fig. 6-4**, it was found that the elevation changed mostly concentrated around -6.3 mm, -4.4 mm, -0.9 mm, and 0 mm for the untreated, ME-170, NB-170, and YE-170 cases, respectively, suggesting that the case of YE-170 had the least soil erosion, which was followed by NB-170 and ME-170. In addition, the apparent accumulation was found in the case of YE-170, which mostly located at the toe part of the slope.

The above results were consistent with the results obtained in the previous chapter. Since the case of YE and NB had the higher ureolytic activity level than ME, it also provided the stronger erosion-resistance to rainfall.

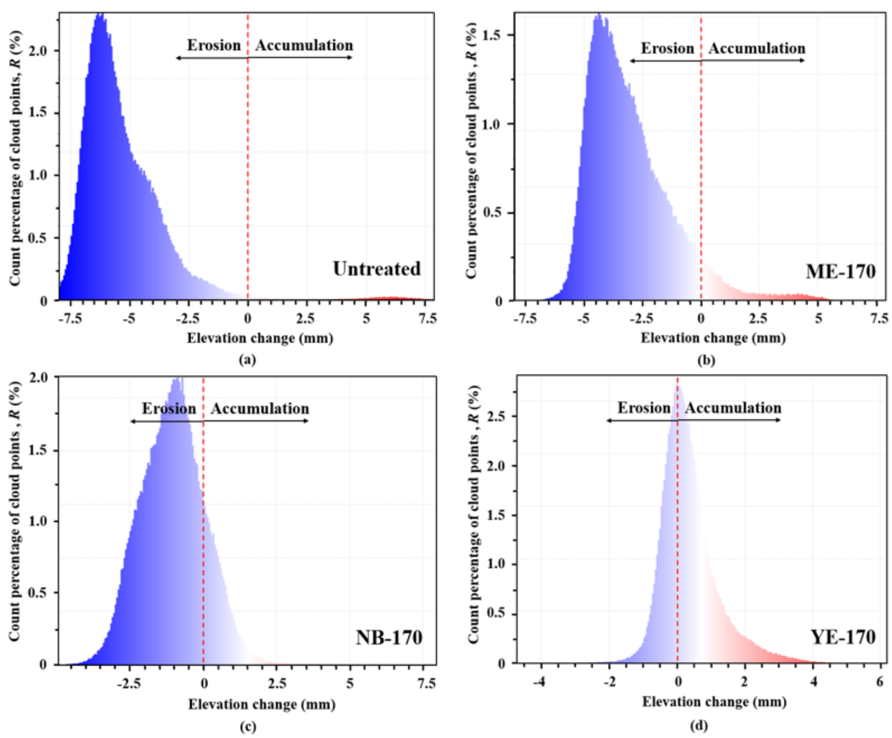

Fig. 6-4 The elevation change distribution histogram (color current: blue→white→red) of (a) untreated slope; (b) ME-170 treated slope; (c) NB-170 treated slope; (d) YE-170 treated slope.

6.4 Conclusions

The results showed that bio-stimulated MICP could significantly reduce the erosion on a sandy slope, especially in case treated by YE-based enrichment medium with 170 initial urea concentration. Furthermore, it is the first time that the photography-based SfM (Structure from Motion) method is applied to evaluate the rainfall-induced erosion of bio-cemented soils, which is a good trial to explore a feasible monitoring way for the future full-scale application in field.

CHAPTER 7. Conclusions

In this dissertation, the applicatiton of bio-stimulated MICP method in calcareous sand was investigated from the biochemical and mechnical aspects. Here are the summaries of major findings throughout this dissertation and suggestions for further research.

7.1 Bio-stimulation under Solution Condition

In this research, A series of batch tests were developed to investigate the effects of the enrichment medium type and initial urea concentration on the enrichment of native ureolytic bacteria in calcareous beach sand under solution condition. The generic and selective enrichment media were compared from the biochemical aspects. This study contributes to the development of bio-stimulated MICP in the following aspects:

(1) The increase in ureolytic activity with time was limited in the generic media, whereas a noticeable increase could be observed in most selective media. In general, YE and NB with higher nitrogen sources have better efficiency than ME. Two different bacterial activities dominate at different stages of bio-stimulation. At the early stage when the cumulative EC value is less than 10 mS cm^{-1}, non-ureolytic bacterial metabolism is dominant. The ureolytic activity due to ureolysis process becomes dominant making the cumulative EC surpass the 10 mS cm^{-1} threshold at the later stage.

(2) Higher initial urea concentration (100 and 170 mM) inhibits the bacterial reproduction at the later stage in the selective media. In generic media and the selective media with 50 mM urea, viable cell number maintained stable until the end of the test.

(3) Reduced nutrients slow down the bacterial reproduction, and further limit the population of ureolytic bacteria, resulting in relatively low ureolytic activity. The amendment of ammonium to the enrichment media, though initially delays the bacteria growth, can finally elevates ureolytic activity due to the elimination of non-ureolytic bacteria at the very start stage of enrichment.

7.2 Bio-stimulated MICP under Sand Column Condition

In this resaerch, the biochemical properties under sand column situation were studied, and a comprehensive experimental program was conducted to systematically investigate the shear behavior of bio-cemented calcareous sand treated by bio-stimulated MICP through direct shear tests. This study contributes to the development of bio-stimulated MICP in the following aspects:

(1) During the enrichment phase, the indigenous ureolytic bacteria can be enriched significantly within 48 hours, though the ureolysis rate was varying with the initial urea concentration. A higher ureolysis rate was maintained in the 170 mM cases until the end of 48 hours, while for 50 mM and 100 mM cases, the ureolysis rate increased slowly or started to drop after 24 h. In addition, the microbial community changed significantly after enrichment stage. The ureolytic species could be found in the sand.

(2) Peak stress ratio (η_p) increased with increasing cementation content and initial D_r, whereas decreased with increasing normal stress. The η_p of low initial relative density (D_r = 16%) samples could be even smaller than that of untreated clean sand when normal stress was higher than 400 kPa. The effects of cementation content and initial D_r on peak strength parameters diminished with the elevated normal stress.

(3) The linear Mohr-Coulomb failure envelopes overestimated the cohesion. Instead, the bilinear failure envelop could more accurately predict the cohesion of bio-cemented sand, especially for the sands with higher cementation level. It was found that the cohesion and peak friction angle increased with elevated cementation level while declined with the increasing normal stress.

(4) For bio-cemented calcareous sand, the stress ratio and dilatancy exhibited a loop-shaped relationship at low normal stress ($\leqslant$ 200 kPa), and an apparent asynchronism between the state of η_p and maximum dilatancy was observed on samples with higher cementation content ranging from 5.87% to 6.33%.

(5) A conceptual framework to analyze peak state shear behavior of bio-cemented calcareous sand was proposed. The interdependence between external influential factors (cementation level, initial D_r, and normal stress) and strength contributors (interparticle friction, dilatancy, particle rearrangement, interparticle bonding, and particle crushing) at

the peak state were illustrated in detail. The validity of this framework was further confirmed through microscopic observations.

7.3 Comprehensive Characteristics of Bio-cemented Calcareous Sand

In this research, the compressive properties of bio-cemented sand treated by bio-stimulated MICP method were studied. A series of one-dimension compression tests were conducted to obtain the compressibility of bio-cemented calcareous sand, which was manifested by the compression curves and particle size distribution curves (PSDs). Then, the relevant parameters including cementation content (*CC*), the coefficient of compressibility (a_v), relative breakage (B_r), and relative agglomeration (A_r) of the bio-cemented sand based on the method proposed by Hardin in 1985 were discussed. This study contributes to the development of bio-stimulated MICP in the following aspects:

(1) The a_v value was found to decrease with the increasing cementation content. Contrarily, the specimens with higher initial D_r had smaller (approximately 20%-70%) a_v values than their counterparts with lower initial D_r. In terms of C_r value, higher initial D_r resulted in a larger C_r, and C_r decreased with the increasing cementation content.

(2) Based on the analysis of PSDs curves after compression, the specimen with higher initial D_r and more *CC* resulted in a smaller B_r and a larger A_r. More fines were generated in bio-cemented specimens with higher cementation content and lower initial D_r. The increased fines mainly came from the debris of calcium carbonate, which is revealed by microscopic images. Additionally, some larger lumps appeared as the result of residual agglomeration effect of some undamaged cementations.

(3) A conceptual framework based on the interparticle contact modes (i.e., G-G; G-C-G; G-C) and their corresponding damage modes (i.e., detachment; debonding; abrasion) during the compression tests was proposed. Compared with G-G and G-C modes, the G-C-G was the strongest contact mode for the bio-cemented sand. During compression, debonding and detachment firstly occurred in the G-C-G and G-C contacts mode, respectively. Abrasion damage mode then became predominant as debonding and detachment progressed during particle rearrangement and relocation.

7.4 The Shearing Behaviors of Biochar-amended Bio-cemented Sand

In this research, the shear behavior of biochar-amended bio-cemented calcareous sand treated via bio-stimulation was investigated through a series of direct shear test. The samples underwent enrichment phase and cementation phase to enrich ureolytic bacteria and form bio-cementation. Upon the completion of bio-stimulated MICP treatment, direct shear test was performed to obtain the shear behaviors and shear parameters including peak stress ratio, friction angle and cohesion. Meanwhile, the specimens were subjected to cementation content measurement and microscopic observations to reveal the fundamentals of the enhancement effect of biochar on bio-cemented calcareous sand. This study contributes to the development of bio-stimulated MICP in the following aspects:

(1) The addition of biochar powders could effectively increase the cementation content of bio-cemented sand treated by bio-stimulation method. Assuming the other conditions were the same, the *CC* increased with the elevated amount of biochar. The addition of biochar yielded a 31%-81% increase in *CC* compared with the specimens without biochar. The specimens with lower initial D_r had slightly higher *CC* than that with higher initial D_r.

(2) The bio-cemented sand with biochar amendment showed a much more significant increase of peak stress ratio (η_p/η_0>1) in the specimens prepared under higher initial D_r than those under lower initial D_r. The primary strength improvement came from the increase of cohesion, and the significant cohesion improvement (c/c_0>1) was also observed under higher initial D_r situation. The friction angle improvement (i.e., ϕ/ϕ_0 >1) was only observed in the specimens with 0.1% biochar content, indicating that the introduction of biochar may reduce the interparticle friction.

(3) Based on the observation of microscopic images, biochar was able to alter the structure of interparticle cementation to influence the shear strength indirectly. It was found that the entombment of biochar within the cementation was a common phenomenon, making the bio-cementation a dark color. Some independent biochar which was not involved in the process of MICP could be observed on the surface of sand particles.

(4) According to the responses of shear strength parameters, the effects of biochar in the shear strength of bio-cemented sands are three folds. Firstly, biochar used as the extra nucleation sites for native ureolytic bacteria, could increase *CC* within specimens. Secondly, too much biochar within bio-cementation may become weak points and thus diminish the contribution of interparticle bonding to the shear strength. Thirdly, as biochar

content increases, more un-entombed tiny biochar powders that are distributed randomly on the surface of sand particles can reduce the interparticle friction.

7.5 Bio-stimulated MICP on Rainfall-induced Erosion Prevention

In this research, a meso-scale laboratory model was made to investigate the deformation on artificial sandy slope treated by bio-stimulated MICP method. Also, it is the first time that the photography-based SfM (Structure from Motion) method is applied to evaluate the rainfall-induced erosion of bio-cemented soils, which is a good trial to explore a feasible monitoring way for the full-scale application in field. This study contributes to the development of bio-stimulated MICP in the following aspects:

(1) The results showed that bio-stimulated MICP could significantly reduce the erosion on a sandy slope, especially in case treated by YE-based enrichment medium with 170 initial urea concentration. Furthermore, it is the first time that the photography-based SfM (Structure from Motion) method is applied to evaluate the rainfall-induced erosion of bio-cemented soils, which is a good trial to explore a feasible monitoring way for the full-scale application in field.

LIST OF PUBLICATIONS

1. **Wang, Y. J.**, Jiang, N. J., Han, X. L., Liu, K., & Du, Y. J. (2022). Biochemical, Strength and Erosional Characteristics of Coral Sand Treated by Bio-Stimulated Microbial Induced Calcite Precipitation. Acta Geotechnica, 1-13.

2. Jiang, N. J., **Wang, Y. J.**, Chu, J., Kawasaki, S., Tang, C. S., Cheng, L., ... & Wang, Y. Z. (2022). Bio - mediated soil improvement: An introspection into processes, materials, characterization and applications. Soil Use and Management, 38(1), 68-93.

3. **Wang, Y. J.**, Han, X. L., Jiang, N. J., Wang, J., & Feng, J. (2020). The effect of enrichment media on the stimulation of native ureolytic bacteria in calcareous sand. International Journal of Environmental Science and Technology, 17(3), 1795-1808.

4. **Wang, Y. J.**, Han, X. L., & Jiang, N. J. (2018, October). Enriching Indigenous Ureolytic Bacteria in Coastal Beach Sand. In The International Congress on Environmental Geotechnics (pp. 340-347). Springer, Singapore.

5. **Wang, Y. J.**, Jiang, N., & Han, X. (2021). A preliminary study of carbonate sand stabilization by bio-stimulation based MICP method. Japanese Geotechnical Society Special Publication, 9(6), 282-286.